University of Venda
Creating Future Leaders

University of Venda

Multiscale Modelling of Environmentally Transmitted Infectious Diseases

by

RENDANI NETSHIKWETA

A Thesis Submitted to the

UNIVERSITY OF VENDA

In Fulfillment of the Requirements for the Degree

of

Doctor of Philosophy (Mathematics)

in the

Department of Mathematics & Applied Mathematics

at

SCHOOL OF MATHEMATICAL & NATURAL SCIENCES

Promoter: Prof. W. GARIRA

Co-Promoter: Dr. D. MATHEBULA

Submitted December 2021

Declaration of Authorship

I, RENDANI NETSHIKWETA, declare that this thesis titled, “Multiscale Modelling of Environmentally Transmitted Infectious Diseases”and the work presented in it are my own. I confirm that:

- This work was done wholly or mainly while in candidature for a research degree at this University.
- Where any part of this thesis has previously been submitted for a degree or any other qualification at this University or any other institution, this has been clearly stated.
- Where I have consulted the published work of others, this is always clearly acknowledged.
- Where I have quoted from the work of others, the source is always given. With the exception of such quotations, this thesis is entirely my own work.
- I have acknowledged all main sources of help.
- Where the thesis is based on work done by myself jointly with others, I have made clear exactly what was done by others and what I have contributed myself.

Author: 

Date: 17-June-2021

Promotor: 

Date: 21-June-2021

Co-Promotor: 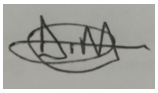

Date: 21-June-2021

Abstract

In the field of mathematical biology, researchers are beginning to witness an overwhelming appreciation of multiscale modelling as an essential and suitable technique as opposed to a traditional single-scale modelling approach in predicting the dynamics of infectious disease systems. Yet, there is still a lack of evidence that generally indicates which among the different categories of multiscale models of infectious disease systems is more appropriate to use in multiscale modelling of infectious disease systems at different levels of their organization. This research study is the first of its kind to compare the suitability of the two fundamental categories of multiscale models of infectious disease systems which are nested multiscale models and embedded multiscale models in predicting disease dynamics with specific reference to environmentally-transmitted diseases. Two environmentally transmitted diseases are used as case studies, namely ruminant paratuberculosis and human ascariasis, to compare the two fundamental categories of multiscale models in predicting disease dynamics. The two environmentally-transmitted diseases considered in this study represent infectious disease systems with replication-cycle at microscale (i.e. ruminant paratuberculosis) and infectious disease systems without replication cycle at the microscale (i.e. human ascariasis). Firstly, the author develop a single-scale model at the host-level that we progressively extend to different categories of multiscale models that we later compare. The findings of this study (through both mathematical and numerical analysis of the multiscale models) are that for ruminant paratuberculosis which has a pathogen replication-cycle at the within-host scale both nested and embedded multiscale models can be used because both the models provide the same prediction of disease dynamics. However, for human ascariasis the findings are such that nested multiscale model is not appropriate in characterizing the disease dynamics, only the embedded is appropriate. Although the comparison of different categories of multiscale models in disease prediction carried out in this study are specific to paratuberculosis in ruminants and human ascariasis, the results obtained in this study are robust enough to be applicable to other infectious disease systems. Our results can be generalized to imply that for any level of organization of an infectious disease systems, if the disease has a replication cycle at the microscale, the nested multiscale and the embedded multiscle model provide the same accuracy in predicting disease dynamics. However, when the disease has no replication cycle at the microscale, only the embedded multiscle model is appropriate for predicting disease dynamics. In such a case, a nested multiscale model is inappropriate. We anticipate that this study will enable modelers to choose appropriate multiscale model category in the study of infectious diseases.

Acknowledgements

First and foremost I would like to give thanks to the Almighty God and Father for His precious gift of life He has given to us. I would like to thank and extend my sincere gratitude to my supervisor, Prof W. Garira, for his support and guidance he extended to me during the entire period of my PhD research work study. I also thank my co-supervisor, Dr D. Mathebula, for all her wonderful contribution she also made to my PhD study. My appreciation goes to all members of Modelling Health and Environmental Linkages Research Group (MHELRG) for their support and unwavering commitment towards my work. My sincere gratitude and gratefulness also goes to my wife, my mother and all my family members for their unwearied support and encouragement throughout my studies. Lastly, I would like to acknowledge the support from South Africa National Research Foundation (NRF) for its financial support, Grant No. IPRR (UID 81235). The work was also supported financially by the Global Infectious Disease Research Training (GIDRT), Award #D43 TW006578 from the Fogarty International Center of the NIH.

Contents

List of Figures

List of Tables

Chapter 1

Introduction

1.1 Background of the Study

Infectious diseases have been and still continued to be a public health threat throughout the world, more especially in low-and-middle income settings where majority of people have limited access to clean water and adequate sanitation facilities as well as health facilities. It has been widely accepted that better insights into transmission mechanisms of infectious diseases using mathematical modelling methods may facilitate the development of new as well as improving existing preventive and control measures against burdens in which these infectious diseases impose across populations. In the past two and half decades and until now, mathematical models in the field of biological systems have been and still continued to play a crucial role in improving our understanding about infectious diseases dynamics across different levels of organization (e.g. cell level, tissue level, organism/host level, population level, etc.). They have also enhanced our understanding regards to the impact of different disease transmission mechanisms (e.g., fecal-oral transmission, sexual-oral transmission mechanism, vector-borne transmission mechanism, etc.) on the transmission risks of many infectious diseases in a given population as well as assisting us to be able to compare and evaluate effectiveness of various health interventions against these infectious diseases either at local or global level. The earliest account of mathematical modelling of infectious disease dynamics can be dated way back in 1766 [3] when Daniel Bernoulli formulated a model for the spread of smallpox to assess the effectiveness of the variolation practice [4, 5]. Since that time until recently, countless mathematical models have been developed to

describe and analyze transmission dynamics of various infectious diseases across different hierarchical levels of biological organization of an infectious disease system (see the work in [4, 6] and reference therein). Additionally, most of these models have further been remarkably useful in addressing many aspects pertaining the transmission dynamics of infectious disease systems such as stages of an infection in a host, susceptibility of the host to infective dose, persistence of a disease in the population, pathogen shedding, pathogen co-evolution, severity of the disease, multi-host infections, and multi-strain infections, etc. Moreover, in the context of infectious disease modelling, it is worthy to mentioning that different models have been and continue to be developed based on different model structures depending on the addressed question(s) of interest under study. These different model structures include susceptible-infected (SI), susceptible-infected-pathogen (SIP), and variations of this paradigm (SIR, SIRP, SEIR, SEIRP, etc) that can be developed at any levels of organization of an infectious disease system (i.e., cell level, tissue level, host level, etc). For instance, the SI model structure and variations of this paradigm (SIS, SIR, SIRS, SEIR, SEIRS, etc) models specifically infectious diseases that are transmitted primarily by direct contact means (see the work in [4] for example and reference therein), while the SIP model structure and variations of this paradigm (SISP, SIRP, SIRSP, SEIRP, SEIRSP, etc) concern with infectious diseases that are transmitted by indirect contact means (see the work in [7] for example and reference therein). Directly transmitted diseases are those infectious diseases that are transmitted from one host to another through host-to-host transmission. Sexually-transmitted infectious diseases such as HIV/AIDS are the most typical examples of directly transmitted diseases. On the other hand, indirectly transmitted diseases are those infectious diseases that a host acquire through ingestion of free-living pathogens located in contaminated physical environment domains such as food, water, air, soil, or contact surface; with the resulting diseases being called environmentally-transmitted diseases. Diarrheal infectious diseases such as cholera, campylobacteriosis, listeriosis, paratuberculosis in ruminants, and soil-transmitted helminth infections are typical examples of environmentally-transmitted diseases. It is so interesting to note that although there is an increasing number of mathematical models that are developed to study transmission dynamics of various infectious disease systems, most of them predominantly studied their dynamics at two scales being the epidemiological scale and the immunological scale. It is again important to note that these two scales have been and continue to be considered separately even for the same infectious disease system. This is despite the fact that infectious disease systems are multiscale, multilevel systems that bridge a wide range of varying spatial and temporal scales, from cellular levels to macroecosystem level [8].

In addition, limited knowledge about how to integrate information from the different sets of scales of biological organization involved in the dynamics of infectious diseases has hampered

progress in controlling, eliminating and even eradicating both social and economical burdens that most of these infectious disease impose throughout the world, particularly in the developing world. Multiscale modelling offers the mathematical technological infrastructure for integrating information from the different sets of scales of biological organization involved in the dynamics of infectious diseases as opposed to traditional single-scale modelling. This is due to the fact that multiscale modelling facilitates the integration of different sets of scales of an infection disease system. Recently, we have witnessed the development and application of different multiscale models for various infectious disease systems (see [9–18] for examples) and the establishment of a broader scientific theory for multiscale of infectious disease systems [8] . In a recent set of landmark papers by Garira [1, 19, 20], the author identified five main different categories of multiscale models of infectious disease systems that can be developed at different levels of organization of an infectious disease system (be the cell level, the tissue level, the host level, etc.) which are: (i) Individual-based multiscale models (IMSMs), (ii) Nested multiscale models (NMSMs), (iii) Embedded multiscale models (EMSMs), (iv) Hybrid multiscale models (HMSMs), and (v) Coupled multiscale models (CMSMs) with each having more than one class within. More details with regards to the categorization of these multiscale models for infectious disease systems a reader is invited to the two papers by Garira ([19, 20]). Here, we only give a brief review of each of the five categories of multiscale model types for infectious disease systems as follow:

(i) ***Category I - Individual based multiscale models (IMSMs)***: In this category, multiscale models are formulated based on the assumption that the individual/lower/micro scale (i.e., within-cell scale, within-tissue scale, within-host scale) sub-model is used to describe the entire infectious disease system across both the within-host scale and between-host scale. The key features in this category are such that (a) there is no information flow from the population/upper/macro scale sub-model to the individual/lower/micro scale sub-model, and the population/upper/macro scale is observed as emergent behaviour of the individual/lower/micro scale entities. Typical examples of the development of multiscale models within this category see the works in [21–29].

(ii) ***Category II - Nested multiscale models (NMSMs)***: These are multiscale models of infectious disease systems that are developed based on the assumption that there is only one-way inter-scale or unidirectional flow of information (i.e., only from the individual/lower/micro sub-model to the population/upper/macro sub-model). In addition, the key features of this category is that (a) the dynamics of the individual/lower/micro is independent from the population/upper/macro scale, and (b) the formalism or mathematical representation that describe both the individual/lower/micro sub-model and the population/upper/macro

sub-model must be the same. The multiscale models in [30–33] are good examples of the development of NMSMs. Another good examples of the development of NMSMs are in [16, 17] in the context of malaria (a vector-borne transmitted disease) and HIV (a direct transmitted disease), respectively.

(iii) ***Category III - Embedded multiscale models (EMSMs)***: These are multiscale models of infectious disease systems in which there is a two-way inter-scale or bidirectional flow of information between the individual/lower/micro sub-model and the population/upper/-macro sub-model. Therefore, the key features in this category are such that (a) there is a reciprocal influence between the individual/lower/micro scale sub-model and population/upper/macro scale sub-model, and (b) both the individual/lower/micro scale sub-model and population/upper/macro scale sub-model must be described by the same formalism or mathematical representation. The papers by [8–11, 14, 34] provide classical examples of the development of EMSMs at the host level.

(iv) ***Category IV - Hybrid multiscale models (HMSMs)***: These are multiscale models that are formulated based on the assumption that the individual/lower/micro sub-model and population/upper/macro model can be modelled in a heterogeneous way using different formalism or mathematical representation as appose to the multiscale models in categories I, II and III, where the within-host scale and the between-host scale can be modelled in a homogeneous way using the same formalism or mathematical representation. Therefore, the key feature in this category is that the individual/lower/micro sub-model and population/upper/macro sub-model are described by different formalism or mathematical representation. The most typical examples of such paired formalisms are deterministic/stochastic, mechanistic/phenomenological, ODE/PDE, and ODE/ABM. Multiscale models of infectious disease systems that are based on this category can be found in the following articles [35–39].

(v) ***Category V - Coupled multiscale models (CMSMs)***: These are multiscale models of infectious disease systems in which multi-strain infections, multi-pathogen infections, multi-group infections, multi-host infections, multi-level infections, multi-geographical environments infections, multi-biological environments infections take into account on the transmission of infectious disease systems. The key features of this category are such that (a) the diversity within a single-host species (multi-group infections) and diversity within a single-pathogen species (multi-strain infections) are considered in multiscale modelling of infectious disease systems, and (b) the other four categories of multiscale models (NMSMs, IMSMs, EMSMs, HMSMs) can be used as sub-models to describe the dynamics of an

infectious disease system across scales in each levels of biological organization. Typical examples of multiscale models in this category are in [40–43].

It is important to mention that IMSMs, NMSMs and EMSMs are fundamental building blocks for the development of most multiscale models that integrate micro-scale and macro-scale dynamics of an infectious disease system across different levels of biological organization. It is further important to note that IMSMs integrate implicitly microscale and macroscale disease dynamics, while both NMSMs and EMSMs integrate explicitly micro-scale and macro-scale disease dynamics. Yet, nothing has been done in investigating which between these two multiscale models (NMSMs and EMSMs) is more suitable in describing the dynamics of infectious disease systems. Therefore, this thesis investigates the suitability of application of NMSMs and EMSMs in modelling infectious disease systems using environmentally-transmitted diseases as example paradigms. The modelling of environmentally transmitted diseases involves the use of pathogen load as a common metric of host infectious and burden of disease across all the seven main biological levels of organization of an infectious disease system (i.e. cell level, tissue level, organ level, micro-ecosystem level, host level, community level, and macro-ecosystem level) [8]. For purposes of implementing multiscale modelling methods, we can demarcate environmentally-transmitted into three different types: (i) type II environmentally transmitted disease - in which there is no replication of their disease-causing pathogens at the microscale, (ii) type I environmentally-transmitted disease - in which their disease-causing pathogens only replicates at the microscale, and (iii) type III environmentally transmitted disease - in which their disease-causing pathogens replicates at both the microscale and macroscale (see [8] and Sec. 1.2 of this thesis for more details).

1.2 Preliminary Comparison of Multiscale Models for Infectious Disease Systems

Despite the increase in the use of multiscale modeling to study the complexity and multiscale nature of infectious diseases dynamics, currently it has been urged by the author in [1] that we cannot be able to draw general conclusions about which of the five categories of infectious disease systems is suitable in addressing the problem of an infectious disease system in different conditions. However, what is now clear as pointed out in [1] is what dictates the selection of a particular category of multiscale models for a particular disease is:

a. IMSMs – their selection is dictated by the need of incorporating heterogeneity into the multiscale model (e.g., heterogeneity in (i) host susceptibility, (ii) the ability of hosts to transmit pathogens to other hosts, (iii) host behavior, and (iv) host immune response).

b. NMSMs – their selection is based on the choice of biological linking mechanisms between two adjacent scales of an infectious disease system (i.e., macroscale and microscale) in which the contribution of super-infection/reinfection at the macro-scale to pathogen replication at the micro-scale is considered irrelevant/insignificant and that the effect of this super-infection/reinfection on the dynamics of an infectious disease can be ignored.

c. EMSMs – their selection is as appose to NMSMs is based on the choice of biological linking mechanisms between two adjacent scales of an infectious disease system (i.e., macro-scale/upper/population scale and micro-scale/lower/individual scale) in which the contribution of super-infection/reinfection at the macro-scale to pathogen replication at the micro-scale is considered significant such and that the effect of this super-infection/reinfection on the dynamics of an infectious disease cannot be ignored.

d. HMSMs – their selection is also dictated by the freedom of the representation of the two scales of an infectious disease system using different mathematical formalizations (e.g., deterministic/stochastic, discrete time/ continues time, mechanistic/phenomenological, ODE/PDE, etc.).

e. CMSMs – their selection is the same as the other four categories of multiscale models (IMSMs, NMSMs, EMSMs, HMSMs), except that in this case the need of incorporating at least the following aspects of infectious disease systems can be considered in the development of multiscale models: (i) multiple levels of biological organization of the infectious disease system, (ii) multiple host species such in the case of vector-borne diseases, (iii) multiple pathogen species/strains such as in the case of co-infections, (iv) multiple communities, and (v) multiple anatomical compartments or organs.

However, there is still lack of evidence that generally indicates which among these categories of multiscale models is more appropriate to use in modelling infectious disease systems for different conditions. The author in [1] further elaborates the need for studies to establish evidence that would guide in the selection of these categories of multiscale models. Thus, the current study is the first of its kind to compare the suitability in characterizing infectious diseases transmission dynamics within these five different categories. We particularly compare the suitability of NMSMs and EMSMs in characterizing the multiscale dynamics of infectious disease systems. This is partly because of their simplicity and partly because both they are fundamental building blocks for the development of other categories of multiscale models of infectious disease

systems that can be developed at any biological organization. The comparison between these two categories of multiscale models in their suitability in predicting the dynamics of infectious disease systems is conducted using environmentally-transmitted disease systems as paradigms. Environmentally-transmitted diseases are infectious diseases that arise or transmitted across populations as a result of interaction of a host (be human, animal, and even plant) with free-living pathogens in the outside-host/physical environmental domain (such as water, food, air, soil or contact surface and objects). In any given population, individual hosts can be exposed to various types of free-living pathogens (e.g., viruses, parasites, bacteria, and fungus) that are capable of living in multiple environments which we can roughly demarcate into two main types as: (i) the outside-host environment - which is generally associated with the pathogen's free-living stages in the geographical environment's physical domains, and (ii) the inside-host/biological environmental domain - which is also associated with the developmental life stages of the pathogen in the biological host environment's organs, tissues, and cells. In the outside-host environment, these free-living pathogens that are solely responsible for causing environmentally-transmitted diseases in the population are generally transmitted from one host to another host through different modes of transmission which can roughly be classified into five classes as follows:

i. ***Food-borne diseases***: These are illnesses that arise from ingestion of spoiled or poisonous food contaminated by microorganisms or toxicants, which may occur at any stage during food processing from production to consumption. The World Health Organization (WHO) reported that every year, 1 in 10 people become infected from eating contaminated food, and further approximately 420 000 people die each year as a result [44]. Bacterial infections such as salmonelliosis, listeriosis and campylobacteriosis, and viral infections such as rotovirus and norovirus infections are among the most common food-borne infectious diseases that afflict millions of people throughout the world annually.

ii. ***Water-borne diseases***: These are infections that are transmitted among hosts through drinking from unsafe water contaminated by infective pathogens. Some of water-borne diseases are transmitted as a result of an individual being exposed to vectors whose life-cycle are influenced by environmental factors, with the resulting disease being termed vector-borne transmitted diseases. According to WHO, four-fifths of all infections in the developing world are caused by water-borne diseases, with diarrhea being the leading cause of death among children under the age of five years [45]. Diarrheal infections such as hepatitis e, cholera and other vector-borne transmitted illnesses such as malaria, typhoid, schistosomiasis, guinea worm infection, and onchocerciasis are the most common examples of water-related diseases.

iii. ***Air-borne diseases***: These are infectious diseases that are transmitted through the air by means of breathing, talking, coughing, sneezing, or any activities which generates aerosol particles or droplets. The most common well-known examples of air-borne related diseases include: anthrax, chickenpox, influenza, measles, smallpox and tuberculosis.

iv. ***Soil-transmitted diseases***: These are infection that are transmitted through walking bare-foot on the contaminated soil contaminated with faecal matters or through the ingestion of worm larvae (eggs) presented in the vegetables, drinking water and raw or undercooked meat. WHO have also reported that soil-transmitted helminth infections are among the most common infections worldwide and affect more than 1.5 billion people, or 24% of the world's population [46]. Typical examples of soil-transmitted diseases are the whip-worm (Trichuris trichiura), the roundworm (Ascaris lumbricoides) and the two species of hookworms (Necator americanus and Ancylostoma duodenale) that are highly prevalent in developing countries.

v. ***Formites-transmitted diseases***: These include infectious diseases which are transmitted through contact with surfaces contaminated with infective free-living pathogens in the environment.

However, it is important to note that this classification is not important in the development of multiscale models of infectious disease systems. In the following we discuss categorization of environmentally-transmitted disease systems which is more suitable for multiscale modelling. Therefore, following the work in [8], we categorize environmentally-transmitted diseases into three main types related to the scale of organization of an infection at which the replication and transmission of their pathogens occur:

i. ***Type I, Environmentally-transmitted diseases***: In this type of environmentally-transmitted infectious disease systems, pathogen replication-cycle do not occur at the micro-scale but only the developmental stages of the pathogen occur at this scale, while the transmission of the pathogen takes place at the macroscale. The most common example of this Type I environmentally-transmitted infectious diseases include schistosomiasis [9], Guinea worm [10], and soil-transmitted diseases such as hookworm [8].

ii. ***Type II Environmentally-transmitted diseases***: In this type of environmentally-transmitted infectious disease systems, pathogen replication-cycle only occurs at the microscale (i.e., at the within-host/within- tissue/within-cell scale) while the transmission of the pathogen occurs at the macroscale (i.e., at the between-host/between-tissue/between-cell scale). Most

air-borne viral infections such as influenza [47] and some food-borne bacterial infections such as paratuberculosis species [48] are good examples of Type II environmentally-transmitted infectious disease systems.

iii. ***Type III Environmentally-transmitted diseases***: In this type of environmentally-transmitted infectious disease systems, replication-cycle of pathogen replicates at both the micro-scale and at the macro-scale while the transmission of the pathogen still happens at the macro-scale. These environmentally-transmitted diseases are typically caused by opportunistic infections such as cholera, salmonella enterica and anthrax (see [8] and reference therein). Additionally, it is important to note from [8] that this type of environmentally-transmitted diseases is the combination of type (I and II) environmentally-transmitted disease systems.

All of these three categories of environmentally-transmitted diseases can be further explained by a conceptual framework of environmentally-transmitted disease systems as shown in Fig. 1.1 which shows four main components of environmentally-transmitted disease systems.

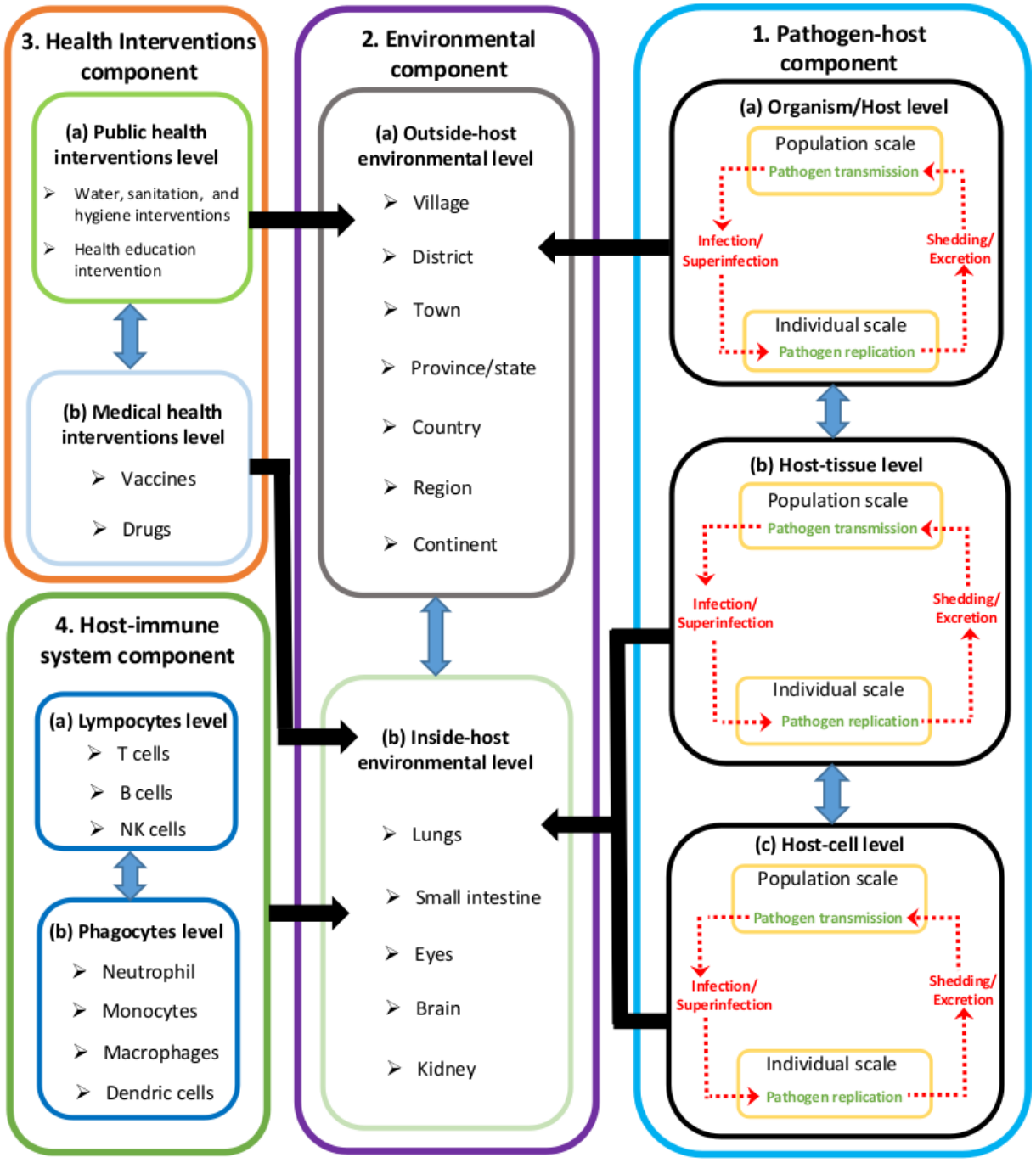

Figure 1.1: *Conceptual diagram showing four main components of an environmentally-transmitted disease system and the associated levels of organization of infection for each component.*

Based on Fig. 1.1, it should be noted that these four main components of environmentally-transmitted disease systems are interdependently to one another and within each of them there is at least two associated levels of biological organization of an infection disease system. These four main components of environmentally-transmitted disease systems are: (a) the pathogen-host

component which consists of (i) organism/host level, (ii) host-tissue level, (iii) host-cell level; (b) the environmental component which also consists of (i) outside-host environmental level, (ii) inside-host environmental level; (c) the health interventions component further consists of (i) public health intervention level, (ii) medical intervention level; and (d) the host-immune system component which again consists of (i) lypocytes level, (ii) phagocytes level. these four components are also described in [20]. In what follows, we briefly describe each components for environmentally-transmitted disease system and their associated levels of biological organization of an infectious disease systems.

1. ***Pathogen-host component***: This could be either the interaction between a free-living pathogen in the physical environmental domains (such as soil, water, air, food, etc.) and a host (such as animal, human or vector) at a host level in the host behavioral physical environment (i.e., outside-host environmental level) or the interaction between pathogen and a host tissue at a host-tissue level within a single infected host (inside-host environmental level) or the interaction between pathogen and a host cell at a host-cell level within an infected individual host (i.e., inside-host environmental level) that could lead to an infection in a host/host-tissue/host-cell populations. From a biological point of view, pathogen-host interaction component generally takes place at different ordered hierarchical levels of biological organization of an infectious disease system ranging from molecule level and cell level to tissue level and to organism/host level and host population level. However, the three main ordered hierarchical levels of organization of an infectious disease system include (a) the organism/host level, (b) the host-tissue level and (c) host-cell level all which serve as the units of multiscale analysis [20]. These three ordered hierarchical levels of biological organization of an infectious disease system can be briefly described as follows [19, 20]:

   (a) *Host level*. This is an upper level of infection in the pathogen-host interaction component at which infection can be observed. At the hierarchical level of the pathogen-host component, empirical studies (i.e., those that are based on experiment, observation, surveillance, clinical trials, etc.) or quantitative studies (i.e., those that are based on mathematical models, statistical models, and computational modellings) that characterize infectious disease systems across two adjacent scales of organization of an infectious disease system can be carried out using a host as a basic unity of multiscale analysis. The disease dynamics at the host level begin within the infection/super-infection of the host by free-living pathogen in the physical environment. Following infection/super-infection of the host by pathogen that has successfully entered inside the host, then pathogen replicate at the micro-scale. The replication of pathogen

within a host in most cases is followed by pathogen shedding/excretion into the physical environment outside the host at the macro-scale. Shedding/excretion of pathogen from host individual level (i.e., within-host scale) into the physical environment at the host population level (i.e., between-host scale) by a single infected host is followed by pathogen transmission between hosts at the host population scale (between-host scale). This close up a circle of transmission-replication at the host level through infection/super-infection and shedding/excretion that link the individual scale and the population scale within this level. Diarrheal infections such cholera and some helminth infections such as hookworm are typical examples of environmentally-transmitted disease systems which can be studied at this order hierarchical level of an environmentally-transmitted disease system.

(b) *Host-tissue level*. This is a central level of infection in the pathogen-host interaction component at which infection happens. At this order of hierarchical level, empirical studies or quantitative studies that characterize infectious disease systems across two adjacent scales and associated four pathogen specific diseases processes within this level can also be conducted using a host-tissue as a basic unity of multiscale analysis. At the host-tissue level disease dynamic begins within the infection/super-infection of the host tissue by invading pathogen at the host tissue individual (within-tissue) scale. Once the infection of the host by pathogen has successfully occur, pathogen replication at the tissue micro-scale follows. The replication of pathogen within a host tissue is followed by pathogen shedding/excretion into the extra-tissue environment outside the host tissue at the host tissue macro-scale. Shedding/excretion of pathogen by a damaged host tissue at the host-tissue individual scale is followed by pathogen transmission between host tissues at the host-tissue population scale (i.e, between-tissue scale). This also close up a transmission-replication circle in the host tissue level. Environmentally-transmitted disease system that can also be studied at this order hierarchical level include bacterial infections such as paratuberculosis and some helminth infections in which their pathogens do infect specific tissue such granulomas and microabscess to cause damage to the host tissues and organs.

(c) *Host-cell level*. This is a lower level of infection in the pathogen-host interaction component at which infection occur. At this order of hierarchical level of the pathogen-host interaction component both empirical and quantitative studies that characterize infectious disease systems across two adjacent scales and associated four pathogen specific diseases processes within this level can also be carried out using a host-cell as a basic unity of multiscale analysis. The disease dynamic at this level begins within the infection of the host cell by cell invasion pathogen within an infected host

at the site of infection (e.g. lung, small intestine, etc.). Once infection of the host cell successfully occurred, pathogen replication at the host-cell individual level follows. The replication of pathogen within a single infected host-cell at the site of infection within an infected host is generally followed by pathogen shedding/excretion by bursting cells into the extracellular environment at the host cell population level. Shedding/excretion of pathogen by bursting cell is followed by pathogen transmission between cells at the host cell population scale (i.e., between-cell scale) at the site of infection inside an infected host. This also close-up a circle of transmission-replication at the host cell level. Typical examples of environmentally-transmitted disease systems which can further be studied at this order hierarchical level of an environmentally-transmitted disease system are bacterial infections such as campylobacteriosis, listeriosis and ruminant paratuberculosis in which their disease-causing pathogens do infect specific cells such as epithelial cells in the host small intestine, and cause damage to these cells.

2. ***Environmental component***: This component constitute both the outside-host and the inside-host environmental levels. At the inside-host environmental level (a) host cells such as epithelial cells and macrophages, (b) host tissues such as granulomas and microabscess, and (c) host organs such as small intestine and lungs all constitute the inside-host (biological) environmental level for an infectious disease system including environmentally-transmitted diseases where pathogen grow, reproduce and spread across host-cell and host-tissue levels. While at the outside-host environmental level geographical environment (such as village, district, town, province/state, country, region, etc.) and the associated physical environment domains (including water, food, soil, contact surfaces and objects, etc.) constitute the outside-host environmental level where both pathogen and host grow, produce and interact with each other within this environmental level. Host individuals are usually exposed to a variety of environmentally-transmitted disease-causing pathogens in the outside-host environmental level through ingesting contaminated food or water with infective pathogens or through direct contact with infective pathogens in the soil. In the context of environmentally-transmitted disease systems, there is always a reciprocal influences between the outside-host and the inside-host environment dynamics of pathogen which are linked through infection of an individual host by the pathogen in the geographical environment (at the host population scale) and the shedding/excretion of the pathogen or its progeny in the biological environment (at the host individual scale) to the geographical environment. Therefore, the outside-host level coupled with the inside-host environmental level strongly determine the nature of health infrastructures and technologies required against epidemics of a particular environmentally-transmitted disease in a specific

village/district/town/province/region/country.

3. ***Health intervention systems component***: This could be public health intervention or medical health intervention or the combination of both depending on the type of an environmentally-transmitted disease system. On one hand, public health interventions are those interventions that are generally administrated at the outside-host or geographical environmental level to interfere with the transmission-replication processes of a pathogen outside the host. Water, sanitation and hygiene (WASH) intervention systems along with health education all are public health intervention level as they target to control, eliminate, and even eradicate an environmentally-transmitted disease system by preventing/reducing/stopping pathogen transmission between hosts at the host population scale in a specific village/district/town/province/region/country. Medical health interventions on other hand are those interventions that are normally administrated at the inside-host or biological environmental level to interfere with the development and establishment of an infection (based on the transmission-replication of pathogen) within a single infected individual (inside-host environmental level). Vaccines and therapeutic drugs as pharmaceutical or medical health intervention level are implemented at the individual level to control, eliminate, and even eradicate an environmentally-transmitted disease system by preventing/reducing/stopping pathogen replication in host cells, tissues or organs at the site of infection in a single infected individual host. Due to the pathogen transmission-replication cycle that occur at the outside-host environmental level and at the inside-host environment, there is also a reciprocal influence between the public health interventions that target to prevent/reduce/stop the movement of pathogen in the physical environment and among individual hosts (at the outside-host environmental level) and the medical health interventions that target to prevent/reduce/stop circulation and replication of pathogen at the host-cell/host-tissue/host-organ levels.

4. ***Host-immune system component***: The host-immune system component of an environmentally-transmitted disease system is made up of a complex network of host-cells, host-tissues and host-organs that work together to protect a host from infection by pathogens, remove toxins, and destroy infected host-cell/tissue/organ or tumor cells. Lymphocytes and phagocytes are the two main levels of the host-immune system component that are involved in fighting against pathogens that are responsible of causing an infection within a host.

   (a) Lymphocytes are small white blood cells that form part of the immune system in a host and play a crucial role in the host immunity. They generate a specific immune response which is referred as adaptive immunity. Lymphocytes mainly circulate in the blood and lymphatic system and they can also found in other host tissues/organs

including bone marrow, peyer's patches, spleen, thymus, liver, lymph nodes, and tonsils to defend the host body from invading pathogen, foreign matter, and infected host cells by pathogen as well as tumor cells. There are three types of lymphocytes which are B cells, T cells and Natural killer (NK) cells. The first type is B cells that are responsible for manufacturing/secreting antibodies which neutralize bacteria and viruses. The second type is T cells that are of three kinds: (i) helper T cells which produce cytokines that stimulate the production of antibodies by the B cells, (ii) cytotoxic T cells which produce granules that induce the apoptosis of the infected cells, and (iii) suppressor T cells which inhabit the immune response towards the self-antigens in the body. The third type is NK cells that are capable to identify and/or induce apoptosis of altered host cells such as tumor cells or infected cells by pathogens.

(b) Phagocytes are also part of white blood cells that are essential for protecting the body from infection by ingesting and destroying or engulfing harmful pathogens, foreign particles, and dead or dying cells at the site of infection within an infected host. They can also be found in different host tissues or organs such as blood, bone marrow and tissue, lymphoid tissue, gut and intestinal peyer's patches, liver, lung, spleen, skin, etc. In contrast to lymphocytes, phagocytes generate a non-specific immune response referred as innate immunity. Example of phagocytes include macrophages, neutrophils, dendritic cells, monocytes, and mast cells.

1.3 Problem statement

In recent years, multiscale modelling of infectious disease systems has begun to receive an overwhelming appreciation over single-scale modelling as a suitable methodology for studying the reciprocal influence between the scales of an infection as well as intervention strategies that operate at different scales. Yet, to the best of our knowledge there has been little that have been done in attempting to compare the suitability in predictions of structurally different multiscale models for the same infectious disease systems. Thus, a comparison study of these structurally different multiscale models is a key component in selecting a suitable multiscale models for predicting infectious disease with various disease properties as well as identifying factors or conditions that are necessary for the control, elimination and even eradication of the burden they cause across the populations. In this study, we bridge this gap by investigating if nested and embedded multiscale models predict the different pattern of multiscale dynamics of infectious diseases using environmentally-transmitted diseases as paradigms. Environmentally-transmitted diseases are

among the most infectious disease systems that remain the leading cause of public health and socioeconomic burden in many parts of the world, most notable in the developing world. In developing countries, more than billion cases of environmentally-transmitted diseases are reported annually. Interestingly, environmentally-transmitted diseases are multilevel and multiscale complex systems as a results of the combined interactions of three subsystems, namely the host sub-system, the free-living pathogen sub-system, and the environment sub-systems.

1.4 Aim and objectives

The current study aimed to compare different categories of structurally different multiscale models of infectious diseases and identify the most appropriate category of multiscale models for a given multiscale modelling problem of an infectious disease system. The specific objectives of the study were as follows:

1. To investigate if nested multiscale models are an appropriate category of multiscale models to characterize the multiscale dynamics of infectious diseases with a replication cycle at microscale using ruminant paratuberculosis as an example.

2. To investigate if embedded multiscale models are an appropriate category of multiscale models to characterize the multiscale dynamics of infectious diseases with a replication cycle at microscale using ruminant paratuberculosis as an example.

3. To compare between nested and embedded multiscale models and identify the most appropriate category of multiscale models to characterize the multiscale dynamics of infectious diseases with a replication cycle at microscale using ruminant paratuberculosis as an example.

4. To compare between nested and embedded multiscale models and identify the most appropriate category of multiscale models to characterize the multiscale dynamics of infectious diseases without a replication cycle at microscale using human ascaris as an example.

1.5 Methodology

The study focused on comparing multiscale models of infectious diseases based on ordinary differential equations that describe the dynamics of environmentally-transmitted diseases at the host-level using ruminant paratuberculosis as an example. We firstly develop an epidemiological

model that describes the transmission dynamics of ruminant paratuberculosis at the between-host scale. This is followed by the development and analysis of two structurally different multiscale models for paratuberculosis that integrate the between-host scale and within-host scale sub-models. We then make a comparison between these two structurally different multiscale models of ruminant paratuberculosis to investigate the most appropriate category in characterizing paratuberculosis transmission dynamics in ruminants. We further illustrate the importance of embedded multiscale models over nested multiscale models by evaluating the reciprocal influence between scales using human ascariasis as a representative of all type I environmentally-transmitted disease as paradigm. We use various mathematical analysis techniques to analyze all the models in this study. which include: (i) Routh-Hurwitz criteria, (ii) Next generation operator, (iii) Center Manifold Theory, and (iv) Lyapunov function. We also conducted sensitivity and numerical analyses for all the models. Sensitivity analysis is conducted using Latin Hypercube Sampling (LHS) and Partial Rank Correlation Coefficients (PRCCs). Also, numerical simulations in all the models are done in order to illustrate analytical results obtained from these multiscale models using Python odeint function in the scipy.integrate which solves any system of differential equations. The methodology for development of multiscale models in this thesis is a variation of the one described in [1].

1.5.1 Process of Multiscale Modelling of Infectious Disease Systems

Traditionally, the developmental process of multiscale models for infectious disease systems, at any hierarchical level of biological organization of an infectious disease system (cell-level, tissue-level, organ-level, host-level, community level, etc.) commonly involves an iterative process between four main stages which are [1]: (a) Formulation stage of multiscale models of infectious disease systems, (b) Testing stage of multiscale models of infectious disease systems, (c) Application stage of multiscale models of infectious disease systems, and (d) communication stage of multiscale models of infectious disease systems. Fig. 1.2 shows schematic diagram of the four main stages of the developmental process for multiscale models of infectious disease systems, which we can briefly describe as follows:

(a) ***Formulation stage of multiscale models of infectious disease systems***: This stage involves development of an appropriate multiscale model to address a particular given problem of an infectious disease system. Within this stage there are three main steps that are involved in order to complete the cycle of the multiscale models development which are:

(i) identification of the infectious disease problem to be addressed,

(ii) identification of the levels/scales of an infectious disease system involved in the infectious disease problem,

(iii) formulation of multiscale models of infectious disease systems to describe the infectious disease problem at appropriate levels/scales being identified,

Therefore, in this stage, a researcher/modeler firstly becomes familiar with the infectious disease problem he/she is intending to address. After identification of the infectious disease problem, a modeler should further define research question(s), aim and objectives of the study as well as stating the hypothesis of the study. Once the infectious disease problem has been identified and well stated, the modeler should clearly identify levels of a biological organization to be incorporated into the multiscale model and their associated scale of infection and further ascertains if there exists any knowledge with regard to the infectious disease problem to be addressed across all the identified scales (i.e., reviewing what has been achieved or done about the problem across all the scales and what is lacking or missing). This can be achieved through either empirical observation or literature review or both. Empirical observation can be made through experiments and data collections. In addition, proper literature review is necessary in attaining the right knowledge required to detail the system under study as well as to understand data and experimental results. After that, the modeler formalizes a biological model that involves detailing the flow of information from one scale to another as well as detailing mechanisms and different relationships of any entities involved in the infectious disease system under observation. This is then followed by the formulation of sub-models for multiscale model that are related to scales of an infection in the biological organization under study. In the formulation of these sub-models of multiscale model for infectious disease problem, a modeler should decide which most features of the system under observation must be included in the models and which must not be included. Following that, the modeler chooses symbols to represent variables included in the multiscale model for infectious disease problem [1].

(b) ***Testing stage of multiscale models of infectious disease systems***: This stage involves testing the quality of the multiscale model of infectious disease through verification, validation and/or sensitivity analysis of the multiscale model results. It is important to verify and validate the results of the multiscale model before trying to do anything else with the model. The testing of the quality of the multiscale model can be analyzed using any available and reliable mathematical techniques. It is at this stage where the modeler decides which technique he/she needs to utilize in analyzing the multiscale model results. It is also at this stage where the modeler determines whether the model is mathematically well-posed through examining the existence and uniqueness of the multiscale model equilibrium

steady states, and further determine their local and global stabilities through analytical and numerical analysis.

(c) ***Application stage of multiscale models of infectious disease systems***: This involves the use of multiscale models of infectious disease systems to (i) evaluate the influence of functionally organized complex systems on infectious disease dynamics, (ii) to analyze the underlying mechanisms of infectious disease dynamics, (iii) predict dynamics of infectious disease, and (iv) inform policy and guide research for the control and elimination of environmentally-transmitted diseases (see for instance the work in [17]).

(d) ***Communication stage of the results of multiscale models for infectious disease systems***: This involves interpreting the results of the models and comparing them with the real-world systems in order to determine whether the outcome behavior of the model matches with what is observed in the system. However, if the outcome behavior of the model matches with the behavior that is observed from the real-world system the results of the model can then be communicated through publication, reports, or writings. Yet, if the outcomes of the models differ with observation made from the system, the formulated model needs to be refined or modified together with assumptions.

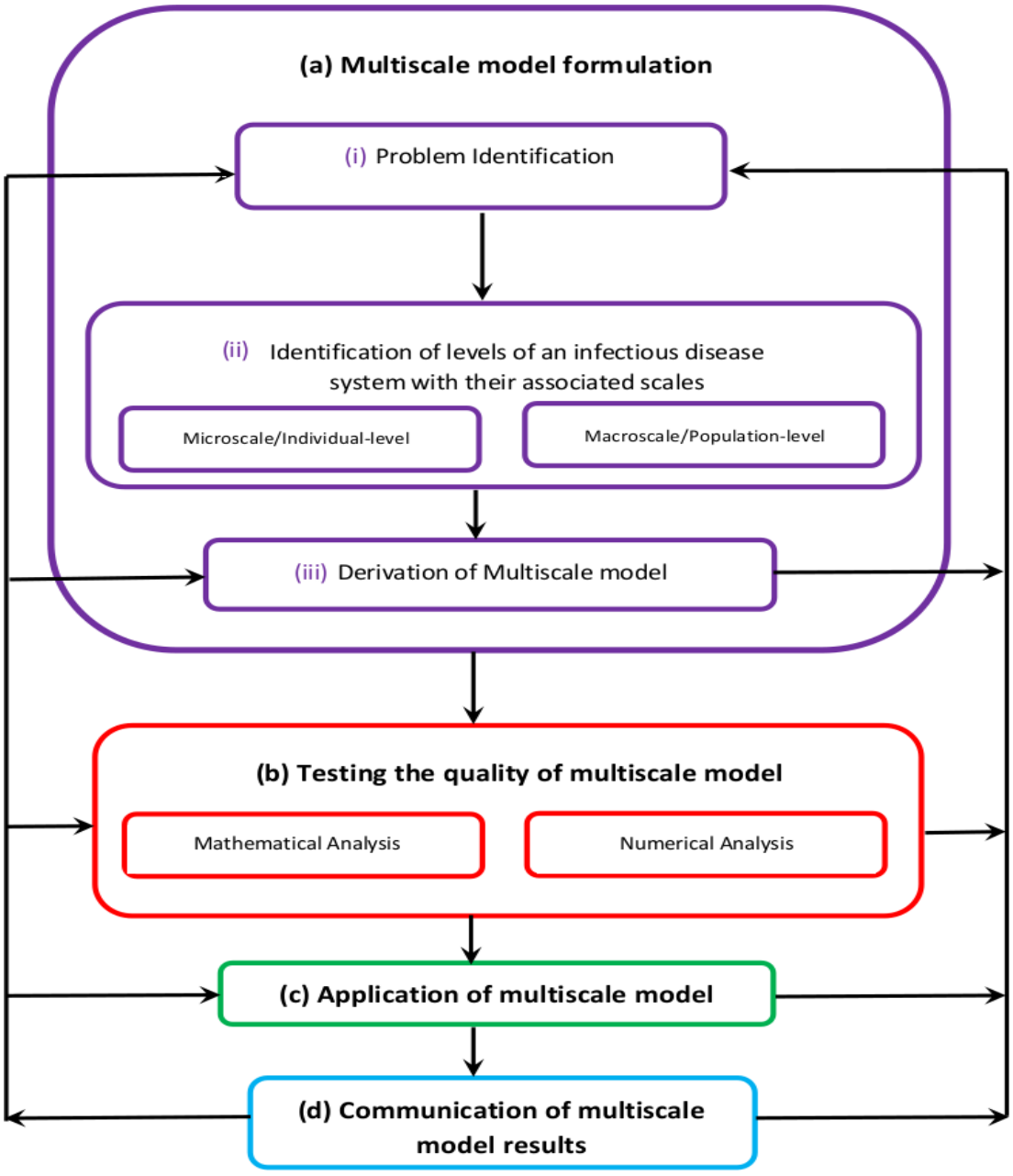

Figure 1.2: *Schematic diagram illustrating the iterative modelling process of multiscale modellings. Adopted from [1]*

In what follows, we give an overview of multiscale models that have been developed in attempting to study multiscale dynamics of environmentally-transmitted diseases at various hierarchical levels of biological organization of an infectious disease system.

1.5.2 Multiscale Modeling and Environmentally-Transmitted Disease Systems

This subsection provides an overview of some of the existing multiscale models that have been developed to describe the multiscale dynamics of environmentally-transmitted diseases in any given population. In the context of environmentally-transmitted diseases, various multiscale models within the five categories of infectious disease systems established in [19, 20] have been developed and analyzed at various scales of biological organization of an infectious disease system. The most studied categories of multiscale models for environmentally-transmitted diseases are the hybrid and the individual based multiscale models as opposed to the other three categories which are nested, embedded and coupled multiscale models. However, since the scope of this study is centered in investigating which between a nested multiscale model an embedded multiscale modelling is appropriate category of multiscale models to characterize the multiscale dynamics of an environmentally-transmitted disease system with different scenarios, we therefore restrict ourselves to those studies that focused on the application of either embedded or nested multiscale models in attempting to broaden our understanding about the complex transmission dynamics of environmentally-transmitted disease systems. In the case of nested multiscale models for environmentally-transmitted disease systems, there has been little progress in their development. To the best of our knowledge, we are only aware of one publication [15], which addresses the development of nested multiscale models for environmentally-transmitted disease systems in the context of ruminant paratuberculosis at the between-pen scale and within within-pen scale dynamics. The authors use nested multiscale model to explore the best combination of control and preventive measures that can minimize the prevalence and incidence of parauberculosis in ruminants as well as the risk of the disease-causing bacteria occurrence in each pen environment and possible in the entire dairy. The study suggests that a combination of test and cull with more frequent manure removal is the most effective method in reducing incidence, prevalence and the risk of the bacteria occurrence as opposed to control measures such as limiting calf-adult cow contacts, raising calves in a disease-free herd or colostrum management. In the context of embedded multiscale models for environmentally-transmitted disease systems on the other hand, there has been also few multiscale models of this types that have been developed and of these few the majority of them have been restricted to studying the transmission dynamics of environmentally transmitted infectious diseases at the host level [9–14]. In particular, the paper by Feng et al. [11], presents a BIDI-EMSM for the transmission dynamics of Toxoplasma gondii (a typical example of type II environmentally transmitted infectious disease system) that integrate within-host sub-model and the between-host sub-model dynamics through the free-living parasite in the environment. Furthermore, the authors simplified BIDI-EMSM into

a SIMP-EMSM based on a singular perturbation argument, which allows for decoupling of the full model by separating the fast- and slow-systems two independent single scale models (i.e., the within-host scale and the between-host scale). In [11], the authors carefully analyzed the within-host scale sub-model and between-host scale sub-model separately and defined new reproductive numbers associated with these two sub-models. In addition, the study established that the reproduction number for the between-host (slow) system dependent on the parameters associated with the within-host (fast) system in a very natural way. In [12, 13], analysis of the multiscale model established in [11] was further carried out using different modifications. The major findings from these studies is that infection may persist at population level even if the isolated between-host reproduction number is less than a unity. Another good examples of BIDI-EMSM are given in [9, 10]. In [9], the authors introduced a superinfection/pathogen-replication approach (i.e., down-scaling and up-scaling method) for development of multiscale models of environmentally-transmitted disease systems at host level (i.e. linking within-host scale and between-host scale) using human schistosomiasis (a type I environmentally-transmitted disease system) as an example. The paper demonstrated in a practical way the idea of scaling up and down in linking scales of an infectious disease system by identifying within-host scale and between-host scale variables and parameters and design a reciprocal influence of these variables and parameters through downscaling and upscaling across the within-host scale and the between-host scale. In [10], the authors followed the method introduced in [9] to Guinea worm disease as a paradigm, which is also a type I environmentally-transmitted disease system. The major findings in these studies is that expressions such as disease reproductive numbers and endemic equilibrium states as well as numerical simulations of the full models all are adequately account for the reciprocal influence of the linked within-host and between-host sub-models. Further example of the development of BIDI-EMSM at the host level is given in [14] in the context of cholera transmission (a type III environmentally-transmitted disease systems). The BIDI-EMSM of this study concurrently study the within-host scale and between-host scale dynamics of cholera, taking into account both direct and environment transmission. Additionally, its development was achieved through presuming a general representation for both the direct transmission and the pathogen shedding, and the interaction between environmental vibrios at between-host scale and human vibrios at within-host scale. Further, the authors simplified BIDI-EMSM into a SIMP-EMSM based using fast- and slow-time scale analysis. Using SIMP-EMSM, the major finding of the study is that the between-host scale sub-model was shown to undergo a backward bifurcation as a result of coupling the within-host scale and between-host scale cholera dynamics.

1.6 Outline of the thesis

The structure of this thesis is as follows.

In **Chapter 2**, we develop a single-scale model for environmentally-transmitted disease systems at the host-level that we progressively extend to develop the different categories of multiscale models.

In **Chapter 3**, we investigate if nested multiscale models are an appropriate category of multiscale models to characterize the multiscale dynamics of infectious diseases with a replication cycle at microscale using paratuberculosis as an example.

In **Chapter 4**, we investigate if embedded multiscale models are an appropriate category of multiscale models to characterize the multiscale dynamics of infectious diseases with a replication cycle at microscale using paratuberculosis as an example.

In **Chapter 5**, we compare between nested and embedded multiscale models and identify the most appropriate category of multiscale models to characterize the multiscale dynamics of infectious diseases with a replication cycle at microscale using paratuberculosis as an example.

In **Chapter 6**, we compare between nested and embedded multiscale models and identify the most appropriate category of multiscale models to characterize the multiscale dynamics of infectious diseases without a replication cycle at microscale using human ascariasis as an example.

Finally, **Chapter 7** provides conclusions and some recommendations for future research directions.

Chapter 2

Single-Scale Model for Environmentally Transmitted Disease Dynamics at the Host-level

2.1 Introduction

In the study of infectious disease systems at any level of their organization, single-scale models have a long history of being used to understanding and interpreting as well as predicting dynamics of many infectious diseases (see [7, 49–51] for and references therein). They have and continue to play a crucial role in guiding control and eliminating burdens imposed by various infectious diseases either at the local or global level. In the context of infectious disease systems, we know that at any level of organization single-scale models describe or characterize dynamics of an infection disease problem only at a single scale. Unlike, multiscale models that describe or characterize an infectious disease problem at more than one scale [1]. In this chapter, we present a single-scale modeling framework for environmentally-transmitted disease systems at the host-level that will be progressively extended to develop different categories of multiscale models. The development of this single-scale model is carried out to examine or test the quality of single-scale models in predicting the dynamics of environmentally-transmitted diseases using Paratuberculosis infection in ruminants as a case study. Paratuberculosis (PTB) infection,

also known as Johnes' disease, is an environmentally-transmitted and important disease in ruminants (e.g., ruminants, goat and sheep) (see [52–54] and references therein) that has been locally and globally reported throughout the world, more especially in countries with temperate climates. The single-scale model will be extended in the chapters that follow to develop the different categories of multiscale models that are compared based on the replication-transmission relativity theory [8], which states that at every level of organization of an infectious disease system, there is no privileged/absolute scale which would determine disease dynamics. However, at every level of organization of an infectious disease system, single scale modelling privileges the macroscale. In the same way, the single-scale model for paratuberculosis developed in this chapter which is developed at the host level privileges the macroscale (i.e. between-host scale) in disease dyanmics. PTB is caused by bacteria called *Mycobacterium avium subspecies paratuberculosis* (MAP) which often infects intestines of many ruminants [53]. This organism is most commonly widespread in dairy ruminants and can lead to a serious economic burdens in livestock industries due to the reduction of milk production and the productive life of ruminants as well [48]. The main clinical outcomes of PTB infection in ruminants are failure growth, increases in weight loss, and chronic diarrhea. Although PTB has not been classified as a zoonotic disease, clinical studies show that most patients with Crohn's disease are found with MAP [55]. Crohn's disease is an inflammatory bowel disease characterized by a persisting, painful, and diarrheal inflammatory disease of the intestinal tract in human [53]. Ruminants in the PTB endemic herd acquire PTB through ingestion of the infective bacteria in colostrum, and from the faeces of infected ruminants contaminating food and surface water/water troughs. The disease can also be transmitted vertically from an infected pregnant ruminant to its foetus. Following the ingestion of MAP bacteria contained in faecal material, and reach the gut of an infected ruminants, MAP are engulfed by macrophages in the submucosal of the ruminant, and the submucosal macrophages become infected [53]. However, the dynamics of MAP among submucosal macrophages within an infected ruminant can be controlled by the ruminant immune response cells (such as T-helper cells). Yet, currently there is no meaningful treatment that has been made available for PTB in ruminant, and control programs implemented in many countries have had limited success [56]. Besides, very few ruminants can resist the infection; and it takes a long time to notice that ruminant has PTB disease because of a long incubation period, and clinical disease is not usually apparent until three to five years-old. Furthermore, clinical studies have reported that infected animals may shed bacteria in the environment through faeces for over a year before clinical signs appear.

2.2 Mathematical Model for Ruminant Paratuberculosis Dynamics at the Host-level

In this section, we present the single-scale model for PTB disease transmission dynamics developed at the host population-level, with the aim of pin-pointing weakness of single-scale models in modelling infectious disease systems. For any infectious disease system, the standard approach for developing single-scale models that describe the dynamics of the infectious disease at the between-host scale is to classify the host population into compartments such as susceptible, infected and recovered (SIR) and variation of this paradigm within which individuals are assumed to behave homogeneously (see [4]). For instance, a paper by Magombedze et al. [52] which investigates the PTB disease dynamics in ruminants is based on the susceptible-exposed-infected framework (SEI) coupled with the environmental dynamics that depict the evolution of MAP bacteria (B) in the environment. The single scale model in [52] divides the class of infected ruminants into three stages: exposed or silent stage, sub-clinical stage and clinical stage. In this case, we only incorporate a single infected class into the between-host scale sub-model. The different classes that the infected ruminant progresses through are accounted for by the within-host scale sub-model. In developing the single scale model at between-host scale for PTB dynamics, we make the following assumptions:

a. The transmission of the infection is only through contact with MAP bacterial load (B_C) in the physical environment. However, if there is any direct transmission, it can be estimated by indirect transmission in terms of environmental MAP bacterial load (B_C).

b. The average extracellular MAP bacteria in each infected ruminant is modelled phenomenologically by $\widehat{N}_c$, which is a proxy for individual ruminant infectiousness.

c. The environmental MAP bacterial (B_C) do not replicate in the environment (outside-host).

From these assumptions, the single scale model for PTB dynamics at between-host scale becomes:

$$\begin{cases} (i)\ \dfrac{dS_C(t)}{dt} &= \Lambda_C - \dfrac{\beta_C B_C(t)}{B_0 + B_C(t)} S_C(t) - \mu_C S_C(t), \\ (ii)\ \dfrac{dI_C(t)}{dt} &= \dfrac{\beta_C B_C(t)}{B_0 + B_C(t)} S_C(t) - (\mu_C + \delta_C) I_C(t), \\ (iii)\ \dfrac{dB_C(t)}{dt} &= \widehat{N}_c \alpha_c I_C(t) - \alpha_C B_C(t), \end{cases} \tag{2.2.1}$$

The single-scale model given by equation (2.2.1), which is later used as a between-host submodel of the nested multiscale model in Chapter (4), is based on monitoring the dynamics of three populations which are susceptible ruminants (S_C), infected ruminants I_C, and MAP bacterial load (B_C) in the physical environment. The first equation of the model system (2.2.1) describes the dynamics of susceptible ruminants. At any time t, new recruits of susceptible ruminants enter the ruminant population through birth and incoming ruminants from other farms at a constant rate Λ_C and this population losses individuals due to natural death at a constant rate μ_C. The susceptible ruminant population also decreases through infection at a rate $\beta_C B_C(t)/(B_0 + B_C(t))$ with β_C being the exposure rate to infective MAP bacterial load (B_C) in the environment and B_0 is the saturation parameter of the bacteria that yield 50 percent chance of a ruminant getting infected with PTB infection after ingesting the bacteria. The infection happens when susceptible ruminants feed from contaminated pasture with faecal material containing infective MAP, or drink from contaminated surface water/water troughs with the bacteria. The second equation in the model system (2.2.1) describes the dynamics of PTB infected ruminants. This population increases through infection of susceptible ruminants and decreases through natural death at a constant rate μ_C. There is additional death at a rate δ_C in the population of infected ruminants due to disease, so that an average lifespan of PTB infected ruminant in the population is $1/(\delta_C + \mu_C)$. We assume that infected ruminants spread the disease through contaminating the environment at a rate $\widehat{N}_c\alpha_c I_C$, where $\widehat{N}_c$ models phenomenologically the average number of the within-host scale MAP bacterial load available for excretion into the environment by each infected ruminants at a rate α_c. Therefore, the population dynamics of MAP bacilli in the environment, described by the last equation of the model system (2.2.1), increases following excretion of MAP bacteria by infected ruminant hosts in faecal material into the environment at a net rate $\widehat{N}_c\alpha_c I_C$. This population of MAP bacilli in the environment is assumed to decrease due to natural death at a rate α_C. The model state variables and parameters are summarized in Table (2.1) and Table (2.2), respectively.

State variables	Description values
$S_C(t)$	The susceptible ruminant population size in the behavioral ruminants environment.
$I_C(t)$	The infected ruminant population size in the behavioral ruminants environment.
$B_C(t)$	The population size of PTB disease-causing bacteria in the physical environment.

Table 2.1: Description of the state variables of the model system (3.1)

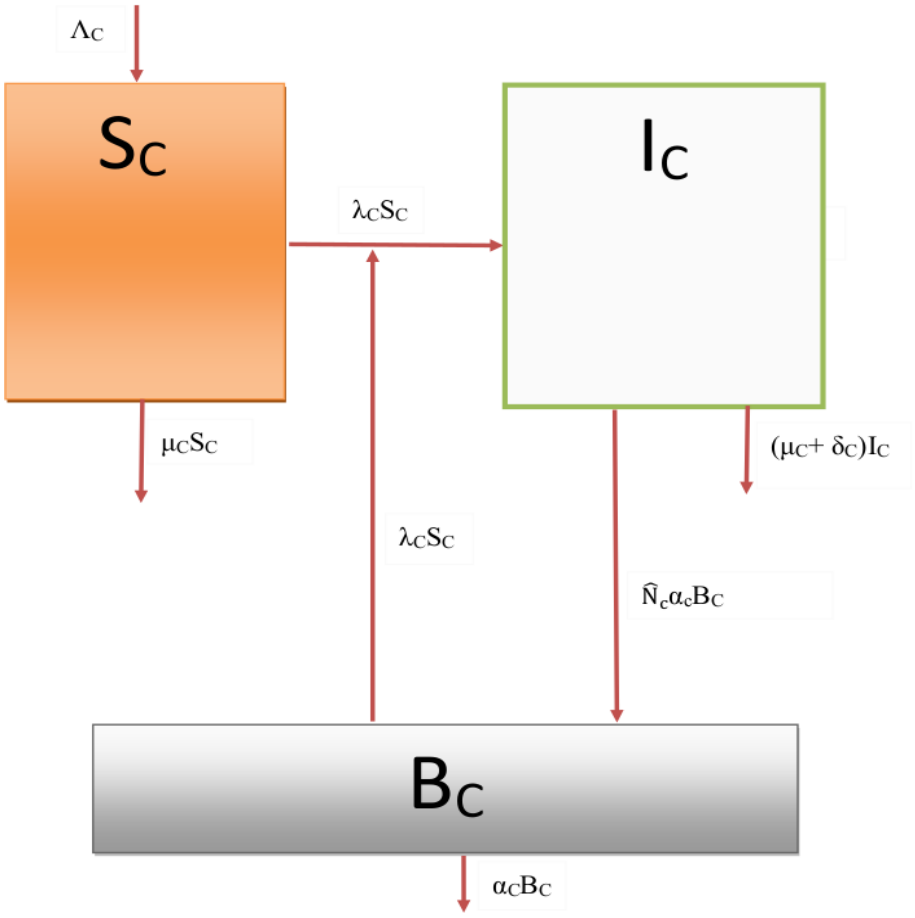

Figure 2.1: *A schematic representation of the transmission-cycle of the Johne's disease in a Herd*

2.3 Mathematical Model Analysis

2.3.1 Basic Properties

In this section, we study mathematical properties of the model system (2.2.1). We start by showing that all the solutions of the model system (2.2.1) will remain positive for all $t \geq 0$. This is followed by showing that the model system (2.2.1) is mathematically and epidemiologically well-posed.

2.3.1.1 Positivity of Solutions

We now consider the positivity of the model system (2.2.1) by showing that if the system starts with non-negative initial conditions ($S_C(0)$, $I_C(0)$, $B_C(0)$), the solutions/trajectories ($S_C(t)$, $I_C(t)$, $B_C(t)$) of the model system (2.2.1) will remain positive for all $t \geq 0$, so that they should be in consistence with the basic aspect of the biological reality. This is summarized in following theorem.

Theorem 2.1. *Given that the initial conditions of the model system (2.2.1) remain non-negative (i.e., $S_C(0) \geq 0, I_C(0) \geq 0, B_C(0) \geq 0$), the resulting solutions ($S_C(t), I_C(t), B_C(t)$) are all positive for all $t \geq 0$.*

Proof: From the first equation of the model system (2.2.1), a differential inequality which describes the dynamics of susceptible ruminant population in time is given by

$$\frac{dS_C(t)}{dt} \geq -(\lambda_C(t) + \mu_C)S_C(t). \tag{2.3.1.1.1}$$

Therefore, the expression of the differential inequality in equation (2.3.1.1.1) can be solved by the separation of variables as follows

$$\frac{dS_C(t)}{S_C(t)} \geq -(\lambda_C(t) + \mu_C)dt. \tag{2.3.1.1.2}$$

Now, letting

$$\hat{t} = sup\{t > 0 : S_C > 0, I_C > 0, B_C > 0\} \in [0, t],$$

and integrating equation (2.3.1.1.2), we thus have

$$\ln(S_C(t)) \geq -\left(\mu_C t + \int_0^t \lambda_C(\hat{t})d\hat{t}\right) + \ln(S_C(0)). \tag{2.3.1.1.3}$$

Thus, the solution of the differential inequality for the susceptible ruminants population is given by

$$S_C(t) \geq S_C(0).\exp\left\{-\left(\mu_C t + \int_0^t \lambda_C(\hat{t})d\hat{t}\right)\right\} > 0. \quad (2.3.1.1.4)$$

This implies that

$$\lim_{t\to\infty} \inf(S_C(t)) \geq 0. \quad (2.3.1.1.5)$$

Using the same principle, it can be shown that

$$\lim_{t\to\infty} \inf(I_C(t)) \geq 0. \quad (2.3.1.1.6)$$

Now, using the second equation of the model system (2.2.1) that describes the evolution of the population of the MAP bacteria in the physical environment, we can have the following differential inequality given as

$$\frac{dB_C(t)}{dt} \geq -\alpha_C B_C(t). \quad (2.3.1.1.7)$$

Therefore, by the separation of variables we obtain

$$B_C(t) \geq B_C(0).\exp\{-\alpha_C t\} > 0. \quad (2.3.1.1.8)$$

This implies that

$$\lim_{t\to\infty} \inf(B_C(t)) \geq 0. \quad (2.3.1.1.9)$$

Thus, when starting with non-negative initial value conditions in the model system (2.2.1), the solutions of the model will remain non-negative for all $t \geq 0$, and this completes the proof.

2.3.1.2 Feasible Region

Letting $N_C(t)$ denotes the total number of ruminant population and adding the first and second equation of the model system (2.2.1), we obtain

$$\frac{dN_C(t)}{dt} = \Lambda_C - \mu_C N_C(t) - \delta_C I_C(t), \quad (2.3.1.2.1)$$

so that

$$\frac{dN_C(t)}{dt} \leq \Lambda_C - \mu_C N_C(t). \tag{2.3.1.2.2}$$

This implies that

$$\lim_{t\to\infty} sup(N_C(t)) \leq \frac{\Lambda_C}{\mu_C}. \tag{2.3.1.2.3}$$

Since $N_C(t)$ is the sum of the state variables for susceptible humans and infected humans, then each of the individual state variables is less or equal to $\frac{\Lambda_C}{\mu_C}$. Now, using the third equation of model system (2.2.1) we obtain the following inequality

$$\frac{dB_C(t)}{dt} \leq \widehat{N}_c\alpha_c\frac{\Lambda_C}{\mu_C} - \alpha_C B_C, \tag{2.3.1.2.4}$$

since $I_C(t) \leq \frac{\Lambda_C}{\mu_C}$. Therefore, the solution of equation (2.3.1.2.4) can be obtained by using a suitable integrating factor ($e^{\alpha_C t}$), to obtain

$$B_C(t) \leq \frac{\widehat{N}_c\alpha_c\Lambda_C}{\alpha_C\mu_C} + C_2 e^{-\alpha_C t}. \tag{2.3.1.2.5}$$

This implies that

$$\lim_{t\to\infty} sup(B_C(t)) \leq \frac{\widehat{N}_c\alpha_c\Lambda_C}{\alpha_C\mu_C}. \tag{2.3.1.2.6}$$

We let

$$\begin{cases} \Omega = \{(S_C(t), I_H(t), P_E(t))|\ 0 \leq S_C(t) + I_C(t) \leq Z_1, \\ \qquad 0 \leq B_C(t) \leq Z_2\}, \end{cases} \tag{2.3.1.2.7}$$

be an invariant region of the model system (2.2.1), where

$$\begin{cases} Z_1 = \dfrac{\Lambda_C}{\mu_C}, \\ \\ Z_2 = \dfrac{\widehat{N}_c\alpha_c\Lambda_C}{\alpha_C\mu_C} > 0. \end{cases} \tag{2.3.1.2.8}$$

Thus, Ω is a positively invariant and attracting region, since all the solutions/trajectories that start in Ω will remain in Ω for all $t \geq 0$. As a result, we can easily conclude that the model

system (2.2.1) is mathematically and epidemiologically well-posed [4]. Therefore it is sufficient to consider the dynamics of the flow generated by model system in Ω.

2.3.2 Disease-free Equilibrium (DFE) and Reproductive Number

The disease-free equilibrium of the model system (2.2.1) was obtained by setting the left-hand side of the model to zero and further assume that $I_C = B_C = 0$ to get

$$E_0 = (X^*, 0) = \left(\frac{\Lambda_C}{\mu_C}, 0, 0\right), \tag{2.3.2.1}$$

where E_0 denotes the disease-free equilibrium of the baseline single-scale model system (2.2.1). In this study, the basic reproductive number of the baseline single-scale model system (2.2.1) was also computed by using the next generation operator approach in [5] to be

$$R_0 = \frac{\beta_C \Lambda_C \widehat{N}_c \alpha_c}{\mu_C(\mu_C + \delta_C) B_0 \alpha_C}, \tag{2.3.2.2}$$

which can be re-written as

$$R_0 = R_{0_{EC}} R_{0_{CE}}, \tag{2.3.2.3}$$

where the quantity $R_{0_{EC}}$ of the above is explained as follows. Consider a single newly infected ruminants entering a contaminated-free environment at an equilibrium point. The expected number of bacteria cells produced by each infected ruminants and contaminate the environment is approximately

$$R_{0_{CE}} = \frac{\widehat{N}_b \alpha_c}{\mu_C(\mu_C + \delta_C)}. \tag{2.3.2.4}$$

Similarly, the quantity $R_{0_{EC}}$ can be interpreted as follows. Consider newly bacterial infectious dose of bacilli cells entering a disease-free population of ruminants at an equilibrium point. The expected number of ruminants infected by this bacteria cells is approximately

$$R_{0_{EC}} = \frac{\beta_C \Lambda_C}{\alpha_C B_0}. \tag{2.3.2.5}$$

Based on the two expressions $R_{0_{EC}}$ and $R_{0_{CE}}$, we can conclude that the epidemiological (between-host) transmission parameters and the immunological (within-host) parameters all contribute to the transmission of ruminant paratuberculosis disease.

2.3.2.1 Local stability of the disease-free equilibrium

In this subsection, we determine the local stability of DFE for the model system (2.2.1) by linearizing the three equations of the model system (2.2.1) to obtain the following Jacobian matrix given as,

$$J(E_0) = \begin{pmatrix} -\mu_C & 0 & -\dfrac{\beta_C \Lambda_C}{B_0 \mu_C} \\ 0 & -(\mu_C + \delta_C) & \dfrac{\beta_C \Lambda_C}{B_0 \mu_C} \\ 0 & \widehat{N}_c \alpha_c & -\alpha_C \end{pmatrix}. \tag{2.3.2.1.1}$$

We test for stability of DFE by calculating the eigenvalues (λ_s) of the above Jacobian matrix at the DFE. The characteristic equation for the eigenvalues is given by

$$(-\mu_H - \lambda)[\lambda^2 + \phi_1 \lambda + \phi_2] = 0, \tag{2.3.2.1.2}$$

where

$$\begin{cases} \phi_1 = \mu_C + \delta_C + \alpha_C, \\ \phi_2 = (\mu_C + \delta_C)\alpha_C(1 - R_0). \end{cases} \tag{2.3.2.1.3}$$

It is clear from equation (2.3.2.1.2) that one of the eigenvalues is equal to $\lambda = -\mu_C$. Now, to determine the remaining eigenvalues of the polynomial

$$P(\lambda) = \lambda^2 + \phi_1 \lambda + \phi_2 = 0, \tag{2.3.2.1.4}$$

we use the Routh-Hurwitz Criteria. In this case, we define the following matrices whose elements are the coefficients (ϕ_S) of the characteristic polynomial $P(\lambda)$ in equation (2.3.2.1.4):

$$H_1 = \begin{pmatrix} \phi_1 \end{pmatrix}, \quad H_2 = \begin{pmatrix} \phi_1 & 1 \\ 0 & \phi_2 \end{pmatrix}. \tag{2.3.2.1.5}$$

Evaluating the determinant of H_1, we obtain

$$\begin{cases} det(H_1) &= \left| \phi_1 \right|, \\ &= \phi_1, \\ &= \mu_C + \delta_C + \alpha_C > 0. \end{cases} \tag{2.3.2.1.6}$$

The determinant of H_2 is given by:

$$\begin{cases} det(H_2) &= \begin{vmatrix} \phi_1 & 1 \\ 0 & \phi_2 \end{vmatrix}, \\ &= \phi_1\phi_2, \\ &= \xi_C(1 - R_0) > 0, \quad \text{whenever} \quad R_0 < 1. \end{cases} \tag{2.3.2.1.7}$$

Where

$$\xi_C = (\mu_C + \delta_C + \alpha_C)(\mu_C + \delta_C)\alpha_C. \tag{2.3.2.1.8}$$

It can be noted that all the coefficients ϕ_1 and ϕ_2 of the polynomial $P(\lambda)$ in equation (2.3.2.1.4) are greater than zero whenever $R_0 < 1$. And also all the determinants of matrices H_1 and H_2 are positive if and only if $R_0 < 1$. Hence, all the roots of the polynomial $P(\lambda)$ are either negative or have negative real parts. These results are summarized by the following theorem.

Theorem 2.2. *The Disease-free equilibrium point of the model system (2.2.1) is locally asymptotically stable if* $R_0 < 1$.

2.3.2.2 Global stability of the disease-free equilibrium

We determine the global stability of DFE of the model system (2.2.1) by using the next generation operator [5]. Thus the system (2.2.1) can be re-written in the form

$$\begin{cases} \dfrac{dX}{dt} &= F(X, Z), \\ \dfrac{dZ}{dt} &= G(X, Z), \end{cases} \tag{2.3.2.2.1}$$

where

- $X = S_C$ represent a compartment of uninfected ruminants, and
- $Z = (I_C, B_C)$ represent compartments of infected ruminants and Infective MAP bacilli bacteria in the physical environment.

We let

$$E_0 = (X^*, 0) = \left(\frac{\Lambda_C}{\mu_C}, 0, 0\right), \tag{2.3.2.2.2}$$

denote the disease-free equilibrium (DFE) of the model system (2.2.1). For X^* to be globally asymptotically stable, the following conditions (H1) and (H2) must be satisfied.

H1. $\frac{dX}{dt} = F(X, 0)$ is globally asymptotically stable (g.a.s),

H2. $G(X, Z) = AZ - \hat{G}(X, Z)$, $\hat{G}((X, Z) \geq 0$ for $(X, Z) \in \mathbb{R}^3_+$ where $A = D_Z G(X^*, 0)$ is an M-matrix and $\mathbb{R}^3_+$is the region where the model makes biological sense.

In this case

$$F(X, 0) = \left[\ \Lambda_C - \mu_C S_C\ \right], \tag{2.3.2.2.3}$$

and the matrix A is given by

$$A = \begin{bmatrix} -(\mu_C + \delta_C) & \frac{\beta_C \Lambda_C}{\mu_C B_0} \\ \\ \widehat{N}_c \alpha_c & -\alpha_C \end{bmatrix}, \tag{2.3.2.2.4}$$

and

$$\hat{G}(X, Z) = \begin{bmatrix} \left(\frac{\Lambda_C}{\mu_C B_0} - \frac{S_C}{B_0 + B_C}\right) \beta_C B_C \\ \\ 0 \end{bmatrix}. \tag{2.3.2.2.5}$$

Since $S^0_C = \Lambda_C/(\mu_C B_0) \geq S_C/(B_0 + B_C)$, it is clear that $\hat{G}(X, Z) \geq 0$ for all $(X, Z) \in \mathbb{R}^3_+$. It is also clear that A is a M-matrix, since the off diagonal elements of A are non-negative. We state a theorem which summarizes the above results.

Theorem 2.3. *The fixed point*

$$E_0 = (X^*, 0) = \left(\frac{\Lambda_C}{\mu_C}, 0, 0\right)$$

of the model system (2.2.1) is global asymptotically stable (GAS) if $R_0 \leq 1$ and the assumptions $(H1)$ and $(H2)$ are satisfied.

2.3.3 Endemic Equilibrium and its Global Stability

For the endemic equilibrium point, we let

$$E^* = (S_C^*, I_C^*, B_C^*), \tag{2.3.3.1}$$

denote the endemic equilibrium point of the system of equations (2.2.1). At the endemic equilibrium point, each of the population variables is constant such that the rate of change of each of the model variables is zero. Thus, we set the left-hand side of the equations of the model system (2.2.1) equal to zero to obtain

$$0 = \Lambda_C - \lambda_C^* S_C^* - \mu_C S_C^*, \tag{2.3.3.2}$$

$$0 = \lambda_C^* S_C^* - (\mu_C + \delta_C) I_C^*, \tag{2.3.3.3}$$

$$0 = \widehat{N}_c \alpha_c I_C^* - \alpha_C B_C^*, \tag{2.3.3.4}$$

where

$$\lambda_C^* = \frac{\beta_C B_C^*}{B_0 + B_C^*}. \tag{2.3.3.5}$$

From (2.3.3.2), the endemic value of susceptible ruminants is given by

$$S_C^* = \frac{\Lambda_C}{\lambda_C^* + \mu_C}. \tag{2.3.3.6}$$

From the expression in equation (2.3.3.6) we note that the susceptible ruminants population at endemic equilibrium is equal to the average time of stay in susceptible class and the rate at which new susceptible ruminants are recruited into the susceptible class through natural birth. The population of susceptible ruminants leave the susceptible class when infected with MAP bacilli in the environment at a rate λ_C, or through natural death at a rate μ_C. The endemic value of infected humans in equation (2.3.3.3) is given by

$$I_C^* = \frac{\lambda_C^* S_C^*}{\alpha_C + \delta_C}. \tag{2.3.3.7}$$

We note from equation (2.3.3.7)) that infected ruminants population at the endemic equilibrium point is equal to the average time of stay in the infected class and the rate at which susceptible ruminants become infected and the density of susceptible ruminants. The endemic value of MAP

bacilli population in the physical environment is given by

$$B_C^* = \frac{\widehat{N}_c \alpha_c I_C^*}{\alpha_C}. \tag{2.3.3.8}$$

We deduce from equation (2.3.3.8) that the average population of MAP bacilli in the environment at the equilibrium point is determined by the rate at which infected ruminants population excretes an average number of the within-ruminants-host MAP bacilli into the physical environment and the average time of stay in the class of MAP bacilli in the physical environment.

2.3.3.1 Existence and uniqueness of the endemic equilibrium state

In this section, we provide some results concerning the existence and uniqueness of an endemic equilibrium point (EEP), $E^* = (S_C^*, I_C^*, B_C^*)$, for model system (2.2.1). We determine the existence and uniqueness of the endemic equilibrium point, E^*, by expressing S_C^* and I_C^* in terms of B_C^* in the form:

$$\begin{cases} S_C^*(B_C^*) &= \dfrac{\Lambda_C(B_0 + B_C^*)}{(\beta_C + \mu_C)B_C^* + \mu_C B_0}, \\ I_C^*(B_C^*) &= \dfrac{\beta_C \Lambda_C B_C^*}{(\delta_C + \mu_C)(\beta_C + \mu_C)B_C^* + \mu_C B_0(\delta_C + \mu_C)}. \end{cases} \tag{2.3.3.1.1}$$

Substituting the expressions in equation (2.3.3.1.1) into the equation for B_C^* which is given by

$$\frac{dB_C(t)}{dt} = \widehat{N}_c \alpha_c I_C(t) - \alpha_C B_C(t),$$

at the endemic equilibrium, we obtain:

$$B_C^*[\alpha_C \mu_C B_0(\delta_C + \mu_C)(R_0 - 1) - \alpha_C(\delta_C + \mu_C)(\beta_C + \mu_C)B_C^*] = 0. \tag{2.3.3.1.2}$$

From equation (2.3.3.1.2), we can either get $B_C^* = 0$, which correspond to disease-free equilibrium point or

$$B_C^* = \frac{\mu_C B_0(\delta_C + \mu_C)}{(\delta_C + \mu_C)(\beta_C + \mu_C)}[R_0 - 1], \tag{2.3.3.1.3}$$

for the endemic equilibrium point. Since $A_C > 0$ and $B_C > 0$, we can easily deduce from equation (2.3.3.1.2) that only a single positive endemic equilibrium point exists for $R_0 > 1$. Therefore, we can conclude that there exists only one unique endemic equilibrium point for model system (2.2.1) whenever $R_0 > 1$.

2.3.3.2 Local stability of the endemic equilibrium

The local stability of the endemic steady state of the model system (2.2.1) is determined by the use of Center Manifold Theory described in [10]. Center Manifold Theory has been used to determine the local stability of a non-hyperbolic equilibrium point. For convenience of interpretation of the stability we state the theorem (see also [57]).

Theorem 2.4. *Consider the following general system of ordinary differential equations with parameter ϕ:*

$$\frac{dx}{dt} = f(x,\phi), \quad f:\mathbb{R}^n \longrightarrow \mathbb{R}, \quad f:\mathbb{C}^2(\mathbb{R}^2\times\mathbb{R}), \tag{2.3.3.2.1}$$

where 0 is an equilibrium point of the system (2.3.3.2.1), i.e., $f(0,\phi)=0, \quad \forall \quad \phi$, and assume that

(1) $A = D_x f(0,0) = \left(\dfrac{\partial f_i(0,0)}{\partial x_i}\right)$ *is a linearization of the system around the equilibrium 0 with ϕ evaluated at 0;*

(2) Zero is a simple eigenvalue of A and other eigenvalues of A have negative real part;

(3) Matrix A has a left eigenvector denoted by $\boldsymbol{u}$ *and a right eigenvector denoted by* $\boldsymbol{v}$*, corresponding to the zero eigenvalue.*

Let f_k be the kth component of f and

$$a = \sum_{k,i,j=1}^{n} v_k u_i u_j \frac{\partial^2 f_k}{\partial x_i \partial x_j}(0,0), \tag{2.3.3.2.2}$$

$$b = \sum_{k,i,j=1}^{n} v_k u_i \frac{\partial^2 f_k}{\partial x_i \partial \phi}(0,0). \tag{2.3.3.2.3}$$

The local dynamics of the system around the equilibrium point 0 is totally governed by the signs of a and b.

(i) $a>0$, $b>0$, when $\phi<0$ with $\mid\phi\mid \ll 1$, 0 is locally asymptotically stable, and there exists a positive unstable equilibrium; when $0<\phi\ll 1$, 0 is unstable and there exists a negative and locally asymptotically stable equilibrium.

(ii) $a<0$, $b<0$, when $\phi<0$ with $\mid\phi\mid \ll 1$, 0 is unstable; when $0<\phi\ll 1$, 0 is locally asymptotically stable, and there exists a positive unstable equilibrium point.

(iii) $a>0$, $b<0$, when $\phi<0$ with $\mid\phi\mid \ll 1$, 0 is unstable and there exists a locally asymptotically stable negative equilibrium; when $0<\phi\ll 1$, 0 is stable and a positive unstable equilibrium appear.

(iv) *$a < 0$, $b > 0$, when ϕ changes from negative to positive, 0 changes its stability from stable to unstable. Correspondingly, a negative unstable equilibrium becomes positive and locally asymptotically stable.*

In our case:

Let $S_C = x_1, I_C = x_2, B_C = x_3$ and $\beta_C = \beta^*$ where β^* is considered as the bifurcation parameter. If we consider $R_0 = 1$;and solve for β^*, we obtain

$$1 = \frac{\widehat{N}_c \alpha_c \beta^* \Lambda_C}{B_0 \mu_C (\mu_C + \delta_C) \alpha_C}, \tag{2.3.3.2.4}$$

so that

$$\beta^* = \frac{B_0 \mu_C (\mu_C + \delta_C) \alpha_C}{\widehat{N}_c \alpha_c \Lambda_C}. \tag{2.3.3.2.5}$$

We also use the vector notation $\bar{x} = (x_1, x_2, x_3)^T$ so that the model system (3.1.3) can be written in the form

$$\frac{d\bar{x}}{dt} = \bar{F}(\bar{x}, \beta^*), \tag{2.3.3.2.6}$$

where

$$\bar{F} = (f_1, f_2, f_3). \tag{2.3.3.2.7}$$

So that

$$\begin{cases} \dot{x_1} = f_1 = \Lambda_C - \dfrac{\beta^* x_1 x_3}{B_0 + x_3} - \mu_C x_1, \\ \dot{x_2} = f_2 = \dfrac{\beta^* x_1 x_3}{B_0 + x_3} - (\mu_C + \delta_C) x_2, \\ \dot{x_3} = f_3 = \widehat{N}_c \alpha_c x_2 - \alpha_C x_3. \end{cases} \tag{2.3.3.2.8}$$

The Jacobian matrix of the model system (2.3.3.2.8) is given by

$$A = \begin{bmatrix} -\mu_C & 0 & -\dfrac{\beta^*\Lambda_C}{\mu_C B_0} \\ 0 & -(\mu_C + \delta_C) & \dfrac{\beta^*\Lambda_c}{\mu_C B_0} \\ 0 & \widehat{N}_c\alpha_c & -\alpha_C \end{bmatrix}. \tag{2.3.3.2.9}$$

The Jacobian matrix of the model system (2.3.3.2.9) has the left eigenvector **u** = $(u_1, u_2, u_3)^T$, where

$$\begin{cases} u_1 = -\dfrac{\beta^*\Lambda_C}{\mu_C^3 B_0^2(\mu_c + \delta_C)}, \\ u_2 = \dfrac{\beta^*\Lambda_C}{B_0(\mu_C + \delta_C)\mu_C}, \\ u_3 = 1 \end{cases} \tag{2.3.3.2.10}$$

and the right eigenvector given by **v** = (v_1, v_2, v_3), where

$$\begin{cases} v_1 = 0, \\ v_2 = \dfrac{\widehat{N}_c\alpha_c}{(\mu_C + \delta_C)}, \\ v_3 = 1. \end{cases} \tag{2.3.3.2.11}$$

The non-zero second order mixed derivatives of **F** with respect to each variables, used to determine the sign of a, are given by

$$\begin{cases} \dfrac{\partial^2 f_1}{\partial x_3^2} = \dfrac{2\beta^*\Lambda_C}{B_0^2\mu_C}, \\ \dfrac{\partial^2 f_2}{\partial x_3^2} = -\dfrac{2\beta^*\Lambda_C}{B_0^2\mu_C}. \end{cases} \tag{2.3.3.2.12}$$

The non-zero partial derivatives with respect to variables and β^*, used to determine the sign of b, are given by

$$\begin{cases} \dfrac{\partial^2 f_1}{\partial x_3 \partial \beta^*} = -\dfrac{\Lambda_C}{\mu_C B_0}, \\ \dfrac{\partial^2 f_2}{\partial x_3 \partial \beta^*} = \dfrac{\Lambda_C}{\mu_C B_0}. \end{cases} \tag{2.3.3.2.13}$$

Substituting expressions (2.3.3.2.10), (2.3.3.2.11), (2.3.3.2.12) and (2.3.3.2.13) into equation (2.3.3.2.2) and (2.3.3.2.3), respectively, we get

$$\begin{cases} a = u_1(v_3)^2 \left(\dfrac{\partial^2 f_1}{\partial x_3^2}\right) + u_2(v_3)^2 \left(\dfrac{\partial^2 f_2}{\partial x_3^2}\right), \\ = \left[\dfrac{2\beta^* \Lambda_C}{B_0^2 \mu_C}\right].u_1.v_3^2 + \left[-\dfrac{2\beta^* \Lambda_C}{B_0^2 \mu_C}\right].u_2.v_3^2, \\ = \left[\dfrac{2\beta^* \Lambda_C}{B_0^2 \mu_C}\right].v_3^2.[u_1 - u_2] < 0, \end{cases} \tag{2.3.3.2.14}$$

since $u_1 - u_2 < 0$, and

$$\begin{cases} b = u_1 v_3 \left(\dfrac{\partial^2 f_1}{\partial x_3 \partial \beta^*}\right) + u_2 v_3 \left(\dfrac{\partial^2 f_2}{\partial x_3 \partial \beta^*}\right), \\ = \left[-\dfrac{\Lambda_C}{B_0 \mu_C}\right].u_1.v_3 + \left[\dfrac{2\Lambda_C}{B_0 \mu_C}\right].u_2.v_3, \\ = \left[\dfrac{2\beta^* \Lambda_C}{B_0^2 \mu_C}\right].v_3.[u_2 - u_1] > 0 \end{cases} \tag{2.3.3.2.15}$$

since $u_2 - u_1 > 0$. Thus, $a < 0$ and $b > 0$. Using **Theorem 2.4**, item (iv), we can conclude that the endemic steady state of the model system (2.2.1) is locally asymptotically stable which holds for $R_0 > 1$ but close to 1. These results are therefore summarized by the following theorem.

Theorem 2.5. *The paratuberculosis endemic steady state of model system (2.2.1) guaranteed by Theorem 3.4 is locally asymptotically stable for $R_0 > 1$ near 1.*

2.3.3.3 Global stability of the endemic equilibrium

To prove that the endemic equilibrium E^* of the model system (2.2.1) is globally asymptotically stable, we state the following theorem:

Theorem 2.6. *The Endemic Equilibrium E^* of the model system (2.2.1) is global asymptotically stable (GAS) whenever $R_0 > 1$.*

Proof: Let's consider a Volterra-type Lyapunov function given by

$$\begin{aligned} L_1 &= L(S_C, I_C, B_C), \\ &= \nu_1 S_C^* g\left(\frac{S_C}{S_C^*}\right) + \nu_2 I_C^* g\left(\frac{I_C}{I_C^*}\right) + \nu_3 B_C^* g\left(\frac{B_C}{B_C^*}\right), \end{aligned} \tag{2.3.3.3.1}$$

where ν_2, ν_2 and ν_3 are positive constants to be determined, and we take advantage of the properties of the function

$$g(x) = x - 1 - \ln(x) \tag{2.3.3.3.2}$$

which is positive in (0, ∞) except at x = 1 where it vanishes. We note that L_1 is non-negative in the interior of Ω and attain zero at E^*. We now need to show that $\dot{L}_1$ is negative definite. Differentiating L_1 along the trajectories of the model system (2.2.1), we obtain

$$\begin{aligned} \dot{L}_1 &= \nu_1 \frac{dS_C}{dt}\left[1 - \frac{S_C^*}{S_C}\right] + \nu_2 \frac{dI_C}{dt}\left[1 - \frac{I_C^*}{I_C}\right] + \nu_3 \frac{dB_C}{dt}\left[1 - \frac{B_C^*}{B_C}\right], \\ &= \nu_1 \left[1 - \frac{S_C^*}{S_C}\right][\Lambda_C - \lambda_C S_C - \mu_C S_C] \\ &\quad + \nu_2 \left[1 - \frac{I_C^*}{I_C}\right][\lambda_C S_C - (\mu_C + \delta_C) I_C] \\ &\quad + \nu_3 \left[1 - \frac{B_C^*}{B_C}\right][\widehat{N}_c \alpha_c I_C - \alpha_C B_C]. \end{aligned} \tag{2.3.3.3.3}$$

Since E^* is an equilibrium point, the following relations hold

$$\begin{cases} \Lambda_C = \lambda_C^* S_C^* + \mu_C S_C^*, \quad (\mu_C + \delta_C) = \dfrac{\lambda_C^* S_C^*}{I_C^*}, \\ \alpha_C = \dfrac{\widehat{N}_c \alpha_c I_C^*}{B_C^*}. \end{cases} \tag{2.3.3.3.4}$$

Using the relations in (2.3.3.3.4), $\dot{L}_1$ becomes

$$\begin{aligned}
\dot{L}_1 &= \nu_1\left[1-\frac{S_C^*}{S_C}\right][\lambda_C^* S_C^* + \mu_C S_C^* - \lambda_C S_C - \mu_C S_C] \\
&\quad + \nu_2\left[1-\frac{I_C^*}{I_C}\right]\left[\lambda_C S_C - \frac{\lambda_C^* S_C^* I_C}{I_C^*}\right] \\
&\quad + \nu_3\left[1-\frac{B_C^*}{B_C}\right]\left[\widehat{N}_c\alpha_c I_C - \frac{\widehat{N}_c\alpha_c I_C^* B_C}{B_C^*}\right], \\
&= -\frac{\nu_1\mu_C}{S_C}(S_C - S_C^*)^2 - \frac{\nu_1\lambda_C^* S_C^{*2}}{S_C} \\
&\quad - \frac{\nu_2\lambda_C S_C I_C^*}{I_C} - \nu_3\widehat{N}_c\alpha_c I_C^*\frac{B_C}{B_C^*} - \nu_3\widehat{N}_c\alpha_c I_C\frac{B_C^*}{B_C} \\
&\quad + \left[\nu_3 N_c\alpha_c - \nu_2\frac{\lambda_C^* S_C^*}{I_C^*}\right] I_C + [\nu_1+\nu_2]\lambda_C^* S_C^* \\
&\quad + [\nu_2-\nu_1]\lambda_C S_C + \nu_1\lambda_C S_C^* + \nu_3\widehat{N}_c\alpha_c I_C^*.
\end{aligned} \tag{2.3.3.3.5}$$

Choose the value of ν_1, ν_2 and ν_3 such that

$$\begin{cases} \nu_1 = \nu_2 = 1, \\ \nu_3\widehat{N}_c\alpha_c - \nu_2\dfrac{\lambda_C^* S_C^*}{I_C^*} = 0, \end{cases} \tag{2.3.3.3.6}$$

from which we get

$$\nu_3 = \frac{\lambda_C^* S_C^*}{\widehat{N}_c\alpha_c I_C^*}. \tag{2.3.3.3.7}$$

Substituting the value of ν_1, ν_2 and ν_3 into equation (2.3.3.3.5), such that

$$\begin{aligned}\dot{L}_1 &= \left[1-\frac{S_C^*}{S_C}\right]\left[\lambda_C^* S_C^* + \mu_C S_C^* - \lambda_C S_C - \mu_C S_C\right] \\ &+ \left[1-\frac{I_C^*}{I_C}\right]\left[\lambda_C S_C - \frac{\lambda_C^* S_C^* I_C}{I_C^*}\right] \\ &+ \frac{\lambda_C^* S_C^*}{\widehat{N}_c \alpha_c I_C^*}\left[1-\frac{B_C^*}{B_C}\right]\left[\widehat{N}_c \alpha_c I_C - \frac{\widehat{N}_c \alpha_c I_C^* B_C}{B_C^*}\right].\end{aligned} \tag{2.3.3.3.8}$$

By direct calculations from equation (2.3.3.3.8), we have that

$$\begin{aligned}&\left[1-\frac{S_C^*}{S_C}\right]\left(\lambda_C^* S_C^* + \mu_C S_C^* - \lambda_C S_C - \mu_C S_C\right) = \left[1-\frac{S_C^*}{S_C}\right]\left(\lambda_C^* S_C^* - \lambda_C S_C\right) \\ &+ \left[1-\frac{S_C^*}{S_C}\right]\left(\mu_C S_C^* - \mu_C S_C\right) = -\mu_C S_C\left[1-\frac{S_C^*}{S_C}\right]^2 + \lambda_C^* S_C^*\left[1-\frac{S_C^*}{S_C}\right]\left[1-\frac{\lambda_C S_C}{\lambda_C^* S_C^*}\right], \\ &\leq \lambda_C^* S_C^*\left[1-\frac{S_C^*}{S_C}\right]\left[1-\frac{\lambda_C S_C}{\lambda_C^* S_C^*}\right]; \\ &\left[1-\frac{I_C^*}{I_C}\right]\left[\lambda_C S_C - \frac{\lambda_C^* S_C^* I_C}{I_C^*}\right] = \lambda_C^* S_C^*\left[1-\frac{I_C^*}{I_C}\right]\left[\frac{\lambda_C S_C}{\lambda_C^* S_C^*} - \frac{I_C}{I_C^*}\right];\end{aligned} \tag{2.3.3.3.9}$$

and

$$\frac{\lambda_C^* S_C^*}{\widehat{N}_c \alpha_c I_C^*}\left[1-\frac{B_C^*}{B_C}\right]\left[\widehat{N}_c \alpha_c I_C - \frac{\widehat{N}_c \alpha_c I_C^* B_C}{B_C^*}\right] = \lambda_C^* S_C^*\left[1-\frac{B_C^*}{B_C}\right]\left[\frac{I_C}{I_C^*} - \frac{B_C}{B_C^*}\right] \tag{2.3.3.3.10}$$

Therefore,

$$\begin{aligned}\dot{L}_1 &\leq \lambda_C^* S_C^*\left[1-\frac{S_C^*}{S_C}\right]\left[1-\frac{\lambda_C S_C}{\lambda_C^* S_C^*}\right] + \lambda_C^* S_C^*\left[1-\frac{I_C^*}{I_C}\right]\left[\frac{\lambda_C S_C}{\lambda_C^* S_C^*} - \frac{I_C}{I_C^*}\right] \\ &+ \lambda_C^* S_C^*\left[1-\frac{B_C^*}{B_C}\right]\left[\frac{I_C}{I_C^*} - \frac{B_C}{B_C^*}\right], \\ &\leq \lambda_C^* S_C^*\left[2 - \frac{\lambda_C S_C I_C^*}{\lambda_C^* S_C^* I_C} + \frac{\lambda_C}{\lambda_C^*} - \frac{S_C^*}{S_C} - \frac{I_C}{I_C^*}\right] + \lambda_C^* S_C^*\left[1 - \frac{I_C B_C^*}{I_C^* B_C} + \frac{I_C}{I_C^*} - \frac{B_C}{B_C^*}\right]\end{aligned} \tag{2.3.3.3.11}$$

By using the function $g(x)$ defined in (2.3.3.3.2), we get

$$
\begin{aligned}
\dot{L}_1 \leq\ & \lambda_C^* S_C^* \left[-g\left(\frac{S_C^*}{S_C}\right) - g\left(\frac{\lambda_C S_C I_C^*}{\lambda_C^* S_C^* I_C}\right) + \frac{\lambda_C}{\lambda_C^*} - \ln\left(\frac{B_C}{B_C^*}\right) - \frac{I_C}{I_C^*} + \ln\left(\frac{I_C}{I_C^*}\right) + \ln\left(\frac{B_0+B_C}{B_0+B_C^*}\right)\right] \\
& + \lambda_C^* S_C^* \left[-g\left(\frac{I_C B_C^*}{I_C^* B_C}\right) - \ln\left(\frac{I_C}{I_C^*}\right) + \frac{I_C}{I_C^*} + \ln\left(\frac{B_C}{B_C^*}\right) - \frac{B_C}{B_C^*}\right], \\
\leq\ & \lambda_C^* S_C^* \left[-g\left(\frac{S_C^*}{S_C}\right) - g\left(\frac{\lambda_C S_C I_C^*}{\lambda_C^* S_C^* I_C}\right) + \frac{B_C}{B_C^*} - \ln\left(\frac{B_C}{B_C^*}\right) - \frac{I_C}{I_C^*} + \ln\left(\frac{I_C}{I_C^*}\right)\right] \\
& + \lambda_C^* S_C^* \left[\frac{B_C(B_0+B_C^*)}{B_C^*(B_0+B_C)} - \frac{B_0+B_C}{B_0+B_C^*} - g\left(\frac{B_0+B_C}{B_0+B_C^*}\right) - \frac{B_C}{B_C^*} - 1\right] \qquad (2.3.3.3.12) \\
& + \lambda_C^* S_C^* \left[-g\left(\frac{I_C B_C^*}{I_C^* B_C}\right) - \ln\left(\frac{I_C}{I_C^*}\right) + \frac{I_C}{I_C^*} + \ln\left(\frac{B_C}{B_C^*}\right) - \frac{B_C}{B_C^*}\right], \\
\leq\ & \lambda_C^* S_C^* \left[\frac{B_C}{B_C^*} - \ln\left(\frac{B_C}{B_C^*}\right) - \frac{I_C}{I_C^*} + \ln\left(\frac{I_C}{I_C^*}\right)\right] \\
& + \lambda_C^* S_C^* \left[\frac{I_C}{I_C^*} - \ln\left(\frac{I_C}{I_C^*}\right) + \ln\left(\frac{B_C}{B_C^*}\right) - \frac{B_C}{B_C^*}\right] = 0
\end{aligned}
$$

From (2.3.3.3.12), we have that the largest invariant subset, where $\dot{L}_1 = 0$, is E^*. Therefore, we conclude from the LaSelle's Invariance Principle that E^* is globally asymptotically stable (*GAS*) when $R_0 > 1$.

2.4 Numerical analysis

Experimental simulations of the baseline single-scale model system (2.2.1)'s behaviour was done using a Python program version V 2.6 which typically uses a package odeint function in the scipy.integrate for solving any nature of system of differential equations. These numerical simulations of the model system (2.2.1) was carried out to illustrate some of the analytical results that we obtained within this chapter. We use the estimated parameter values presented in Table (2.2) for sensitivity and numerical analysis. It is important to mention that parameter values used for numerical simulations, some are from published literature and some were assumed as values of some parameters are generally not reported in literature. The initial conditions used for simulation are given by $S_C(0) = 2000$, $I_C(0) = 0$, $B_C(0) = 10000$.

Parameter	Description	Unit	Initial values	Source
Λ_C	Cattle birth rate	day^{-1}	0.27	[52, 54]
β_C	Ruminant infection rate	day^{-1}	0.00027	Assumed
μ_C	Death rate of Ruminants	day^{-1}	0.0001	[52]
δ_C	Ruminant removal rate due to PTB infection	day^{-1}	0.0008	Assumed
α_C	Environmentally bacteria death rate	day^{-1}	0.0018	[52]
B_0	Saturation rate of bacteria	day^{-1}	10000	[54]
$\widehat{N}_c$	Number of MAP bacteria available for excretion	day^{-1}	1000	Assumed
α_c	Excretion rate	day^{-1}	0.01	[54]

Table 2.2: Model parameter values associated with the transmission dynamics of Paratuberculosis

2.4.1 Sensitivity analysis

In this sub-section, we conduct a sensitivity analysis of the two PTB transmission metrics derived from the baseline PTB dynamics single-scale model system (2.2.1). The two PTB transmission metrics derived from the baseline PTB single-scale model system (2.2.1) are: the reproduction number, R_0, which generally describes the dynamics of a disease at the beginning of an infection and the endemic value of the environmental bacteria load, B_C^*, which generally describes the dynamics of a disease at the epidemic level. For any epidemic model that describe the dynamics of any diseases in a population, a sensitivity analysis study is essential to perform as it helps to identify model's parameters which can be targeted for disease control, elimination or even eradication, and also be monitored and controlled during an outbreak of the disease. In this case, sensitivity analysis of both the PTB transmission metrics (R_0 and B_C^*), with respect to the variation of the baseline PTB single-scale model system (2.2.1)'s parameters is conducted using Latin Hypercube Sampling and partial rank correlation coefficients (PRCCs). We use 1000 simulations per run to investigate the impact of each model parameters on both the basic reproduction numbers (R_0) and the endemic value of the environmental bacteria load (B_C^*). The sensitivity results of R_0 and B_C^* on the model parameters when they changes are given in the Tornado plots, Figure (2.2) and Figure (2.3), respectively.

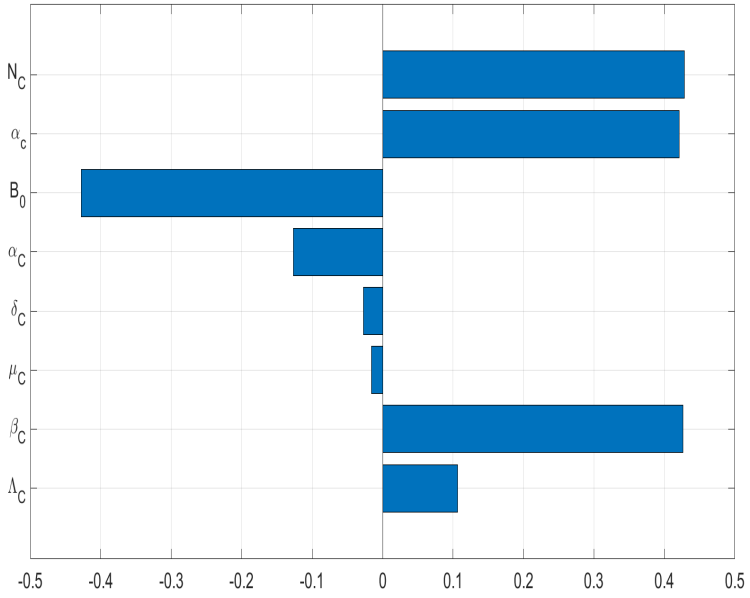

Figure 2.2: *Tornado plot of partial rank correlation coefficients (PRCCs) of all the model parameters that influence the PTB transmission metric* R_0.

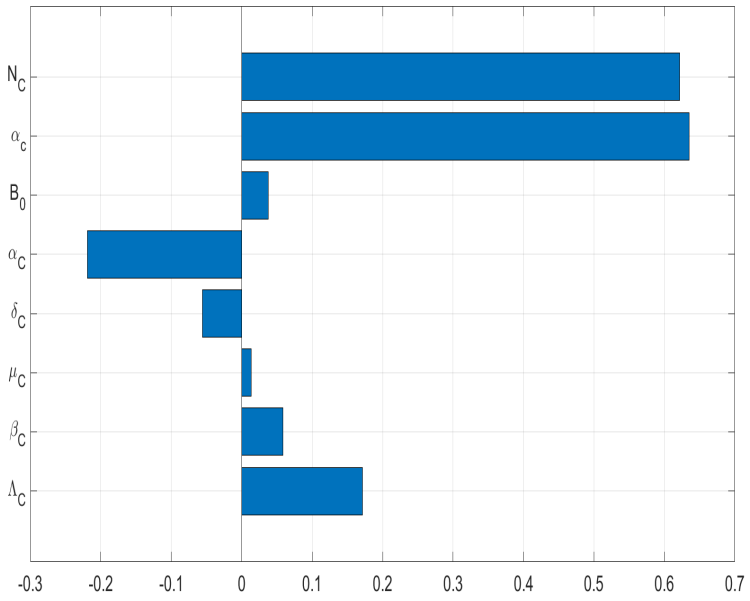

Figure 2.3: *Tornado plot of partial rank correlation coefficients (PRCCs) of all the model parameters that influence the PTB transmission metric* B^*_C.

From the sensitivity analysis results of both R_0 and B_C^* to all the baseline model (2.2.1)'s parameters in Figure (2.3), we deduce the following results:

(a) Some of the baseline PTB single-scale model (2.2.1)'s parameters have positive PRCCs and some have negative PRCCs. This indicates that, parameters with positive PRCCs will increase the values for both R_0 and B_C^* when they are increased, while parameters with negative PRCCs will decrease the values for both R_0 and B_C^* when they are increased. For instance, increasing parameter like bacteria transmission rate β_C at the between-host level will eventually increase the value of R_0 as well as the value of B_C^*, and also increasing parameters like decay rate of bacteria in the environment α_C will the lead to a reduction in the value of R_0 as well as the value of B_C^*.

(b) The PTB transmission metric R_0 is highly sensitive to the six of the disease parameters (β_C, B_0, $\widehat{N}_c$, α_c, α_C, Λ_C) is relatively high, but more highly and approximately equal sensitive to β_C, B_0, $\widehat{N}_c$, and α_c. However, the sensitivity of B_C^* to the same parameters is variable, with B_C^* being least sensitive to β_C and B_0 while remaining highly sensitive and having approximately the same sensitivity to $\widehat{N}_c$ and α_c as for R_0. Since R_0 characterizes transmission of PTB disease at the start of the epidemic while B_C^* characterizes transmission of the disease when the disease has reach an endemic level. We make the following conclusions regarding the sensitivity of R_0 and B_C^* to the PTB model system (2.2.1)'s parameters.

(i) Since both R_0 and B_C^* are significantly sensitive to (β_C, B_0, $\widehat{N}_c$, α_c, α_C, Λ_C), this implies that care must be taken to the accuracy of these six PTB transmission model (2.2.1)'s parameters during the data collection if the validity and utility of the model system (2.2.1) is to be improved.

(ii) Since B_C^* is less sensitive to β_C and B_0 while R_0 is significantly sensitive to β_C and B_0, this implies that PTB interventions such as environmental-hygiene management (which reduce MAP concentration in the environment through cleaning as we as preventing contact of ruminant with the MAP in the environment) and vaccination (which reduce susceptibility of ruminants to infection) would have more effect in controlling the transmission of PTB infection at the start of the epidemic than when the disease is already endemic in the herd.

(iii) Since both R_0 and B_C^* are significantly sensitive to $\widehat{N}_c$, we note that $\widehat{N}_c$ phenomenologically model the within-host dynamics of the infection which can be modified by the within-host health intervention mechanisims such as drugs that kill MAP bacterial cells at the ruminant individual level.

2.4.2 Numerical simulations of the basiline PTB model transmission dynamics

In this subsection, we use numerical simulations to verify some results we have obtained from the sensitivity analysis for both R_0 and B_C^* and analytical results of the model. The numerical simulations are conducted using the baseline parameter values given in Table (2.2). We illustrate the influence of four PTB transmission parameters (β_C, B_0, $\widehat{N}_c$, α_C) on the model variables (S_C, I_C, B_C). These parameters were only chosen partly because they are significantly sensitive to both R_0 and B_C^*.

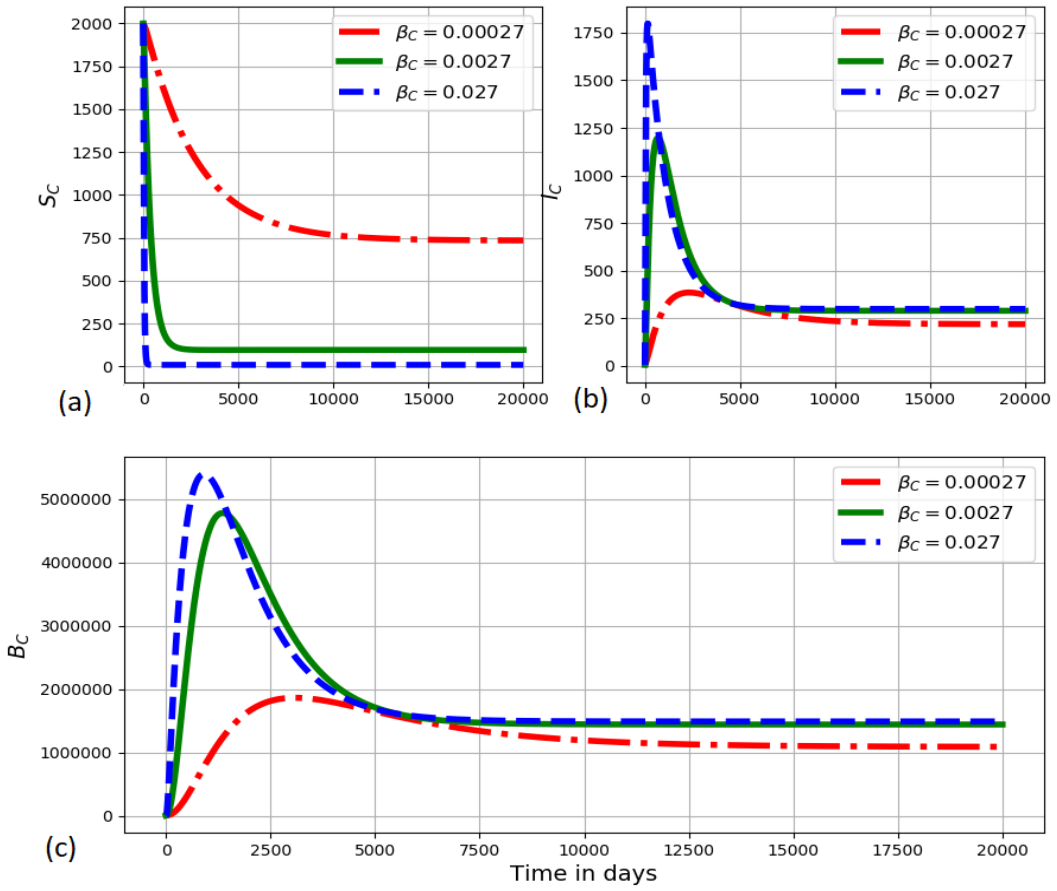

Figure 2.4: *Graphs of numerical solutions of the model system (2.2.1) showing evolution in time of (a) population of susceptible ruminants (S_C), (b) population of infected ruminants (I_C), and (c) population of environmental MAP bacterial load (B_C) for different values of ruminant infection rate β_C: $\beta_C = 0.00027$, $\beta_C = 0.0027$, and $\beta_C = 0.027$.*

Figure (2.4) shows changes in (a) population of susceptible ruminants (S_C), (b) population of infected ruminants (I_C), and (c) population of environmental MAP bacteria load (B_C) for different values of the rate at which ruminants became infected with PTB infection: β_C: $\beta_C = 0.3$,

$\beta_C = 0.03$, and $\beta_C = 0.003$. The results in Figure (2.4) show that higher rates of infection at the ruminant population level result in increased population of environmental MAP bacteria B_C and infected ruminants I_C and a significant noticeable increase in the population of susceptible ruminants S_C. Therefore, environmental-hygiene management measures practiced by farmers which prevent ruminants from contact with MAP bacteria in the environment reduce the transmission risk of the disease at the ruminant population/herd level.

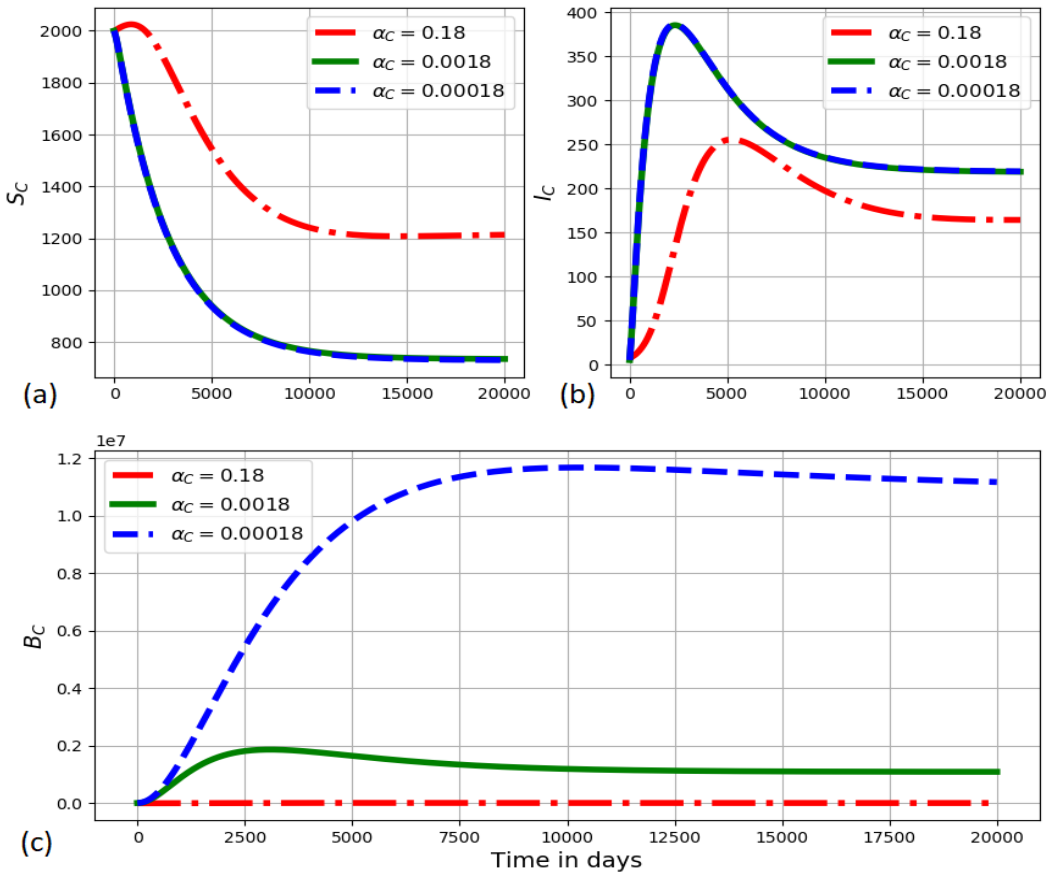

Figure 2.5: *Graphs of numerical solutions of the model system (2.2.1) illustrating the variation of (a) population of susceptible ruminants (S_C), (b) population of infected ruminants (I_C), and (c) between-host MAP bacterial load (B_C) for different values of natural death rate of the MAP bacterial load in the physical environmental domains α_C: $\alpha_C = 0.18$, $\alpha_C = 0.00018$, and $\alpha_C = 0.000018$.*

Figure (2.5) also shows graphs of numerical solutions of the between-host scale model system (2.2.1) illustrating dynamics of (a) population of susceptible ruminants (S_C), (b) population of infected ruminants (I_C), and (c) environmental MAP bacteria load (B_C) for different values of natural death rate of the MAP bacilli in the environmental domains α_C: $\alpha_C = 0.18$, $\alpha_C = 0.0018$, and $\alpha_C = 0.00018$. The results also show the environmental conditions which enhance death of

MAP bacteria in the environment affect transmission of PTB disease in the ruminant population. This imply that increasing death of MAP bacteria population in the environment will reduce transmission risk of the disease at the ruminant population level. Therefore, environmental-hygiene management which enhance the killing of MAP bacteria in the physical environment reduces transmission risk of the disease among ruminants in the herd.

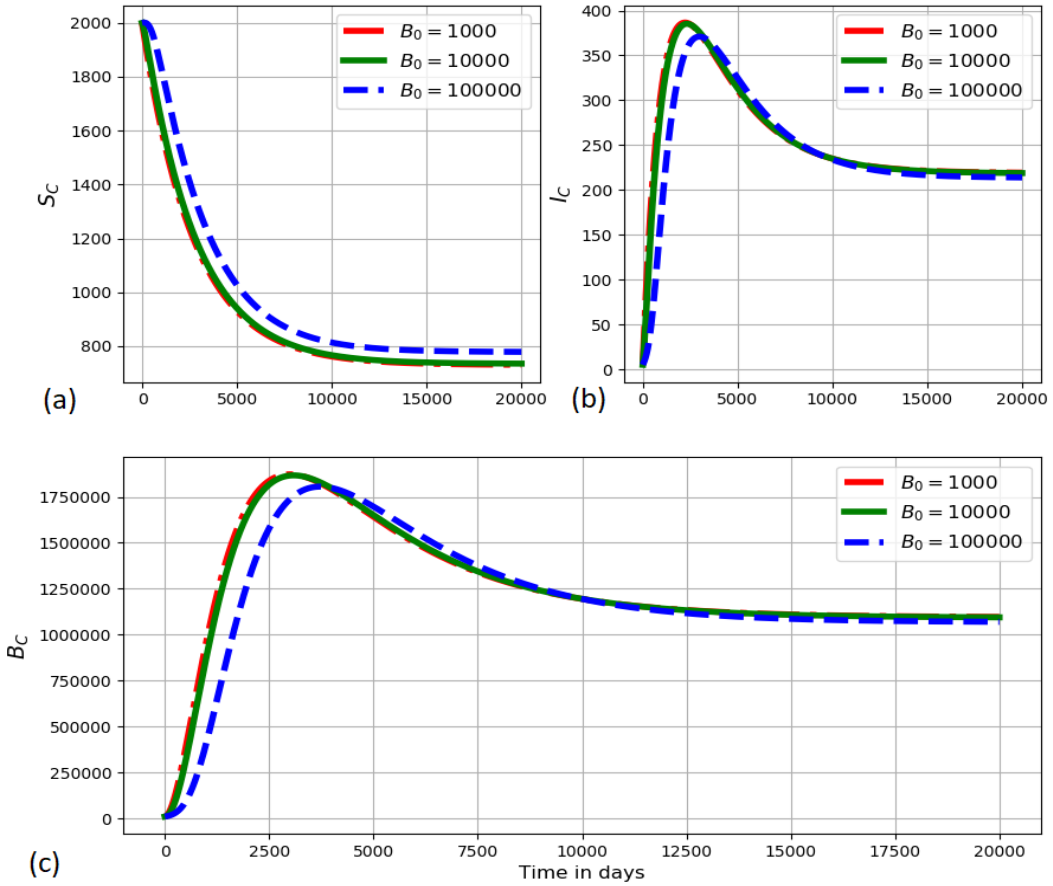

Figure 2.6: *Graph of numerical solutions of model system (2.2.1) further showing propagation of (a) population of susceptible ruminants (S_C), (b) population of infected ruminants (I_C), and (c) environmental MAP bacteria load (B_C) for different values of disease induce death rate B_0:* $B_0 = 1000$, $B_0 = 10000$, *and* $B_0 = 100000$.

Figure (2.6) further shows changes in (a) population of susceptible ruminants (S_C), (b) population of infected ruminants (I_C), and (c) population of environmental MAP bacteria load (B_C) for different values of natural decay rate of the within-host MAP bacilli bacteria cells: B_0: $B_0 = 1000$, $B_0 = 10000$, and $B_0 = 100000$. The results in Figure (2.6) show that as the death rate of the within-host bacterial load increases, there is a noticeable reduction in the population of environmental MAP bacteria B_C and the population of infected ruminants I_C as well as an increase in the population of susceptible ruminants S_C. Therefore, vaccination interventions

that reduces susceptibility of ruminants to infection would have a significant impact on reducing transmission risk of PTB infections at the ruminant population/herd level.

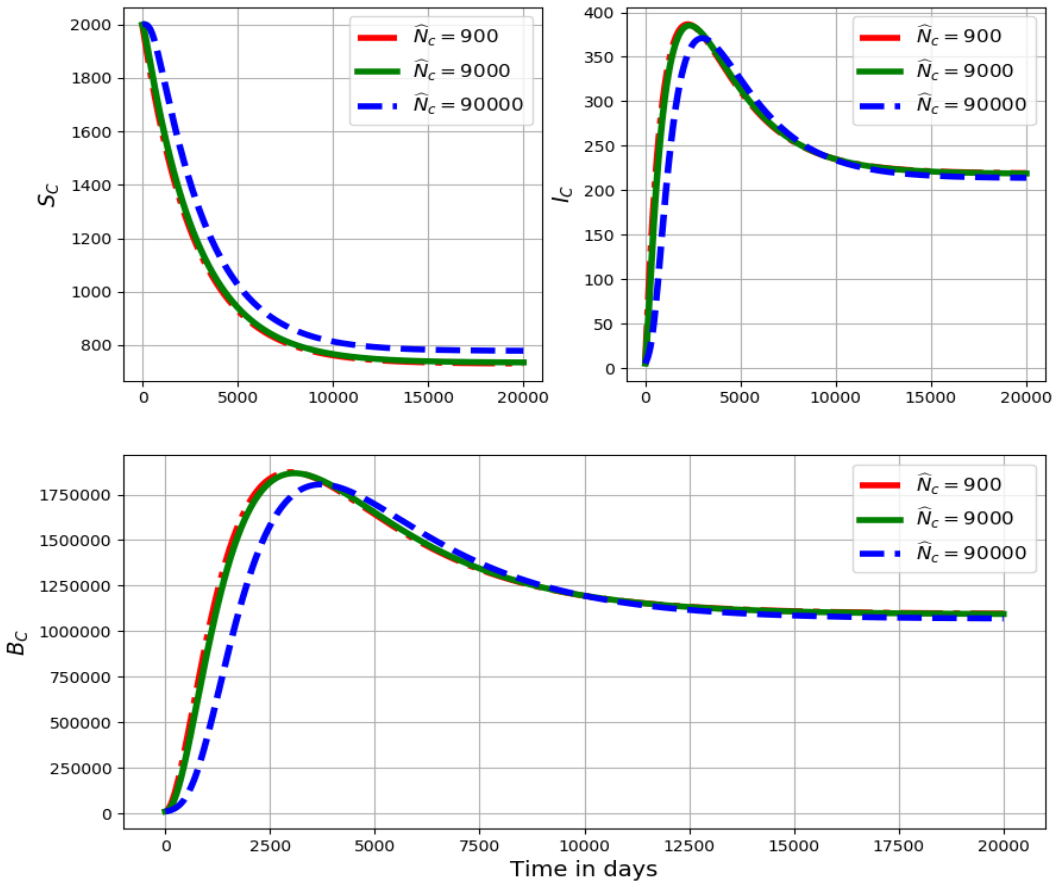

Figure 2.7: *Graphs of numerical solutions of the model system (2.2.1) showing dynamics in (a) population of susceptible ruminants (S_C), (b) population of infected ruminants (I_C), and (c) population of environmental MAP bacterial load (B_C) for different values of the average number of within-host MAP bacteria produced per bursting infected macrophage cell N_c:$\widehat{N}_c = 900$, $\widehat{N}_c = 9000$, $\widehat{N}_c = 90000$.*

Figure (2.7) shows dynamics in the (a) population of susceptible ruminants (S_C), (b) population of infected ruminants (I_C), and (c) population of environmental MAP bacterial load (B_C) for different values of the average number of within-host MAP bacteria excreted in the environment by each infected ruminants N_c: $\widehat{N}_c = 900$, $\widehat{N}_c = 9000$, $\widehat{N}_c = 90000$. The numerical results in Figure (2.7) show that the within-host process that enhance killing of MAP bacteria load at the site of PTB infection within an infected ruminant affect transmission of the disease at the ruminant population level. Therefore, any mechanism that intend to kill within-host MAP bacteria load at the ruminant individual level would have an influence on the transmission risk of PTB infection among ruminants in the herd.

2.5 Summary

In this chapter, we presented a single-scale model that describes the intrinsic dynamics of a given environmentally-transmitted disease that can be modeled at the host level using paratuberculosis in ruminants as paradigm. The model was formulated based on the susceptible-infected endemic framework coupled with the compartment of free-living pathogen in the environment (SIP) which describes the population dynamics of susceptible ruminants S_C, infected ruminants I_C, and MAP bacteria B_C at any time t. We study the mathematical properties of the model system (2.2.1) and established that the model is mathematically and epidemiologically well-posed. This has been achieved by establishing the positiveness and boundedness of the model system (2.2.1) solutions and determining the basic reproductive number for the model and the two equilibrium states which are the disease-free equilibrium state (E_0) and the endemic equilibrium state (E^*). The basic reproductive number, R_0, of the model system (2.2.1) was then used to prove both local and global stability of E_0 as well as the existence and uniqueness of E^* along with local and global stability of E^*. Additionally, we noted that when the basic reproductive number of the model is less than a unity the disease-free equilibrium state is asymptotically stable and globally attracting. However, when the basic reproductive number of the model is greater than a unity there exist a unique endemic equilibrium state which is locally and globally asymptotically stable. Sensitivity analysis of the basic reproductive number and the endemic value of the infective MAP bacteria in the physical environment as the two main disease transmission metrics which generally characterize the dynamics of the disease at the start of infection and when it has already at an endemic level has been conducted. We further carried out numerical simulations of the model with the aim of verifying mathematical analysis derived from the model. Although both the mathematical and numerical analysis of this single-scale model of the dynamics of ruminant paratuberculosis was easy, a major weakness of this model is that it describes the replication dynamics of the MAP bacteria within an infected ruminant host in a phenomenological manner which makes the model unrealistic in predicting the dynamics of the disease. We anticipated that this kind of limitation of single-scale models in predicting dynamics of environmentally-transmitted diseases can be overcome by extending the single-scale model to a multiscale model.

Chapter 3

A Nested Multiscale Modelling of Paratuberculosis Dynamics in Ruminants

3.1 Introduction

It is widely appreciated that infectious diseases are typical example of complex systems because of their multilevel and multiscale nature [1]. Due to this common key feature of multilevel and multiscale in infectious disease systems, several authors in the field of mathematical biology have turned their attention to multiscale modelling as a scientific method for studying the dynamics of infectious diseases at different levels of their organizations. Multiscale models facilitate integration of more than one scale that are involved in the dynamics of an infectious disease systems. In this chapter, we present a nested multiscale model that integrates microscale and macroscale at a host level of an infectious disease system that has a pathogen replication-cycle at the microscale with application to paratuberculosis in ruminants. The most important feature of nested multiscale models at any level of organization of an infectious disease system [1, 8]: cell level, tissue level, organ level, microecosystem level, host level, community and macroecosystem level is that the macroscale influences the microscale through the initial infective inoculum. Our objective in this chapter is to investigate how the initial inoculum influences disease dynamics for a pathogen with a replication-cycle at the microscale. Therefore, we investigate the impact of the variation in size of initial inoculum on the dynamics of the disease. This is unlike embedded multiscale models in which the macroscale influences the microscale through super-infection [1]. We use this

key feature of nested multiscale models to investigate if they are an appropriate category of multiscale models to characterize the multiscale dynamics of environmentally-transmitted infectious diseases with a replication-cycle at microscales using Paratuberculosis (PTB) in ruminants as an example. In the subsequent chapters of this research, we will further compare this key feature of nested multiscale models with the features of embedded multiscale models of infectious diseases systems. In the context of an environmentally-transmitted disease system at the host level, the within-host scale and the between-host scale serve as building blocks in the development of multiscale models. In the case of PTB infection in dairy ruminants as an environmentally-transmitted disease system, the within-host scale on one hand is associated with the interaction of MAP with ruminant macrophages (target cells) and other immune response cells that happens inside an infected ruminant. It is at this scale where the process outcomes of infection within a single infected ruminant level determine if, when and how much the ruminant will further transmit the bacteria into the environment, and in turn affecting the spread of the disease at the ruminant population-level. The processes of PTB infection at the within-host scale can be modified by the within-host conditions and medical interventions. The between-host scale on other hand, however, is associated with the transmission dynamics of MAP bacteria that typically occurs between ruminants and their physical environment domains. This takes place when ruminants feed from contaminated pasture with fecal material containing infective MAP or drink from contaminated surface water/water troughs with the bacteria. The processes at the between-ruminant-host scale can be modified by control measures such as reducing fecal contamination of food, water and pasture (which can be achieved by raising feed and water troughs, strip grazing, or use of mains/piped water rather than surface/pond water); avoid spreading yard manure on pasture; and maintain proper hygiene practices particularly in buildings/yards and calving boxes [58].

To date, most of PTB disease dynamics models in the literature have been devoted to study the dynamics of PTB infection in ruminants and evaluating the effect of control measures aim at controlling, eliminating and even eradicating this disease using a single-scale modelling approach (see [52, 59, 60] and references therein). This is despite the fact that PTB infection is a complex and multiscale disease system. However, we have to date, witnessed the development of few models in the literature that consider the complexity and multiscale nature of PTB infection in attempting to study its dynamics [54, 61–63]. The multiscale models in [54, 61] use the time-since-infection approach to link the within-host sub-model with the between-host sub-model for PTB infection as well as the dependence of some epidemiological parameters on the within-host MAP bacteria load. This coupling principle employed in [54, 61] was suggested for the first time by Gilchrist and Sasaki [35]. In addition, it is also worthy to note that the multiscale models in

[54, 61] are categorized as hybrid multiscale models (see [19, 20]). To the best of our knowledge the nested multiscale in this study is the first of its kind to be developed to characterize the dynamics of PTB in ruminants. Moreover, although the multiscale models in [54, 61] and the multiscale model developed in this study all characterize the reciprocal influence between the within-host scale and the between-host scale disease dynamics, there are important differences between these multiscale models. Specifically, in the current nested multiscale model, both the within-host scale and the between-host scale sub-models are all described by the same formalism or mathematical representation (i.e. a system of ODEs). However, the multiscale models in [54, 61] are hybrid multiscale models, where only the within-host scale sub-models are represented by ODEs, while their between-host sub-models are represented by partial differential equations (PDEs).

.

3.2 Derivation of Nested Multiscale Model for the Dynamics of Ruminant Paratuberculosis (PTB)

As mentioned previously, for infectious disease systems at host level, the between-host scale sub-model and the within-host scale sub-model are the building blocks upon which multiscale models are developed. In this case, we derive a nested multiscale model that integrates the between-host sub-model associated with the transmission dynamics of PTB disease and the within-host sub-model associated with the replication dynamics of MAP bacteria within an infected ruminant at the site of infection. In the following sections, we begin by presenting two independent sub-models for PTB transmission dynamics at two distinct scales, one at the between-host scale and other at the within-host scale and then integrate them into a single multiscale model in sec 3.2.3.

3.2.1 The between-host scale submodel for the PTB multiscale model dynamics

The between-host scale submodel for the multiscale dynamics of PTB in ruminants is described by the system of ordinary differential equations given in Chapter 2, which we can re-write here for quick reference as:

$$\begin{cases} i.\ \dfrac{dS_C(t)}{dt} &= \Lambda_C - \dfrac{\beta_C B_C(t) S_C(t)}{B_0 + B_C(t)} - \mu_C S_C(t), \\ ii.\ \dfrac{dI_C(t)}{dt} &= \dfrac{\beta_C B_C(t) S_C(t)}{B_0 + B_C(t)} - (\mu_C + \delta_C) I_C(t), \\ iii.\ \dfrac{dB_C(t)}{dt} &= \widehat{N}_c \alpha_c I_C(t) - \alpha_C B_C(t). \end{cases} \tag{3.2.1.1}$$

From the model system (3.2.1.1), we make the following assumption that the dynamics of S_C, I_C and B_C occur at a slow time scale, t, compared to the within-host scale PTB transmission dynamics variables, so that $S_C = S_C(t)$, $I_C = I_C(t)$ and $B_C = B_C(t)$. It is also important to note from the model system (3.2.1.1), that $\widehat{N}_c$ is treated as a single value parameter whereas $\widehat{N}_c$ is a composite parameter that summarize the disease dynamics within an infected individual host and this make the model system (3.2.1.1) being unrealistic. We shall also urge that it is note easy to estimate $\widehat{N}_c$ using a single-scale models. However, an alternative approach for estimating $\widehat{N}_c$ is to use a nested multiscale model based on the within-host disease dynamics. In section 3.3, we simplified a full nested multiscale model nested multiscale in order to estimate $\widehat{N}_c$.

3.2.2 The within-host scale submodel for the PTB multiscale model dynamics

Further, for the derivation of the current nested multiscale model for PTB in ruminants considered in this study, the within-host submodel dynamics is adopted from a more elaborative single-scale model framework from the work by Magombedze et al. [53] with minor modifications which are based on multiscale considerations. However, the main multiscale consideration incorporated into the model in [53] is the excretion/shedding rate α_c, which is an important multiscle consideration since in general the within-host scale sub-model is linked to the between-host scale sub-model through pathogen shedding/excretion [19]. The resulting within-host model describes the interactions of six population: susceptible macrophages, M_ϕ which are target cells, infected macrophages, I_m which are macrophages which have internalized extracellular MAP bacteria cells, MAP bacterial load, B_c at the extracellular environment, specific naive CD4+ T cells T_0, Th1 immune response cells, T_1, and Th2 phenotype immune response cells, T_2 (see the work in [53]). We also modify the model in [53] by making the following assumptions:

a. Transmission of the infection between cells is only through contact with the extracellular MAP bacterial load B_c in the extracellular environment at the site of infection.

b. The within-host scale disease processes happen at fast time scale, τ, compared to the between-host scale PTB submodel variable so that $M_\phi = M_\phi(\tau)$, $I_m = I_m(\tau)$, $B_c = B_c(\tau)$, $T_0 = T_0(\tau)$, $T_1 = T_1(\tau)$ and $T_2 = T_2(\tau)$.

c. The extracellular MAP bacterial load modelled mechanistically by $B_c = B_c(\tau)$ is a proxy for individual ruminant infectiousness.

d. The extracellular MAP bacteria cannot replicate outside the macrophage cells of an individual ruminant.

e. The depletion of MAP bacteria in the extracellular environment through engulfment by macrophages is negligible.

These assumptions lead to the following submodel of ordinary differential equations for the within-host scale PTB transmission dynamics:

$$\begin{cases} i.\ \dfrac{dM_\phi(\tau)}{d\tau} &= \Lambda_\phi - \beta_\phi M_\phi(\tau) B_c(\tau) - \mu_\phi M_\phi(\tau), \\ ii.\ \dfrac{dI_m(\tau)}{d\tau} &= \beta_\phi M_\phi(\tau) B_c(\tau) - \gamma_m T_1(\tau) I_m(\tau) \\ & \quad -(k_m + \mu_\phi) I_m(\tau), \\ iii.\ \dfrac{dB_c(\tau)}{d\tau} &= N_m k_m I_m(\tau) - (\mu_c + \alpha_c) B_c(\tau), \\ iv.\ \dfrac{dT_0(\tau)}{d\tau} &= \Lambda_0 - (\delta_m I_m(\tau) + \delta_b B_c(\tau)) T_0(\tau) \\ & \quad -\mu_0 T_0(\tau), \\ v.\ \dfrac{dT_1(\tau)}{d\tau} &= \theta_1 \delta_m I_m(\tau) T_0(\tau) - \mu_1 T_1(\tau), \\ vi.\ \dfrac{dT_2(\tau)}{d\tau} &= \theta_2 \delta_b B_c(\tau) T_0(\tau) - \mu_2 T_2(\tau). \end{cases} \tag{3.2.2.1}$$

In the within-host scale sub-model (3.2.2.1), the first two equations describe the dynamics of the within-ruminant-host macrophage population which is divided into two groups. The first group is

of susceptible macrophage cells $M_\phi(\tau)$ (these are macrophages which are healthy and are susceptible to the Paratuberculosis at the site of infection). The second group is of infected macrophage cells $I_m(t)$ (these are macrophages which are infected by the MAP bacteria). We assume that, at any time τ, new macrophage recruits enter the population of susceptible macrophages through the supply of macrophage cells from progenitor monocytes that are recruited from the blood to the site of infection at a constant rate Λ_ϕ and this population losses individuals due to natural death at a constant rate μ_ϕ. Susceptible macrophages acquire infection through engulfing extracellular MAP bacilli bacteria at a rate β_ϕ. We assume that in the population of infected macrophages there is an additional death due to bursting of infected cells at a rate k_m and due to cell removal by T_1 immune response at a rate γ_m. In addition, when infected macrophages burst at constant rate k_m, they are assumed to release an average number of intracellular MAP bacilli N_m into the extracellular environment, so that the total number of intracellular bacteria released into the extracellular environment is $N_m k_m I_m$. The third equation of the model system (3.2.2.1) describes the changes in time of the population size of MAP bacteria in the extracellular environment which is generated following the release of the intracellular MAP bacilli into the extracellular environment when each infected macrophage bursts. We assume that the population of MAP bacteria in the extracellular environment decays naturally at a constant rate μ_c and are excreted out of the body of infected ruminant into the physical environment through feces at a constant rate α_c. The last three equations of the model system (3.2.2.1) describe the evolution in time of the population of ruminant immune response cells at the site of infection in the gut which are specific naive CD4+ T cells (T_0), and the two subsets of the MAP specific immune response, Th1 (T_1) and Th2 (T_2) cells (see [53] and reference therein). The population of specific naive CD4+ T cells (T_0) for MAP bacilli are produced at a constant rate Λ_0 from the thymus. We assume that these specific naive CD4+ T cells decay naturally at a rate μ_0. Following the work in [53], we assume that T_0 cells become T_1 or T_2 immune response cells at per capita rates δ_m and δ_b, respectively. Thus, the population of T_1 and T_2 immune response cells are proliferated at a rate $\theta_1\delta_m I_m T_0$ and $\theta_1\delta_b B_m T_0$, respectively. We assume that both the population of T_1 and T_2 immune response cells decay naturally at rates μ_1 and μ_2, respectively.

3.2.3 Integration of the between-host and within-host submodels of PTB dynamics into a nested multiscale model

In the previous sections we presented the two submodels for the dynamics of PTB infection (between-host submodel (3.2.1.1) and within-host submodel (3.2.2.1)) that separately describe the two key processes of PTB disease dynamics (transmission and replication of MAP bacteria processes) which occur at two distinct scales (within-host scale and between-host scale). We

now integrate them into a single multiscale model as shown in flow diagram in Fig. 3.1. We achieve this by replacing the parameter $\widehat{N}_c$ which phenomenologically models within-host scale pathogen replication by a variable $B_c(\tau)$ which mechanistically models the within-host scale pathogen replication to get:

$$
\begin{cases}
i.\ \dfrac{dS_C(t)}{dt} &= \Lambda_C - \dfrac{\beta_C B_C(t)}{B_0 + B_C(t)} S_C(t) - \mu_C S_C(t), \\
ii.\ \dfrac{dI_C(t)}{dt} &= \dfrac{\beta_C B_C(t)}{B_0 + B_C(t)} S_C(t) - (\mu_C + \delta_C) I_C(t), \\
iii.\ \dfrac{dB_C(t)}{dt} &= \alpha_c B_c(\tau) I_C(t) - \alpha_C B_C(t), \\
iv.\ \dfrac{dM_\phi(\tau)}{d\tau} &= \Lambda_\phi - \beta_\phi M_\phi(\tau) B_c(\tau) - \mu_\phi M_\phi(\tau), \\
v.\ \dfrac{dI_m(\tau)}{d\tau} &= \beta_\phi M_\phi(\tau) B_c(\tau) - \gamma_m T_1(\tau) I_m(\tau) \\
&\quad -(k_m + \mu_\phi) I_m(\tau), \\
vi.\ \dfrac{dB_c(\tau)}{d\tau} &= N_m k_m I_m(\tau) - (\mu_c + \alpha_c) B_c(\tau), \\
vii.\ \dfrac{dT_0(\tau)}{d\tau} &= \Lambda_0 - (\delta_m I_m(\tau) + \delta_b B_c(\tau)) T_0(\tau) \\
&\quad -\mu_0 T_0(\tau), \\
viii.\ \dfrac{dT_1(\tau)}{d\tau} &= \theta_1 \delta_m I_m(\tau) T_0(\tau) - \mu_1 T_1(\tau), \\
ix.\ \dfrac{dT_2(\tau)}{d\tau} &= \theta_2 \delta_b B_c(\tau) T_0(\tau) - \mu_2 T_2(\tau).
\end{cases}
\tag{3.2.3.1}
$$

Based on the categorization of multiscale models of infectious disease systems presented in [19, 20], the multiscale model for PTB disease dynamics given by (3.2.3.1) falls in the category of nested multiscale models of class 2.

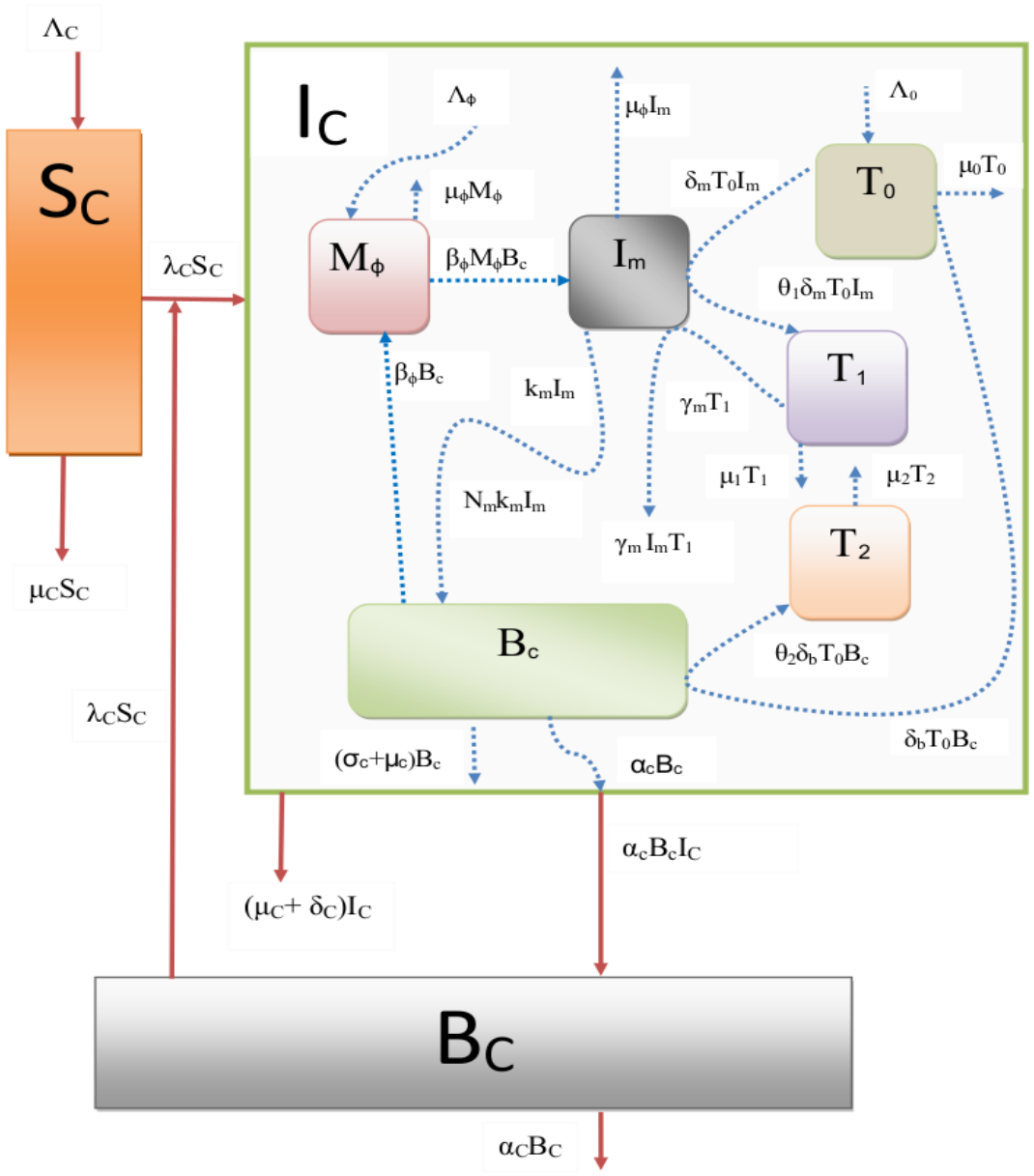

Figure 3.1: *A schematic representation of the nested multiscale model of Johne's disease in a herd*

3.2.4 Analysis of the multiscale model using fast-low time-scale analysis

We note from the full nested multiscale model system given by (3.2.3.1) has two different time scales involved which are the between-host time scale (t) associated with the transmission dynamics of PTB at the population level and the within-host time scale (τ) associated with the replication dynamics of PTB infectious agent at an individual ruminant level. This makes the analysis of the full nested multiscale model system (3.2.3.1) more difficult to perform. However, the analysis of the multiscale model system (3.2.3.1) can be simplified by expressing the slow

time-scale and the fast time-scale in terms of each other by using the relationship $t = \epsilon\tau$, where $0 < \epsilon << 1$ and ϵ being a constant highlighting the fast time-scale dynamics of the within-host model compared to the slow time-scale of the between-host scale dynamics, so that the full nested multiscale model system (3.2.3.1) becomes:

$$
\begin{cases}
i.\ \dfrac{dS_C(t)}{dt} &= \Lambda_C - \dfrac{\beta_C B_C(t)}{B_0 + B_C(t)} S_C(t) - \mu_C S_C(t), \\
ii.\ \dfrac{dI_C(t)}{dt} &= \dfrac{\beta_C B_C(t)}{B_0 + B_C(t)} S_C(t) - (\mu_C + \delta_C) I_C(t), \\
iii.\ \dfrac{dB_C(t)}{dt} &= \alpha_c B_c(t) I_C(t) - \alpha_C B_C(t), \\
iv.\ \epsilon\dfrac{dM_\phi(t)}{dt} &= \Lambda_\phi - \beta_\phi M_\phi(t) B_c(t) - \mu_\phi M_\phi(t) \\
v.\ \epsilon\dfrac{dI_m(t)}{dt} &= \beta_\phi M_\phi(t) B_c(t) - \gamma_m T_1(t) I_m(t) \\
&\quad -(k_m + \mu_\phi) I_m(t) \\
vi.\ \epsilon\dfrac{dB_c(t)}{dt} &= N_m k_m I_m(t) - (\mu_c + \alpha_c) B_c(t) \\
vii.\ \epsilon\dfrac{dT_0(t)}{dt} &= \Lambda_0 - (\delta_m I_m(t) + \delta_b B_c(t)) T_0(t) \\
&\quad -\mu_0 T_0(t) \\
viii.\ \epsilon\dfrac{dT_1(t)}{dt} &= \theta_1 \delta_m I_m(\tau) T_0(\tau) - \mu_1 T_1(t) \\
ix.\ \epsilon\dfrac{dT_2(t)}{dt} &= \theta_2 \delta_b B_c(t) T_0(t) - \mu_2 T_2(t).
\end{cases}
\tag{3.2.4.1}
$$

In the next two sub-sections, we assessed through numerical simulations of the full nested multi-scale model system given by equation (3.2.4.1) the reciprocal influence between the between-host scale and the within-host scale dynamics of PTB infection. We achieved this by demonstrating (i) the influence of the between-host scale on the within-host scale through the initial infective inoculum that susceptible ruminants may acquire by interacting with MAP bacteria in contaminated environment, and (ii) the influence of the within-host scale parameters on the between-host

disease dynamics. The parameter values used for simulations are tabulated in Table 3.1. In addition, initial values used for simulations for the full nested multiscale model system (3.2.4.1) are as follows: $S_C(0) = 2000$, $I_C(0) = 5$, $B_c(0) = 10$, $M_\phi(0) = 500$, $I_m(0) = 0$, $T_0(0) = 0$, $T_1(0) = 0$, $T_2(0) = 0$, $B_C(0) = 1000$.

Parameter	Description	Unit	Initial value	Source
Λ_C	Ruminants birth rate	day^{-1}	0.27	[52, 54]
β_C	Ruminant infection rate	day^{-1}	0.00027	Assumed
μ_C	Death rate of Ruminants	day^{-1}	0.0001	[52]
δ_C	Ruminant removal rate due to PTB infection	day^{-1}	0.0008	Assumed
α_C	Environmentally bacteria death rate	day^{-1}	0.0018	[52]
B_0	Saturation rate of Bacteria	day^{-1}	1000	[54]
Λ_ϕ	Macrophages supply rate	day^{-1}	10	[53]
β_ϕ	Macrophages infection rate	day^{-1}	0.002	[53]
μ_ϕ	Macrophages natural death rate	day^{-1}	0.02	[53]
N_m	Burst size of intracellular MAP bacteria	day^{-1}	100	[53]
k_m	Burst rate of infected macrophages	day^{-1}	0.00075	[53]
γ_m	T_1 lytic effect	day^{-1}	0.01	[53]
μ_c	Bacteria's death rate	day^{-1}	0.03	[53]
α_c	Excretion rate of extracellular MAP bacteria	day^{-1}	0.01	[54]
Λ_0	T_0 supply rate	day^{-1}	0.001	[53]
μ_0	T_0 death rate	day^{-1}	0.01	[53]
μ_1	T_1 death rate	day^{-1}	0.03	[53]
μ_2	T_2 death rate	day^{-1}	0.02	[53]
δ_m	T_0 differentiation into T_1 cells	day^{-1}	0.01	[53]
δ_b	T_0 differentiation into T_2 cells	day^{-1}	0.01	[53]
θ_1	T_1 cells clonal expansion	day^{-1}	9000	[53]
θ_2	T_2 cells clonal expansion	day^{-1}	9000	[53]

Table 3.1: Model parameter values associated with the within-host scale and between-host scale dynamics of Paratuberculosis

3.2.4.1 The influence of initial inoculum on the within-host scale of PTB infection dynamics

In this subsection, we demonstrate through numerical simulations of the full nested multiscale model system (3.2.4.1) the influence of between-host scale dynamics on within-host scale variables for PTB infection dynamics. This is achieved by varying the initial value condition of the infective inoculum $B_c(0)$ that susceptible ruminants may acquire by interacting with MAP bacteria in contaminated environment for different values and assess its impact on the dynamics of four selected key within-host variables, I_m, B_c, T_1 and T_2. The results of the influence of between-host scale dynamics on the within-host scale variables for the PTB infection are as follows:

a. Fig. 3.2 shows the effect of varying $B_c(0)$ for different values on the within-host variables (I_m, B_c, T_1, T_2). $B_c(0)$: $B_c(0) = 10$, $B_c(0) = 100$, and $B_c(0) = 1000$.

b. Fig 3.3 also shows the effect of varying $B_c(0)$ for different values on the within-host variables (I_m, B_c, T_1, T_2). $B_c(0)$: $B_c(0) = 1000$, $B_c(0) = 10000$, and $B_c(0) = 100000$.

c. Fig 3.4 further shows the effect of varying $B_c(0)$ for different values on the within-host variables (I_m, B_c, T_1, T_2). $B_c(0)$: $B_c(0) = 1000000$, $B_c(0) = 10000000$, and $B_c(0) = 100000000$.

Collectively, from all these three sets of numerical results in Fig. 3.2, Fig. 3.3, and Fig. 3.4, we notice that as the initial infective inoculum $B_c(0)$ increases beyond the minimum infectious dose (MID), there is a noticeable but minimal changes in the dynamics of the within-host scale variables I_m, B_c, T_1, T_2. This is because, once the host is infected, the replication of the MAP bacteria at the within-host scale sustains the disease dynamics at this scale.

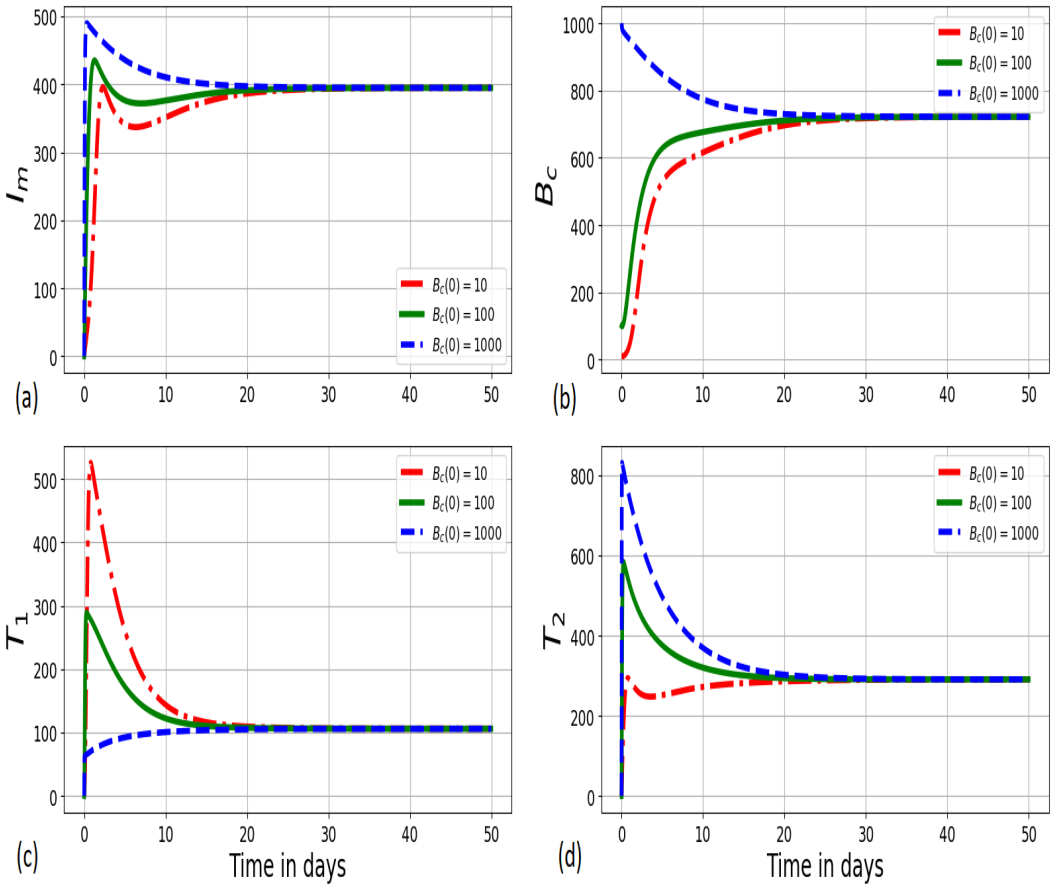

Figure 3.2: *Graphs of numerical solutions of the multiscale model system (3.2.4.1) showing evolution of (a) infected macrophage population (I_m), (b) within-host MAP bacteria population (B_c), (c) MAP-Specific Th1 response cells (T_1), and (d) MAP-Specific Th2 response cells (T_2) for different values of initial value condition of the within-host MAP bacterial load $B_c(0)$: $B_c(0) = 10$, $B_c(0) = 100$, and $B_c(0) = 1000$.*

Fig. 3.2 shows the solution profile of the population of (a) infected macrophage population (I_m), (b) within-host MAP bacteria population (B_c), (c) MAP-Specific Th1 response cells (T_1), and (d) MAP-Specific Th2 response cells for different initial values of the within-host MAP bacterial load $B_c(0)$: $B_c(0) = 10$, $B_c(0) = 100$, and $B_c(0) = 1000$. The results in Fig. 3.2 illustrate that when the initial inoculum vary from $B_c(0) = 10$, $B_c(0) = 100$, and $B_c(0) = 1000$ this only affect the dynamics of the disease at the within-host scale within the first 20 days. However, after that there is no different in the dynamics of the disease. This implies that different initial inoculum values converge to the same endemic state after a period of about 20 days. Therefore, these results confirm that once the minimum infectious dose is consumed, the long term disease dynamics is independent of the initial inoculum.

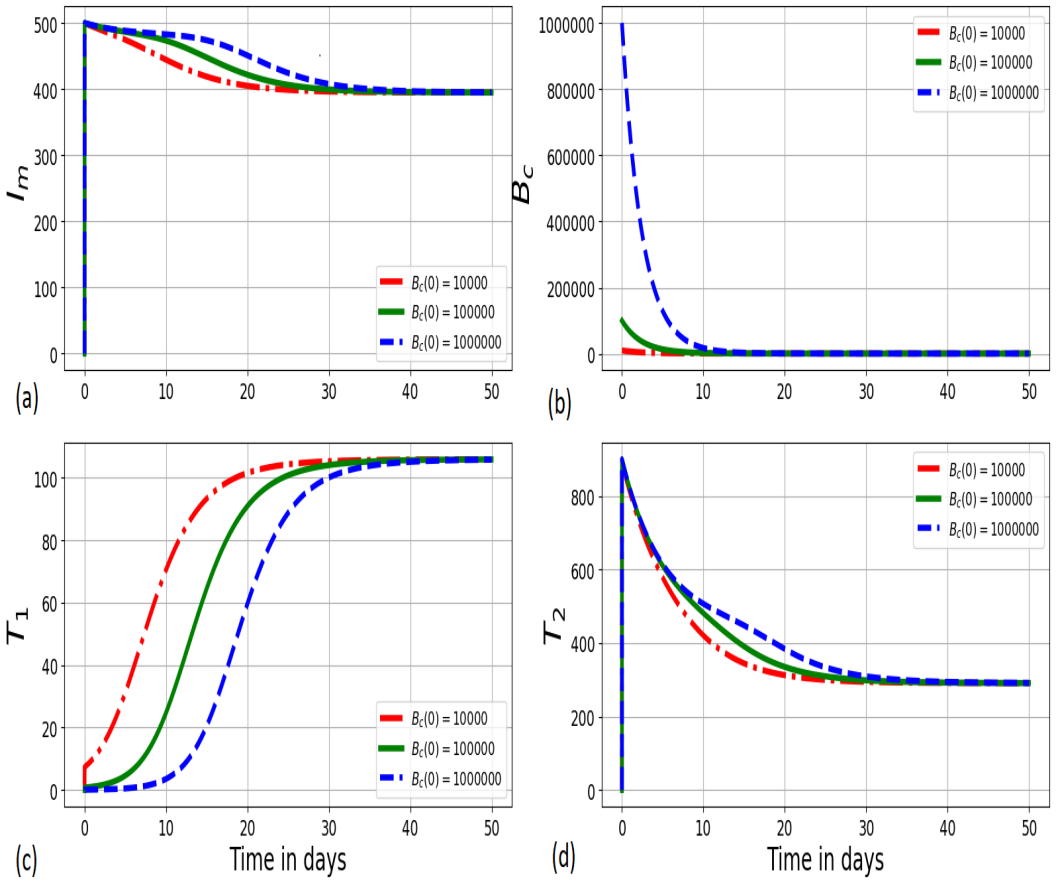

Figure 3.3: *Graphs of numerical solutions of the multiscale model system (3.2.4.1) showing propagation of (a) infected macrophage population (I_m), (b) within-host MAP bacteria population (B_c), (c) MAP-Specific Th1 response cells (T_1), and (d) MAP-Specific Th2 response cells (T_2) for different values of initial value condition of the within-host MAP bacterial load $B_c(0)$:* $B_c(0) = 1000$, $B_c(0) = 10000$, *and* $B_c(0) = 100000$.

Fig. 3.3 shows the solution profile of the population of (a) infected macrophage population (I_m), (b) within-host MAP bacteria population (B_c), (c) MAP-Specific Th1 response cells (T_1), and (d) MAP-Specific Th2 response cells for different values of initial value condition of the within-host MAP bacterial load $B_c(0)$: $B_c(0) = 10$, $B_c(0) = 100$, and $B_c(0) = 1000$. The results in Fig. 3.3 illustrate that when the initial inoculum vary from $B_c(0) = 1000$, $B_c(0) = 10000$, and $B_c(0) = 100000$ this only affects the dynamics of the disease at the within-host scale within the first 30 days. However, after that there is also no different in the dynamics of the disease. This also implies that different initial inoculum values converge to the same endemic state after a period of about 30 days. Therefore, these results also confirm that once the minimum infectious dose is consumed, the long term disease dynamics is independent of the initial inoculum.

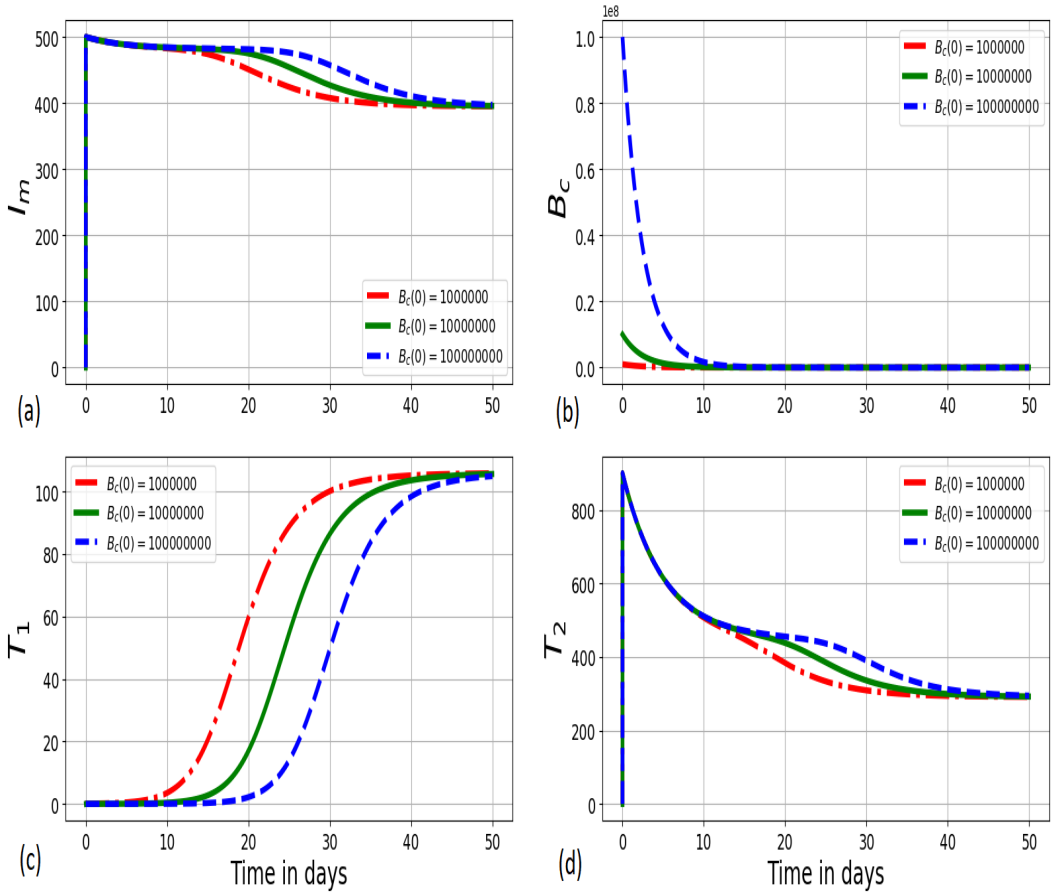

Figure 3.4: *Graphs of numerical solutions of the multiscale model system (3.2.4.1) showing changes of (a) infected macrophage population (I_m), (b) within-host MAP bacteria population (B_c), (c) MAP-Specific Th1 response cells (T_1), and (d) MAP-Specific Th2 response cells (T_2) for different values of initial value condition of the within-host MAP bacterial load $B_c(0)$: $B_c(0) = 1000000$, $B_c(0) = 10000000$, and $B_c(0) = 100000000$.*

Fig 3.4 shows the solution profiles of the population of (a) infected macrophage population (I_m), (b) within-host MAP bacteria population (B_c), (c) MAP-Specific Th1 response cells (T_1), and (d) MAP-Specific Th2 response cells for different values of initial inoculum of MAP bacterial load $B_c(0)$: $B_c(0) = 10$, $B_c(0) = 100$, and $B_c(0) = 1000$ at within-host scale. The results in Figure (3.4) also illustrate that the variation in the initial inculom from $B_c(0) = 1000000$, $B_c(0) = 10000000$, and $B_c(0) = 100000000$ influence with the dynamics of the disease at the within-host scale between 20 and 50 days. However, after that the dynamics of the disease reach an endemic level. Similarly, this also implies that different initial inoculum values converge to the same endemic state after a period of about 50 days. In the same way as the results in Fig. 3.2 and Fig. 3.3, these results also confirm that once the minimum infectious dose is consumed, the long term disease dynamics is independent of the initial inoculum. However, the all the three

figures confirm (i.e. Fig. 3.2, Fig. 3.3 and Fig. 3.4) that as the initial inoculum increases, the time to reach the endemic state also increases.

3.2.4.2 The influence of initial inoculum on the between-host scale of PTB infection dynamics

In this subsection, we investigated through numerical simulations of the full nested multiscale model system (3.2.4.1) the influence of initial inoculum on between-host scale variables for PTB infection dynamics. This is achieved by varying the initial value condition of the infective inoculum $B_c(0)$ that susceptible ruminants may acquire by interacting with MAP bacteria in contaminated environment for different values and assess its impact on the dynamics of all the three between-host variables: S_C, I_C, and B_C. The results of the influence of initial inoculum on the between-host scale variables for the PTB infection are as follows:

a. Fig. 3.5 shows the effect of varying $B_c(0)$ for different values on the between-host variables (S_C, I_C, B_C). $B_c(0)$: $B_c(0) = 10$, $B_c(0) = 100$, and $B_c(0) = 1000$.

b. Fig. 3.6 also shows the effect of varying $B_c(0)$ for different values on the between-host variables (S_C, I_C, B_C). $B_c(0)$: $B_c(0) = 1000$, $B_c(0) = 10000$, and $B_c(0) = 100000$.

c. Fig. 3.7 again shows the effect of varying $B_c(0)$ for different values on the between-host variables (S_C, I_C, B_C). $B_c(0)$: $B_c(0) = 1000000$, $B_c(0) = 10000000$, and $B_c(0) = 100000000$.

Collectively, from all these three sets of numerical results in Fig. 3.5, Fig. 3.6, and Fig. 3.7, we notice the same trends that as the initial value of the infective inoculum $B_c(0)$ increases beyond the minimum infectious dose (MID), there is a noticeable but minimal changes in the dynamic of the between-host scale variables S_C, I_C, B_C.

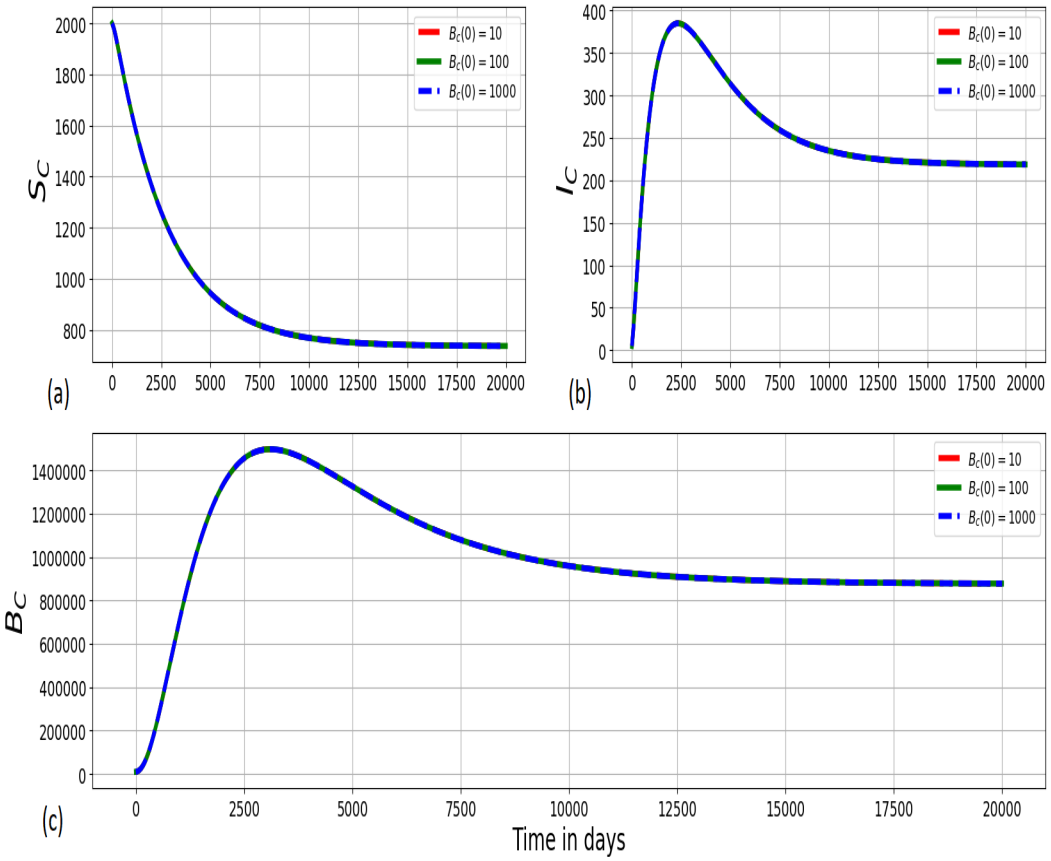

Figure 3.5: *Graphs of numerical solutions of the multiscale model system (3.2.4.1) showing evolution of (a) population of susceptible ruminants (S_C), (b) population of infected ruminants (I_C), and (c) between-host MAP bacterial load (B_C) for different values of initial value of the within-host MAP bacterial load $B_c(0)$: $B_c(0) = 10$, $B_c(0) = 100$, and $B_c(0) = 1000$.*

Fig. 3.5 shows graphs of numerical solutions of the model system (3.2.4.1) showing dynamics of (a) population of susceptible ruminants (S_C), (b) population of infected ruminants (I_C), and (c) environmental MAP bacteria load (B_C) for different values of initial value of the within-host MAP bacterial load $B_c(0)$: $B_c(0) = 10$, $B_c(0) = 100$, and $B_c(0) = 1000$. The results in Fig. 3.5 show that an increase in the initial inoculum from $B_c(0) = 10$ to $B_c(0) = 1000$ makes no different in the transmission dynamics of the disease at the between-host scale as the between-host scale variables (S_C, I_C, B_C) remain constant as the initial inoculum changes.

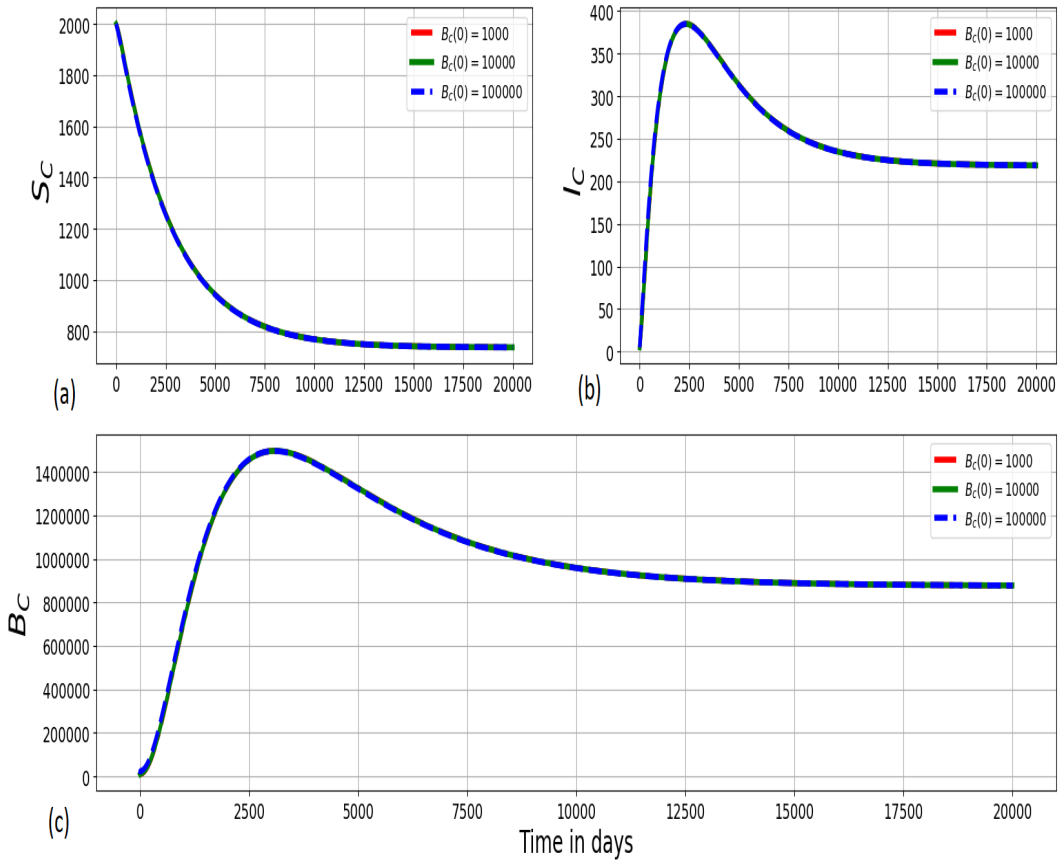

Figure 3.6: *Graphs of numerical solutions of the multiscale model system (3.2.4.1) showing propagation of (a) population of susceptible ruminants (S_C), (b) population of infected ruminants (I_C), and (c) between-host MAP bacterial load (B_C) for different values of initial value of the within-host MAP bacterial load $B_c(0)$: $B_c(0) = 1000$, $B_c(0) = 10000$, and $B_c(0) = 100000$.*

Fig. 3.6 shows graphs of numerical solutions of the model system (3.2.4.1) showing dynamics of (a) population of susceptible ruminants (S_C), (b) population of infected ruminants (I_C), and (c) environmental MAP bacteria load (B_C) for different values of initial value condition of the within-host MAP bacterial load $B_c(0)$: $B_c(0) = 1000$, $B_c(0) = 10000$, and $B_c(0) = 100000$. The results in Fig. 3.6 show that an increase in the initial inculum from $B_c(0) = 1000$ to $B_c(0) = 100000$ also makes no different in the transmission dynamics of the disease at the between-host scale as the between-host scale variables (S_C, I_C, B_C) remain constant as the initial inoculum changes.

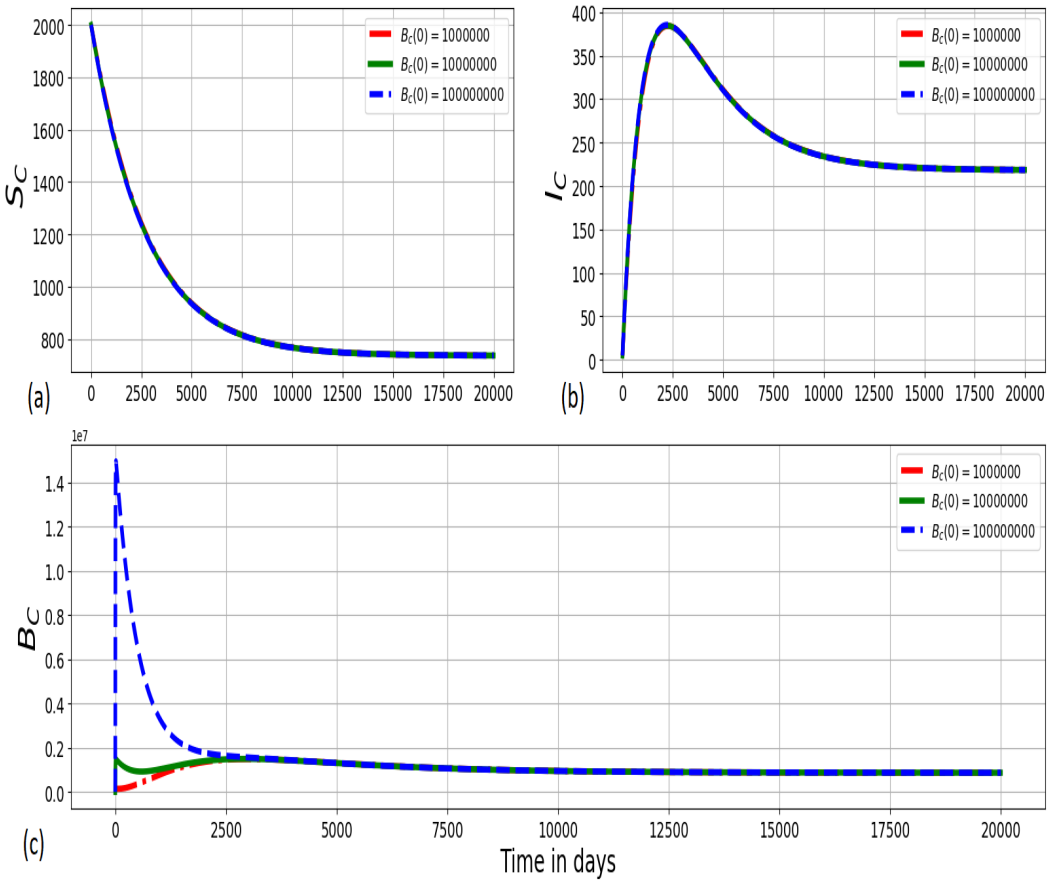

Figure 3.7: *Graphs of numerical solutions of the multiscale model system (3.2.4.1) showing changes of (a) population of susceptible ruminants (S_C), (b) population of infected ruminants (I_C), and (c) between-host MAP bacterial load (B_C) for different values of initial value of the within-host MAP bacterial load $B_c(0)$: $B_c(0) = 1000000$, $B_c(0) = 10000000$, and $B_c(0) = 100000000$.*

Fig. 3.7 shows graphs of numerical solutions of the model system (3.2.4.1) showing dynamics of (a) population of susceptible ruminants (S_C), (b) population of infected ruminants (I_C), and (c) environmental MAP bacteria load (B_C) for different values of initial value of the within-host MAP bacterial load $B_c(0) = 1000000$, $B_c(0) = 10000000$, and $B_c(0) = 100000000$. The results in Fig. 3.7 show that an increase in the initial inculum from $B_c(0) = 1000$ to $B_c(0) = 100000$ only associated with the increase in the between-host scale MAP bacteria within the first 2500 days as both the susceptable and infected ruminants remain constant with the increase in the initial inoculum.

3.2.4.3 The influence of within-host scale parameters on the between-host scale PTB infection dynamics

In this subsection, we illustrate through numerical simulations of the full nested multiscale model system (3.2.4.1) the influence of within-host scale parameters on between-host scale variables for PTB infection dynamics. We vary the within-host scale parameters, α_c, μ_c and N_m and assess their impact on the dynamics of the between-host scale variables.

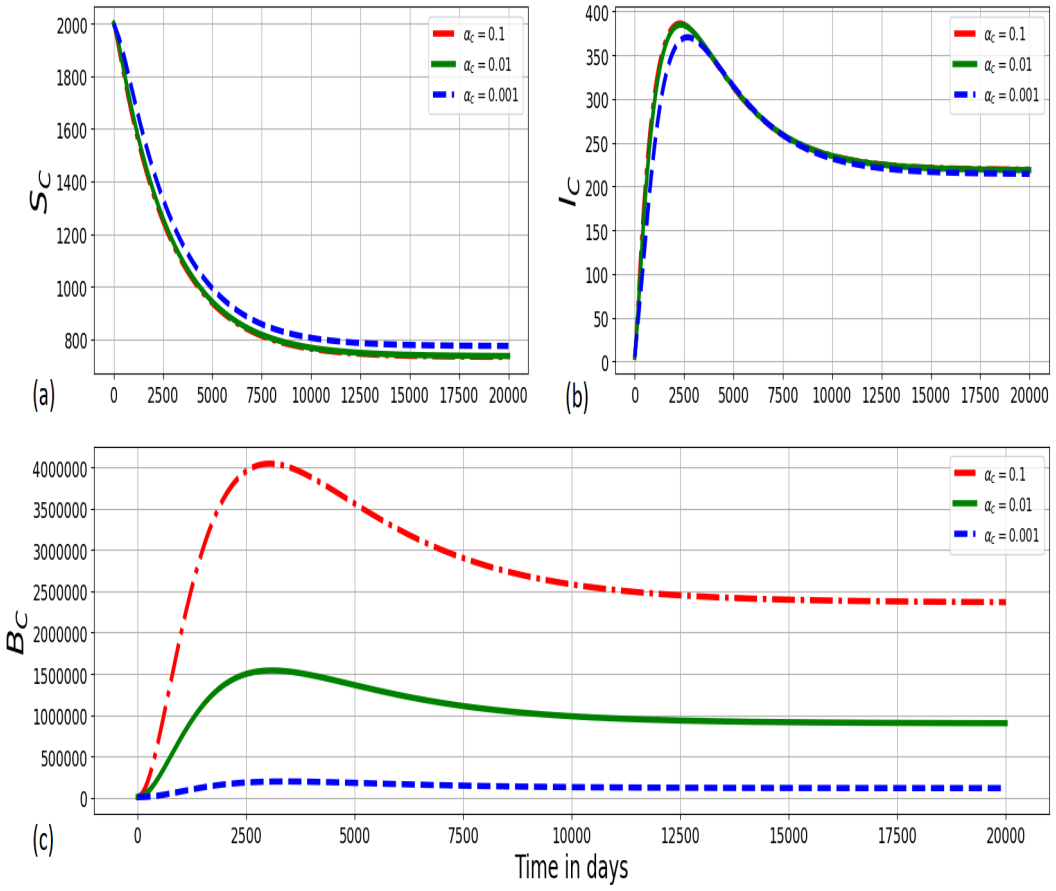

Figure 3.8: *Graphs of numerical solutions of the multiscale model system (3.2.4.1) showing the evolution in time of (a) population of susceptible ruminants (S_C), (b) population of infected ruminants (I_C), and (c) between-host MAP bacterial load (B_C) for different values of excretion rate of the within-host MAP bacterial load into the environment α_c: $\alpha_c = 0.1$, $\alpha_c = 0.01$, and $\alpha_c = 0.001$.*

Fig. 3.8 shows graphs of numerical solutions of the model system (3.2.4.1) showing dynamics of (a) population of susceptible ruminants (S_C), (b) population of infected ruminants (I_C), and (c) environmental MAP bacteria load (B_C) for different values of excretion rate of the within-host scale MAP bacilli into the environment α_c: $\alpha_c = 0.1$, $\alpha_c = 0.01$, and $\alpha_c = 0.001$. The

results show that an increase in the excretion rate of the within-host scale bacterial load into the physical environment by each infected ruminant individual has important public health effects at the between-host scale dynamics of PTB infection as there is a noticeable increase in the population of environmental MAP bacteria B_C and the population of infected ruminants I_C as well as a decrease in the population of susceptible ruminants S_C.

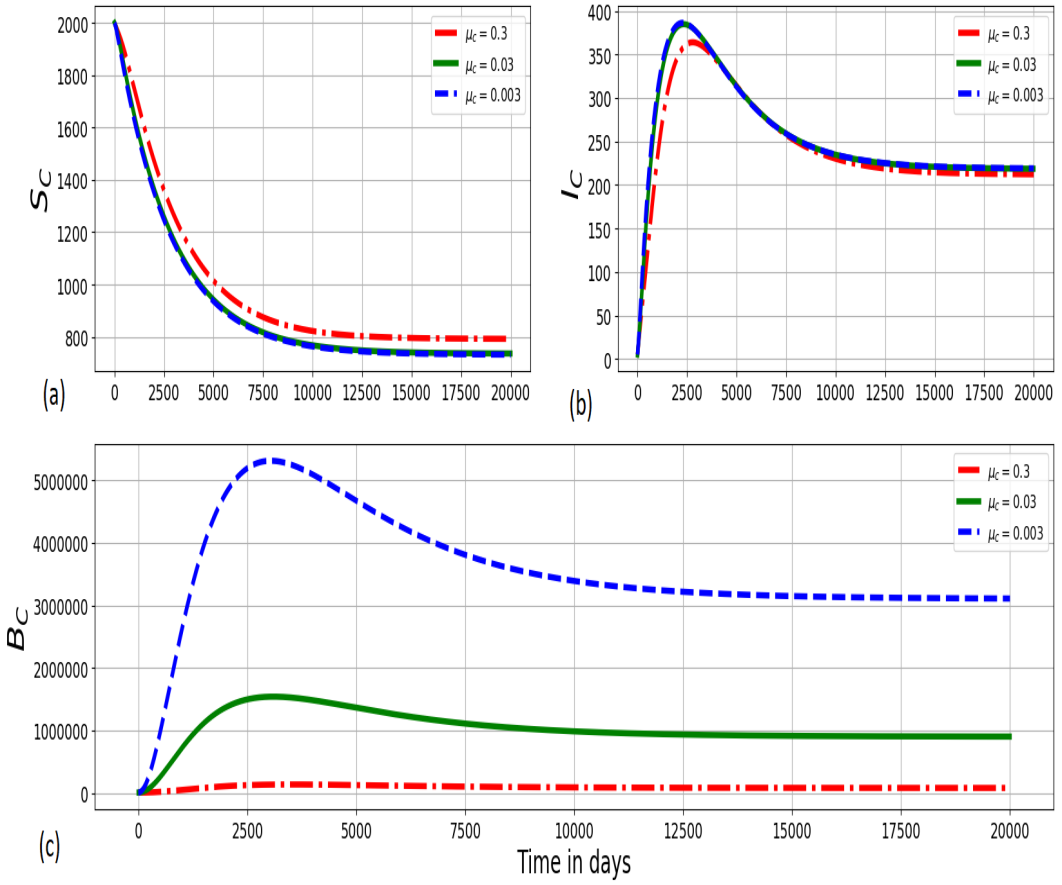

Figure 3.9: *Graphs of numerical solutions of the multiscale model system(3.2.4.1) showing changes in (a) population of susceptible ruminants (S_C), (b) population of infected ruminants (I_C), and (c) population of environmental MAP bacterial load (B_C) for different values of death rate of the within-host MAP bacterial load μ_b: $\mu_c = 0.3$, $\mu_c = 0.03$, and $\mu_c = 0.003$.*

Fig. 3.9 shows changes in (a) population of susceptible ruminants (S_C), (b) population of infected ruminants (I_C), and (c) population of environmental MAP bacteria load (B_C) for different values of natural decay rate of the within-host scale MAP bacteria cells: μ_c: $\mu_c = 0.3$, $\mu_c = 0.03$, and $\mu_c = 0.003$. The results in Fig. 3.9 show that as the death rate of the within-host scale bacterial load increases, there is also noticeable reduction in the population of environmental MAP bacteria B_C and the population of infected ruminants I_C as well as an increase in the population of susceptible ruminants S_C at between-host scale. Therefore, any treatment measures

that kills the MAP bacteria at within-host scale are equally good for both the individual ruminant and the population because a single infected ruminant will no longer pose a threat for transmitting infection in the population/herd which consequently reduces the transmission risk of the disease among the ruminants in the population/herd.

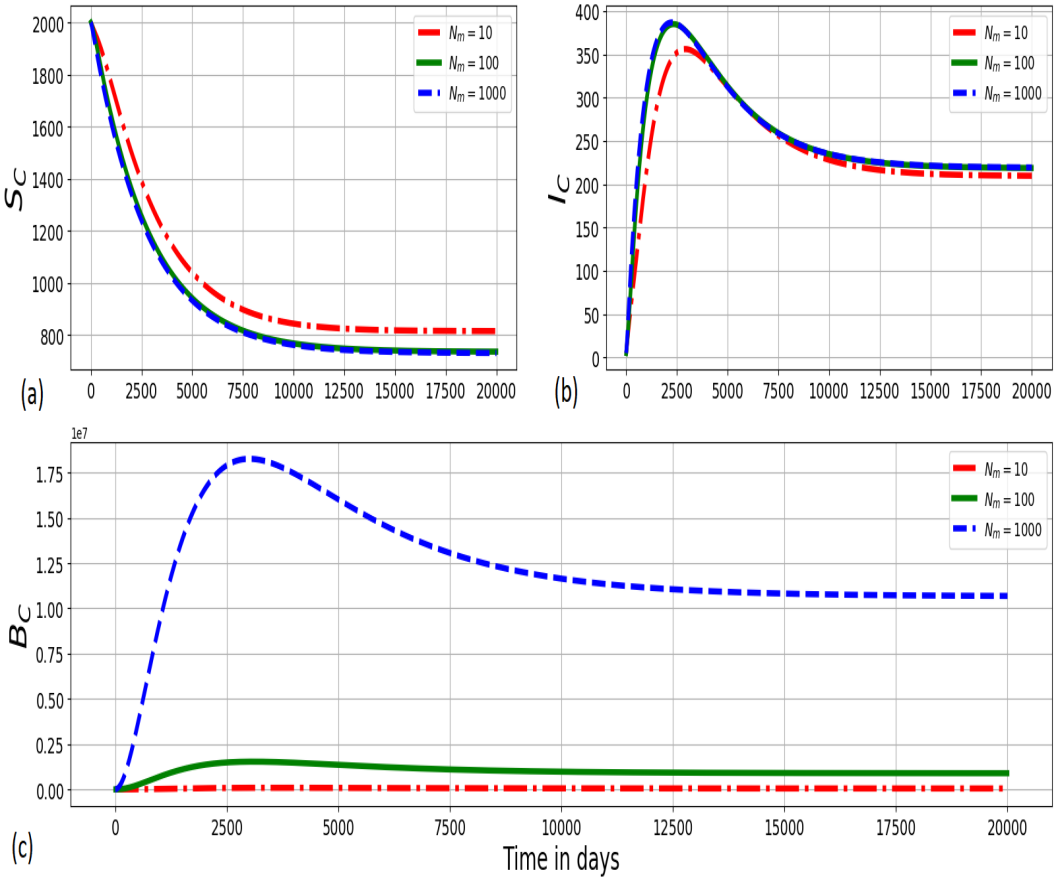

Figure 3.10: *Graphs of numerical solutions of the multiscale model system(3.2.4.1) showing dynamics in (a) population of susceptible ruminants (S_C), (b) population of infected ruminants (I_C), and (c) population of environmental MAP bacterial load (B_C) for different values of within-host scale MAP bacteria produced per bursting infected macrophage cell N_m: $N_m = 100$, $N_m = 1000$, $N_m = 10000$.*

Fig. 3.10 shows the dynamics in the (a) population of susceptible ruminants (S_C), (b) population of infected ruminants (I_C), and (c) population of environmental MAP bacterial load (B_C) for different values of within-host scale bursting size of each infected macrophage cell N_m: $N_m = 100$, $N_m = 1000$, $N_m = 10000$. The numerical results in Fig. 3.10 show that as an average replication rate of the within-host MAP bacteria within infected macrophage cells at the site of infection increases, transmission of PTB infection at the population/herd level of ruminants also increases. Therefore, these results demonstrate the benefit of treatment that can restrict the

replication of MAP bacteria at individual ruminant level on the transmission of the disease at the population/herd level of ruminants. Collectively, we note from the results in Fig. 3.8 - Fig. 3.10, that the between-host scale variables (S_C, I_C, B_C) are significantly sensitive to the variation of the three selected within-host scale parameters (α_c, μ_c and N_m), particularly the decay rate μ_c of the within-host scale MAP bacteria.

Overall, the results in Fig. 3.5 - Fig. 3.10 show that:

a. The between-host scale influences the within-host scale through the initial inoculum of the infectious agent.

b. Once the initial inoculum has been introduced from the between-host scale, then the infection at within-host scale is sustained by pathogen replication.

c. As the initial inoculum acquired from the between-host scale increases beyond the MID, the time taken for the infection at within-host scale to reach equilibrium increases.

d. The between-host scale variables (S_C, I_C, B_C) are significantly sensitive to the variation of the three selected within-host scale parameters (α_c, μ_c and N_m), particularly the decay rate μ_c of the within-host scale MAP bacteria.

This indeed indicates that during the dynamics for PTB infection in ruminants once the infection has successfully established at the within-host scale, the contribution of initial infective inoculum to the total pathogen load becomes negligible compared to the contribution of the replication-cycle.

3.3 Estimation of $\widehat{N}_c$ from the Full Nested Multiscale Model

In this section, we estimate $\widehat{N}_c$ parameter in the single scale model for the dynamics of PTB infection using the nested multiscale model system (3.2.4.1). This is achieved by assumming that $0 < \epsilon << 1$, so that to reasonable approximation we can set $\epsilon = 0$ in the the full nested multiscale model system (3.2.4.1). Thus, we consider the last six equations of the PTB transmission dynamics multiscale model system (3.2.4.1) re-written here as a quick reference

$$
\begin{cases}
i.\ \epsilon\dfrac{dM_\phi(t)}{dt} &= \Lambda_\phi - \beta_\phi M_\phi(t)B_c(t) - \mu_\phi M_\phi(t), \\
ii.\ \epsilon\dfrac{dI_m(t)}{dt} &= \beta_\phi M_\phi(t)B_c(t) - \gamma_m T_1(t)I_m(t) \\
&\quad -(k_m + \mu_\phi)I_m(t), \\
ii.\ \epsilon\dfrac{dB_c(t)}{dt} &= N_m k_m I_m(t) - (\mu_c + \alpha_c)B_c(t), \\
iv.\ \epsilon\dfrac{dT_0(t)}{dt} &= \Lambda_0 - (\delta_m I_m(t) + \delta_b B_c(t))T_0(t) \\
&\quad -\mu_0 T_0(t), \\
v.\ \epsilon\dfrac{dT_1(t)}{dt} &= \theta_1\delta_m I_m(\tau)T_0(\tau) - \mu_1 T_1(t), \\
vi.\ \epsilon\dfrac{dT_2(t)}{dt} &= \theta_2\delta_b B_c(t)T_0(t) - \mu_2 T_2(t).
\end{cases}
\tag{3.3.1}
$$

Since $0 < \epsilon << 1$, we can set ϵ to zero so that the within-host scale PTB replication dynamics submodel becomes independent of time and we obtain:

$$
\begin{cases}
i. & \Lambda_\phi - \beta_\phi M_\phi^* B_c^* - \mu_\phi M_\phi^* = 0, \\
ii. & \beta_\phi M_\phi^* B_c^* - \gamma_m T_1^* I_m^* - (k_m + \mu_\phi)I_m^* = 0, \\
iii. & N_m k_m I_m^* - (\mu_c + \alpha_c)B_c^* = 0, \\
iv. & \Lambda_0 - (\delta_m I_m^* + \delta_b B_c^*)T_0^* - \mu_0 T_0^* = 0, \\
v. & \theta_1\delta_m I_m^* T_0^* - \mu_1 T_1^* = 0, \\
vi. & \theta_2\delta_b B_c^* T_0^* - \mu_2 T_2^* = 0.
\end{cases}
\tag{3.3.2}
$$

From (3.3.2) we get

$$\begin{cases} i.\ M_{\phi}^{*} &= \dfrac{2\Lambda_{\phi}(\mu_c+\alpha_c)}{\beta_{\phi}N_m k_m M + 2\mu_{\phi}(\mu_c+\alpha_c)}, \\ ii.\ I_m^{*} &= \dfrac{M}{2}, \\ iii.\ B_c^{*} &= \dfrac{N_m k_m M}{2(\mu_c+\alpha_c)}, \\ iv.\ T_0^{*} &= \dfrac{2\Lambda_0(\mu_c+\alpha_c)}{2\mu_0(\mu_c+\alpha_c)+[\delta_m(\mu_c+\alpha_c)+\delta_b N_m k_m]M}, \\ v.\ T_1^{*} &= \dfrac{\theta_1\delta_m\Lambda_0(\mu_c+\alpha_c)M}{2\mu_0\mu_1(\mu_c+\alpha_c)+\mu_1[\delta_m(\mu_c+\alpha_c)+\delta_b N_m k_m]M}, \\ vi.\ T_1^{*} &= \dfrac{\theta_2\delta_b\Lambda_0 N_m k_m M}{2\mu_2\mu_0(\mu_c+\alpha_c)+\mu_2[\delta_m(\mu_c+\alpha_c)+\delta_b N_m k_m]M}. \end{cases} \tag{3.3.3}$$

In the expression (3.3.3),

$$\begin{cases} M &= -\phi_1 + \sqrt{\phi_1^2 + 4\phi_2} \\ \phi_1 &= \dfrac{k_3 + \mu_1\mu_0 k_2 - k_1 Q}{k_2 k_1}, \\ \phi_2 &= \dfrac{\mu_1\mu_0 Q}{k_2 k_1}, \end{cases} \tag{3.3.4}$$

with

$$\begin{cases} Q & = & \mu_\phi(\mu_\phi+\delta_\phi)(R_{0_W}-1), \\ k_1 & = & \dfrac{\mu_1\delta_m(\mu_c+\alpha_c)+\mu_1\delta_b N_m k_m}{(\mu_c+\alpha_c)}, \\ k_2 & = & \dfrac{\beta_\phi N_m k_m(\mu_\phi+k_m)}{(\mu_c+\alpha_c)}, \\ k_3 & = & k_0+\mu_\phi\gamma_m\theta_1\delta_m\Lambda_0, \\ k_0 & = & \dfrac{\beta_\phi N_m k_m\gamma_m\theta_1\delta_m\Lambda_0}{(\mu_c+\alpha_c)}, \\ R_{0_W} & = & \dfrac{\beta_\phi\Lambda_\phi N_m k_m}{\mu_\phi(\mu_\phi+k_m)(\mu_c+\alpha_c)}. \end{cases} \tag{3.3.5}$$

Further, in the expression (3.3.5) the quantity

$$R_{0_W}=\frac{\beta_\phi\Lambda_\phi N_m k_m}{\mu_\phi(\mu_\phi+\delta_\phi)(\mu_c+\alpha_c)},$$

is the within-host scale basic reproductive number. Therefore, the fast-slow analysis reduces the within-host scale submodel system (3.2.2.1) to the algebraic equations given in (3.3.3) which can be fed into the parameters of the between-host scale submodel and become

$$\begin{cases} i.\ \dfrac{dS_C(t)}{dt} & = & \Lambda_C-\dfrac{\beta_C B_C(t)}{B_0+B_C(t)}S_C(t)-\mu_C S_C(t), \\ ii.\ \dfrac{dI_C(t)}{dt} & = & \dfrac{\beta_C B_C(t)}{B_0+B_C(t)}S_C(t)-(\mu_C+\delta_C)I_C(t), \\ iii.\ \dfrac{dB_C(t)}{dt} & = & \alpha_c B_c^* I_C(t)-\alpha_C B_C(t). \end{cases} \tag{3.3.6}$$

We note that from the model system given by (3.3.6) that the total number of extracellular MAP bacilli excreted by each infected ruminant into the physical environment $B_c I_C$ is now approximated by $B_c^* I_C$. Using the notation that $N_c = B_c^*$, a composite parameter which can be interpreted as the average number of the within-host scale MAP bacterial load (B_c) at the endemic equilibrium that is available for excretion into the environment by each infected ruminant, the

full multiscale model (3.2.3.1) of PTB transmission dynamics is simplified to become

$$\begin{cases} i. \ \dfrac{dS_C(t)}{dt} &= \Lambda_C - \dfrac{\beta_C B_C(t)}{B_0 + B_C(t)} S_C(t) - \mu_C S_C(t), \\ ii. \ \dfrac{dI_C(t)}{dt} &= \dfrac{\beta_C B_C(t)}{B_0 + B_C(t)} S_C(t) - (\mu_C + \delta_C) I_C(t), \\ iii. \ \dfrac{dB_C(t)}{dt} &= N_c \alpha_c I_C(t) - \alpha_C B_C(t) \end{cases} \tag{3.3.7}$$

where the composite parameter N_c which estimates $\widehat{N}_c$ is given by

$$N_c = \frac{N_m k_m}{2(\mu_c + \alpha_c)} \left[-\phi_1 + \sqrt{\phi_1^2 + 4\phi_2} \right]. \tag{3.3.8}$$

In the expression for N_c given by equation (3.3.8),

$$\begin{cases} \phi_1 &= \dfrac{k_3 + \mu_1 \mu_0 k_2 - k_1 Q}{k_2 k_1}, \\ \phi_2 &= \dfrac{\mu_1 \mu_0 Q}{k_2 k_1} \end{cases} \tag{3.3.9}$$

with

$$\begin{cases} Q &= \mu_\phi(\mu_\phi + \delta_\phi)(R_{0_W} - 1), \\ k_1 &= \dfrac{\mu_1 \delta_m(\mu_c + \alpha_c) + \mu_1 \delta_b N_m k_m}{(\mu_c + \alpha_c)}, \\ k_2 &= \dfrac{\beta_\phi N_m k_m (\mu_\phi + k_m)}{(\mu_c + \alpha_c)}, \\ k_3 &= k_0 + \mu_\phi \gamma_m \theta_1 \delta_m \Lambda_0, \\ k_0 &= \dfrac{\beta_\phi N_m k_m \gamma_m \theta_1 \delta_m \Lambda_0}{(\mu_c + \alpha_c)}, \\ R_{0_W} &= \dfrac{\beta_\phi \Lambda_\phi N_m k_m}{\mu_\phi(\mu_\phi + k_m)(\mu_c + \alpha_c)}. \end{cases} \tag{3.3.10}$$

Based on the categorization of the multiscale models of infectious disease systems in [19, 20], the multiscale model system given by (3.3.7) is a nested multiscale model of class 3. After

estimating $\widehat{N}_c$ as well as establishing the simplified nested multiscale model system given by (3.3.7), we now analyze the behavior of this nested multiscale model system (3.3.7). In the next section we present some results from mathematical analysis and numerical simulations of the behaviour of the simplified nested multiscale model (3.3.7).

3.4 Mathematical Analysis of the Simplified Nested Multiscale Model For PTB Infection in Ruminants

The PTB dynamics multiscale model system (3.3.7) can be analyzed in a region $\Gamma \subset \mathbb{R}^3_+$ of biological interest, which is given by

$$\begin{aligned} \Gamma &= \{(S_C; I_C; B_C) \in \mathbb{R}^3_+ : \\ &\quad 0 \leq S_C + I_C \leq S_1,\ 0 \leq B_C \leq S_2\} \end{aligned} \tag{3.4.1}$$

where the constant S_1 and S_2 are such that

$$\begin{cases} S_1 = \dfrac{\Lambda_C}{\mu_C}, \\ S_2 = \dfrac{N_c \alpha_c \Lambda_C}{\alpha_C \mu_C}. \end{cases} \tag{3.4.2}$$

It can be easily shown that all solutions for the simplified multiscale model system (3.3.7) with positive initial conditions remain bounded within the invariant region Γ given by (3.4.1). Therefore, it is sufficient to consider the dynamics of the flow generated by the simplified nested model system (3.3.7) in Γ.

In the following three subsections, we evaluate global stability of both the disease-free and endemic equilibrium states for the PTB dynamics multiscale model system (3.3.7) as well as evaluating sensitivity of the two main between-host transmission metrics which are the basic reproductive number (R_0) and the endemic value of the nested multiscale model (3.3.7) MAP bacteria (B^*_C).

3.4.1 Disease-free equilibrium and reproductive number of the simplified nested multiscale model for PTB infection in ruminants

The disease-free equilibrium of the nested multiscale model system (3.3.7) was obtained by setting the left-hand side of the model to zero and further assume that $I_C = B_C = 0$ to get

$$\widehat{E}_0 = (X^*, 0) = \left(\frac{\Lambda_C}{\mu_C}, 0, 0\right), \tag{3.4.1.1}$$

where $\widehat{E}_0$ denotes the disease-free equilibrium of the nested multiscale model system (3.3.7).

3.4.1.1 Derivation of the reproductive number of the simplified multiscale model for PTB infection in ruminants

The basic reproduction number denoted by R_0, is a threshold value that is often used as a public health measure to determine whether a disease will persist or die out. In this study, we computed the basic reproductive number of the simplified multiscale model system (3.3.7) by using the next generation operator approach in [5] to obtain

$$R_0 = \frac{\beta_C \Lambda_C N_c \alpha_c}{\mu_C(\mu_C + \delta_C) B_0 \alpha_C} \tag{3.4.1.1.1}$$

which can be re-written as

$$R_0 = R_{0_a} R_{0_b} \tag{3.4.1.1.2}$$

where the quantity R_{0_a} is explained as follows:

a. Consider a single newly infected ruminant entering a contaminated-free environment at an equilibrium point. The expected number of bacteria cells produced by this ruminant and contaminate the environment is approximately

$$R_{0_a} = \frac{N_c \alpha_c}{\mu_C(\mu_C + \delta_C)}. \tag{3.4.1.1.3}$$

From the expression (3.4.1.1.3) we deduce that the quantity R_{0_a} depends on the average MAP bacterial load within an infected ruminant N_c which is excreted into the physical environment at a rate α_c , where it becomes infectious to other ruminants during feeding from contaminated food or water with MAP bacterial load. In this study, we consider N_c as a composite parameter which is interpreted as the endemic value of the within-host

scale MAP bacterial load B_c^* which we have already determined from the within-host PTB disease dynamics sub-model as given in equation (3.3.8). Therefore, the quantity R_{0_a} quantifies how much an infected ruminant can contribute to the spread of the disease in the herd during its entire period of infectiousness, with $1/(\mu_C + \delta_C)$ describes the average life span of an infected ruminant.

b. Similarly, consider a newly bacterial infectious dose of MAP bacilli cells entering a disease-free population of a ruminant population at an equilibrium point. The expected number of ruminants infected by this dose of bacteria cells is approximately

$$R_{0_b} = \frac{\beta_C \Lambda_C}{\alpha_C B_0}. \tag{3.4.1.1.4}$$

We can also deduce that the quantity R_{0_b} in (3.4.1.1.4) depends on the supply rate of susceptible ruminants Λ_C, the rate at which susceptible ruminants contract MAP bacteria in the physical environment domains during feeding β_C, the average life span of each susceptible ruminant host $1/\mu_C$, the average life span of MAP bacteria load in the physical environment domains and the susceptibility coefficient to PTB infection in the ruminant community/herd, where B_0 is the bacterial load that results in 50% chance of the people being infected.

Collectively, based on the two expressions R_{0_a} and R_{0_b}, we conclude that the epidemiological (between-host scale) transmission parameters and the immunological (within-host scale) parameters all contribute to the transmission of ruminant paratuberculosis disease.

3.4.1.2 Global stability of the disease-free equilibrium

In this subsection, we determine the global stability of DFE of the simplified multiscale model system (3.3.7) by using a next generation operator [5] as in **Chapter 2**. Thus the system (3.3.7) can be re-written in the form

$$\begin{cases} \dfrac{dX}{dt} &= F(X, Z), \\ \dfrac{dZ}{dt} &= G(X, Z), \end{cases} \tag{3.4.1.2.1}$$

where

- $X = S_C$ represents a compartment of uninfected ruminants, and

- $Z = (I_C, B_C)$ represents compartments of infected ruminants and Infective MAP bacteria in the physical environment.

We let

$$E_0 = (X^*, 0) = \left(\frac{\Lambda_C}{\mu_C}, 0, 0\right), \tag{3.4.1.2.2}$$

denote the disease-free equilibrium (DFE) of the model system (3.3.7). For X^* to be globally asymptotically stable, the following conditions (H1) and (H2) must be satisfied.

H1. $\frac{dX}{dt} = F(X, 0)$ is globally asymptotically stable (g.a.s),

H2. $G(X, Z) = AZ - \hat{G}(X, Z)$, $\hat{G}((X, Z) \geq 0$ for $(X, Z) \in \mathbb{R}^3_+$ where $A = D_Z G(X^*, 0)$ is an M-matrix and $\mathbb{R}^3_+$ is the region where the model makes biological sense.

In this case,

$$F(X, 0) = \left[\ \Lambda_C - \mu_C S_C\ \right], \tag{3.4.1.2.3}$$

and the matrix A is given by

$$A = \begin{bmatrix} -(\mu_C + \delta_C) & \frac{\beta_C \Lambda_C}{\mu_C B_0} \\ N_c \alpha_c & -\alpha_C \end{bmatrix} \tag{3.4.1.2.4}$$

and

$$\hat{G}(X, Z) = \begin{bmatrix} \left(\frac{\Lambda_C}{\mu_C B_0} - \frac{S_C}{B_0 + B_C}\right) \beta_C B_C \\ 0 \end{bmatrix}. \tag{3.4.1.2.5}$$

Since $S_C^0 = \frac{\Lambda_C}{\mu_C B_0} \geq \frac{S_C}{B_0 + B_C}$, it is clear that $\hat{G}(X, Z) \geq 0$ for all $(X, Z) \in \mathbb{R}^3_+$. It is also clear that A is a M-matrix, since the off diagonal elements of A are non-negative. We state a theorem which summarizes the above results.

Theorem 3.1. *The fixed point*

$$E_0 = (X^*, 0) = \left(\frac{\Lambda_C}{\mu_C}, 0, 0\right)$$

of the multiscale model system (3.3.7) is globally asymptotically stable (GAS) if $R_0 \leq 1$ *and the assumptions* $(H1)$ *and* $(H2)$ *are satisfied.*

3.4.2 Endemic Equilibrium and its Global Stability

In ths subsection, we determine the endemic equilibrium state of the simplified nested multiscale model system (3.3.7) by setting the left-hand side of the simplified nested multiscale model system (3.3.7) to zero but assuming that I_C and B_C are non-zero, so that

$$E^* = (S_C^*, I_C^*, B_C^*) \tag{3.4.2.1}$$

where

$$\begin{cases} S_C^* &= \dfrac{\Lambda_C(\mu_C[R_0 - 1] + (\beta_C + \mu_C))}{(\beta_C + \mu_C)\mu_C R_0}, \\ I_C^* &= \dfrac{\beta_C \Lambda_C [R_0 - 1]}{(\mu_C + \delta_C)(\beta_C + \mu_C)R_0}, \\ B_C^* &= \dfrac{\mu_C B_0}{\beta_C + \mu_C}[R_0 - 1], \\ R_0 &= \dfrac{\beta_C \Lambda_C N_c \alpha_c}{\mu_C(\mu_C + \delta_C)B_0 \alpha_C}. \end{cases} \tag{3.4.2.2}$$

We deduce that only a single positive endemic equilibrium point exists whenever $R_0 > 1$. To this effect, we conclude that there exists only one unique endemic equilibrium point for model system (3.3.7) whenever $R_0 > 1$. We can then further determine the global stability of the endemic equilibrium for the simplified multiscale model system (3.3.7) since we have established the existence of E^* without providing any information about its stability. The global stability of the endemic equilibrium E^* of the multiscale model system (3.3.7) is summarized in the following theorem:

Theorem 3.2. *The Endemic Equilibrium* E^* *of the multiscale model system (3.3.7) is globally asymptotically stable (GAS) whenever* $R_0 > 1$.

Proof: The proof is not needed since the global stability of the endemic equilibrium is a consequence of **Theorem 2.6** in **Chapter 2**.

3.4.3 Sensitivity analysis

In this sub-section, we conduct a sensitivity analysis of the two PTB transmission metrics derived from the simplified nested multiscale model given by (3.3.7) to the parameters of the model. As mentioned previously, the two PTB transmission metrics derived from the baseline PTB multiscale model system (3.3.7) are: the reproduction number, R_0, which generally describes the dynamics of a disease at the beginning of an infection and the endemic value of the environmental bacteria load, B_C^*, which generally describes the dynamics of a disease at the endemic level. For any epidemic model that describes the dynamics of any diseases in a population, a sensitivity analysis study is an essential to perform as it helps to identify model's parameters which can be targeted for disease control, elimination or even eradication, and also be monitored and controlled during an outbreak of the disease. In this case, sensitivity analysis of both the PTB multiscale transmission metrics (R_0 and B_C^*), with respect to the variation of the baseline PTB multiscale model system (3.3.7)'s parameters is conducted using Latin Hypercube Sampling and partial rank correlation coefficients (PRCCs). We used 1000 simulations per run to investigate the impact of each model parameter on both the basic reproduction numbers (R_0) and the endemic value of the environmental bacteria load (B_C^*). The sensitivity results of R_0 and B_C^* to the model parameters are given in the Tornado plots, Fig. 3.11 and Fig. 3.12, respectively.

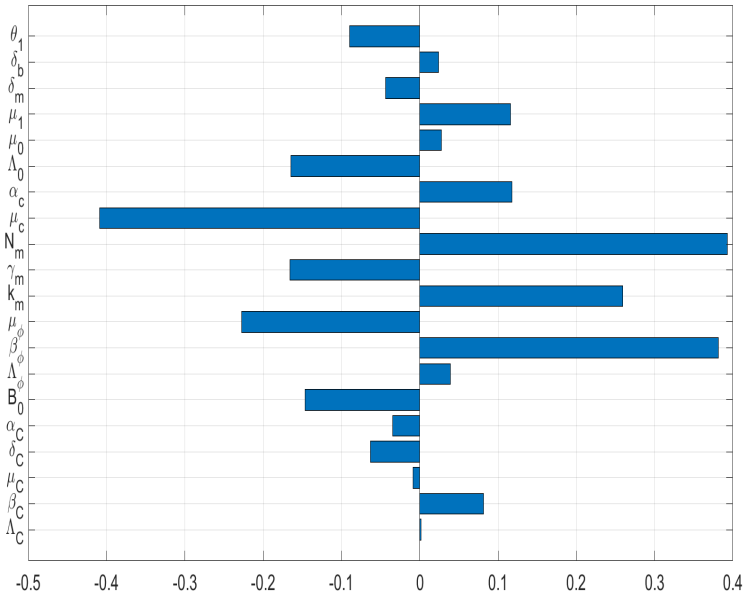

Figure 3.11: *Tornado plot of partial rank correlation coefficients (PRCCs) of the model parameters that influence the PTB transmission metric* R_0.

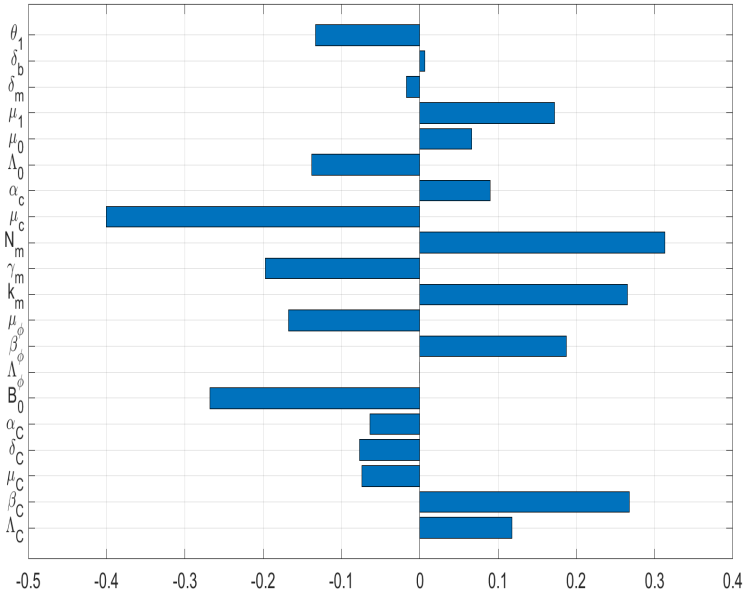

Figure 3.12: *Tornado plot of partial rank correlation coefficients (PRCCs) of the model parameters that influence the PTB transmission metric* B_C^*.

Fig. 3.11 and Fig. 3.12 show the results of the evaluating the sensitivity of the two PTB transmission metrics derived from the PTB simplified multiscale model (3.3.7). From the sensitivity analysis results of both R_0 and B_C^* to baseline PTB multiscale model (3.3.7)'s parameters in Fig. 3.11 and Fig. 3.12, we deduce that some of the baseline PTB multiscale model (3.3.7)'s parameters have positive PRCCs and some have negative PRCCs. This indicates that, parameters with positive PRCCs will increase the value of both R_0 and B_C^* when they are increased, while parameters with negative PRCCs will decrease the value of R_0 and B_C^* when they are increased. For instance, increasing a parameter like bacteria transmission rate β_C at the between-host scale eventually increases the value of R_0 and B_C^*, and also increasing parameters like B_0 will lead to a reduction in the value of both R_0 and B_C^*. Therefore, since R_0 characterizes transmission of PTB infection at the start of the epidemic while B_C^* characterizes transmission of PTB when the disease is now endemic in a herd, we make the following conclusions regarding the sensitivity of both R_0 and B_C^*:

a. The PTB transmission metric R_0 is relatively sensitive to the variation of the within-host scale and between-host scale parameters of the multiscale model system (3.3.7), but more highly sensitive to the five within-host scale parameters (μ_c, N_m, μ_ϕ, β_ϕ, k_m). From the results of the sensitivity analysis of R_0, we can easily notice that the influence of the between-host scale parameters on the changes of R_0 is negligible. This is contrary to

the results of sensitivity analysis of the single-scale model basic reproductive number in Chapter 2 which indicate that the between-host parameters such as β_C and B_0 have the higher sensitive PRCC indexes of about more than 0.4. This might be due to the fact that single-scale models characterize the dynamics of an infection at the microscale of organization.

b. Similarly, the PTB transmission metric B_C^* is also relatively sensitive to the variation of the within-host scale and between-host scale parameters of the multiscale model system (3.3.7), but highly sensitive to only three within-host scale parameters (μ_c, N_m, k_m) and two between-host scale parameters (β_C, B_0). This means that when PTB is at the endemic level, interventions such as (a) vaccination that reduces susceptibility of ruminant to infection, (b) drug treatments if available that would reduce the population of the within-host MAP bacterial cells, and (c) environmental hygiene management that reduces the risk of a ruminant to interact with environmental MAP bacterial cells in the environment need to be highly considered as they are likely to have the highest benefits in reducing the transmission of PTB among ruminants in the herd. This is also contrary to the output of results of sensitivity analysis of the single-scale model basic reproductive number in Chapter 2 which indicate that the two between-host parameters β_C and B_0 have the least sensitive PRCC indexes of about less than 0.1. This also can be due to the fact that single-scale models phenomenologically characterize the dynamics of an infection at the microscale of organization.

3.5 Summary

The major innovation in this chapter to scientific knowledge is the use of a nested multiscale model to investigate if the initial infective inoculum increases beyond the minimum infectious dose (MID) has an impact on the dynamics of an infectious disease system in which the pathogen replication-cycle occurs only at the microscale. The numerical results in this chapter demonstrate that once the minimum infectious dose is consumed, then the infection at the within-host scale is sustained by pathogen replication. These results also show that as the initial inoculum increases, the time to reach the endemic state also increases at this scale domain. However, at the between-host scale, the results further show that when initial inoculum increases beyond the MID makes no different in the transmission dynamics of the disease in the ruminant population. From these results it seem like superinfection might have an insignificant effect on the dynamics of PTB in ruminants. However, at this stage we cannot precisely conclude if superinfection does not effect

on the dynamics of the disease. This would be investigated in the next chapter (i.e. Chapter 4) using an embedded multiscale model. Furthermore, through the reduction of the dimension in order of full nested multiscale model enable us to estimate a composite parameter, $\widehat{N}_c$, that is difficult to estimate using single-scale models. The estimation of $\widehat{N}_c$ facilitate in enhancing single-scale model framework that can be developed at host level to predict the dynamics of paratuberculosis in ruminants. This is largely because single-scale models consider pathogen transmission as the only major disease process, while multiscale models consider both pathogen transmission and pathogen replication as the two major disease processes. We also perform a sensitivity analysis to the two main disease dynamics metrics of the simplified nested multiscale model, namely the basic reproductive number and the endemic value of the MAP bacteria in the environment to determine important parameters of paratuberculosis disease dynamics. The sensitive analysis results show that at the start of PTB infection and when it has reach at the endemic level, the two key within-host parameters (μ_c and N_m) are relatively sensitive to PTB disease dynamics. This is unlike the sensitivity results of the basic reproductive number and the endemic value of the MAP bacteria in the environment in the single-scale model for PTB developed in Chapter 2 which only provide a general indication about the influential of the within-host dynamics significantly influence the dynamics of the PTB disease, but not specifically indicating parameters that have potential influence on the disease dynamics.

Chapter 4

An Embedded Multiscale Model to Study Paratuberculosis Dynamics in Ruminants

4.1 Introduction

In the previous chapter, we developed a nested multiscale model for ruminant paratuberculosis. We used the nested multiscale model to investigate the influence of initial inoculum on ruminant paratuberculosis disease dynamics. What we do not know is whether an embedded multiscale model can be used to model the same disease system with comparable accuracy. The most defining feature of an embedded multiscale model is that at any level of organization of a disease the macroscale influences the microscale through super-infection [1]. This is unlike the nested multiscale model in which the macroscale influences the microscale through initial infective inoculum. In this chapter, we presented an embedded multiscale model to investigate the influence of super-infection on the dynamics of infectious diseases that has a pathogen replication-cycle at microscale using Paratuberculosis in ruminants as a case study. Therefore, the objective in this chapter was to investigate how the super-infection influences disease dynamics for a pathogen with a replication cycle at the microscale. In the next chapter we compare the suitability of the embedded multiscale model in prediction of PTB transmission dynamics with the nested multiscale model described in the previous chapter. To the best of our knowledge, there is no embedded multiscale models in the literature that we are aware of which characterize the dynamics of infectious diseases that have a pathogen replication-cycle at the microscale of organization of an

infectious disease system. The embedded multiscale model presented in this study is the first of its kind to be developed to characterize infectious disease dynamics with a pathogen replication-cycle at the microscale. However, the only application of the embedded multiscale models that we aware of is that of hookworm infection [8] which is an environmentally-transmitted disease systems of type II in which there is no pathogen replication-cycle at the microscale. Moreover, the multiscale models such as in [9] and [10] use embedded multiscale models as sub-models in the context of schistosomiasis and guinea worm infection, respectively. Unlike hookworm infection in [8] and schistosomiosis in [9] as well as guinea worm infection in [10] in which their disease-causing agents have no replication-cycle inside a host, paratuberculosis (PTB) in ruminant considered in this study is caused by the bacteria that has a replication-cycle that occur inside a host. The bacteria which is responsible for PTB infection in ruminants is called *Mycobacterium Avium Subspecies Paratuberculosis* (MAP) [52–54] which is the most notorious obligate pathogen affecting domestic ruminants and wild animals throughout the world. As previously mentioned, MAP is commonly widespread in dairy cattle and can significantly pose a serious economic burdens in dairy cattle industries due to the reduction of milk production, increased cattle mortality and premature culling of infected cattle as well as reduction of sale price for cattle in regions with high PTB prevalence [48]. Additionally, in the dairy cattle, PTB is manifested by cattle's failure to grow, increases in weight loss and chronic diarrhea.

For the transmission-replication dynamics of PTB in the dairy ruminants at the host level, there are two important disease processes that usually occur at different scales of PTB infection. One is the outside-host (i.e., within-host scale) disease process which is associated with the transmission of MAP at the ruminant population-level. The other is the inside-host (i.e., between-host scale) disease process which is associated with the replication of MAP at the ruminant individual-level. It is worthy to mentioning that there is a reciprocal influence between these two disease processes on the dynamics of PTB in the dairy ruminants. Mathematical models that integrate these two disease processes of PTB in dairy ruminants into multiscale modelling have been developed using either individual-based multiscale such as [62] or hybrid multiscale modelling such as [54, 61]. It is also worth mentioning that although an IMSM in [62] and a HMSM in [54] both have respectively shed some lights into the multiscale nature of PTB infection and the impact of health interventions against the disease, there are important differences between them and the current embedded multiscale model presented in this research study. Therefore, the following differentiate our model from the models in [54], our model uses pathogen load as a common metric for infectiousness and disease transmission potential, whereas in [54] different metrics were used for disease transmission across scales. Additionally, the within-host scale model in [54] use pathogen load as the metric for disease transmission while at between-host scale disease

class (i.e. infected class or prevalence) is used as the metric for disease transmission.

4.2 Embedded Multiscale Model for the PTB Transmission-Replication Dynamics in Ruminants

To investigate explicitly if superinfection has an influence on the dynamics of infectious diseases with a pathogen replication-cycle at the microscale of their organizations using ruminant paratuberculosis as an example, we developed a multiscale model which takes into account the reciprocal influence of the macroscale on the microscale through superinfection on the disease dynamics. For the PTB in ruminants, the within-host sub-model that characterize the dynamics of the disease at the microscale was adopted with minor modifications from a single-scale model framework in Magombedze et al. [53]. However, the only minor extension to the model in [53] is the addition of the excretion/shedding rate parameter α_c. While the between-host sub-model that describes the dynamics of the disease at the microscale is based on a susceptible-infected-pathogen (SIP) epidemic framework as described in Chapter 2. Therefore, integrating the between-host epidemic framework developed in Chapter 2) and the adopted within-host model in [53] through super-infection and pathogen replication method introduced in [9] result to embedded multiscale model for ruminant paratuberculosis transmission-replication dynamics which is consequently based on monitoring the dynamics of nine populations: susceptible ruminant (S_C), infected ruminant (I_C) and the between-host MAP bacilli bacterial load (B_C) in the environment at the between-host scale; and susceptible macrophages (M_Φ), infected macrophages (I_m), within-host MAP bacilli bacterial load (B_c) at the extracellular environment, specific naive CD4+ T cells (T_0), Th1 response cells (T_1), and Th2 phenotype response cells (T_2) at the within-host scale within an infected ruminant-host level. We made the following assumption for this model:

(i) Infected ruminants do not naturally recover from MAP infection,

(ii) Transmission of infection is only through indirect means and if there is any direct transmission, it will be estimated by an indirect expression,

(iii) There is no vertical transmission, and ruminant hosts are not vaccinated or treated and so the infection state of the ruminant hosts (exposed, subclinical, clinical, etc.) is only determined by the level of immune response in each ruminant host.

(iv) The recruitment of ruminants in the herd is through birth and incoming ruminant from other farms.

(v) All the new recruited ruminants are assumed to be healthy and have not been previously exposed to the disease.

(vi) The extracellular MAP bacterial load $B_c = B_c(t)$ is a proxy for individual ruminant infectiousness and is excreted out of the body of an individual ruminant through feces.

(vii) There is no bacteria replication in the physical environment, and the loss of MAP bacteria in the environment due to uptake by susceptible ruminant hosts is negligible,

(viii) The depletion of MAP bacteria in the extracellular environment through engulfment by macrophages is negligible.

(ix) Clonal expansion of the T_0 cells into T_1 is only due to infected macrophages while clonal expansion of the T_2 is only due to MAP bacteria in the infected ruminant host.

Based on the above mentioned assumptions and the diagram presented in Fig. 4.1, the embedded multiscale model for PTB transmission dynamics is given by the following system of ordinary differential equations:

$$
\begin{cases}
i. \quad \dfrac{dS_C(t)}{dt} &= \Lambda_C - \dfrac{\beta_C B_C(t)}{B_0 + B_C(t)} S_C(t) - \mu_C S_C(t), \\
ii. \quad \dfrac{dI_C(t)}{dt} &= \dfrac{\beta_C B_C(t)}{B_0 + B_C(t)} S_C(t) - [\mu_C + \delta_C] I_C(t), \\
iii. \quad \dfrac{dB_C(t)}{dt} &= \alpha_c [I_C(t) + 1] B_c(t) - \alpha_C B_C(t), \\
iv. \quad \dfrac{dB_c(t)}{dt} &= \dfrac{\beta_C B_C(t)[S_C(t) - 1]}{[B_0 + B_C(t)]\Phi_C[I_C(t) + 1]} + N_m k_m I_m(t) - [\mu_c + \alpha_c] B_c(t), \\
v. \quad \dfrac{dM_\phi(t)}{dt} &= \Lambda_\phi - \beta_\phi M_\phi(t) B_c(t) - \mu_\phi M_\phi(t), \\
vi. \quad \dfrac{dI_m(t)}{dt} &= \beta_\phi M_\phi(t) B_c(t) - [k_m + \mu_\phi] I_m(t) - \gamma_m T_1(t) I_m(t), \\
vii. \quad \dfrac{dT_0(t)}{dt} &= \Lambda_0 - [\delta_m I_m(t) + \delta_b B_c(t)] T_0(t) - \mu_0 T_0(t), \\
viii. \quad \dfrac{dT_1(t)}{dt} &= \theta_1 \delta_m I_m(t) T_0(t) - \mu_1 T_1(t), \\
ix. \quad \dfrac{dT_2(t)}{dt} &= \theta_2 \delta_b B_c(t) T_0(t) - \mu_2 T_2(t).
\end{cases}
\tag{4.2.1}
$$

The first two equations of the model system (4.2.1), equations (1) and (2), describe the dynamics of susceptible and infected ruminant hosts respectively. At any time t, new recruits susceptible ruminant enter the ruminant population through birth and incoming ruminant from other farms at a constant rate Λ_C. Susceptible ruminant population losses its individuals due to natural death at a constant rate μ_C and through infection at a rate variable $\lambda_C(t)S_C(t)$. Susceptible ruminants acquire PTB infection when feed from contaminated pasture with fecal material containing infective MAP, or drink from contaminated surface water/water troughs with MAP bacilli cells. The infected ruminant is generated when susceptible ruminants become infected and join the group at a rate variable $\lambda_C(t)S_C(t)$. The infected group decreases due to natural death at a constant rate μ_C or through death induced removal rate at δ_C, so that an average lifespan of PTB infected ruminant in the population is determined by $1/(\delta_C + \mu_C)$. We assume that infected ruminant spread the disease in the population through contaminating the environment with fecal material containing the MAP bacteria cells at a variable rate $\alpha_c B_c(t)(I_C(t) + 1)$ as shown in Fig. (4.1).

Therefore, the population dynamics of MAP bacilli in the physical environment, described by equation (3) of the model system (4.2.1) is generated through excretion of fecal material containing the MAP bacteria cells by each infected ruminant individual host at a rate $\alpha_c B_c(t) I_c(t)$. We assume that the population of MAP bacteria in the physical environment decreases due to natural death at a rate α_C. Equation (4) of the model system (4.2.1) describes the changes in time of the within-host MAP bacteria cells at the site of infection within a single infected ruminant host. The within-host MAP bacteria cells at the site of infection within an infected ruminant host are generated following uptake of average between-host MAP bacteria cells in the physical environment through ingesting contaminated food or water and the release of the intracellular MAP bacilli into the extracellular environment when each infected macrophage burst. Generally, in the ruminant population, the uptake of contaminated food or water which contain between-host MAP bacterial cells, is the transmission of the MAP bacteria from the physical environment to susceptible ruminant and become infected ruminant. Following the methodology as described in [8–10] for modelling re-infection (superinfection) for environmentally-transmitted infectious disease systems, we model the average rate at which a single susceptible ruminant host uptake MAP bacterial cells in the physical environment through ingesting contaminated food or water and become an infected ruminant host by the expression

$$\lambda_c(t) S_c(t) = \frac{\lambda_C(t)[S_C(t) - 1]}{\Phi_C[I_C(t) + 1]}, \tag{4.2.2}$$

where $\lambda_C(t)$, $S_C(t)$ and $I_C(t)$ are as defined previously, and

$$(S_C(t), I_C(t), B_C(t)) \to (S_C(t) - 1, I_C(t) + 1, B_C(t)). \tag{4.2.3}$$

being a single transition used for down-scaling and up-scaling between PTB transmission dynamics at the population level and at the within ruminant host level. Moreover, this term $\lambda_c(t) S_c(t)$ models increases of the within-host MAP bacteria at the within-host scale through super-infection, and thus downscaling population infectiousness into and individual infectiousness. Furthermore, in the within ruminant level, the burst of infected macrophages to release an average number of intracellular MAP bacteria cells into the extracellular environment is modeled phenomenological. The burst rate represents the transmission of the MAP bacteria between cells at the site of infection within an infected ruminant host. Infected macrophages burst at constant rate k_m to release an average number of intracellular MAP bacilli N_m into the extracellular environment, so that the total number of intracellular bacteria released into the extracellular environment is determined by $N_m k_m I_m$. Therefore, the average number of within-host MAP bacterial cells at the site of infection, $B_c(t)$ within a single infected ruminant host increases at a mean rate $\lambda_h(t) S_h(t)$ and $N_m k_m I_m$. We assume that the population of MAP bacilli in the extracellular environment decay

naturally at a constant rate μ_c and excreted out of the body of an infected ruminant into the physical environment through fecal material at a constant rate α_c. Equations (5) and (6) of the model system (4.2.1) describe the dynamics of the susceptible macrophage cells $M_\phi(t)$ and infected macrophage cells $I_m(t)$ at the site of infection within a single infected ruminant host. Similarly, at any time t, new susceptible macrophages are recruited through the supply of macrophage cells from progenitor monocytes that are recruited from the blood to the site of infection at a constant rate Λ_ϕ and the population losses individuals due to natural death at a constant rate μ_ϕ. In that way an average lifespan of each susceptible macrophages cells in the site of infection within an infected ruminant is $1/\mu_\phi$. Susceptible macrophages acquire infection through engulfing extracellular MAP bacilli bacteria at a rate β_ϕ. The infected macrophage cells at a site of infection within an infected ruminant host is generated when susceptible macrophages become infected and join the group of infected macrophages at a rate β_ϕ. We assume that in the population of infected macrophages there is an additional death rate related to infection and due to removal by T_1 response at a rate k_m and γ_m, respectively, so that the lifespan in the population of infected macrophages is $1/(k_m + \mu_\phi + \gamma_m T_1)$. The last three equations of the model system (4.2.1), equations (7) - (9) describe the evolution in time of the population of ruminant response cells at a site of infection in the gut which are specific naive CD4+ T cells (T_0), and the two subsets of the MAP specific immune response, Th1 (T_1) and Th2 (T_2) cells (see [53] and reference therein). The population of specific naive CD4+ T cells (T_0) for MAP bacilli are produced at a constant rate Λ_0 from the thymus. We assume that these specific naive CD4+ T cells decay naturally at a rate μ_0, so that their average lifespan is $1/\mu_0$. Following the work in (4.2.1), we also assume that T_0 cells become T_1 and T_2 immune response cells at per capita rates δ_m and δ_b, respectively. Thus, the population of T_1 and T_2 immune response cells are proliferated at a rate $\theta_1\delta_m I_m T_0$ and $\theta_1\delta_b B_m T_0$, respectively. We also assume that both the population of T_1 and T_2 immune response cells decay naturally at a rate μ_1 and μ_2, respectively.

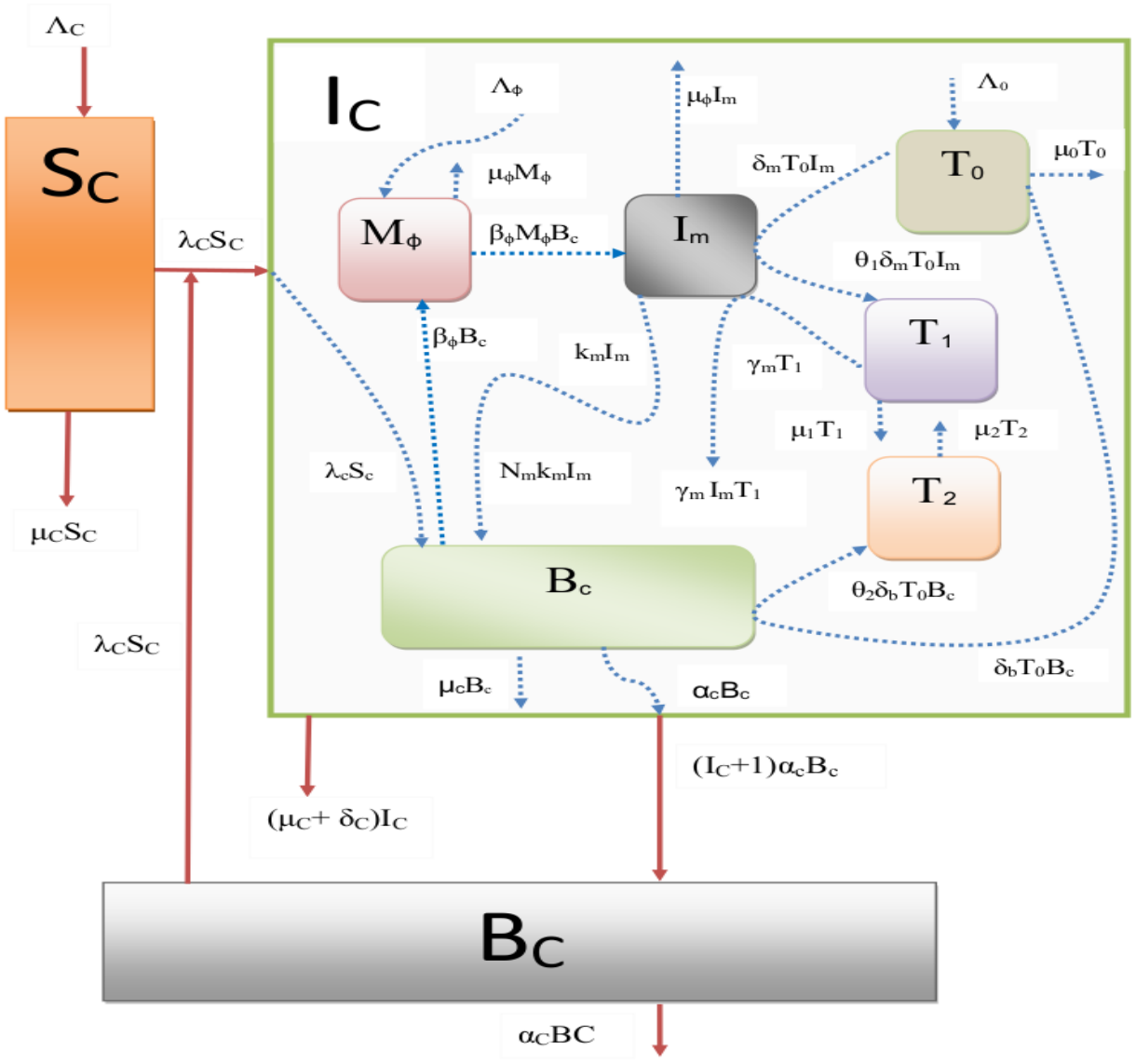

Figure 4.1: *A conceptual diagram of the multiscale model of PTB transmission dynamics in ruminant population.*

4.3 Mathematical Analysis of the Embedded Multiscale Model for PTB Transmission-Replication Dynamics in Ruminants

4.3.1 Feasible Region of the Equilibria of the Model

The embedded multiscale model system (4.2.1) for PTB transmission dynamics can be analyzed in a region $\Gamma \in R^+$ of biological interest. Now assuming that all parameters and state variables for model system (4.2.1) are positive for all $t > 0$, it can be shown that all solutions for the

model system (4.2.1) with positive initial conditions remain bounded. Letting $N_C = S_C + I_C$ and $N_\phi = M_\phi + I_m$, and further add the 1^{st} and 2^{nd}, and 5^{th} and 6^{th} equations of the model system (4.2.1), respectively, we obtain

$$\begin{cases} 1.\ \dfrac{dN_C(t)}{dt} &= \Lambda_C - \mu_C N_C - \delta_C I_C, \\ 2.\ \dfrac{dN_\phi(t)}{dt} &= \Lambda_\phi - \mu_\phi N_\phi - [\gamma_m T_1 + k_m] I_m. \end{cases} \tag{4.3.1}$$

It follows that

$$\begin{cases} 1.\ \dfrac{dN_C(t)}{dt} &\leq \Lambda_C - \mu_C N_C, \\ 2.\ \dfrac{dN_\phi(t)}{dt} &\leq \Lambda_\phi - \mu_\phi N_\Phi. \end{cases} \tag{4.3.2}$$

From which we get

$$\begin{cases} 1.\ N_C(t) &\leq N_C(0)e^{-\mu_C t} + \dfrac{\Lambda_C}{\mu_C}\left[1 - e^{-\mu_C t}\right], \\ 2.\ N_\phi(t) &\leq N_\phi(0)e^{-\mu_\phi t} + \dfrac{\Lambda_\phi}{\mu_\phi}\left[1 - e^{-\mu_\phi t}\right] \end{cases} \tag{4.3.3}$$

where $N_C(0)$ represents the value of total ruminant population at the between-host scale in the population-host level and $N_\phi(0)$ represents the value of total macrophage cell population at the within-host scale within a single infected ruminant-host level evaluated at the initial values of the respective variables. Taking the limits of both $N_C(t)$ and $N_\phi(t)$ in (4.3.3) as time gets larger, we get the following expressions

$$\begin{cases} 1.\ \lim\limits_{t\to\infty} sup(N_C(t)) &\leq \dfrac{\Lambda_C}{\mu_C}, \\ 2.\ \lim\limits_{t\to\infty} sup(N_\phi(t)) &\leq \dfrac{\Lambda_\phi}{\mu_\phi}. \end{cases} \tag{4.3.4}$$

Now, considering the 7^{th} equation of the model system (4.2.1) given by

$$\frac{dT_0(t)}{dt} = \Lambda_0 - [\delta_m I_m(t) + \delta_b B_c(t)]T_0(t) - \mu_0 T_0(t), \tag{4.3.5}$$

it is true that

$$\frac{dT_0}{dt} \leq \Lambda_0 - \mu_0 T_0, \tag{4.3.6}$$

from which we get

$$T_0(t) \leq T_0(0)e^{-\mu_0 t} + \frac{\Lambda_0}{\mu_0}\left[1 - e^{-\mu_0 t}\right], \tag{4.3.7}$$

where $T_0(0)$ denoting the value of total naïve immune response cell population at the within-host scale within an infected ruminant-host level evaluated at the initial values of T_0. Taking the limits of $T_0(t)$ as time gets larger, we get the following

$$\lim_{t\to\infty} sup(T_0(t)) \leq \frac{\Lambda_0}{\mu_0}. \tag{4.3.8}$$

From the 8^{th} equation of the of the model system (4.2.1), we get

$$\frac{dT_1}{dt} \leq \frac{\theta_1 \delta_m \Lambda_0 \Lambda_\phi}{\mu_\phi \mu_0} - \mu_1 T_1. \tag{4.3.9}$$

From which we get

$$T_1(t) \leq T_1(0)e^{-\mu_1 t} + \frac{\theta_1 \delta_m \Lambda_0 \Lambda_\phi}{\mu_\phi \mu_1 \mu_0}\left[1 - e^{-\mu_1 t}\right], \tag{4.3.10}$$

with $T_1(0)$ being the value of total Th1 immune response cell population at the within-host scale within a single infected ruminant-host level evaluated at the initial values of T_1. This implies that

$$\lim_{t\to\infty} sup(T_1(t)) \leq \frac{\theta_1 \delta_m \Lambda_0 \Lambda_\phi}{\mu_\phi \mu_1 \mu_0}. \tag{4.3.11}$$

Therefore, substituting $N_C \leq \frac{\Lambda_C}{\mu_C}$, $N_\phi \leq \frac{\Lambda_\phi}{\mu_\phi}$ and $T_1 \leq \frac{\theta_1 \delta_m \Lambda_0 \Lambda_\phi}{\mu_\phi \mu_1 \mu_0}$ into the 3^{rd}, 4^{th} and 9^{th} equations of the model system (4.2.1), we obtain the following

$$\begin{cases} 1.\ \dfrac{dB_C(t)}{dt} \leq \dfrac{\alpha_c(\Lambda_C + \mu_C)}{\mu_C} B_c - \alpha_C B_C, \\ 2.\ \dfrac{dB_c(t)}{dt} \leq \dfrac{\beta_C(\Lambda_C - \mu_C)B_C}{\Phi_C(\Lambda_C + \mu_C)(B_0 + B_C)} + \dfrac{N_m k_m \Lambda_\phi}{\mu_\phi} - (\mu_c + \alpha_c)B_c, \\ 3.\ \dfrac{dT_2(t)}{dt} \leq \dfrac{\theta_2 \delta_b \Lambda_0}{\mu_0} B_c - \mu_2 T_2, \end{cases} \tag{4.3.12}$$

with

$$a_1 = (\mu_c + \alpha_c). \tag{4.3.13}$$

From which we get

$$\begin{cases} 1.\ B_C & \leq & \dfrac{\alpha_c(\Lambda_C + \mu_C)}{\mu_C \alpha_C} B_c, \\ 2.\ B_c & \leq & \dfrac{\beta_C(\Lambda_C - \mu_C)B_C}{\Phi_C(\Lambda_C + \mu_C)(B_0 + B_C)(\mu_c + \alpha_c)} + \dfrac{N_m k_m \Lambda_\phi}{\mu_\phi(\mu_c + \alpha_c)}, \\ 3.\ T_2 & \leq & \dfrac{\theta_2 \delta_b \Lambda_0}{\mu_0 \mu_2} B_c. \end{cases} \tag{4.3.14}$$

Following some algebraic solving we obtain

$$\begin{cases} 1.\ B_C & \leq & \dfrac{\alpha_c(\Lambda_C + \mu_C)}{2\mu_C \alpha_C} \left[\xi_1 + \sqrt{\xi_1^2 + 4\xi_2}\right], \\ 2.\ B_c & \leq & \dfrac{1}{2}\left[\xi_1 + \sqrt{\xi_1^2 + 4\xi_2}\right], \\ 3.\ T_2 & \leq & \dfrac{\theta_2 \delta_b \Lambda_0}{2\mu_0 \mu_2} \left[\xi_1 + \sqrt{\xi_1^2 + 4\xi_2}\right], \end{cases} \tag{4.3.15}$$

where the constants ξ_1 and ξ_2 are as follows

$$\begin{cases} \xi_1 & = & \nu_0(\nu_1 + \nu_2) - B_0, \\ \xi_2 & = & \nu_0 \nu_2 B_0, \end{cases} \tag{4.3.16}$$

with

$$\begin{cases} \nu_0 &= \dfrac{\alpha_c(\Lambda_C+\mu_C)}{\mu_C\alpha_C}, \\ \nu_1 &= \dfrac{\beta_C(\Lambda_C-\mu_C)}{\Phi_C(\Lambda_C+\mu_C)(\mu_c+\alpha_c)}, \\ \nu_2 &= \dfrac{N_m k_m \Lambda_\phi}{\mu_\phi(\mu_c+\alpha_c)}, \end{cases} \tag{4.3.17}$$

This implies that

$$\begin{cases} 1.\ \lim\limits_{t\to\infty} sup(B_C(t)) &\leq \dfrac{\alpha_c(\Lambda_C+\mu_C)}{2\mu_C\alpha_C}\left[\xi_1+\sqrt{\xi_1^2+4\xi_2}\right], \\ 2.\ \lim\limits_{t\to\infty} sup(B_c(t)) &\leq \dfrac{1}{2}\left[\xi_1+\sqrt{\xi_1^2+4\xi_2}\right], \\ 3.\ \lim\limits_{t\to\infty} sup(T_2(t)) &\leq \dfrac{\theta_2\delta_b\Lambda_0}{2\mu_0\mu_2}\left[\xi_1+\sqrt{\xi_1^2+4\xi_2}\right]. \end{cases} \tag{4.3.18}$$

Therefore, all feasible solutions of the model system (4.2.1) are positive and enter a region defined by

$$\begin{cases} \Gamma &= \{(S_C, I_C, B_C, B_c, M_\phi, I_m, T_0, T_1, T_2) \in R_+^9 : \\ & 0 \leq S_C + I_C \leq S_1,\ 0 \leq M_\phi + I_m \leq S_2,\ 0 \leq B_C \leq S_3, \\ & 0 \leq B_c \leq S_4,\ 0 \leq T_0 \leq S_5,\ 0 \leq T_1 \leq S_6,\ 0 \leq T_2 \leq S_7\}, \end{cases} \tag{4.3.19}$$

which is positively invariant and attracting for all $t > 0$, where

$$\begin{cases} S_1 = \dfrac{\Lambda_C}{\mu_C}, \\ S_2 = \dfrac{\Lambda_\phi}{\mu_\phi}, \\ S_3 = \dfrac{\alpha_c(\Lambda_C + \mu_C)}{2\mu_C\alpha_C}\left[\xi_1 + \sqrt{\xi_1^2 + 4\xi_2}\right], \\ S_4 = \dfrac{1}{2}\left[\xi_1 + \sqrt{\xi_1^2 + 4\xi_2}\right], \\ S_5 = \dfrac{\Lambda_0}{\mu_0}, \\ S_6 = \dfrac{\theta_1\delta_m\Lambda_0\Lambda_\phi}{\mu_\phi\mu_1\mu_0}, \\ S_7 = \dfrac{\theta_2\delta_b\Lambda_0}{2\mu_0\mu_2}\left[\xi_1 + \sqrt{\xi_1^2 + 4\xi_2}\right], \\ \xi_1 = \nu_0(\nu_1 + \nu_2) - B_0, \\ \xi_2 = \nu_0\nu_2 B_0. \end{cases} \tag{4.3.20}$$

Therefore, it is sufficient to consider solutions of the model system (4.2.1) in Ω, since all solutions starting in Ω remain there for all $t \geq 0$. Hence, the multiscale model system (4.2.1) is mathematically and epidemiologically well-posed. It is sufficient to consider the dynamics of the flow generated by model system (4.2.1) in Ω whenever $\Lambda_C > \mu_C$ and $\nu_0(\nu_1 + \nu_2) > B_0$. We shall assume in all that follows (unless stated otherwise) that $\Lambda_C > \mu_C$ and $\nu_0(\nu_1 + \nu_2) > B_0$. In the next two subsections, we provide some results concerning the equilibrium states of the multiscale model system (4.2.1) and their stabilities. The multiscale model system (4.2.1) has two equilibrium states: the disease-free equilibrium state (DFE) and the endemic equilibrium state (EPP).

4.3.2 Disease-Free Equilibrium and Reproduction Number

We obtained the disease-free equilibrium point of the model system (4.2.1) by setting the left-hand side of the equations of model system (4.2.1) equal to zero and also assuming that $I_C = B_C = B_c = I_m = T_1 = T_2 = 0$. Thus, we let

$$E_0 = \left(\frac{\Lambda_C}{\mu_C}, 0, 0, 0, \frac{\Lambda_\phi}{\mu_\phi}, 0, \frac{\Lambda_0}{\mu_0}, 0, 0\right), \tag{4.3.2.1}$$

denote the disease-free equilibrium of the model system (4.2.1). For the purpose of analyzing the stability of the DFE, we make use of the basic reproductive number, R_0. We employed the next generation operator approach described in [5] to compute the basic reproduction number of the embedded multiscale model (4.2.1). Therefore, the model system (4.2.1) can also be written in the form

$$\begin{cases} \dfrac{dX}{dt} = f(X, Y, Z), \\ \dfrac{dY}{dt} = g(X, Y, Z), \\ \dfrac{dZ}{dt} = h(X, Y, Z), \end{cases} \tag{4.3.2.2}$$

where

i. $X = (S_C, M_\phi, T_0, T_1, T_2)$ represents all compartments of individuals who are not infected,

ii. $Y = (I_C, I_m)$ represents all compartments of infected individuals who are not capable of infecting others,

iii. $Z = (B_C, B_c)$ represents all compartments of infected individuals who are capable of infecting.

In this case, we let the disease free-equilibrium of the model (4.2.1) be denoted by the following expression

$$\bar{U}_0 = \left(\frac{\Lambda_C}{\mu_C}, 0, 0, 0, \frac{\Lambda_\phi}{\mu_\phi}, 0, \frac{\Lambda_0}{\mu_0}, 0, 0\right). \tag{4.3.2.3}$$

Following [5], we let

$$\tilde{g}(X^*, Z) = (\tilde{g}_1(X^*, Z),\ \tilde{g}_2(X^*, Z)) \tag{4.3.2.4}$$

with

$$\begin{cases} \tilde{g}_1(X^*, Z) &= \dfrac{\beta_C \Lambda_C B_C}{\mu_C(\mu_C + \delta_C)(B_0 + B_C)}, \\ \tilde{g}_2(X^*, Z) &= \dfrac{\beta_\phi \Lambda_\phi B_c}{\mu_\phi(\mu_\phi + \delta_\phi)}. \end{cases} \tag{4.3.2.5}$$

We deduce that

$$h(X, Y, Z) = (h_1(X, Y, Z), h_2(X, Y, Z)), \tag{4.3.2.6}$$

with

$$\begin{cases} h_1(X, Y, Z) &= \dfrac{K_0 B_C B_m}{(B_0 + B_m)} + \alpha_c B_c - \alpha_C B_C, \\ h_2(X, Y, Z) &= \dfrac{K_1 B_C}{(K_3 + K_2 B_C)} + K_4 B_c - (\mu_c + \alpha_c) B_c, \end{cases} \tag{4.3.2.7}$$

where

$$\begin{cases} K_0 &= \dfrac{\beta_C \Lambda_C \alpha_c}{\mu_C(\mu_C + \delta_C)}, \\ K_1 &= \dfrac{\beta_C(\Lambda_C - \mu_C)(\mu_C + \delta_C)}{\Phi_C}, \\ K_2 &= \beta_C \Lambda_C + \mu_C(\mu_C + \delta_C), \\ K_3 &= \mu_C(\mu_C + \delta_C) B_0, \\ K_4 &= \dfrac{\beta_\phi \Lambda_\phi N_m k_m}{\mu_\phi(\mu_\phi + k_m)}. \end{cases} \tag{4.3.2.8}$$

A matrix

$$A = D_Z h(X^*, \tilde{g}(X^*, 0), 0) = \begin{bmatrix} -\alpha_C & \alpha_c \\ \dfrac{K_1}{K_3} & K_4 - (\mu_c + \alpha_c) \end{bmatrix} \tag{4.3.2.9}$$

can be written in the form $A = M - D$, so that

$$M = \begin{bmatrix} 0 & \alpha_c \\ \dfrac{K_1}{K_3} & K_4 \end{bmatrix} \tag{4.3.2.10}$$

and

$$D = \begin{bmatrix} \alpha_C & 0 \\ 0 & (\mu_c + \alpha_c) \end{bmatrix}. \tag{4.3.2.11}$$

The basic reproductive number is the spectral radius (dominant eigenvalue) of the matrix $T = MD^{-1}$, that is,

$$R_0 \quad = \quad \rho(T). \tag{4.3.2.12}$$

Hence, in this case, the basic reproductive number of the embedded multiscale model (4.2.1) is expressed by the following quantity

$$R_0 \quad = \quad \frac{1}{2}\left[R_{0_c} + \sqrt{R_{0_c}^2 + 4R_{0_C}}\right] \tag{4.3.2.13}$$

where

$$R_{0_c} = \frac{\beta_\phi \Lambda_\phi N_m k_m}{\mu_\phi(\mu_\phi + k_m)(\mu_c + \alpha_c)} \tag{4.3.2.14}$$

characterizes a partial within-host basic reproductive number and

$$R_{0_C} = \frac{\beta_C(\Lambda_C - \mu_C)\alpha_c}{\alpha_C \mu_C \Phi_C(\mu_c + \alpha_c)} \tag{4.3.2.15}$$

characterizes a partial between-host basic reproduction number. However, we can conclude from the expression (4.3.2.13) of the reproductive number that it is a function of both the within-host

scale parameters and the between-host scale parameters. Therefore, the obtained results here show that the within-host scale and the between-host scale influence each other in a reciprocal way. We further made use of the basic reproductive number (4.3.2.13) to test both the local and global stability of the disease-free equilibrium (E_0) of the multiscale model system (4.2.1). We then established that if the basic reproductive number is less than a unity, then E_0 is locally and globally stability asymptotically stable. Details of the local and global stability of E_0 are given in the next two subsections.

4.3.3 Stability Analysis of the Embedded Multiscale Model Disease-Free Equilibrium State

4.3.3.1 Local stability analysis of analysis of the embedded multiscale disease-free equilibrium state

In this subsection, we determined the local stability of DFE of the model system (4.2.1) by linearizing all the equations of the model system (4.2.1) to obtain a Jacobian matrix. Then we evaluate the Jacobian matrix of the system at the disease-free equilibrium

$$E_0 = \left(\frac{\Lambda_C}{\mu_C},\ 0,\ 0,\ 0, \frac{\Lambda_\phi}{\mu_\phi},\ 0,\ \frac{\Lambda_0}{\mu_0},\ 0,\ 0\right). \tag{4.3.3.1.1}$$

Evaluating the Jacobian matrix of the model system (4.2.1) at the disease-free equilibrium state (DFE), we get

$$J(E_0) = \begin{pmatrix} -\mu_C & 0 & -\frac{\beta_C \Lambda_C}{\mu_C B_0} & 0 & 0 & 0 & 0 & 0 & 0 \\ 0 & -a_0 & \frac{\beta_C \Lambda_C}{\mu_C B_0} & 0 & 0 & 0 & 0 & 0 & 0 \\ 0 & 0 & -\alpha_C & \alpha_c & 0 & 0 & 0 & 0 & 0 \\ 0 & 0 & A_1 & -a_1 & 0 & N_m k_m & 0 & 0 & 0 \\ 0 & 0 & 0 & -\frac{\beta_\phi \Lambda_\phi}{\mu_\phi} & -\mu_\phi & 0 & 0 & 0 & 0 \\ 0 & 0 & 0 & \frac{\beta_\Phi \Lambda_\phi}{\mu_\phi} & 0 & -a_2 & 0 & 0 & 0 \\ 0 & 0 & 0 & -\frac{\delta_b \Lambda_0}{\mu_0} & 0 & -\frac{\delta_m \Lambda_0}{\mu_0} & -\mu_0 & 0 & 0 \\ 0 & 0 & 0 & 0 & 0 & \frac{\theta_1 \delta_m \Lambda_0}{\mu_0} & 0 & -\mu_1 & 0 \\ 0 & 0 & 0 & \frac{\theta_2 \delta_b \Lambda_0}{\mu_0} & 0 & 0 & 0 & 0 & -\mu_2 \end{pmatrix} \tag{4.3.3.1.2}$$

where

$$\begin{cases} a_0 = (\mu_C + \delta_C), \\ a_1 = (\mu_c + \alpha_c), \\ a_2 = (\mu_\phi + k_m), \\ A_1 = \frac{\beta_C (\Lambda_C - \mu_C)}{\Phi_C \mu_C B_0}. \end{cases} \tag{4.3.3.1.3}$$

Now, considering stability of DFE by calculating the eigenvalues (λ_s) of the Jacobian matrix given by equation (4.3.3.1.2), characteristic equation for the eigenvalues is given by

$$Q_0[\lambda^3 + \Phi_1\lambda^2 + \Phi_2\lambda + \Phi_3] = 0, \tag{4.3.3.1.4}$$

where the coefficient Q_0 is as follows

$$Q_0 = (-\mu_C - \lambda)(-\mu_\phi - \lambda)(-\mu_0 - \lambda)(-\mu_1 - \lambda)(-\mu_2 - \lambda)(-a_0 - \lambda). \tag{4.3.3.1.5}$$

We noticed from equation (4.3.3.1.4), that there are six negative eigenvalues (-μ_C ,-μ_ϕ, -μ_0, -a_0,-μ_1 and -μ_2). The stability of the DFE can be concluded by using the Routh-Hurwitz criteria to determine the sign of the remaining eigenvalues of the polynomial

$$\lambda^3 + \Phi_1\lambda^2 + \Phi_2\lambda + \Phi_3 = 0 \tag{4.3.3.1.6}$$

where

$$\begin{cases} \Phi_1 &= \alpha_C + a_1 + a_2, \\ \Phi_2 &= (\alpha_C + a_2)a_1 + \alpha_C a_2(1 - R_{0_C}), \\ \Phi_3 &= a_1 a_2[R_{0_c} + \alpha_C(1 - R_{0_C})]. \end{cases} \tag{4.3.3.1.7}$$

Employing the Routh-Hurwitz stability criterion, we can deduce that the equilibrium state associated with the model system (4.2.1) would be stable if and only if the determinants of all the Hurwitz matrices associated with the characteristic equation (4.3.3.1.6) are positive, that is

$$Det(H_j) > 0; \quad j = 1, 2, ..., 6 \tag{4.3.3.1.8}$$

where

$$\begin{cases} H_1 = \begin{pmatrix} \Phi_1 \end{pmatrix}; \quad H_2 = \begin{pmatrix} \Phi_1 & 1 \\ \Phi_3 & \Phi_2 \end{pmatrix}; \\ H_3 = \begin{pmatrix} \Phi_1 & 1 & 0 \\ \Phi_3 & \Phi_2 & \Phi_1 \\ 0 & 0 & \Phi_3 \end{pmatrix}. \end{cases} \tag{4.3.3.1.9}$$

The Routh-Huiwitz criterion applied to expressions in equation (4.3.3.1.9) requires that the following conditions $C1$ and $C2$ be satisfied, in order to guarantee the local stability of the disease-free equilibrium point of the model system (4.2.1).

$$\begin{cases} C1.\ \Phi_1,\ \Phi_2,\ \Phi_3 > 0, \\ C2.\ \Phi_1\Phi_2 - \Phi_3 > 0, \end{cases} \tag{4.3.3.1.10}$$

From equations (4.3.3.1.6) and (4.3.3.1.9) we noted that all the coefficients Φ_1, Φ_2, and Φ_3 of the polynomial $P(\lambda)$ are greater than zero whenever $R_0 < 1$. And we also noted that the conditions above are satisfied if and only if the basic reproductive number of the model system (4.2.1) is less than a unit (i.e., $R_0 < 1$). Hence all the roots of the polynomial $P(\lambda)$ are either negative or have negative real parts. The results are summarized in the following theorem.

Theorem 4.1. *The Disease-free equilibrium point of the model system (4.2.1) is locally asymptotically stable whenever* $R_0 < 1$.

4.3.3.2 Global stability analysis of the embedded multiscale disease-free equilibrium state

We determined the global stability of DFE of the embedded multiscale model system (4.2.1) by using a next generation operator [5]. Thus the system (4.2.1) can be re-written in the form

$$\begin{cases} \dfrac{dX}{dt} &= F(X,Z), \\ \dfrac{dY}{dt} &= G(X,Z) \end{cases} \tag{4.3.3.2.1}$$

where

- $X = S_C, M_\phi, T_0, T_1, T_2$ represents compartment of uninfected ruminant, and
- $Z = (I_C, B_C, B_c, I_m)$ represents compartments of infected ruminant and Infective MAP bacilli bacteria in the physical environment.

We let

$$E_0 = (X^*, 0) = \left(\frac{\Lambda_C}{\mu_C},\ 0,\ 0,\ 0, \frac{\Lambda_\phi}{\mu_\phi},\ 0,\ \frac{\Lambda_0}{\mu_0},\ 0,\ 0\right), \tag{4.3.3.2.2}$$

denote the disease-free equilibrium (DFE) of the embedded multiscale model system (4.2.1). For X^* to be globally asymptotically stable, the following conditions (H1) and (H2) must be satisfied.

H1. $\dfrac{dX}{dt} = F(X,0)$ is globally asymptotically stable (g.a.s),

H2. $G(X,Z) = AZ - \hat{G}(X,Z)$, $\hat{G}((X,Z) \geq 0$ for $(X,Z) \in R^9_+$ where $A = D_Z G(X^*, 0)$ is an M-matrix and R^9_+ is the region where the model makes biological sense.

In this case,

$$F(X,0) = \begin{bmatrix} \Lambda_C - \mu_C S_C \\ \Lambda_\phi - \mu_\phi M_\phi \\ 0 \\ 0 \end{bmatrix} \tag{4.3.3.2.3}$$

and the matrix A is given by

$$A = \begin{bmatrix} -(\mu_C + \delta_C) & \frac{\beta_C \Lambda_C}{B_0 \mu_C} & 0 & 0 \\ 0 & -\alpha_C & \alpha_c & 0 \\ 0 & \frac{\beta_C(\Lambda_C - \mu_C)}{B_0 \Phi_C \mu_C} & -(\alpha_c + \mu_c) & N_m k_m \\ 0 & 0 & \frac{\beta_\phi \Lambda_\phi}{\mu_\phi} & -(\mu_\phi + k_m) \end{bmatrix} \tag{4.3.3.2.4}$$

with $\hat{G}(X, Z)$ given by

$$\hat{G}(X, Z) = \begin{bmatrix} \left(\frac{\Lambda_C}{B_0 \mu_C} - \frac{S_C}{B_0 + B_C}\right) \beta_C B_C \\ 0 \\ 0 \\ \left(\frac{\Lambda_\phi}{\mu_\phi} - M_\phi\right) \beta_\phi B_c + \gamma_m T_1 I_m \end{bmatrix}. \tag{4.3.3.2.5}$$

It is clear that $\hat{G}(X, Z) \geq 0$ for all $(X, Z) \in R_+^9$, since $\frac{\Lambda_C}{\mu_C B_0} \geq \frac{S_C}{B_0 + B_C}$ and $\frac{\Lambda_\phi}{\mu_\phi} \geq M_\phi$. It is also clear that A is an M-matrix, since the off diagonal elements of A are non-negative. We state a theorem which summarizes the above result.

Theorem 4.2. *The disease-free equilibrium of model system (4.2.1) is globally asymptotically stable if $R_0 \leq 1$ and the assumptions $(H1)$ and $(H2)$ are satisfied.*

4.3.4 Endemic Equilibrium State of the embedded multiscale model

The endemic equilibrium state of the multiscale model system (4.2.1) is given by

$$E^* = \left(S_C^*, I_C^*, B_C^*, B_c^*, M_\phi^*, I_m^* T_0^* T_1^*, T_2^*\right)$$

satisfies

$$\begin{cases} 0 &= \Lambda_C - \lambda_C(t)S_C(t) - \mu_C S_C(t), \\ 0 &= \lambda_C(t)S_C(t) - [\mu_C + \delta_C]I_C(t), \\ 0 &= \alpha_c B_c(t)I_c(t) - \mu_B B_C(t), \\ 0 &= \lambda_c S_c + N_m k_m I_m(t) - [\mu_c + \alpha_c]B_c(t), \\ 0 &= \Lambda_\phi - \beta_\phi M_\phi(t)B_c(t) - \mu_\phi M_\phi(t), \\ 0 &= \beta_\Phi M_\phi(t)B_c(t) - \gamma_m T_1(t)I_m(t) - [k_m + \mu_\phi]I_m(t), \\ 0 &= \Lambda_0 - [\delta_m I_m(t) + \delta_b B_c(t)]T_0(t) - \mu_0 T_0(t), \\ 0 &= \theta_1 \delta_m I_m(t)T_0(t) - \mu_1 T_1(t), \\ 0 &= \theta_2 \delta_b B_c(t)T_0(t) - \mu_2 T_2(t) \end{cases} \tag{4.3.4.1}$$

where

$$\begin{cases} \lambda_C &= \dfrac{\beta_C B_C}{B_0 + B_C}, \\ \lambda_c &= \dfrac{\beta_C B_C(S_C - 1)}{(B_0 + B_C)\Phi_C(I_C + 1)} \end{cases} \tag{4.3.4.2}$$

for all $S_C^*, I_C^*, B_C^*, B_c^*, M_\phi^*, I_m^*, T_0^*, T_1^*, T_2^* > 0$.

Based on the expressions in (4.3.4.1), we can therefore estimate the disease burden of PTB in ruminants. We achieved this by estimating the endemic values of the PTB disease variables $S_C^*, I_C^*, B_C^*, B_c^*, M_\phi^*, I_m^*, T_0^*, T_1^*, T_2^*$. The endemic value of susceptible ruminants is given by

$$S_C^* = \frac{\Lambda_C}{\lambda_C^* + \mu_C}. \tag{4.3.4.3}$$

From Eqn. (4.3.4.3) the susceptible ruminant population at endemic equilibrium is given by

the rate at which new susceptible ruminant individuals entering into the susceptible class at a constant rate Λ_C and the average time of stay in the susceptible class. Susceptible ruminants leave the susceptible class either through infection or death. The endemic value of infected ruminants is given by

$$I_C^* = \frac{\lambda_C^* S_C^*}{\mu_C + \delta_C}. \tag{4.3.4.4}$$

From Eqn. (4.3.4.4) the population of infected ruminants at the endemic equilibrium steady state is determined by the rate at which susceptible ruminants become infected and the density of susceptible ruminants and the average time of stay in the infected class. The endemic value of between-host scale MAP bacterial load in the environment at the equilibrium steady state is given by

$$B_C^* = \frac{\alpha_c B_c^* (I_C^* + 1)}{\alpha_C}. \tag{4.3.4.5}$$

From Eqn. (4.3.4.5) the between-host MAP bacterial load in the environment at the equilibrium steady state is given by the rate of excretion of the average number of the within-host MAP bacterial load by each infected ruminant individual into the environment and the average life-span of the bacteria in the environment. It should be noted that this expression provides a link between the dynamics of the within-host MAP bacterial load and the transmission dynamics of the disease at the ruminant population level. The endemic value of within-host scale MAP bacterial load within a single infected ruminant is given by

$$B_c^* = \frac{\lambda_c^* S_c^* + N_m k_m I_m^*}{(\alpha_c + \mu_c)}. \tag{4.3.4.6}$$

From Eqn. (4.3.4.6) the population of within-host MAP bacteria within a single infected ruminant at endemic equilibrium steady state is determined by the average dose of the between-host bacterial load in the environment are ingested and the average life-span of within-host bacterial load at the site of infection within an infected ruminant and the average number rate of the within-host MAP bacilli bacteria produced by bursting infected macrophage cells at a site of infection. It should also be noted that this expression provides a link between the dynamics of the between-host MAP bacterial load in the environment and the within-host infection dynamics within a single infected ruminant. The value of susceptible macrophage population within a single infected ruminant at equilibrium steady state is given by

$$M_\phi^* = \frac{\Lambda_\phi}{\beta_\phi B_c^* + \mu_\phi}. \tag{4.3.4.7}$$

From Eqn. (4.3.4.7) the susceptible macrophage population at endemic equilibrium within an infected ruminant host is proportional to the average time of stay in susceptible macrophage class and the rate at which new susceptible macrophage are supplied into the susceptible macrophage class at the site of infection within this infected ruminant. The endemic value of infected macrophage population is given by

$$I_m^* = \frac{\beta_\phi B_c^* M_\phi^*}{k_m + \mu_\phi + \gamma_m T_1^*}. \tag{4.3.4.8}$$

From Eqn. (4.3.4.8) the infected macrophage population at the endemic equilibrium steady state is proportional to the average time of stay in the infected macrophage class at the site of infection, the rate at which susceptible macrophages become infected and the density of susceptible macrophages. The endemic value of naïve CD4 T cell population within a single infected ruminant at the site of infection is given by

$$T_0^* = \frac{\Lambda_0}{\delta_m I_m^* + \delta_b B_c^* + \mu_0}. \tag{4.3.4.9}$$

The average population of naïve immune response cells at a site of infection within an infected human at endemic equilibrium point is equal to the average life-span of naïve CD4 T cells and the supply rate of naïve CD4 T cells into a site of infection from the source within an infected ruminant body. The endemic value of a single ruminant MAP-specific immune response Th1 effector cells within a single infected ruminant at the site of infection is given by

$$T_1^* = \frac{\theta_1 \delta_m I_m^* T_0^*}{\mu_1}, \tag{4.3.4.10}$$

The average population of MAP-specific immune response Th1 effector cells within an infected ruminant is proportional to the differential rate of naïve CD4 T cells into the class of MAP-specific immune response cell Th1 effector population after a detection of infected macrophage cells at the site of infection. The endemic value of a single ruminant MAP-specific immune response Th2 effector cell within a single infected ruminant at the site of infection is given by

$$T_2^* = \frac{\theta_2 \delta_b B_c^* T_0^*}{\mu_2}. \tag{4.3.4.11}$$

From Eqn. (4.3.4.11) that the MAP-specific immune response Th1 effector cell population within a single infected ruminant at equilibrium point is proportional to the differential rate of naïve CD4 T cells into the class of MAP-specific immune response Th2 effector population after a detection of the within-host MAP bacterial load at the site of infection.

From the endemic equilibrium values of the model system (4.2.1) given by expressions (4.3.4.3)-(4.3.4.11), we deduce that the between-host scale expression B_C^* depends on both the within-host and the between-host disease variables, while the within-host scale expression B_c^* is determined by both the within-host and the between-host disease variables. Therefore, the obtained results here show that the within-host scale and the between-host scale dynamics influence each other in a reciprocal way.

4.3.5 Stability Analysis of the Embedded Multiscale Model Endemic Equilibrium State

In this sub-section, we evaluated the local stability of the endemic steady state of the model system (4.2.1) by using the center manifold theory in [57] as in the previous chapters. In this case, we employed Center Manifold Theory by making the following changes of variables: letting $S_C = x_1$, $I_C = x_2$, $B_C = x_3$, $B_c = x_4$, $M_\phi = x_5$, $I_m = x_6$, $T_0 = x_7$, $T_1 = x_8$ and $T_2 = x_9$. We used the vector notation $\mathbf{x} = (x_1, x_2, x_3, x_4, x_5, x_6, x_7, x_8, x_9)^T$ so that the model system (4.2.1) can be written in the form

$$\frac{d\mathbf{x}}{dt} = \mathbf{f}(\mathbf{x}, \beta^*) \tag{4.3.5.1}$$

where

$$\mathbf{f} = (f_1, f_2, f_3, f_4, f_5, f_6, f_7, f_8, f_9). \tag{4.3.5.2}$$

Therefore, model system (4.2.1) can be re-written as:

$$\begin{cases} i.\ \ \dot{x}_1 &= \Lambda_C - \dfrac{\beta_C x_3(t)}{B_0 + x_3(t)} x_1(t) - \mu_C x_1(t), \\ ii.\ \ \dot{x}_2 &= \dfrac{\beta_C x_3(t)}{B_0 + x_3(t)} x_1(t) - [\mu_C + \delta_C] x_2(t), \\ iii.\ \ \dot{x}_3 &= \alpha_c x_4(t)(x_2(t) + 1) - \alpha_C x_3(t), \\ iv.\ \ \dot{x}_4 &= \dfrac{\beta_C x_3(t)(x_1(t) - 1)}{(B_0 + x_3(t))\Phi_C(x_2 + 1)} + N_m k_m x_6(t) - [\mu_c + \alpha_c] x_4(t), \\ v.\ \ \dot{x}_5 &= \Lambda_\phi - \beta_\phi x_5(t) x_4(t) - \mu_\phi x_5(t), \\ vi.\ \ \dot{x}_6 &= \beta_\phi x_5(t) x_4(t) - \gamma_m x_8(t) x_6(t) - [k_m + \mu_\phi] x_6(t), \\ vii.\ \ \dot{x}_7 &= \Lambda_0 - [\delta_m x_6(t) + \delta_b x_4(t)] x_7(t) - \mu_0 x_7(t), \\ viii.\ \ \dot{x}_8 &= \theta_1 \delta_m x_6(t) x_7(t) - \mu_1 x_8(t), \\ ix.\ \ \dot{x}_9 &= \theta_2 \delta_b x_4(t) x_7(t) - \mu_2 x_9(t). \end{cases} \tag{4.3.5.3}$$

The Jacobian matrix associated with the system of equations (4.3.5.3) evaluated at the disease-free equilibrium (E_0) is given by

$$J(E_0) = \begin{pmatrix} -\mu_C & 0 & -\frac{\beta_C \Lambda_C}{\mu_C B_0} & 0 & 0 & 0 & 0 & 0 & 0 \\ 0 & -z_0 & \frac{\beta_C \Lambda_C}{\mu_C B_0} & 0 & 0 & 0 & 0 & 0 & 0 \\ 0 & 0 & -\alpha_C & \alpha_c & 0 & 0 & 0 & 0 & 0 \\ 0 & 0 & q_1 & -z_1 & 0 & N_m k_m & 0 & 0 & 0 \\ 0 & 0 & 0 & -\frac{\beta_\phi \Lambda_\phi}{\mu_\phi} & -\mu_\phi & 0 & 0 & 0 & 0 \\ 0 & 0 & 0 & \frac{\beta_\phi \Lambda_\phi}{\mu_\phi} & 0 & -z_2 & 0 & 0 & 0 \\ 0 & 0 & 0 & -\frac{\delta_b \Lambda_0}{\mu_0} & 0 & -\frac{\delta_m \Lambda_0}{\mu_0} & -\mu_0 & 0 & 0 \\ 0 & 0 & 0 & 0 & 0 & \frac{\theta_1 \delta_m \Lambda_0}{\mu_0} & 0 & -\mu_1 & 0 \\ 0 & 0 & 0 & \frac{\theta_2 \delta_b \Lambda_0}{\mu_0} & 0 & 0 & 0 & 0 & -\mu_2 \end{pmatrix} \tag{4.3.5.4}$$

where

$$\begin{cases} z_0 = (\mu_C + \delta_C), \\ z_1 = (\mu_c + \alpha_c), \\ z_2 = (\mu_\phi + k_m), \\ q_1 = \frac{\beta_C (\Lambda_C - \mu_C)}{\Phi_C \mu_C B_0}. \end{cases} \tag{4.3.5.5}$$

Using the similar approach as in the previous Chapters, the basic reproductive number of model system (4.3.5.3) is

$$R_0 = \frac{1}{2}\left[R_{0_c} + \sqrt{R_{0_c}^2 + 4R_{0_C}}\right] \tag{4.3.5.6}$$

where

$$R_{0_c} = \frac{\beta_\phi \Lambda_\phi N_k k_m}{\mu_\phi(\mu_\Phi + \delta_\phi)(\mu_c + \sigma_c + \alpha_c)} \tag{4.3.5.7}$$

and

$$R_{0_C} = \frac{\beta_C(\Lambda_C - \mu_C)\alpha_c}{\mu_B B_0 \mu_C(\mu_c + \alpha_c)\Phi_C}. \tag{4.3.5.8}$$

Now, let us consider $\beta_\phi = k\beta_C$, regardless of whether $k \in (0,1)$ or $k \geq 1$ and let $\beta_C = \beta^*$ be a bifurcation parameter of the model system (4.3.5.3). Considering $R_0 = 1$, and solve for β^* in equation (4.3.5.6), we obtain:

$$\beta^* = \frac{(\mu_c + \alpha_c)\mu_\phi(\mu_\phi + \delta_\phi)\alpha_C B_0 \mu_C \Phi_C}{k\Lambda_\phi N_m k_m \alpha_C \mu_C B_0 \mu_C \Phi_C + \alpha_c(\Lambda_C - \mu_C)\mu_\phi(\mu_\phi + k_m)}. \tag{4.3.5.9}$$

We noted that the linearized system of the transformed equations (4.3.5.3) with bifurcation point β^* has a simple zero eigenvalue. Hence, the Center Manifold Theory [57] can be used to analyze the dynamics of (4.3.5.3) near $\beta_C = \beta^*$. We, therefore, apply Theorem 4.1 in Castillo-Chavez and Song [5] stated below as Theorem 4.3 for convenience, to show the local asymptotic stability of the endemic equilibrium point of (4.3.5.3) (which is the same as the endemic equilibrium point of the original system (4.2.1) for $\beta_C = \beta^*$).

Theorem 4.3. *Consider the following general system of ordinary differential equations with parameter ϕ:*

$$\frac{dx}{dt} = f(x,\phi), \quad f : R^n \times R \longrightarrow R, \quad f : C^2(R^2 \times R), \tag{4.3.5.10}$$

where 0 is an equilibrium of the system, that is $f(0,\phi) = 0$ for all ϕ, and assume that

A1. $A = D_x f(0,0) = ((\partial f_i/\partial x_j)(0,0))$ *is a linearization matrix of the model system (4.3.5.10) around the equilibrium 0 with ϕ evaluated at 0. Zero is a simple eigenvalue of A and other eigenvalues of A have negative real parts,*

A2. matrix A has a right eigenvector u and a left eigenvector v corresponding to the zero eigenvalue.

Let f_k be the k^{th} component of f and

$$\begin{aligned} a &= \sum_{k,i,j=1}^{n} u_k v_i v_j \frac{\partial^2 f_k}{\partial x_i \partial x_j}(0,0), \\ b &= \sum_{k,i=1}^{n} u_k v_i \frac{\partial^2 f_k}{\partial x_i \partial \phi}(0,0). \end{aligned} \tag{4.3.5.11}$$

The local dynamics of (4.3.5.10) around 0 are totally governed by a and b and are summarized as follows.

1. *$a > 0$, $b > 0$. When $\phi < 0$ with $|\phi| \ll 1$, 0 is locally asymptotically stable and there exists a positive unstable equilibrium; when $0 < \phi \ll 1$, 0 is unstable and there exists a negative and locally asymptotically stable equilibrium.*

2. *$a < 0$, $b < 0$. When $\phi < 0$ with $|\phi| \ll 1$, 0 is unstable; when $0 < \phi \ll 1$, 0 is locally asymptotically stable and there exists a positive unstable equilibrium;*

3. *$a > 0$, $b < 0$. When $\phi < 0$ with $|\phi| \ll 1$, 0 is unstable and there exists a locally asymptotically stable negative equilibrium; when $0 < \phi \ll 1$, 0 is stable and a positive unstable equilibrium appears;*

4. *$a < 0$, $b > 0$. When ϕ changes from negative to positive, 0 changes its stability from stable to unstable. Correspondingly, a negative unstable equilibrium becomes positive and locally asymptotically stable.*

In order to apply Theorem 4.3, the following computations are necessary (it should be noted that we are using β^* as the bifurcation parameter, in place of ϕ in Theorem 4.3).

Eigenvectors of J_{β^*}: For the case when $R_0 = 1$, it can be shown that the Jacobian matrix of (4.3.5.4) at $\beta_C = \beta^*$ (denoted by J_{β^*}) has a right eigenvector associated with the zero eigenvalue given by

$$\mathbf{u} = [u_1, u_2, u_3, u_4, u_5, u_6, u_7, u_8, u_9]^T \tag{4.3.5.12}$$

where

$$\begin{cases} u_1 &= -\dfrac{\beta^*\Lambda_C}{\mu_C^2 B_0 \alpha_C}, \\ u_2 &= \dfrac{\alpha_c \beta^*\Lambda_C}{B_0\mu_C(\mu_C+\delta_C)\alpha_C}, \\ u_3 &= \dfrac{\alpha_c}{\alpha_C}, \\ u_4 &= 1, \\ u_5 &= -\dfrac{k\beta^*\Lambda_\phi}{\mu_\phi^2}, \\ u_6 &= \dfrac{k\beta^*\Lambda_\Phi}{\mu_\phi(\mu_\phi+\delta_\phi)}, \\ u_7 &= -\left[\dfrac{\delta_b\Lambda_0}{\mu_0^2}+\dfrac{\delta_m\Lambda_0 k\beta^*\Lambda_\Phi}{\mu_0^2(\mu_\phi+k_m)\mu_\phi}\right], \\ u_8 &= \dfrac{\theta_1\delta_m\Lambda_0 k\beta^*\Lambda_\phi}{\mu_0(\mu_\phi+k_m)\mu_\phi\mu_1}, \\ u_9 &= \dfrac{\theta_2\delta_b\Lambda_0}{\mu_0\mu_2}. \end{cases} \tag{4.3.5.13}$$

In addition, the left eigenvector of the Jacobian matrix in (4.3.5.4) associated with the zero eigenvalue at $\beta_C = \beta^*$ is given by

$$\mathbf{v} = [v_1, v_2, v_3, v_4, v_5, v_6, v_7, v_8, v_9]^T, \tag{4.3.5.14}$$

where

$$\begin{cases} v_1 &= 0, \\ v_2 &= 0, \\ v_3 &= \dfrac{\beta^*(\Lambda_C - \mu_C)}{\alpha_C \mu_C \Phi_C B_0}, \\ v_4 &= 1, \\ v_5 &= 0, \\ v_6 &= \dfrac{N_m k_m}{(\mu_\phi + k_m)}, \\ v_7 &= 0, \\ v_8 &= 0, \\ v_9 &= 0. \end{cases} \tag{4.3.5.15}$$

Computation of bifurcation parameters a and b:

We evaluated the non-zero second order mixed derivatives of **f** with respect to the variables and β^* in order to determine the signs of a and b. The sign of a is associated with the following non-vanishing partial derivatives of **f**:

$$\begin{cases} \dfrac{\partial^2 f_1}{\partial x_3^2} &= \dfrac{2\beta^* \Lambda_C}{B_0^2 \mu_C}, \\ \dfrac{\partial^2 f_2}{\partial x_3^2} &= -\dfrac{2\beta^* \Lambda_C}{B_0^2 \mu_C}, \\ \dfrac{\partial^2 f_3}{\partial x_3^2} &= -\dfrac{2\beta^* (\Lambda_C - \mu_C)}{B_0^2 \mu_C \Phi_C}. \end{cases} \tag{4.3.5.16}$$

The sign of b is associated with the following non-vanishing partial derivatives of $\mathbf{f}$:

$$\begin{cases} \dfrac{\partial^2 f_1}{\partial x_3 \partial \beta^*} = -\dfrac{\Lambda_C}{\mu_C B_0}, \\ \dfrac{\partial^2 f_2}{\partial x_3 \partial \beta^*} = \dfrac{\Lambda_C}{\mu_C B_0}, \\ \dfrac{\partial^2 f_4}{\partial x_3 \partial \beta^*} = \dfrac{(\Lambda_C - \mu_C)}{\mu_C B_0 \Phi_C}, \\ \dfrac{\partial^2 f_5}{\partial x_4 \partial \beta^*} = -\dfrac{\Lambda_\phi}{\mu_\phi}, \\ \dfrac{\partial^2 f_6}{\partial x_4 \partial \beta^*} = \dfrac{k\Lambda_\phi}{\mu_\phi}. \end{cases} \tag{4.3.5.17}$$

Substituting expressions (4.3.5.13), (4.3.5.15) and (4.3.5.16) into equation (4.3.5.11), we get

$$\begin{cases} a = u_1 v_3^2 \dfrac{\partial^2 f_1}{\partial x_3^2} + u_2 v_3^2 \dfrac{\partial^2 f_2}{\partial x_3^2} + u_4 v_3^2 \dfrac{\partial^2 f_4}{\partial x_3^2} + \\ \quad = u_1 v_3^2 \left[\dfrac{2\beta^* \Lambda_C}{B_0^2 \mu_C}\right] + u_2 v_3^2 \left[\dfrac{-2\beta^* \Lambda_C}{B_0^2 \mu_C}\right] + u_4 v_3^2 \left[\dfrac{-2\beta^*(\Lambda_C - \mu_C)}{\Phi_C B_0^2 \mu_C}\right] \\ \quad = \dfrac{2\beta^* \Lambda_C}{B_0^2 \mu_C}.v_3^2 \left[u_1 - u_2\right] - u_4 v_3^2 \left[\dfrac{2\beta^*(\Lambda_C - \mu_C)}{\Phi_C B_0^2 \mu_C}\right] < 0 \end{cases} \tag{4.3.5.18}$$

since $(u_1 - u_2) < 0$, $u_4 > 0$, and $v_3 > 0$.

Similarly, substituting expressions (4.3.5.13) (4.3.5.15) and (4.3.5.17) into equation (4.3.5.11), we get

$$\begin{cases} b = u_1 v_3 \dfrac{\partial^2 f_1}{\partial x_3 \partial \beta^*} + u_2 v_3 \dfrac{\partial^2 f_2}{\partial x_3 \partial \beta^*} + u_4 v_3 \dfrac{\partial^2 f_4}{\partial x_3 \partial \beta^*} + u_5 v_4 \dfrac{\partial^2 f_4}{\partial x_{10} \partial \beta^*} + u_6 v_4 \dfrac{\partial^2 f_6}{\partial x_4 \partial \beta^*}, \\ \quad = v_3 \left[\dfrac{\Lambda_C}{B_0 \mu_C}.u_2 - \dfrac{\Lambda_C}{B_0 \mu_C}.u_1 + \dfrac{(\Lambda_C - \mu_C)}{\Phi_C B_0 \mu_C}.u_4\right] + v_4 \left[\dfrac{k\Lambda_\phi}{\mu_\phi}.u_6 - \dfrac{k\Lambda_\phi}{\mu_\phi}.u_5\right], \\ \quad = \dfrac{\Lambda_C}{B_0 \mu_C}.v_3 \left[u_2 - u_1\right] + \dfrac{(\Lambda_C - \mu_C)}{\Phi_C B_0 \mu_C}.v_3 u_4 + \dfrac{k\Lambda_\phi}{\mu_\phi}.v_4 \left[u_6 - u_5\right] > 0 \end{cases} \tag{4.3.5.19}$$

since $(u_2 - u_1) > 0$, $(u_6 - u_5) > 0$, $u_4 > 0$, and $v_3 > 0$.

Thus, $a < 0$ and $b > 0$. Using Theorem 4.3, item (iv), we have established the following result which only holds for $R_0 > 1$ but close to 1:

Theorem 4.4. *The endemic equilibrium guaranteed by the Center Manifold Theorem 4.3 is locally asymptotically stable for $R_0 > 1$ near 1.*

4.3.6 Sensitivity Analysis

In this section, we conducted sensitivity analysis to evaluate the relative change in a proposed PTB health intervention metric when the within-host and between-host parameters of the multiscale model system (4.2.1) changes. We achieved this by using Latin Hypercube Sampling (LHS) and Partial Rank Correlation Coefficients (PRCCs). The proposed PTB health intervention metric in this study is the basic reproductive number obtained from the multiscale model (4.2.1). Therefore, we used 1000 simulations per run to investigate the impact of each of the multiscale model system (4.2.1)'s parameters on the proposed PTB dynamics metric. The results of the evaluation of the sensitivity of the PTB dynamic metric to the baseline PTB multiscale model system (4.2.1)'s parameters are shown in the Tornado plots in Fig 4.2. Therefore, based on Fig.4.2, it can be note that some of the model parameters have positive PRCCs and some have negative PRCCs. Thus, parameters with positive PRCCs will increase the PTB dynamics metric, R_0, when they are increased, whereas parameters with negative PRCCs will decrease R_0 when they are increased. For instance, increasing parameter like N_m increases the value of R_0 and also increasing parameters like μ_c reduces the value of R_0.

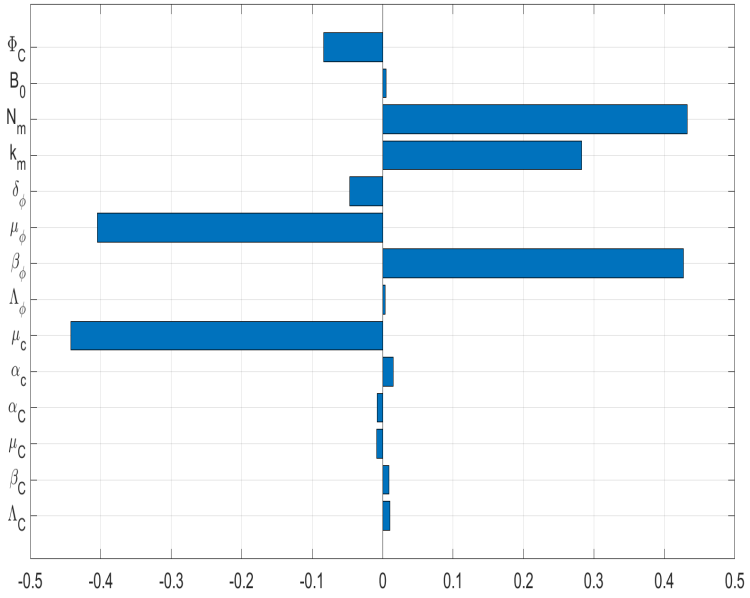

Figure 4.2: *Tornado plots of partial rank correlation coefficients (PRCCs) of all the model parameters that influence the PTB transmission metric* R_0

Therefore, from Fig. 4.2, we make the following deductions:

(i) The most sensitive parameters to the PTB embedded multiscale model disease metric R_0 are N_m, k_m, μ_ϕ, μ_c and β_ϕ, with all being the within-host scale PTB parameters. This is in agreement with sensitive results of the nested multiscale model in Chapter 3 which show that the impact of the within-host scale on the dynamics of the disease is vital compare to the between-host scale parameters. This implies that care should be taken in improving the accuracy of these five within-host scale parameters during data collection if the validity and utility of both the nested and embedded multiscale models of PTB transmission given by (4.2.1) are to be improved. From the assessment of the sensitivity of R_0 to two additional parameters that we can have the most control over (N_m and μ_c), we note that R_0 is also significantly sensitive to these two within-host scale parameters while having the highest sensitivity to N_m. We conclude that administration of PTB drug treatment that kill and restrict the reproduction of the within-host bacteria cells will likely yield the highest benefits in reducing the transmission of PTB at the herd level.

(ii) The sensitivity output results of the embedded multiscale model metric in Fig. 4.2 show the similar trends as to the sensitive output results of the nested multiscale model in Chapter 3 which show that the threshold R_0 is less sensitive to the all three between-host scale

parameters (β_C, α_C, B_0) that we can have a significant control over through some preventive and control intervention measures such as environmentally-hygiene management and vaccinations.

4.4 Numerical Analysis of the baseline multiscale model of ruminant PTB transmission-replication dynamics

This section presented evidence about the reciprocal influence between the immunology and the epidemiology of PTB infection which we get from the numerical simulations of the embedded multiscale model that describes the dynamics of the disease. The numerical values of the parameters used in the numerical simulations are given in Table (4.1).

Parameter	Description	Unit	Initial values	Source
Λ_C	Ruminants birth rate	day^{-1}	0.27	[52, 54]
β_C	Ruminants infection rate	day^{-1}	0.00027	
μ_C	Natural death rate of Ruminant population	day^{-1}	0.0001	[52]
δ_C	Ruminants removal rate due to PTB infection	day^{-1}	0.0008	Assumed
α_C	Environmentally bacteria death rate	day^{-1}	0.0018	[52]
B_0	Saturation rate of bacteria	day^{-1}	1000	[54]
Φ_C	Down-scaling parameter	day^{-1}	0.03	Assumed
Λ_ϕ	Macrophages supply rate	day^{-1}	10	[53]
β_ϕ	Macrophages infection rate	day^{-1}	0.002	[53]
μ_ϕ	Macrophages natural death rate	day^{-1}	0.02	[53]
N_m	Burst size of intracellular MAP	day^{-1}	100	[53]
k_m	Burst rate of infected macrophages	day^{-1}	0.00075	[53]
γ_m	T_1 lytic effect	day^{-1}	0.01	[53]
μ_c	Bacteria's death rate	day^{-1}	0.03	[53]
α_c	Excretion rate of extracellular MAP	day^{-1}	0.01	[54]
Λ_0	T_0 supply rate	day^{-1}	0.001	[53]
μ_0	T_0 death rate	day^{-1}	0.01	[53]
μ_1	T_1 death rate	day^{-1}	0.03	[53]
μ_2	T_2 death rate	day^{-1}	0.02	[53]
δ_m	T_0 differentiation into T_1 cells	day^{-1}	0.01	[53]
δ_b	T_0 differentiation into T_2 cells	day^{-1}	0.01	[53]
θ_1	T_1 cells clonal expansion	day^{-1}	9000	[53]
θ_2	T_2 cells clonal expansion	day^{-1}	9000	[53]

Table 4.1: Model parameter values used for Simulations

4.4.1 The influence of between-host scale on the within-host PTB disease dynamics

In this sub-section, we assessed numerically the effect of the between-host submodel parameters on the within-host submodel PTB pathogen-cell interactions within a single infected ruminant.

Fig. 4.3) - Fig. 4.5 show the impact in the variation of four between-host parameters (β_C, α_C, B_0) on the dynamics of four selected with-host scale variables (I_m, B_c, T_1, T_2).

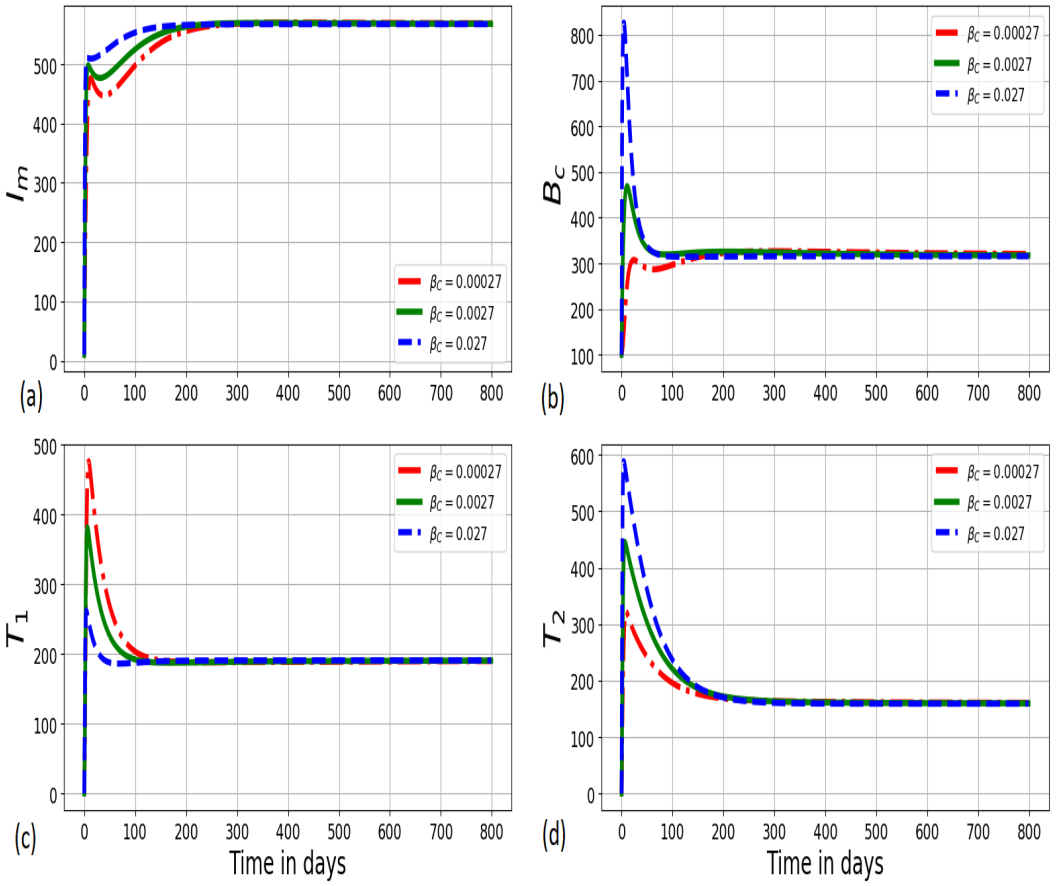

Figure 4.3: *Graph of numerical solutions of model system (4.2.1) showing the evolution in time of (a) infected macrophage population (I_m), (b) within-host MAP bacteria population (B_c), (c) MAP-Specific Th1 response cells (T_1), and (d) MAP-Specific Th2 response cells for different values of between-host transmission rate β_C: β_C = 0.00027, β_C = 0.0027, and β_C = 0.027.*

In Fig. 4.3, we showed the effects of the variation of the infection rate parameter β_C: β_C = 0.00027, β_C = 0.0027, and β_C = 0.027 associated with the between-host scale dynamics on the within-host scale selected variable (a) infected macrophage population (I_m), (b) top right: within-host MAP bacteria population (B_c), (c) MAP-Specific Th1 response cells (T_1), and (d) MAP-Specific Th2 response cells. The results showed that the increase in infection rate at the population level of ruminants will only influence the within-host disease dynamics at the start of an infection within 100 days. But after that there is no difference in the population dynamics of the within-scale MAP bacterial (B_c), MAP-Specific Th2 response cells (T_2), MAP Specific Th1 response cells (T_1), and infected macrophages (I_m) in the long run. This also implies that the variation of infection rate for different values influence the within-host scale disease dynamics

only at the start of infection of about 100 days, after that then converge to the same endemic state. Therefore, these results further confirm that once the minimum infectious dose is consumed, the long term disease dynamics is independent to superinfection.

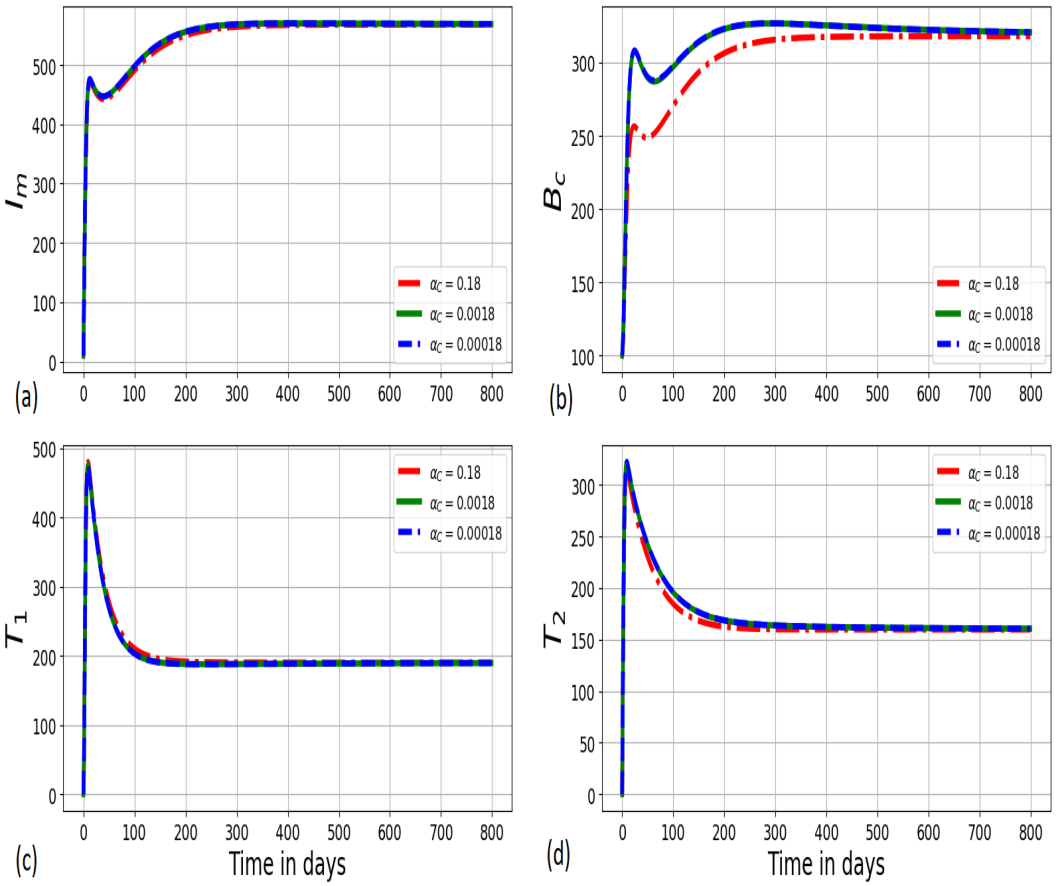

Figure 4.4: *Simulations of model system (4.2.1) showing propagation of (a) infected macrophage population (I_m), (b) within-host MAP bacteria population (B_c), (c) MAP-Specific Th1 response cells (T_1), and (d) bottom right: MAP-Specific Th2 response cells for different values of environmentally MAP bacilli death rate α_C: α_C = 0.18, α_C = 0.018, and α_C = 0.0018.*

In Fig. 4.4, we also illustrated the effects of the variation of natural death rate of MAP bacilli in the environment α_C: α_C = 0.18, α_C = 0.018, and α_C = 0.0018 at the between-host scale on the within-host scale selected variable (a) top left: infected macrophage population (I_m), (b) within-host MAP bacteria population (B_c), (c) MAP-Specific Th1 response cells (T_1), and (d) MAP-Specific Th2 response cells for different values. The results also indicated that increasing the environmentally MAP bacilli death rate will only influence the within-host disease dynamics at the start of an infection within 100 days. However after that there would be no difference in the population dynamics of the within-scale MAP bacterial load (B_c), MAP-Specific Th2 response cells (T_2), MAP Specific Th1 response cells (T_1), and infected macrophages (I_m) in the long run.

This also implies that the variation of infection rate for different values influence the within-host scale disease dynamics only at the start of infection of about 100 days, after that then converge to the same endemic state. Therefore, these results confirm that once the minimum infectious dose is consumed, the long term disease dynamics is independent to superinfection.

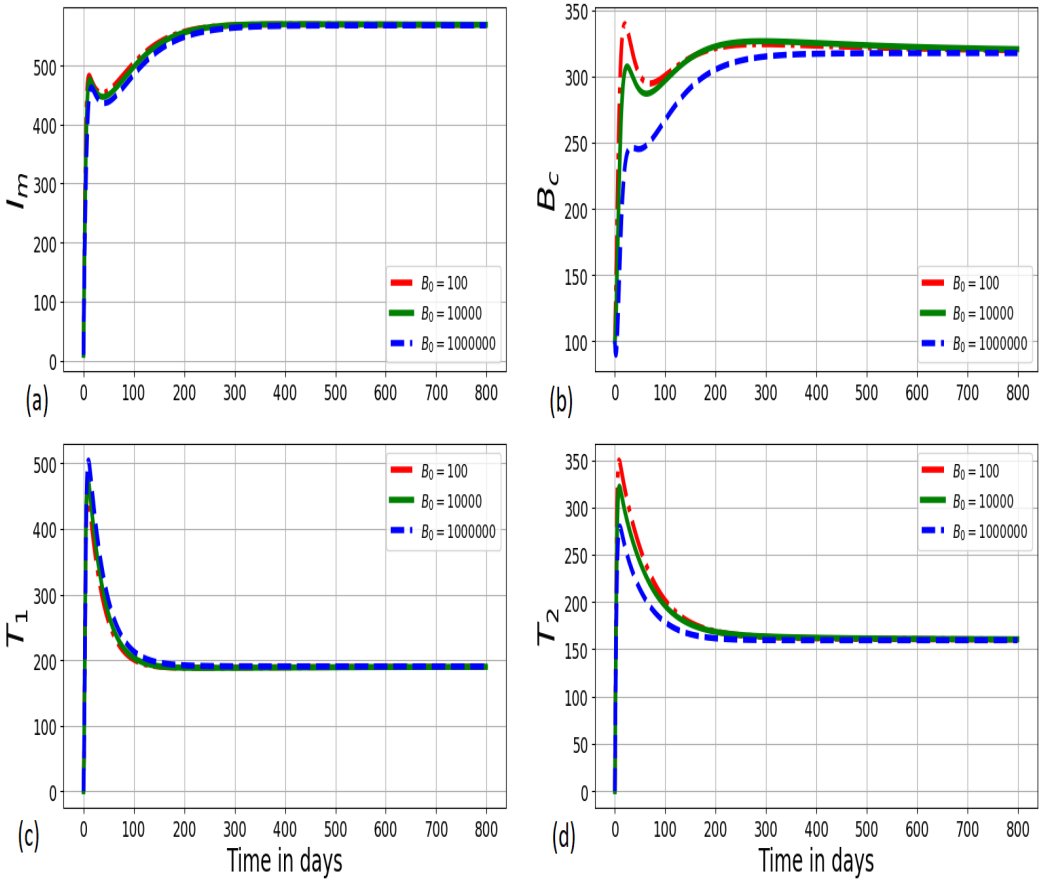

Figure 4.5: *Graph of numerical solutions of model system (4.2.1) showing propagation of (a) infected macrophage population (I_m), (b) top right: within-host MAP bacteria population (B_c), (c) MAP-Specific Th1 response cells (T_1), and (d) MAP-Specific Th2 response cells population for different values of disease induce death rate B_0: $B_0 = 1000$, $B_0 = 10000$, and $B_0 = 100000$.*

In Fig. 4.5, we further showed the effects of variation of the bacteria half saturation constant B_0: $B_0 = 1000$, $B_0 = 10000$, and $B_0 = 100000$ associated with infection of ruminants at the between-host scale on the within-host scale selected variables (a)infected macrophage population (I_m), (b) within-host MAP bacteria population (B_c), (c) MAP-Specific Th1 response cells (T_1), and (d) MAP-Specific Th2 response cells for different values of. Fig. 4.5 show that the health mechanisms that reduce the susceptibility of ruminants to the disease (e.g. administration of vaccine) again will only have a considerable effect on the within-host disease dynamics at

the start of an infection within 100 days. But after that there is no difference in the population dynamics of the within-scale MAP bacterial load (B_c), MAP-Specific Th2 response cells (T_2), MAP Specific Th1 response cells (T_1), and infected macrophages (I_m) in the long run. This again implies that the variation of infection rate for different values influence the within-host scale disease dynamics only at the start of infection of about 100 days, after that then converge to the same endemic state. Therefore, these results again confirm that once the minimum infectious dose is consumed, the long term disease dynamics is independent to superinfection.

Collectively, based on the numerical results in Fig. 4.3 - Fig. 4.3, we noticed that the when the between-host scale parameters are varied, there is a noticeable but minimal changes in the dynamics of the within-host scale variables: I_m, B_c, T_1, T_2. This is because, once the host is infected, superinfection becomes irrelevant as the replication of the MAP bacterial load at the within-host scale sustains the disease dynamics at this scale.

4.4.2 The influence of within-host scale on the between-host PTB disease dynamics

This sub-subsection highlights some numerical assessment results of the influence of the within-host submodel parameters on the between-host submodel PTB transmission dynamics. Fig. 4.6 - Fig. 4.8 show the impact in the variation of three within-host parameters (α_c, N_c, μ_c) on the dynamics of three key between-host scale variables (S_C, I_C, B_C).

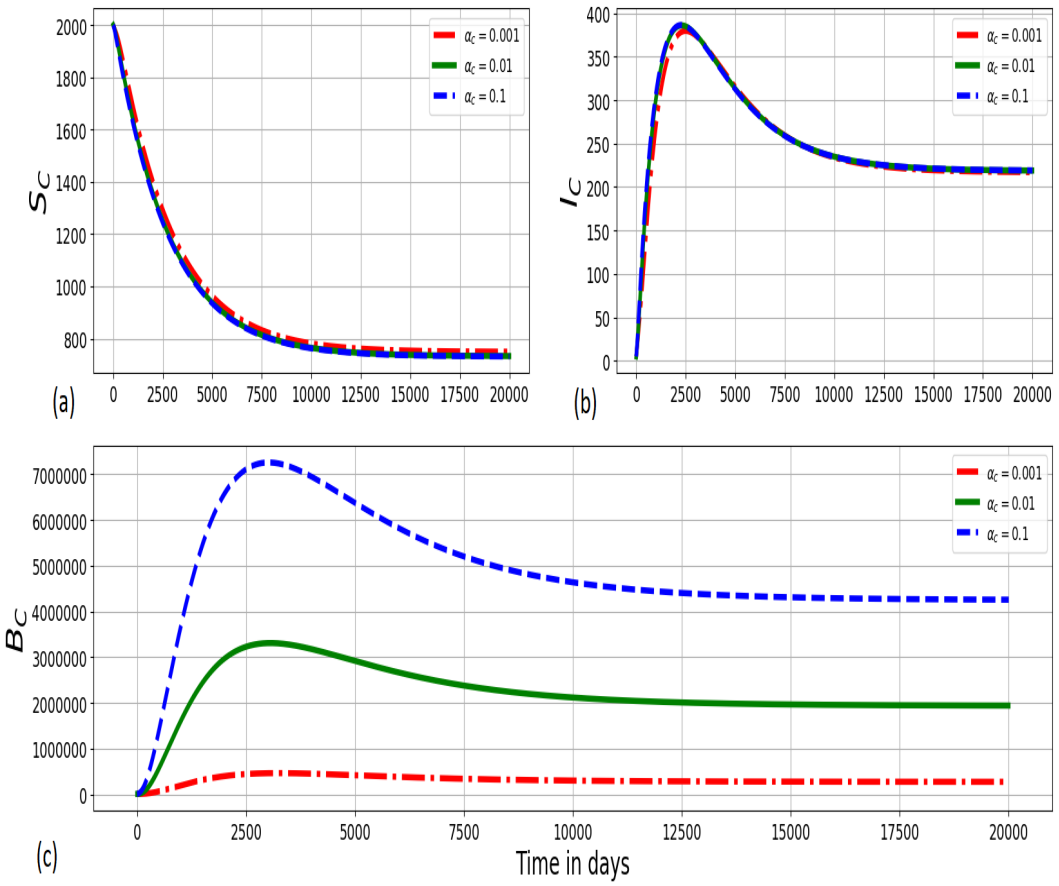

Figure 4.6: *Graph of numerical solutions of the model system (4.2.1) showing the evolution in time of (a) population of susceptible ruminants (S_C), (b) population of infected ruminants (I_C), and (c) between-host MAP bacterial load (B_C) for different values of excretion rate of within-host MAP bacterial load, B_c, α_c: $\alpha_c = 0.001$, $\alpha_c = 0.01$, and $\alpha_c = 0.1$.*

Fig. 4.6 shows graphs of numerical solutions of the model system (4.2.1) showing propagation of (a) population of susceptible ruminants (S_C), (b) population of infected ruminants (I_C), and (c) between-host MAP bacterial load (B_C) for different values of excretion rate of within-host MAP MAP bacilli into the environment α_c: $\alpha_c = 0.001$, $\alpha_c = 0.01$, and $\alpha_c = 0.1$. The results Fig. 4.6 showed that an increase of excretion rate of the within-host bacterial load into the physical environment by each infected ruminant individual has important public health effect at the ruminant population-level in that there is a noticeable increase in the between-host MAP bacteria B_C and population of infected ruminant I_C as well as decrease in the population of susceptible ruminant S_C.

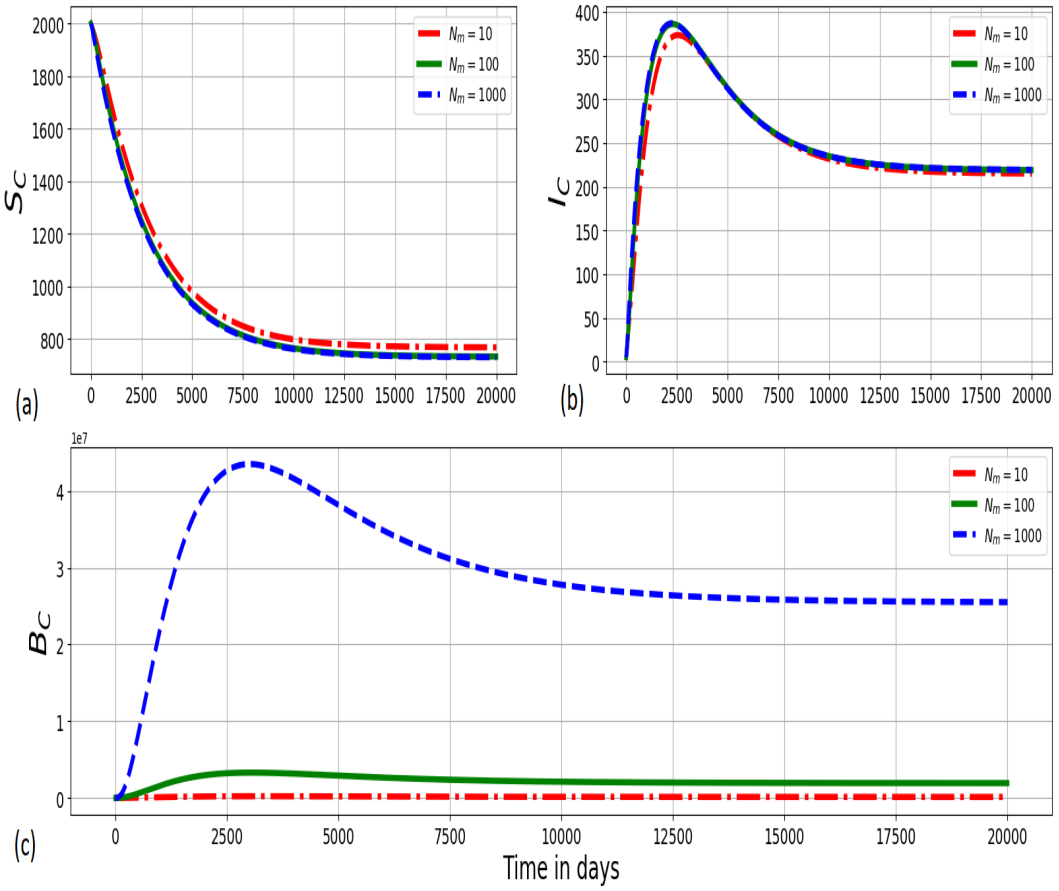

Figure 4.7: *Graphs showing changes in (a) population of susceptible ruminants (S_C), (b) population of infected ruminants (I_C), and (c) between-host MAP bacterial load (B_C) for different values of within-host MAP bacteria produced per bursting infected macrophage cell N_m:* $N_m = 10$, $N_m = 100$, $N_m = 1000$.

Fig. 4.7 shows graphs of numerical solutions of the model system (4.2.1) showing variation of (a) population of susceptible ruminants (S_C), (b) population of infected ruminants (I_C), and (c) between-host MAP bacterial load (B_C) for different values of within-host MAP bacteria produced per bursting infected macrophage cell N_m: $N_m = 10$, $N_m = 100$, $N_m = 1000$. This shows that as an average replication rate of the within-host MAP bacilli bacteria at an infected macrophage cell-scale at individual ruminant level increases, transmission of PTB infection at herd-level of ruminant also increases.

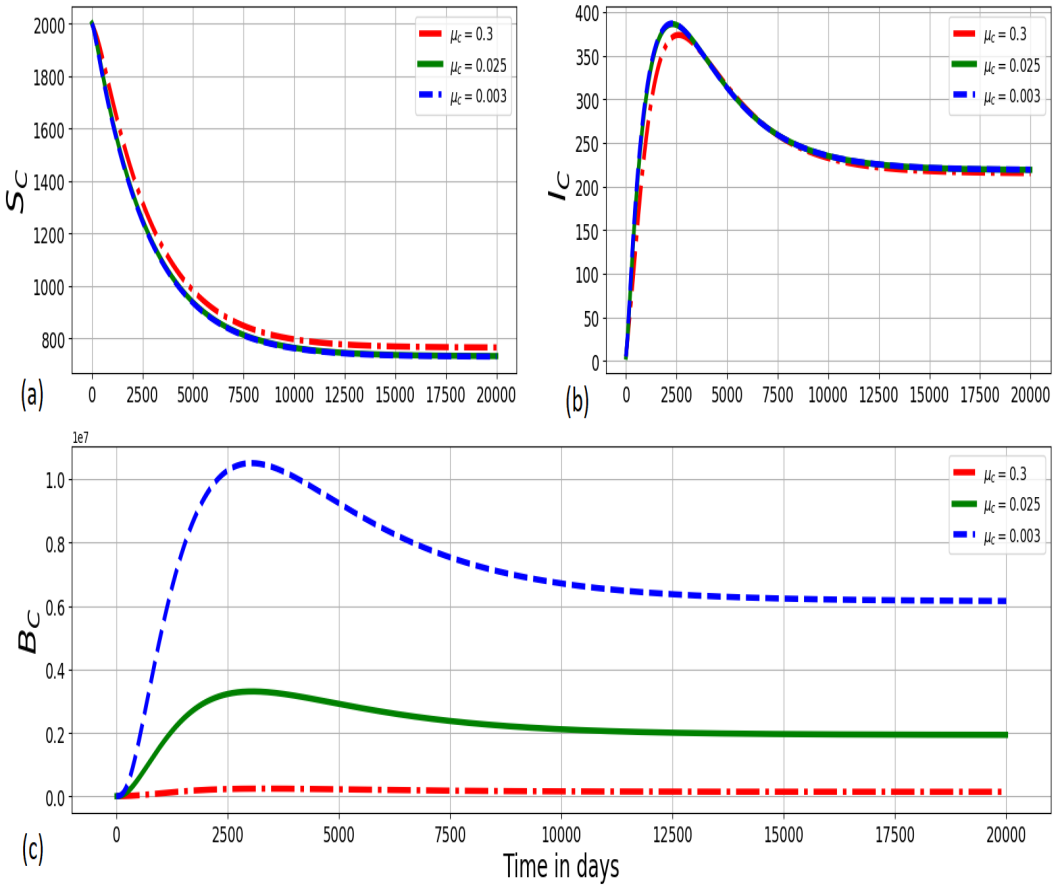

Figure 4.8: *Simulations of model system (4.2.1) showing changes of (a) top left: population of susceptible ruminants (S_C), (b) top right:population of infected ruminants (I_C), and (c) bottom: between-host MAP bacterial load (B_C) for different values of death rate of the within-host MAP bacterial load, μ_c: $\mu_c = 0.3$, $\mu_c = 0.025$, and $\mu_c = 0.003$.*

Fig. 4.8 illustrates the solution profile of the multiscale model system (4.2.1) showing variations of (a) population of susceptible ruminants (S_C), (b) population of infected ruminants (I_C), and (c) between-host MAP bacterial load (B_C) for different values of natural death rate of within-host MAP bacilli at the site of infection within an infected ruminant μ_c: $\mu_c = 0.3$, $\mu_c = 0.025$, and $\mu_c = 0.003$. The results in Fig. 4.8 showed that as the death rate of the within-host MAP bacilli increase, there is a noticeable decrease in the between-host MAP bacterial load, B_C and population of infected ruminant, I_C as well as increase in the population of susceptible ruminant S_C. This again confirms the influence of the between-host parameters on the infection dynamics at the ruminant population-level.

Overall, based on the numerical results in Fig. 4.3 - Fig. 4.8, we can conclude that:

a. The between-host scale influences the within-host scale through the superinfection of the infectious agent.

b. Once the minimum infectious dose is consumed, superinfection makes no different on the dynamics of the disease when the infection at the within-host scale has successfully been established because the infection at this domain scale is sustained by pathogen replication.

c. The within-host scale continuously influence the dynamics of the disease at the between-host scale throughout the infection.

This indeed indicates that during the dynamics for paratuberculosis infection in ruminants, the contribution of initial infective inoculum to the total pathogen load becomes negligible compared to the contribution of the replication-cycle.

4.5 Summary

The contribution of this chapter to scientific knowledge is the use of embedded multiscale model developed to investigate the effect of super-infection on the intrinsic dynamics of Paratuberculosis in ruminants as a representative of all type II environmentally-transmitted disease systems in which a pathogen replication-cycle occurs only at the microscale. To the best of our knowledge, the embedded multiscale model developed in this study is the first of its kind to characterize an infectious diseases in which pathogen replication occurs only at the microscale. Similar to the nested multiscale model results in Chapter 3, the embedded multiscale model results in this chapter (through numerical simulation) also illustrate that the transmission of the PTB disease at the between-host scale only influences the disease dynamics at the within-host scale at the start of the infection, while once the infection has been established, the replication of MAP bacteria at the within-host scale sustain the dynamics of PTB disease. This means that once the minimum infectious dose is consumed, superinfection become irrelevant when the infection at the within-host scale has successfully been established. This implies that repeated infection of the ruminant by the bacteria before it recovers from prior infection by PTB infection does not significantly alter the total pathogen load within an infected ruminant. Sensitivity analysis of the model parameters was also carried out using the basic reproduction number of the embedded multiscale model as the disease metric that characterized the infection at the start of an infection. The sensitivity analysis of the embedded multiscale model basic reproductive number was based on the Latin Hypercube Sampling (LHS) scheme. The results output of sensitivity analysis of the basic reproductive number of the embedded multiscale model in this chapter are consistent with the sensitivity analysis results of the basic reproductive numberwe obtain from the nested multiscale

model in the previous chapter (i.e, Chapter 3) that indicate that the variation of the decay rate in the within-host MAP bacteria population has a significant effect on the transmission risk of the disease at the ruminant population level. Therefore, taking into account that there are no drugs for PTB infection (intervention which is administrated at within-host scale), these results suggest that the development of a drug that kills and restrict replication of MAP bacteria at within-host scale would have the highest impact on the reduction of the transmission risk of the disease among the ruminants at the herd level. Although the embedded multiscale modelling framework developed here to specific disease system of paratuberculosis in ruminants, we anticipate it to be robust enough to be applicable to other infectious diseases of type II environmentally-transmitted diseases beyond paratuberculosis in ruminants.

Chapter 5

Comparison of the Multiscale Models in Predicting Dynamics of Infectious Diseases

5.1 Introduction

In Chapter 3 and Chapter 4, we respectively developed both a nested multiscale model (NMSM) and an embedded multiscale model (EMSM) which we used to study the intrinsic dynamics of Partuberculosis (PTB) in ruminants as a typical example of type II environmentally-transmitted diseases in which the pathogen has a replication-cycle at the microscale (i.e. at within-host scale). A key feature of disease dynamics at any level of organization is that it is characterized by the replication-transmission relativity [8]. The theory posits that at any level of organization of an infectious disease there is a multiscale cycle/loop that involves the reciprocal influence of the microscale and the macroscale. Both NNSMs and EMSMs describe this invariant feature of the multiscale dynamics of infectious disease systems. However, the underlying difference is that in NMSMs the macroscale influences the micro-scale through pathogen initial inoculum, whereas in EMSMs the macroscale influences the microscale through super-infection (i.e. repeated infection by a pathogen of the same species/strain before the host recovers from prior infection by the same pathogen species/strain). At this stage what we know is that PTB disease dynamics in ruminants involves a pathogen replication-cycle at the microscale (i.e. at within-host scale). We also know that when the infection of the host involves a minimum infectious dose, then this is the one that triggers the replication. The contribution of any subsequent infections to the total pathogen

load becomes negligible compared to the contribution of the replication cycle. This means that repeated infection of the host by the bacteria before the host recovers from prior infection by PTB does not significantly alter the total pathogen load within an infected host. This in turn means that superinfection would not make a difference in disease dynamics. Thus both the NMSM and the EMSM can equally be used to characterize an infectious disease that involves a pathogen replication-cycle at the microscale such as PTB. What we do not know is whether the NMSM and the MSM would predict similar trends in disease dynamics. The fundamental question is whether the NMSM and the EMSM would predict the same pattern of the intrinsic dynamics of an infectious disease system and whether the predicted pattern would change under the influence of health interventions. To the best of our knowledge no previous studies have investigated this fundamental question. Thus, the objective of this chapter is to compare between these two multiscale model categories (NMSM and EMSM), in order to establish the most appropriate category of multiscale models in predicting the dynamics of an infectious disease system using PTB in ruminants as a paradigm. The comparison consists of simulating the transmission of PTB disease in ruminants without and with the influence of preventive and control measures using different multiscale models for PTB disease dynamics that we have derived in previous chapters which are: (a) the full nested multiscale model, (b) the simplified nested multiscale model and (c) the embedded multiscale model.

5.2 Three Multiscale Models to be Compared

In this section, we provided the three multiscale models which we want to compare which are: (a) the full nested multiscale model, (b) the simplified nested multiscale model, and (c) the embedded multiscale model for quick reference. All these three different multiscale models describe the dynamics of PTB infection in ruminants. The three multiscale models are given as follows:

a. ***The full nested multiscale model for PTB transmission dynamics in ruminants***: The full nested multiscale model for PTB transmission dynamics in ruminants is:

$$\begin{cases} i.\ \dfrac{dS_C(t)}{dt} &= \Lambda_C - \dfrac{\beta_C B_C(t)}{B_0 + B_C(t)} S_C(t) - \mu_C S_C(t), \\ ii.\ \dfrac{dI_C(t)}{dt} &= \dfrac{\beta_C B_C(t)}{B_0 + B_C(t)} S_C(t) - (\mu_C + \delta_C) I_C(t), \\ iii.\ \dfrac{dB_C(t)}{dt} &= \alpha_c B_c(t) I_C(t) - \alpha_C B_C(t), \\ iv.\ \epsilon\dfrac{dM_\phi(t)}{dt} &= \Lambda_\phi - \beta_\phi M_\phi(t) B_c(t) - \mu_\phi M_\phi(t) \\ v.\ \epsilon\dfrac{dI_m(t)}{dt} &= \beta_\phi M_\phi(t) B_c(t) - \gamma_m T_1(t) I_m(t) - (k_m + \mu_\phi) I_m(t) \\ vi.\ \epsilon\dfrac{dB_c(t)}{dt} &= N_m k_m I_m(t) - (\mu_c + \alpha_c) B_c(t) \\ vii.\ \epsilon\dfrac{dT_0(t)}{dt} &= \Lambda_0 - (\delta_m I_m(t) + \delta_b B_c(t)) T_0(t) - \mu_0 T_0(t) \\ viii.\ \epsilon\dfrac{dT_1(t)}{dt} &= \theta_1 \delta_m I_m(\tau) T_0(\tau) - \mu_1 T_1(t) \\ ix.\ \epsilon\dfrac{dT_2(t)}{dt} &= \theta_2 \delta_b B_c(t) T_0(t) - \mu_2 T_2(t). \end{cases} \tag{5.2.1}$$

For a complete description of the full nested multiscale model system (5.2.1) and its derivation see Chapter 3. The full nested multiscale model can be reduced in order by using a first-slow time-scale method [17]. For details of the reduction of the order of the full nested multiscale model see Chapter 3.

b. ***The simplified/reduced nested multiscale model for PTB transmission dynamics***: The simplified nested multiscale model for PTB transmission dynamics in ruminants is:

$$\begin{cases} i. \ \dfrac{dS_C(t)}{dt} &= \Lambda_C - \dfrac{\beta_C B_C(t)}{B_0 + B_C(t)} S_C(t) - \mu_C S_C(t), \\ ii. \ \dfrac{dI_C(t)}{dt} &= \dfrac{\beta_C B_C(t)}{B_0 + B_C(t)} S_C(t) - [\mu_C + \delta_C] I_C(t), \\ iii. \ \dfrac{dB_C(t)}{dt} &= N_c \alpha_c I_C(t) - \alpha_C B_C(t) \end{cases} \tag{5.2.2}$$

where the composite parameter N_c which estimates $\widehat{N}_c$ is given by

$$N_c = \frac{N_m k_m}{2(\mu_c + \alpha_c)} \left[-\phi_1 + \sqrt{\phi_1^2 + 4\phi_2} \right] \tag{5.2.3}$$

with

$$\begin{cases} \phi_1 &= \dfrac{k_3 + \mu_1 \mu_0 k_2 - k_1 Q}{k_2 k_1}, \\ \phi_2 &= \dfrac{\mu_1 \mu_0 Q}{k_2 k_1} \end{cases} \tag{5.2.4}$$

and

$$\begin{cases} Q &= \mu_\phi(\mu_\phi + \delta_\phi)(R_{0_c} - 1), \\ k_1 &= \dfrac{\mu_1 \delta_m(\mu_c + \alpha_c) + \mu_1 \delta_b N_m k_m}{(\mu_c + \alpha_c)}, \\ k_2 &= \dfrac{\beta_\phi N_m k_m(\mu_\phi + k_m)}{(\mu_c + \alpha_c)}, \\ k_3 &= k_0 + \mu_\phi \gamma_m \theta_1 \delta_m \Lambda_0, \\ k_0 &= \dfrac{\beta_\phi N_m k_m \gamma_m \theta_1 \delta_m \Lambda_0}{(\mu_c + \alpha_c)}, \\ R_{0_c} &= \dfrac{\beta_\phi \Lambda_\phi N_m k_m}{\mu_\phi(\mu_\phi + k_m)(\mu_c + \alpha_c)}. \end{cases} \tag{5.2.5}$$

Further, the quantity $R_{0_c} = \dfrac{\beta_\phi \Lambda_\phi N_m k_m}{\mu_\phi(\mu_\phi + k_m)(\mu_c + \alpha_c)}$ in expression (5.2.5) is the within-host PTB basic reproductive number as previously explained. Also, the derivation of this simplified version of the full PTB multiscale model has been previously done in chapter Chapter 3.

c. ***The embedded multiscale model for PTB transmission dynamics in ruminants***: The embedded multiscale model for PTB transmission dynamics in ruminants is given here for a quick reference as:

$$
\begin{cases}
i. \quad \dfrac{dS_C(t)}{dt} &= \Lambda_C - \dfrac{\beta_C B_C(t)}{B_0 + B_C(t)S_C(t)} - \mu_C S_C(t) \\[2ex]
ii. \quad \dfrac{dI_C(t)}{dt} &= \dfrac{\beta_C B_C(t)}{B_0 + B_C(t)S_C(t)} - [\mu_C + \delta_C] I_C(t) \\[2ex]
iii. \quad \dfrac{dB_C(t)}{dt} &= \alpha_c [I_C(t) + 1] B_c(t) - \alpha_C B_C(t) \\[2ex]
iv. \quad \dfrac{dB_c(t)}{dt} &= \dfrac{\beta_C B_C(t)[S_C(t) - 1]}{[B_0 + B_C(t)]\Phi_C[I_C(t) + 1]} + N_m k_m I_m(t) - [\mu_c + \alpha_c] B_c(t) \\[2ex]
v. \quad \dfrac{dM_\phi(t)}{dt} &= \Lambda_\phi - \beta_\phi M_\phi(t) B_c(t) - \mu_\phi M_\phi(t) \\[2ex]
vi. \quad \dfrac{dI_m(t)}{dt} &= \beta_\phi M_\phi(t) B_c(t) - [k_m + \mu_\phi] I_m(t) - \gamma_m T_1(t) I_m(t) \\[2ex]
vii. \quad \dfrac{dT_0(t)}{dt} &= \Lambda_0 - [\delta_m I_m(t) + \delta_b B_c(t)] T_0(t) - \mu_0 T_0(t) \\[2ex]
viii. \quad \dfrac{dT_1(t)}{dt} &= \theta_1 \delta_m I_m(t) T_0(t) - \mu_1 T_1(t) \\[2ex]
ix. \quad \dfrac{dT_2(t)}{dt} &= \theta_2 \delta_b B_c(t) T_0(t) - \mu_2 T_2(t).
\end{cases}
\tag{5.2.6}
$$

For a complete description of the embedded multiscale model system (5.2.6) and its derivation see Chapter 4.

In what follows, we compared these three types of multiscale models.

5.3 Comparison of three types of multiscale models in predicting the intrinsic dynamics of PTB infection from numerical simulations

In this section, we presented some of the results concerning the comparison in predictions of the intrinsic dynamics of environmentally-transmitted disease systems by the three different types of multiscale models (i.e., a full nested multiscale model, a simplified nested multiscale model, and a embedded multiscale model) using PTB in ruminants as a case study. We achieved this by numerical simulating the two key between-host scale variables in all the three multiscale models for PTB transmission dynamics. The two key between-host scale variables are (i) the population infected ruminants, I_C and (ii) the population of the between-host scale MAP bacterial load, B_C). The simulations of these two key between-host scale variables (I_C and B_C) we carried out under the influence of the selected parameters when they are varied from different values in all the three multiscale models. The initial condition used for the simulations of these multiscale models are: $S_C(0)$ = 20000, $I_C(0)$ = 0, $B_C(0)$ = 10000 , $B_c(0)$ = 100 , $M_\phi(0)$ = 500, $I_m(0)$ = 0, $T_0(0)$ = 0.1 , $T_1(0)$ = 0, and $T_2(0)$ = 0. The parameter values used for simulations of these three multiscale models are tabulated in Table 4.1 of Chapter 4. The comparison of the predicted output from all the three multiscale models (FULL-NMSM, SIMP-NMSM and BIDI-EMSM) are presented in Fig. 5.1 and Fig. 5.2 as follows:

a. Camparing the suitability of the three multiscale models in predicting the profile of I_C, over time.

(i) Fig. 5.1(a) shows evolution of I_C from the three multiscale models when μ_c varying from high level, $\mu_c = 0.3$ to low level, $\mu_c = 0.003$.

(ii) Fig. 5.1(b) shows evolution of I_C from the three multiscale models when α_c varying from high level, $\alpha_c = 0.1$ to low level, $\alpha_c = 0.001$.

(iii) Fig. 5.1(c) shows evolution of I_C from the three multiscale models when α_c varying from high level, $N_m = 10$ to low level, $N_m = 1000$.

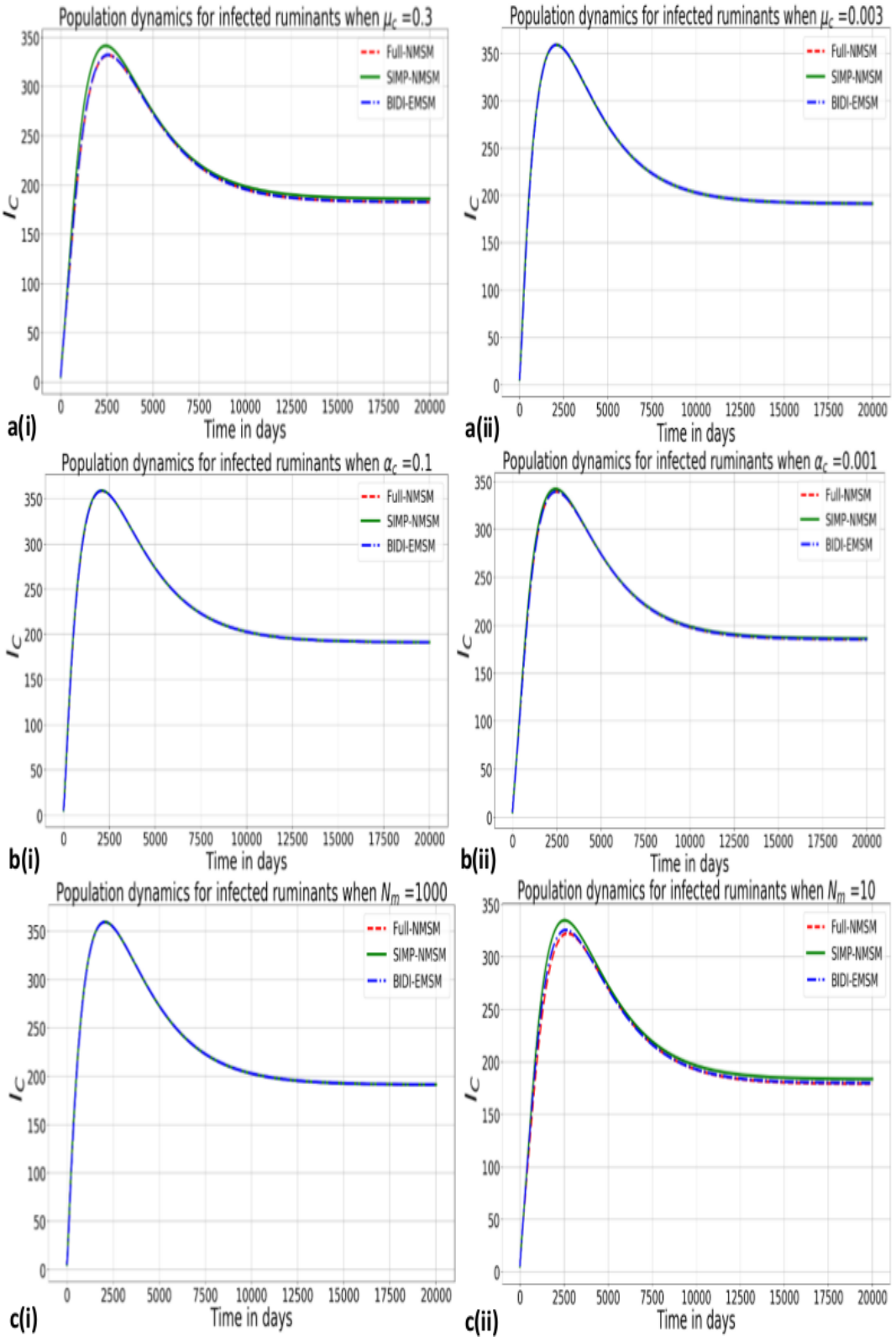

Figure 5.1: *Graphs of numerical solutions of the three multiscale models (Full-NMSM, SIMP-NMSM and BIDI-EMSM) showing the profile of infected ruminants for different values of selected within-host parameters (α_c, μ_c, N_m).*

From on the results in Figure 5.1, we made the following deduction:

1. The numerical results in Fig. 5.1(a) showed that when the natural decay rate (μ_c) of the within-host MAP bacteria population changes from high level (i.e., $\mu_c = 0.3$) to low level (i.e., $\mu_c = 0.003$), there is noticeable but negligible difference among the three multiscale models in predicting the profile of I_C as the trajectory of I_C in all the multiscale models increase to a marginally different peak values of about less than 350 infected ruminants when μ_c is at the high level. When μ_c is at the low level I_C increases to an approximately equal peak value of about more than 350 infected ruminants in all the multiscale models. Furthermore, we also noticed that in the long run, trajectories of infected ruminants in all the multiscale models decrease and converge to approximately equal equilibrium steady state when μ_c is at high level and when it is at the low level it converge to a strictly equal equilibrium steady state.
2. The numerical results in Fig. 5.1(b) showed that the variation in the excretion rate (α_c) of the within-host MAP bacteria population from high level (i.e., $\alpha_c = 0.1$) to low level (i.e., $\alpha_c = 0.001$) makes no difference in predicting the profile of I_C among the three multiscale models as the trajectories of I_C in all the multiscale models increase to an approximately equal peak values as well as converging to a strictly equal equilibrium steady state in the long run in all the cases (i.e., when α_c is at high level and when it is at low level).
3. The numerical results in 5.1(c) show that the variation in the average number (N_m) of the intracellular MAP bacteria load into the extracellular environment by each infected macrophages upon bursting from high level (i.e., $N_m = 1000$) to low level (i.e., $N_m = 10$) again there is a noticeable but negligible difference among the three multiscale models in predicting the profile of I_C as the trajectories of I_C in all the multiscale models increase to a marginally different peak values when N_m = 10. However, when N_m = 1000, all the three multiscale models (Full-NSMS, SIMP-NMSM and BIND-EMSM) provide the same prediction of the profile of I_C.

Collectively, based on all the three sets of numerical results presented in Fig. 5.1 (i.e., Fig. 5.1(a - c)), we can easily note that the variation in the selected key PTB within-host parameters α_c, μ_c and N_m from different values contribute to a negligible difference in predicting the profile of I_C from the three multiscale models. This means that all the three multiscale models (Full-NSMS, SIMP-NMSM and BIND-EMSM) can equally be used to characterize the dynamic of an infectious disease that has a pathogen replication at the microscale, although the SIMP-NMSM provide a

worse case scenario. This might be due to the fact that in the SIMP-NMSM infection at the microscale has been allowed to reach an endemic before contributing to the dynamics of the disease at the between-host scale.

b. Camparing the suitability of the three multiscale models in predicting the profile of B_C over time.

(i) Fig. 5.2(a) shows evolution of B_C from the three multiscale models when μ_c varying from high level, $\mu_c = 0.3$ to low level, $\mu_c = 0.003$.

(ii) Fig. 5.2(b) shows evolution of B_C from the three multiscale models when α_c varying from high level, $\alpha_c = 0.1$ to low level, $\alpha_c = 0.001$.

(iii) Fig. 5.2(c) shows evolution of B_C from the three multiscale models when α_c varying from high level, $N_m = 10$ to low level ($N_m = 1000$).

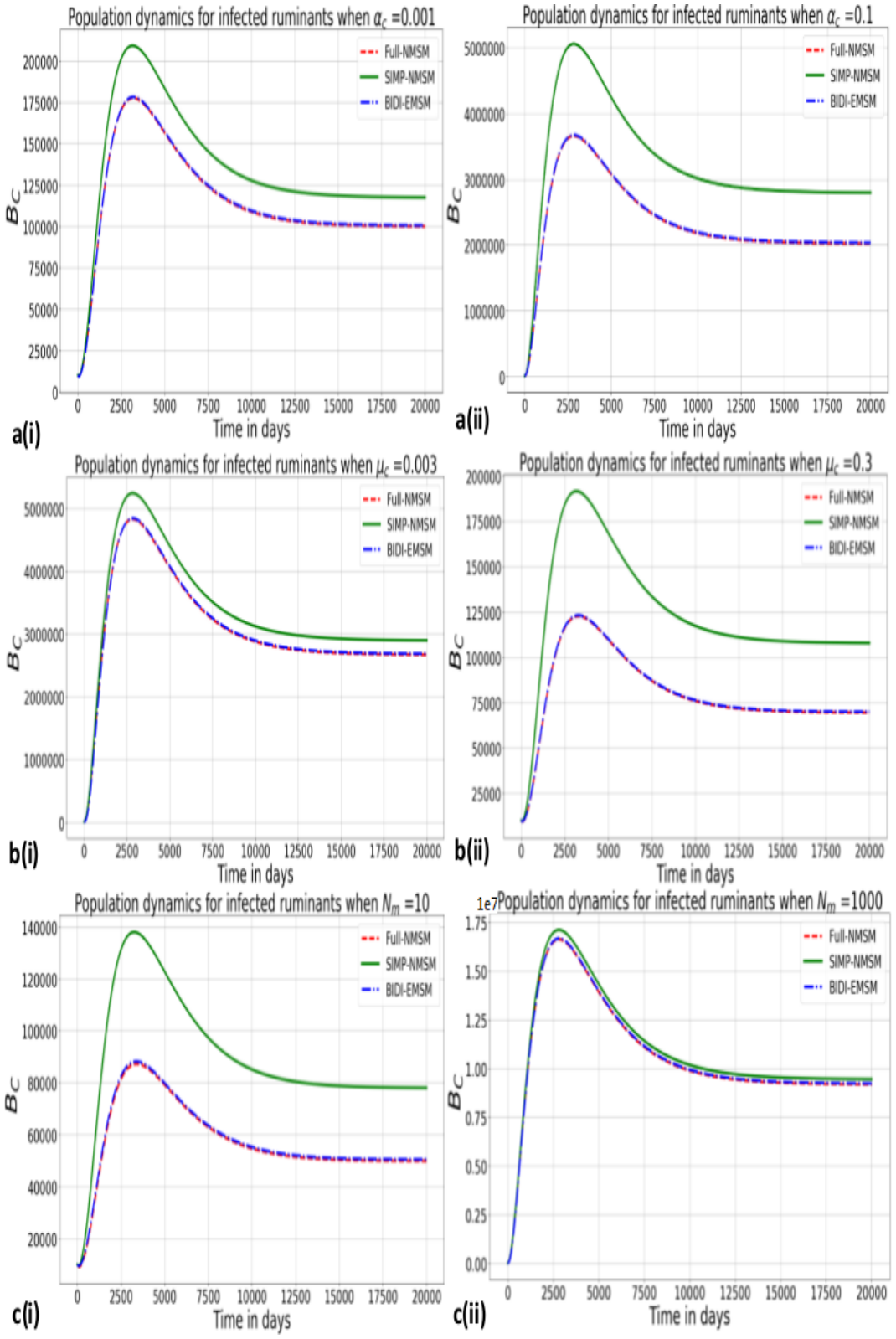

Figure 5.2: *Graphs of numerical solutions of the three multiscale models (Full-NMSM, SIMP-NMSM and BIDI-EMSM) showing the profile of infected ruminants for different values of selected within-host parameters (α_c, μ_c, N_m).*

From the results in Figure 5.2, we make the following deductions:

1. The numerical results in Fig. 5.2(b) show that as the natural decay rate (μ_c) of the within-host MAP bacteria population vary from low level ($\mu_c = 0.003$) to high level ($\mu_c = 0.3$) there is a noticeable difference among the three multiscale models in predicting the profile of B_C, with the simplified nested multiscale models predicting high population size of B_C compared to full nested and embedded multiscale models in which both predict approximately equal population size of B_C.
2. The numerical results in Fig. 5.2(b) show that when the excretion rate (α_c) of the within-host MAP bacteria load into the physical environmental domain by each infected ruminant individuals increases from low level ($\alpha_c = 0.001$) to high level ($\alpha_c = 0.1$) there is also a noticeable difference among the three multiscale models in predicting the profile of B_C, with the simplified nested multiscale models predicting high population size of B_C compare to full nested and embedded multiscale models in which both predict approximately equal population size of B_C.
3. The numerical results in Fig. 5.2(c) show that when the average number of the intracellular MAP bacterial load into the extracellular environment by each infected macrophages upon bursting (N_m) increase from low level ($N_m = 10$) to high level ($N_m = 1000$) there is a significant difference in predicting the population size of B_C, with the simplified nested multiscale models still predicting high population size of B_C compare to both the full nested and the embedded multiscale models in which both predict approximately equal population size of B_C.

Collectively, from all the three sets of numerical results in Fig. 5.2 (i.e., Fig. 5.2(a - c)), we notice that as the selected key PTB within-host parameters α_c, μ_c and N_m change from different levels contribute to the variation in the three multiscale models in predicting the profile of B_C, with the simplified multiscale predicting a high number of MAP bacterial cells in the environment compared to both the full nested and embedded multiscale models in which all predict an approximately equal number of infective MAP bacterial cells in the environment. This is largely because in the simplified nested multiscale model the replication-cycle of pathogen is allowed to reach an endemic level first before contributing to the dynamics of the diseases at the population level.

Overall, the numerical results shown in Fig. 5.1 and Fig. 5.2 illustrate that during PTB disease dynamics, although there is reciprocal influence between the within-host scale (micro-scale) and

the between-host scale (macro-scale) when the within-host scale varies for different values, the comparative different between the nested and embedded multiscale models in predicting the dynamics of PTB in the ruminant population is negligible. This generally implies that at any level of biological organization of an infectious disease system in which the replication-cycle of pathogen only occurs at the micro-scale either a nested multiscale model or an embedded multiscale model can equally be used to characterize its intrinsic dynamics. This is largely because the results that can be obtained using an embedded multiscale modelling can also be obtained by using a nested multiscale modelling.

5.4 Comparison of three types of multiscale models in predicting the dynamics of PTB infection under the influence of PTB interventions

In this section, we further investigate which among the full nested, simplified nested and embedded multiscale models would be more appropriate in guiding control and elimination of the burden of Paratuberculosis (PTB) in the ruminant population. We extend all the three baseline multiscale models introduced in Chapter 3 and Chapter 4, respectively, to incorporate two major PTB health interventions which are: (i) environmentally-hygiene management (EHM) and (ii) medical-based prevention and therapy (MBPT). We Achieve this by firstly evaluating how well the three extended multiscale models that incorporate the two PTB health interventions (EHM and MBPT) can translate existing knowledge about efficacy at the individual ruminant scale (i.e., within-ruminant-host scale) into outcomes of effectiveness that can be predicted at the ruminant population scale (i.e., between-ruminant-host scale) in public health decision making. It is important to note that both EHM and MBPT are complex intervention systems as they are composed of a number of components, which may act independently or inter-dependently. For instance, EHM have two components which are: (i) health and sanitary education effect of EHM and (ii) killing of environmental bacilli bacteria effect of EHM. Similarly, MBPT have three components which are (i) PTB vaccination effect of MBPT, (ii) PTB test and culling effect of MBPT and (iii) PTB test and curing effect of MBTP. In addition, it should also be noted that these two PTB health interventions in ruminant (EHM and MBPT) are generally administered at different scale domains of the PTB disease system, with EHM administered at between-host scale while MBPT administrated at within-host scale. Below is the description of the two main PTB interventions:

(i) **Environmentally-hygiene management**: This intervention strategy has two effects: (i) health and sanitary education effect which has the net effect of reducing the infection rate in

the ruminant population (r), and (ii) treatment of dams or water troughs effect using some chemical for killing bacterial load in water which also have the net effect of increasing the natural death of MAP in the physical water environment (k). Therefore, if we assume that health and sanitary education intervention and treatment of water are administered then the rate of ruminant contact with the physical environmental bacterial load parameter β_C is modified to become $\beta_C(1-r)$ where r is the efficacy of health and sanitary education effect, with $0 < r < 1$. The natural death rate of the environmental bacterial load in the physical water environment is modified to become $\alpha_C(1-k)$ where k is the efficacy of killing effect, with $0 < k < 1$. Thus, $\beta_C(1-r)$ measures the probability of the reduction of susceptible ruminant contact with unsafe water bodies or other contaminated physical environments due to health education campaigns and changes in behavioral practices that aims to reduce the transmission risk of the disease in ruminant animals. The quantity $\alpha_C(1-k)$ measures the probability at which the population of MAP bacilli bacteria is reduced in the physical environment due to the treatment of unsafe water with some chemicals.

(ii) **Medical-based prevention and treatment**: This intervention strategy also has multiple effects: (i) PTB preventive vaccine effect which has the net effect of reducing susceptibility of ruminants to PTB infection (v), (ii) PTB immune stimulation effect which has the net effect of boosting Th_1 cells at the site of an infection within an infected ruminant (b), (iii) killing of extracellular MAP bacteria effect which net effect of increasing natural death rate in the population of extracellular MAP bacilli (d) and (iv) restricting growth of intracellular MAP bacteria effect which has a net effect of preventing infected macrophages from bursting and further transmit MAP bacteria to other cells (m). Assuming that PTB preventive vaccine are administered as PTB health intervention, coefficient $1/B_0$ is reduced to become $1/B_0(1+v)$, where v is the efficacy of the preventive vaccine and $0 < v < 1$. Thus, $B_0(1+v)$ measures the probability of reducing the susceptibility of ruminant when contact with the environmental bacterial load. Assuming further that any health intervention mechanism that stimulates the response of Th_1 cells against the infection at the within-host scale is administered, then θ_1 becomes $\theta_1(1+b)$ where b is the efficacy of Th_1 stimulation and $0 < b < 1$. Thus, $\theta_1(1+b)$ measures the probability of increasing the proliferation of Th_1 cells. Also, if we assume that test and treatment with drugs is administered, the μ_c is modified to be $\mu_c(1+d)$, where d is the efficacy of drug therapy intervention and $0 < d < 1$ and also d is a parameter that relates to the treatment of each ruminant using the drugs after tested positive to PTB infection. Thus, $\mu_c(1+d)$ measures the probability of killing the within-host bacterial load. Assuming that any health intervention mechanism that restricts the growth of intracellular MAP bacteria

within an infected macrophages, then N_m become $N_m(1+d)$. Thus, $N_m(1+d)$ measures the probability of restriction of the replication of intracellular bacteria within each infected macrophages. Overall, health-sanitary education and the administration of PTB vaccination in the herd modify λ_C and λ_c to become $\widetilde{\lambda}_C$ and $\widetilde{\lambda}_c$, respectively. Where

$$\begin{cases} \widetilde{\lambda}_C(t) = \dfrac{\beta_C(1-r)B_C(t)}{B_0(1+v)+B_C(t)}, \\ \\ \widetilde{\lambda}_c(t) = \dfrac{\beta_C(1-r)B_C(t)}{[B_0(1+v)+B_C(t)]\Phi_C[I_C(t)+1]}. \end{cases} \tag{5.4.1}$$

A summary of the modifications of the two multiscale models parameters of PTB dynamics due to effects of the two PTB health interventions (EHM and MBPT) is given in Table 5.1.

Health Interventions	Transformation	Efficacy Value Range
Reducing contact rate effect of EHM (r)	$\beta_C \longrightarrow \beta_C(1-r)$	0.1 - 0.8
Killing of between-host MAP bacteria effect of EHM (k)	$\alpha_C \longrightarrow \alpha_C(1+k)$	0.1 - 0.8
Reducing susceptibility of ruminants to infection effect of MBPT (v)	$B_0 \longrightarrow B_0(1+v)$	0.1 - 0.8
Proliferation of Th_1 cells effect of MBPT (b)	$\theta_1 \longrightarrow \theta_1(1+b)$	0.1 - 0.8
Killing of extracellular MAP bacteria effect of MBPT (d)	$\mu_c \longrightarrow \mu_c(1+d)$	0.1 - 0.8
Retricting growth of intracellular MAP bacteria effect of MBPT (m)	$N_m \longrightarrow N_m(1-m)$	0.1 - 0.8

Table 5.1: Summary of the actions of the components of the two PTB health interventions against the PTB infection dynamics in ruminants.

Taking into account all the modifications as in Fig. 5.1, the full nested, simplified and embedded multiscale models for PTB infection dynamics that incorporate the effects of the two PTB health interventions in ruminant (EHM and MBPT) are given as follows:

a. ***The full nested multiscale model incorporating the two PTB health intervention is given as***:

$$
\begin{cases}
i.\ \dfrac{dS_C(t)}{dt} &= \Lambda_C - \dfrac{\beta_C(1-r)B_C(t)}{B_0(1+v)+B_C(t)}S_C(t) - \mu_C S_C(t), \\
ii.\ \dfrac{dI_C(t)}{dt} &= \dfrac{\beta_C(1-r)B_C(t)}{B_0(1+v)+B_C(t)}S_C(t) - (\mu_C+\delta_C)I_C(t), \\
iii.\ \dfrac{dB_C(t)}{dt} &= \alpha_c B_c(t)I_C(t) - \alpha_C(1-k)B_C(t), \\
iv.\ \epsilon\dfrac{dM_\phi(t)}{dt} &= \Lambda_\phi - \beta_\phi M_\phi(t)B_c(t) - \mu_\phi M_\phi(t) \\
v.\ \epsilon\dfrac{dI_m(t)}{dt} &= \beta_\phi M_\phi(t)B_c(t) - \gamma_m T_1(t)I_m(t) - (k_m+\mu_\phi)I_m(t) \\
vi.\ \epsilon\dfrac{dB_c(t)}{dt} &= N_m(1-m)k_m I_m(t) - (\mu_c(1+d)+\alpha_c)B_c(t) \\
vii.\ \epsilon\dfrac{dT_0(t)}{dt} &= \Lambda_0 - (\delta_m I_m(t)+\delta_b B_c(t))T_0(t) - \mu_0 T_0(t) \\
viii.\ \epsilon\dfrac{dT_1(t)}{dt} &= \theta_1(1+b)\delta_m I_m(\tau)T_0(\tau) - \mu_1 T_1(t) \\
ix.\ \epsilon\dfrac{dT_2(t)}{dt} &= \theta_2\delta_b B_c(t)T_0(t) - \mu_2 T_2(t).
\end{cases}
\tag{5.4.2}
$$

As previously indicated, the extended nested baseline multiscale model (5.4.2) can not be analyzed mathematically due to its structural feature in which the between-host scale dynamics only influence the within-host scale dynamics through the initial value condition of the within-host MAP bacteria population. However, the numerical analysis of the extended nested baseline multiscale model (5.4.2) can be performed.

b. ***The simplified/reduced nested multiscale model for PTB transmission dynamics in ruminants is given as follow***:

$$\begin{cases} i.\ \dfrac{dS_C(t)}{dt} &= \Lambda_C - \dfrac{\beta_C(1-r)B_C(t)}{B_0(1+v)+B_C(t)}S_C(t) - \mu_C S_C(t), \\ ii.\ \dfrac{dI_C(t)}{dt} &= \dfrac{\beta_C(1-r)B_C(t)}{B_0(1+v)+B_C(t)}S_C(t) - [\mu_C+\delta_C]I_C(t), \\ iii.\ \dfrac{dB_C(t)}{dt} &= N_c\alpha_c I_C(t) - \alpha_C(1+k)B_C(t) \end{cases} \tag{5.4.3}$$

with

$$N_c = \frac{N_m(1-b)k_m}{2(\mu_c(1+d)+\alpha_c)}\left[-\phi_1 + \sqrt{\phi_1^2+4\phi_2}\right] \tag{5.4.4}$$

where

$$\begin{cases} \phi_1 &= \dfrac{k_3+\mu_1\mu_0k_2-k_1Q}{k_2k_1}, \\ \phi_2 &= \dfrac{\mu_1\mu_0Q}{k_2k_1} \end{cases} \tag{5.4.5}$$

and

$$\begin{cases} Q &= \mu_\phi(\mu_\phi+\delta_\phi)(R_{0_c}-1), \\ k_1 &= \dfrac{\mu_1\delta_m(\mu_c(1+d)+\alpha_c)+\mu_1\delta_bN_m(1-m)k_m}{(\mu_c(1+d)+\alpha_c)}, \\ k_2 &= \dfrac{\beta_\phi N_m(1-m)k_m(\mu_\phi+k_m)}{(\mu_c(1+d)+\alpha_c)}, \\ k_3 &= k_0+\mu_\phi\gamma_m\theta_1\delta_m\Lambda_0, \\ k_0 &= \dfrac{\beta_\phi N_m(1-m)k_m\gamma_m\theta_1(1+b)\delta_m\Lambda_0}{(\mu_c(1+d)+\alpha_c)}, \\ R_{0_c} &= \dfrac{\beta_\phi\Lambda_\phi N_m(1-m)k_m}{\mu_\phi(\mu_\phi+k_m)(\mu_c(1+d)+\alpha_c)}. \end{cases} \tag{5.4.6}$$

c. ***The PTB embedded multiscale model incorporating the two PTB health intervention becomes***:

$$
\begin{cases}
i. \quad \dfrac{dS_C(t)}{dt} &= \Lambda_C - \dfrac{\beta_C(1-r)B_C(t)}{B_0(1+v)+B_C(t)}S_C(t) - \mu_C S_C(t), \\
ii. \quad \dfrac{dI_C(t)}{dt} &= \dfrac{\beta_C(1-r)B_C(t)}{B_0(1+v)+B_C(t)}S_C(t) - [\mu_C+\delta_C]I_C(t), \\
iii. \quad \dfrac{dB_C(t)}{dt} &= \alpha_c[I_C(t)+1]B_c(t) - \alpha_C(1+k)B_C(t), \\
iv. \quad \dfrac{dB_c(t)}{dt} &= \dfrac{\beta_C(1-r)B_C(t)(S_C(t)-1)}{[B_0(1+v)+B_C(t)]\Phi_C[I_C(t)+1]} + N_m(1-m)k_m I_m(t) - \\
&\quad [\mu_c(1+d)+\alpha_c]B_c(t), \\
v. \quad \dfrac{dM_\phi(t)}{dt} &= \Lambda_\phi - \beta_\phi M_\phi(t)B_c(t) - \mu_\phi M_\phi(t), \\
vi. \quad \dfrac{dI_m(t)}{dt} &= \beta_\phi M_\phi(t)B_c(t) - [k_m+\mu_\phi]I_m(t) - \gamma_m T_1(t)I_m(t), \\
vii. \quad \dfrac{dT_0(t)}{dt} &= \Lambda_0 - [\delta_m I_m(t)+\delta_b B_c(t)]T_0(t) - \mu_0 T_0(t), \\
viii. \quad \dfrac{dT_1(t)}{dt} &= \theta_1(1+b)\delta_m I_m(t)T_0(t) - \mu_1 T_1(t), \\
iv. \quad \dfrac{dT_2(t)}{dt} &= \theta_2\delta_b B_c(t)T_0(t) - \mu_2 T_2(t).
\end{cases}
\tag{5.4.7}
$$

The comparison of the suitability of the three multiscale models in predicting the effectiveness of PTB health interventions operated at different scales on the dynamics of I_C over time are presented as follows:

(i) Fig. 5.3(a) shows evolution of I_C from all the three multiscale models when all the six component efficacy values of the two PTB health interventions are assume to have a low level of 10% in all the three multiscale models.

(ii) Fig. 5.3(b) shows evolution of I_C from all the three multiscale models when all the six component efficacy values of the two PTB health interventions are assume to have a median level of 40% in all the three multiscale models.

(iii) Fig. 5.3(c) shows evolution of I_C from all the three multiscale models when all the six component efficacy values of the two PTB health interventions are assume to have a high level of 80% in all the three multiscale models.

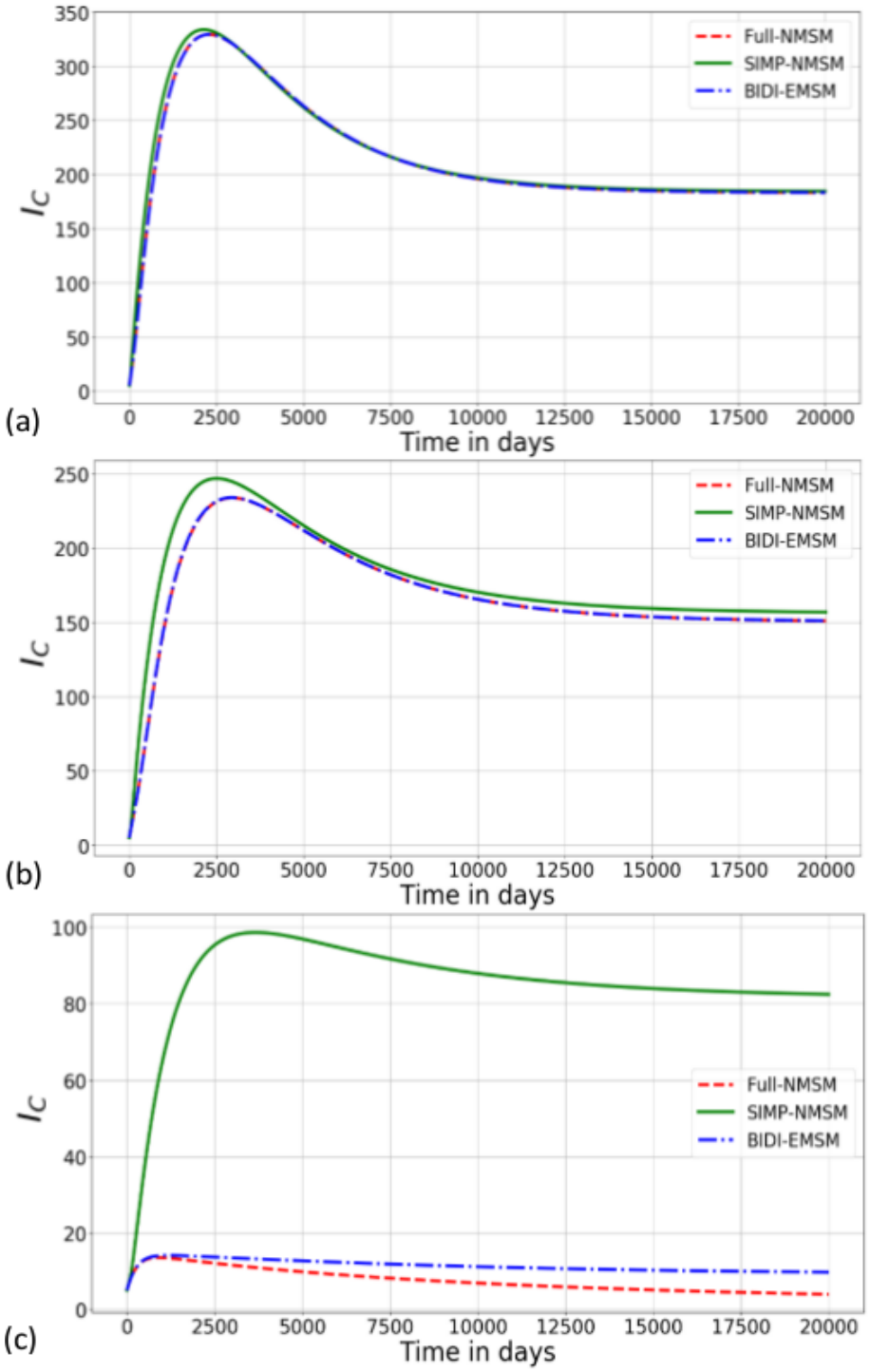

Figure 5.3: *Graphs of numerical solutions of the three multiscale models (Full-NMSM, SIMP-NMSM and BIDI-EMSM) showing the profile of infected ruminants for different efficacy values of all the six components of the two PTB health interventions.*

From the results in Figure 5.3, we make the following deduction:

1. The variation in the efficacy values of the six individual interventions from different levels (0.1, 0.4, 0.8) in all the three multiscale models have a significant and considerable benefit in reducing the prevalence at the population level as there is a noticeable reduction of the population size of infected ruminants I_C in all the multiscale models from more than 350 infected ruminants to less than 100 infected ruminants.

2. However, when each of the six individual interventions is assumed to have the same efficacy value of 0.1, the comparative difference in predicting the effectiveness of these interventions in all the three multiscale models in Fig. 5.3(a) is negligible as the population of infected ruminants (I_C) in all the multiscale models increase to a negligible different peak values. We also observe that in a long run the profiles of I_C in all the three multiscale models converge to approximately equal equilibrium steady state. But the simplified nested multiscale model predicts a slightly low effectiveness of reducing the population size of infected ruminants compared to the full nested multiscale model and embedded multiscale model in which both predict high and approximately equal effectiveness of reducing the population size of infected ruminants.

3. When each of the six individual interventions is assumed to have the same efficacy value of 0.4, the comparative difference in predicting the effectiveness of these interventions in all the three multiscale models in Fig. 5.3(b) is significant as the population of infected ruminants (I_C) in all the multiscale models increase to a noticeable different peak values. We also observe that in a long run the profiles of I_C in all the three multiscale models converge a negligible different equilibrium steady states, with the simplified nested multiscale model predict a slightly low effectiveness of reducing the population size of infected ruminants compared to the full nested multiscale model and embedded multiscale model in which both predict high and approximately equal effectiveness of reducing the population size of infected ruminants.

4. When each of the six individual interventions is assumed to have the same efficacy value of 0.8, the comparative difference in predicting the effectiveness of these interventions in all the three multiscale models in Fig. 5.3(c) is extremely significant as the population of infected ruminants (I_C) in all the multiscale models increase to a noticeable different peak values. We further observe that profiles of I_C in all the three multiscale models converge to a considerable different endemic levels compared to when each of the six individual interventions is assumed to have the same efficacy value of 0.1 and 0.4, respectively. However, we also observe that when each of the six individual interventions is assumed to have the same efficacy value of 0.8 the simplified multiscale model predict a low effectiveness of reducing the population of infected ruminants, while the embedded multiscale model

predict an intermediate effectiveness of reducing the population of infected ruminants and the full nested multiscale model predict a high effectiveness of reducing the population of infected ruminants.

The comparison of the suitability of the three multiscale models in predicting the effectiveness of PTB health interventions operated at different scales on the dynamics of B_C over time are presented as follows:

(i) Fig. 5.4(a) shows evolution of B_C from the three multiscale models when all the six component efficacy values of the two PTB health interventions are assume to have a low level of 10%.

(ii) Fig. 5.4(b) shows evolution of B_C from the three multiscale models when all the six component efficacy values of the two PTB health interventions are assume to have a median level of 40%.

(iii) Fig. 5.4(c) shows evolution of B_C from the three multiscale models when all the six component efficacy values of the two PTB health interventions are assume to have a high level of 80%.

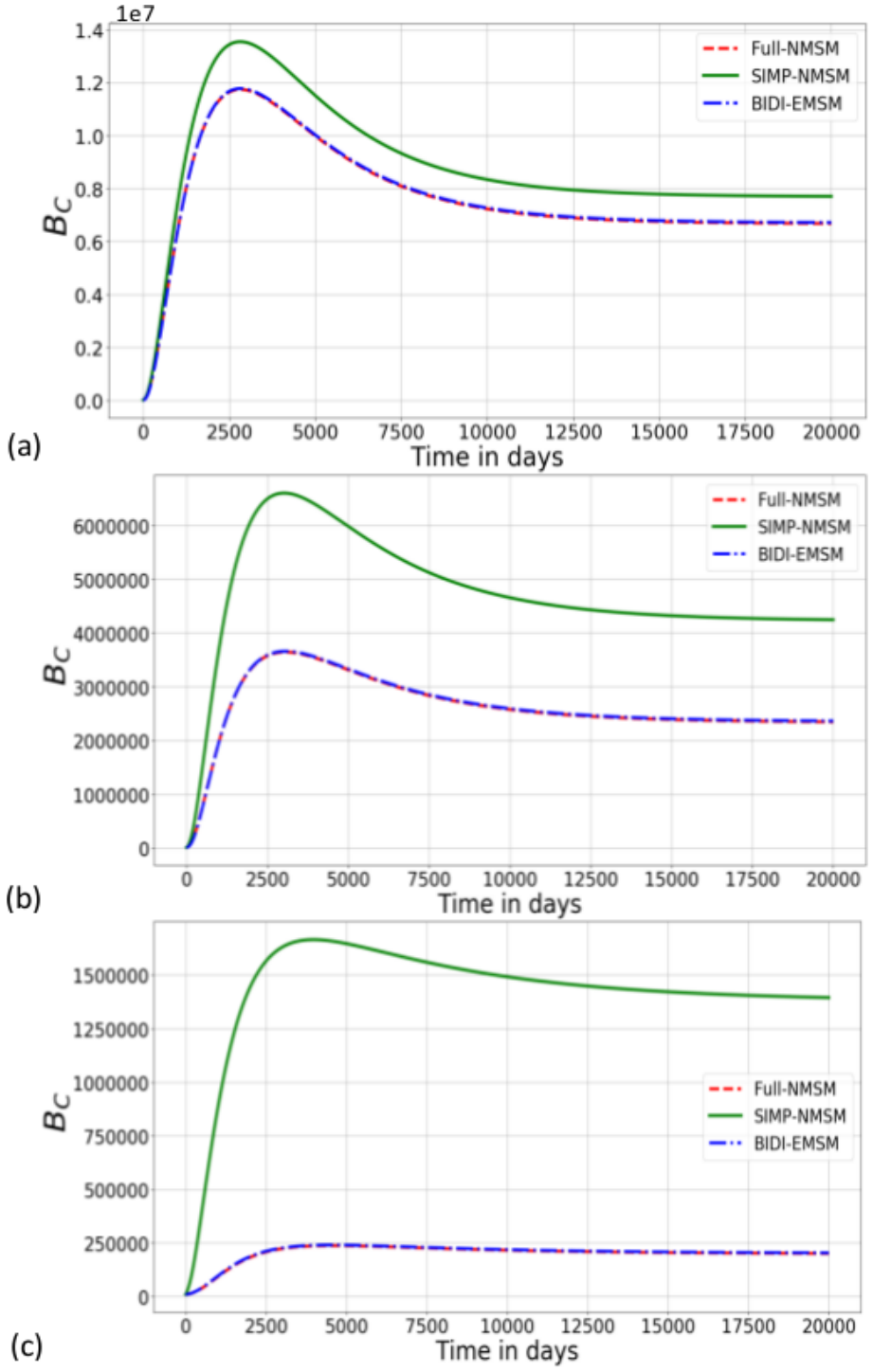

Figure 5.4: *Graphs of numerical solutions of the three multiscale models (Full-NMSM, SIMP-NMSM and BIDI-EMSM) showing the profile of infected ruminants for different efficacy values of all the six components of the two PTB health interventions.*

From on the results in Figure 5.4, we make the following deduction:

1. Similarly, the variation in the efficacy values of the six individual interventions from different levels (0.1, 0.4, 0.8) in all the three multiscale models have a more considerable benefit in reducing the prevalence at the population level as there is a noticeable reduction of the population size of the between-host MAP bacteria load B_C in all the multiscale models from more than 130 million MAP bacteria cells to less than 1.6 million MAP bacteria cells.

2. In Fig. 5.4(a), when each of the six individual interventions is assumed to have the same efficacy value of 0.1, there is a minimal comparative difference in predicting the effectiveness of these interventions in reducing the population of MAP bacterial cells at the population level in all the three multiscale models. We observe that the profiles of B_C in all the three multiscale models increases to a noticeable but slightly different peak values, with the simplified multiscale model predict the high peak value of MAP bacteria cells while both the full nested and embedded multiscale models predict approximately equal peak value of MAP bacteria cells. We also observe that in a long run the profiles of B_C in all the three multiscale models converge to a noticeable but slightly different equilibrium steady states, with the simplified nested multiscale model predict a slightly low effectiveness of reducing the MAP bacterial load in the physical environmental entities compared to the full nested multiscale model and embedded multiscale model in which both predict high and approximately equal effectiveness of reducing the MAP bacterial load in the physical environment.

3. In Fig. 5.4(b), when each of the six individual interventions is assumed to have the same efficacy value of 0.4 , the comparative difference in predicting the effectiveness of these interventions in all the three multiscale models is significant. We observe that the profiles of B_C in all the multiscale models increases to a noticeable different peak values, with the simplified multiscale model predict the high peak value of MAP bacteria cells while both the full nested and embedded multiscale models predict approximately equal peak value of MAP bacteria cells. We also observe that in a long run the profiles of B_C in all the three multiscale models converge to a noticeable different equilibrium steady states, with the simplified nested multiscale model predict a low effectiveness of reducing the MAP bacterial load in the physical environmental entities compared to the full nested multiscale model and embedded multiscale model in which both predict high and approximately equal effectiveness of reducing the MAP bacterial load in the physical environment.

4. In Fig. 5.4(c), when each of the six individual interventions is assumed to have the same efficacy value of 0.8, the comparative difference in predicting the effectiveness of these interventions in all the three multiscale models is extremely significant as B_C in all the

multiscale models increase to a more considerable different peak values. We observe that the simplified multiscale model predict a low effectiveness of reducing the population of MAP bacteria cells in the environment, while both the embedded multiscale model and the full nested multiscale model predict a high and equal effectiveness of reducing the population of MAP bacterial load at the population level.

Collectively, the numerical results shown in Fig. 5.3 and Fig. 5.4 show that during PTB transmission-replication dynamics, the simplified nested multiscale model predict a worse case scenario of the effectiveness of the six individual intervention in reducing MAP bacterial load at the population level. While both the full nested and embedded multiscale models predict approximately equal effectiveness of reducing the number of infected ruminants and MAP bacterial load in the environment. Similarly, this also indicates that both the full nested and the embedded multiscale models can equally be used to characterize the dynamics of an infectious disease that involves a pathogen replication-cycle at the microscale under the influence of health interventions.

5.5 Summary

In this chapter, we compared the predictions of three different types of multiscale models in characterizing disease dynamics with pathogen replication cycle that occurs only at the microscale using ruminant paratuberculosis as a paradigm. Based on the simulations of population dynamics of infected ruminants as well as the population dynamics of the free-living MAP bacteria in the environment in all the three multiscale models (FULL-NSMS, SIMP-NMSM and EMSM), we were able to established the fact that all of them would predict the same pattern of the intrinsic dynamics of an infectious disease system. These results indicate that both the NMSM and the EMSM can equally be used to characterize intrinsic dynamics of an infectious disease that involves a pathogen replication-cycle at the microscale such as PTB. We further extended the three baseline models described in **Chapter 3** and **Chapter 4**, respectively, to incorporate two main health intervention strategies for ruminant paratuberculosis, with the aim of investigating further if the predicted pattern by the NMSM and the EMSM would change under the influence health interventions. Similarly, the findings show that both the full nested and the embedded multiscale models would predict the same pattern of the dynamics of an infectious disease system under the influence of health intervention mechanisms. However, the simplified multiscale model provide a worse case scenario. In conclusion, although the focus of this chapter was on investigating if a NMSM and an EMSM would predict the same pattern of an infectious disease system using paratuberculosis in ruminants as a example of type II environmentally-transmitted diseases, we

anticipated that the results of the chapter can be robust enough in the selection of multiscale modelling framework to characterize other infectious diseases beyond PTB in ruminants.

Chapter 6

An Embedded Multiscale Model For Dynamics of Ascariasis Population Biology

6.1 Introduction

In Chapter 5, we compared nested and embedded multiscale models to determine the most appropriate category to characterize the multiscale dynamics of infectious diseases without a replication cycle of pathogen at microscale of organization of an infectious disease system. At this stage, what we know is that both nested and embedded multiscale models can be used to characterize the dynamics of infectious diseases that has a pathogen replication at the microscale as both nested and embedded multiscale models equally predict the same disease dynamics. However, what we do not know is whether a nested multiscale model and embedded multiscale model would predict the same dynamics of an infectious disease system in which there is no pathogen replication at the microscale. Therefore, the objective of this chapter is to compare and identify the most appropriate category to model the multiscale dynamics of infectious diseases with a replication cycle of pathogen at microscale using human ascariasis as an example. To achieve this objective, start by investigating the potential influence of super-infection on the dynamics of type I environmentally-transmitted diseases from an embedded multiscale model through testing or examining the reciprocal influence between the inside-host scale and outside-host scale disease processes of human ascariasis as a paradigm. This is followed by investigating if nested multiscale models are an appropriate category of multiscale models to characterize the multiscale

dynamics of infectious diseases that have no pathogen replication-cycle at microscale. Human ascariasis is one of the soil-transmitted helminth infections of the small intestine and also a neglected tropical disease that has been and continue to be a cause of public health concern in many countries [64]. Together, soil-transmitted helminths (hookworm, ascariasis, and whipworm) are environmentally-transmitted disease systems of type I [8] and they account for a major burden of parasitic disease worldwide [2], with an estimation of 807 million - 1.2 billion people infected with human ascariasis [65]. In general, soil-transmitted helminths commonly affect people living in tropical and sub-tropical regions, with about 10 percent from the developing world infected with intestinal worms [2]. The causal agent of human ascariasis is the parasite ascaris lumbricoides, which is a species of roundworm. Additionally, The parasite ascaris lumbricoides has been implicated in the health welfare of many people world-widely, more especially in the impoverished regions with inadequate sanitation and poor hygiene practices [66]. People become infected with human ascariasis after accidentally swallowed ascaris lumbricoides eggs from the soil that have been contaminated by human feces or from raw vegetables or untreated water contaminated by soil containing the eggs. The main two environments that directly attribute in the life-cycle of ascaris lumbricoides are (i) the physical environment - which is associated with the outside-host developmental stages and transmission of ascaris lumbricoides at the population level (i.e., the between-host scale or macroscale) and (ii) the biological-host environment - which is associated with the inside-host developmental stages and migration of ascaris lumbricoides across various organs of the body (e.g., small intestine, heart, liver and lungs) at an individual level (i.e., the within-host scale or microscale). In the following three subsections, we provide some basic information about the life-cycle of the parasite that is resposible for the disease, preventive and control measures against the disease, and an overview of some mathematical models that have been developed to study the dynamics of the disease in the populations.

6.1.1 Life-Cycle of the Parasite of Human Ascariasis

This subsection highlights the complex life-cycle of ascaria lumbricoides. It involves seven important stages (see Figure 6.1). Five of these seven stages of the life-cycle of ascaria lumbricoides occur in the biological/inside-host environment (i.e. at the within-host scale or microscale) and the other two occur outside-host/geographical environment (i.e. at the between-host scale or macroscale). For more details on the life cycle of ascaria lumbricoides see the published works [67, 68]. Here, we only give a brief description. The transmission of human ascaris parasite begins when a human swallows food or water contaminated with fertilized ascaris worm eggs containing ascaris worm larvae (L3 larvae). After ingestion, the fertilized worm eggs hatch L3 larvae in the small intestine. Then the hatched larvae migrate to the lungs through bloodstream

where they mature. After maturing, the roundworms leave the lungs and migrate to the small intestine for the second time, where they become adult worms. It is at this stage where worms mate and lay eggs, which are then excreted to the physical-soil environment in feces. The cycle continues when another person ingests the eggs from contaminated soil.

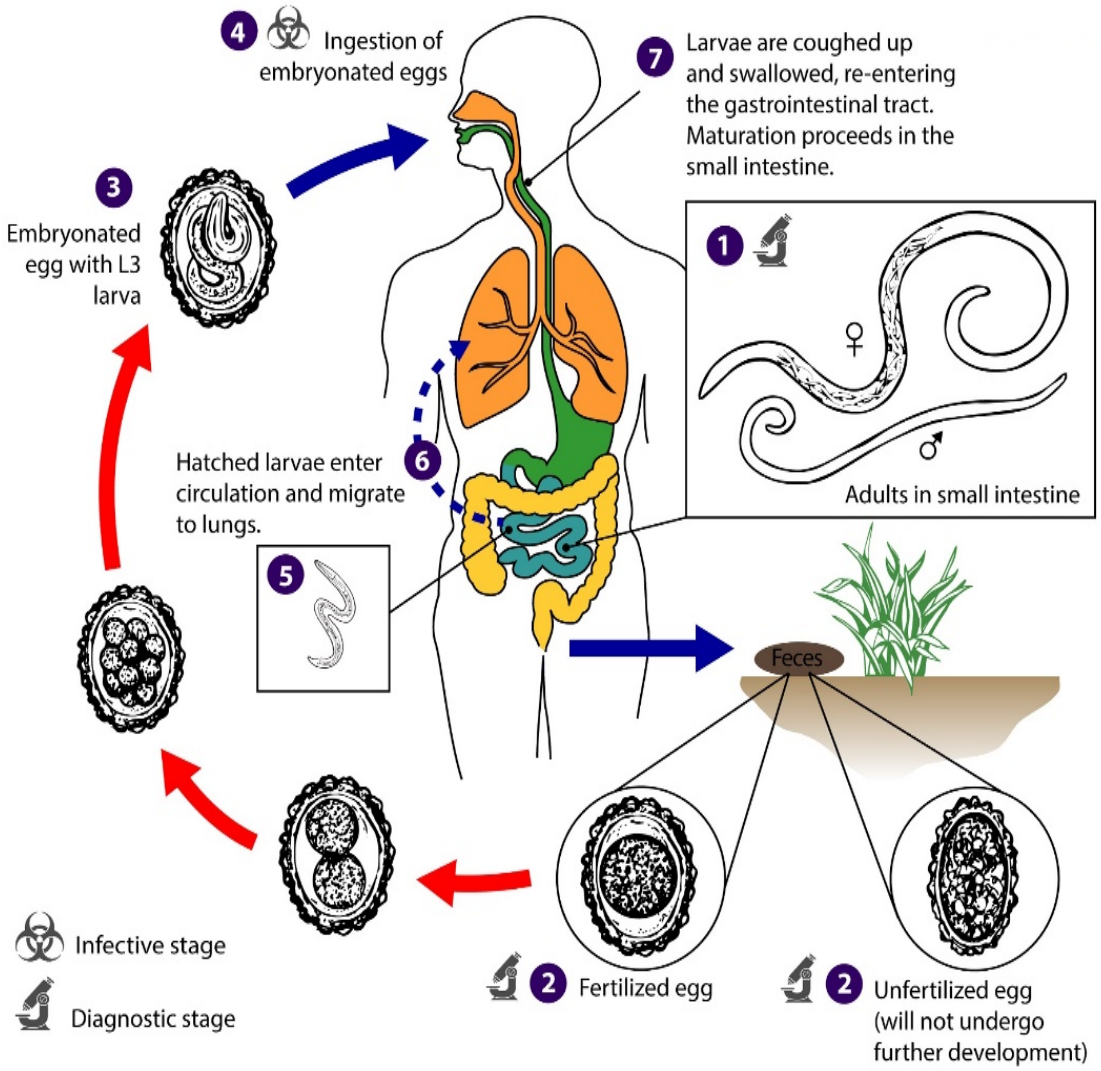

Figure 6.1: A Conceptual Diagram Showing the Life-cycle of Human Ascariasis Parasite. Source: [2]

6.1.2 Preventive and Control Measures Against Human Ascariasis

In general, the complexity of the life-cycle of ascaria lumbricoides makes human ascariasis being among the most challenging but preventable environmentally-transmitted infectious diseases to eliminate and even eradicate. Although, ascariasis infection rarely cause morbidity, however, if left untreated a high number of worms in the small intestine or lungs can lead to a sever complications such as intestinal blockage and impair growth in children. Additionally, people infected with this infection often show no symptoms. We briefly discuss some of control and preventive measures that have been proposed and implemented against human ascarisis. Currently, there is no vaccine against human ascariasis. Yet, efforts against the spread of human ascariasis across populations are only centered on control and preventive measures which include the following:

1. ***Health education [68]***: This involves educating people in a community about the disease and ensuring that they adopt and maintain behavioral practices that are aimed at reducing cases of human ascariasis. These behavioral practices include (i) improvement of personal hygiene practices such as washing of hands before handling or eating food as well as washing, peeling, or cooking all raw vegetables and fruits before eating, (ii) avoiding contact with soil that may be contaminated with human feces and (iii) always make a use of improved latrines for defecating.

2. ***Prevention of fecal contamination of soil [68]***: This involves control of parasitic movement from an infected individual to the physical environment through the means of providing sanitary disposal of human excreta to the households in communities with high risk of heavy ascariasis infections to ensure that people do not defect in open spaces. Generally, provision of sanitary disposal of human excreta in communities can be achieved through government's programs/campaigns that focus on breaking the parasite's life-cycle outside the host environment (i.e. at the between-host scale).

3. ***Administration of Anthelminthic medications for prevention and treatment [68]***: This involves provision and administration of drugs such as Albendazole and Mebendazole for treating people who are already infected with the disease. In addition the effectiveness of administration of anthelminthic medications is through killing the parasite. Moreover, the administration of anthelminthic medications also involves treating groups of people who are identified to be at higher risk for the infection without a prior stool examination by means of mass drug administration. Preschool and school-aged children as well as women of childbearing age (including pregnant women in the 2nd and 3rd trimesters and lactating women) are particularly identified as the high-risk groups for soil-transmitted helminth infections by the World Health Organization. In most cases, school-age children are often

treated through school-health programs while preschool children and pregnant women are treated during their visits to health clinics. Collectively, all of these measures focus on breaking the life-cycle of the parasite inside the host environment (i.e. at the within-host scale).

4. ***Removal of Parasitic Eggs from Water, Soil and Food [68]***: This include the treatment of wastewater, boiling of drinking water, and thorough cooking of raw vegetables, particularly those that have been grown in soil that has been fertilized with human excreta. Thus, this control measures have an effect of killing the parasite and thereby reduce parasite population in the water or vegetables.

Despite the aforementioned efforts for controlling and preventing human ascariasis together with the other soil-transmitted diseases (hookworm and Trichuris diseases), these infections continue to be a major public health concerned in many impoverished populations living in the tropical and subtropical regions of the world [68].

6.1.3 Overviews of Mathematical Models for the Transmission Dynamics of Human Ascariasis

In the past few decades, a number of mathematical models have been and continue to be used in attempting to gain a deeper understanding about the complexity of human ascariasis population biology and characterize its persist in a given population. The earliest account of mathematical models that describe the transmission dynamics and population biology of human ascariasis can be dated way back in 1980s, a period when mathematical modelling for helmnith infections was in its infancy [67]. It is in this period where Anderson and May introduced the first and simplest model structure of the population biology of ascaris. The model describes the dynamics of the mature adult worms (M) in the human host and the free-living infective egg stage (E) in the environment. Following the mathematical model developed in [67], we have witnessed a growing interest in mathematical modelling of human ascariasis and different modifications from this model by several authors have been carried out to take into account various aspects pertaining the population biology and transmission dynamics of human ascariasis which include: (i) age-structure, (ii) different host exposure and excretion/shedding rates of the parasite and (iii) control and preventive measures against human ascariasis burden across population (see for examples [67, 69–71] and references therein). Contrary to the previous studies of the transmission dynamics for human ascarisasis, the current study thought to use process of multiscale modelling as a way of thinking about human ascariasis population biology as a multiscale infectious disease system, in order to explicitly integrate the outside-host and inside-host environment life stages of

the parasite ascaria lumbricoides. This has been achieved through explicitly integrating ascaria disease processes that typically occur at the between-host scale in the physical environment as well as at the within-host scale in the human biological environment. In addition, this multiscale modeling for human ascariasis population biology presented in this current study is an extension of the application of the general method in [8] of type I environmentally-transmitted diseases.

6.2 Formulation of Embedded Multiscale Model of Human Ascariasis Dynamics

To explicitly capture the relevant and significant details of the population biology for human ascariasis, we use a general multiscale model in [8] that integrates the within-host scale and the between-host scale dynamics of environmentally-transmitted disease systems of type I. We used the general multiscale model for type I environmentally-transmitted infectious disease system to ascertain the potential influence of super-infection/reinfection on the spread of human ascariasis in the population. The multiscale model for human ascariasis presented in this section takes into consideration the reciprocal influence between the life stages of human ascariasis parasite in the inside-host/biological environment and the outside-host/geographical environment as shown in Figure 6.2. Thus, Figure 6.2 is a conceptual diagram of the multiscal model of human ascariasis showing the dynamics of the nine populations at any time t, namely: susceptible humans $S_H(t)$ and infected humans $I_H(t)$ in the human behavioural environment; fertilized worm eggs $P_E(t)$ and infective worm eggs $P_H(t)$ in the physical soil-environment; infective worm eggs $P_h(t)$ and hatched worm larvae $P_s(t)$ in the small intestine; mature worm $P_m(t)$ in the lungs; and adult worm larvae $P_a(t)$ and released worm eggs $P_e(t)$ by adult worm larvae in the small intestine.

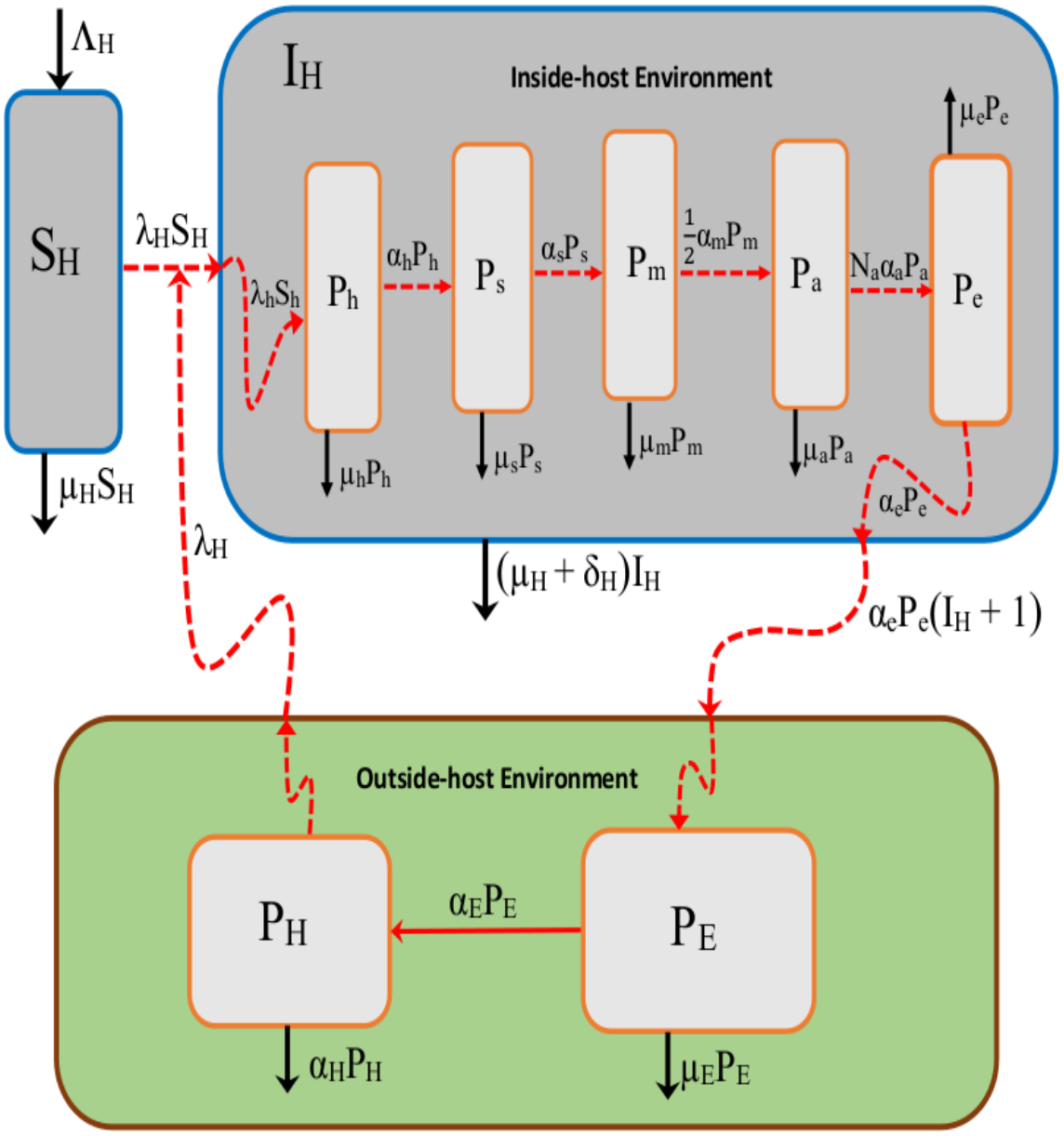

Figure 6.2: A conceptual diagram of the multiscale model of Human Ascariasis disease system. In this Figure $\lambda_h S_h = \dfrac{\lambda_H[S_h(t)-1]}{\Phi_H[I_H(t)+1]}$, where $\lambda_H = \dfrac{\beta_H P_H(t)}{P_0 + P_H(t)}$.

We make the following assumption for the multiscale model of human ascariasis dynamics:

(i) There is no vertical transmission of the disease,

(ii) The transmission of the disease is only through ingestion of infective eggs (P_H) in the physical environmental's entities (such soil, food or water),

(iii) The infected human population do not recover naturally from the infection,

(iv) There is no immune response in the human population,

(v) All the new recruited humans are assumed be healthy and have not been previously exposed to the disease.

(vi) The within-host scale parasitic load $P_a = P_a(t)$ is a proxy for individual human infectiousness.

(vii) The production of eggs is only by female adult worms $P_a(t)$ in the small intestine.

(viii) The population of unfertilized eggs in the soil is negligible as it has no impact on the transmission risk of the disease in the human population.

Based on the above mentioned assumptions and the diagram presented in Figure (6.2), the multiscale model for human ascariasis transmission dynamics is given by the following system of ordinary differential equations:

$$
\begin{cases}
i. \quad \dfrac{dS_H(t)}{dt} &= \Lambda_H - \dfrac{\beta_H P_H(t) S_H(t)}{P_0 + P_H(t) S_H(t)} - \mu_H S_H(t), \\
ii. \quad \dfrac{dI_H(t)}{dt} &= \dfrac{\beta_H P_H(t) S_H(t)}{P_0 + P_H(t)} - [\mu_H + \delta_H] I_H(t), \\
iii. \quad \dfrac{dP_E(t)}{dt} &= [I_H(t) + 1]\alpha_e P_e(t) - [\mu_E + \alpha_E] P_E(t), \\
iv. \quad \dfrac{dP_H(t)}{dt} &= \alpha_E P_E(t) - \alpha_H P_H(t), \\
v. \quad \dfrac{dP_h(t)}{dt} &= \dfrac{\beta_H P_H(t)[S_H(t) - 1]}{[P_0 + P_H(t)]\Phi_H[I_H(t) + 1]} - [\mu_h + \alpha_h] P_h(t), \\
vi. \quad \dfrac{dP_s(t)}{dt} &= \alpha_h P_h(t) - [\mu_s + \alpha_s] P_s(t), \\
vii. \quad \dfrac{dP_m(t)}{dt} &= \alpha_s P_s(t) - [\mu_m + \alpha_m] P_m(t), \\
viii. \quad \dfrac{dP_a(t)}{dt} &= \dfrac{\alpha_m}{2} P_m(t) - \mu_a P_a(t), \\
iv. \quad \dfrac{dP_e(t)}{dt} &= N_a \alpha_a P_a(t) - [\mu_e + \alpha_e] P_e(t).
\end{cases}
\tag{6.2.1}
$$

The first two equations of the model system (6.2.1) describe the dynamics of susceptible and infected human populations, respectively, in the behavioural human environment. The population of susceptible humans is assumed to increase at a constant rate Λ_H. This population is depleted through infection of susceptible humans at a variable rate $\lambda_H(t)S_H(t)$ and natural death at a constant rate μ_H. The infected human population increases through infection of susceptible humans, and decreases through natural death at a rate μ_H and through disease induced death at a rate δ_H, so that an average lifespan of infected humans in the population is determined by $1/(\delta_H + \mu_H)$.

The third equation in the model system (6.2.1) describe the dynamics of fertilized worm eggs in the physical soil-environment, which is generate through excretion of fecal material containing the within-host worm eggs at a variable rate $\alpha_e P_e(t)(I_H(t) + 1)$ derived following [9] and further refined in [8] which involves up scaling of individual infectiousness to population infectiousness. We assume that the fertilized worm eggs in the soil deplete through natural death at a rate μ_E and through developmental changes to become infective worm eggs at a rate α_E.

Equation (4) of the model system (6.2.1) describes the changes in time of the infective worm eggs in the physical environment, which also is generated following the developmental changes undergone by fertilized worm eggs at a rate α_E. The population of infective worm eggs in the physical environment is assumed to deplete naturally at a constant rate α_H.

Equation (5) of the model system (6.2.1) describes the dynamics of the inside-host infective worm eggs in the small intestine. The population of the inside-host infective worm eggs in the small intestine is generated following the ingestion of the outside-host infective worm eggs in the contaminated water or food by susceptible human host and becomes an infected human host at a mean rate $\lambda_h(t)S_h(t)$ derived also following [9] and further refined in [8] which involves down scaling of population infectiousness into individual infectiousness. This population of the inside-host infective worm eggs is assumed to decrease through natural death at a constant rate μ_h and through hatching at a constant rate α_h.

Equation (6) of the model system (6.2.1) describes the variation in time of the immature worm larvae in the small intestine. This population is generated through each egg hatching into immature worm larvae at a rate α_h. We assume that the population of immature worm larvae in the intestine depleted through natural death at a rate μ_s and through migration to the lungs at a rate α_s, where they develop and grow into mature worms.

Equation (7) of the model system (6.2.1) describes the evolution in time of the population of

mature worm larvae in the lungs, which is generated following the developmental changes undergone by immature worm larvae to become mature worm larvae at a rate α_s. This population is assumed to decrease through natural death at the rate μ_m and through migration to the small intestine at a rate α_m where they develop and grow to become adult worm larvae.

The last two equations of the multiscale model system (6.2.1) describe the changes in time of adult female worm larvae and released worm eggs by adult female worms in the small intestine, respectively. The population of adult female worm larvae is generated following developmental changes undergone by mature worms to become adult female worms at a rate $\alpha_m/2$. These developmental changes result in mature worms reaching sexual maturity and pairing up. Therefore, the introduction of the fraction 1/2 multiplying the parameter α_m models the pairing of immature worms on reaching sexual maturity. We assume that mature worms die naturally at a rate μ_a. The population of worm eggs in the intestine is generated when each pair laying an average number N_a of eggs at a rate α_a. We model the rate at which these eggs die in the human small intestine by the parameter μ_e and the rate at which they are excreted by the human host into the physical soil environment by μ_e.

No.	Variable	Description
1.	$S_H(t)$	Population of susceptible human hosts at time t.
2.	$I_H(t)$	Population of infected human hosts at time t.
3.	$P_E(t)$	Mean population of fertilized eggs in the environment at time t.
4.	$P_E(t)$	Mean population of infective eggs in the environment at time t.
5.	$P_h(t)$	Mean population of infective worm per infected human host at time t.
6.	$P_s(t)$	Mean population of immature worms per infected human host at time t.
7.	$P_m(t)$	Mean population of mature worms per infected human host at time t.
8.	$P_a(t)$	Mean population of female worms per infected human host at time t.
9.	$P_e(t)$	Mean population of worm eggs per infected human at time t.

Table 6.1: A summary of the variables of the human ascariasis multiscale model system (6.2.1).

6.3 Mathematical analysis of the embedded multiscale model of human ascariasis dynamics

In this section, we analyze the multiscale model system (6.2.1) by studying its properties, computing its basic reproductive number an use it to determine the stabilities of the model equilibrium states. The multiscale model system (6.2.1) has two equilibrium states: the disease-free equilibrium state (DFE) and the endemic equilibrium state (EEP).

6.3.1 Feasible Region of the Equilibria of the Multiscale Model

The multiscale model system (6.2.1) describes the transmission cycle of ascaria parasite in two distinct environments which are: (i) the inside-human-host scale environment and (ii) the outside-human-host scale environment. The multiscale model system (6.2.1) for human ascariasis transmission dynamics can be analyzed in a region $\Gamma \in R^+$ of biological interest. Assuming that all parameters and state variables for model system (6.2.1) are positive for all $t > 0$, it can be verified that all solutions for the model system (6.2.1) with non-negative initial conditions remain bounded. Therefore, letting $N_H = S_H + I_H$ and further add the 1^{st} and 2^{nd} equations in system (6.2.1) gives

$$\frac{dN_H(t)}{dt} = \Lambda_H - \mu_H N_H - \delta_H I_H. \tag{6.3.1}$$

It follow that

$$\frac{dN_H(t)}{dt} \leq \Lambda_H - \mu_H N_H \tag{6.3.2}$$

from which we get

$$N_H(t) \leq N_H(0)e^{-\mu_H t} + \frac{\Lambda_H}{\mu_H}\left[1 - e^{-\mu_H t}\right]. \tag{6.3.3}$$

Where $N_H(0)$ represents the value of total human population at the between-host scale in the population-host level evaluated at the initial values of the variables. Taking the limits of both $N_H(t)$ in (6.3.3) as time gets larger, we get the following expressions

$$\lim_{t\to\infty} sup(N_H(t)) \leq \frac{\Lambda_H}{\mu_H}. \tag{6.3.4}$$

Using the same principle as in equation (6.3.4), similar expressions can be derived for the remaining model variables. Hence, all feasible solutions of the model system (6.2.1) are positive and enter a region define by

$$\begin{cases} \Gamma = \{(S_H, I_H, P_E, P_H, P_h, P_s, P_m, P_a, P_e) \in R_+^9 : \\ \quad 0 \leq S_H + I_H \leq S_1, \ 0 \leq P_E \leq S_2, \ 0 \leq P_H \leq S_3, \\ \quad 0 \leq P_h \leq S_4, \ 0 \leq P_s \leq S_5, \ 0 \leq P_m \leq S_6, \ 0 \leq P_a \leq S_7, \\ \quad 0 \leq P_e \leq S_8\} \end{cases} \tag{6.3.5}$$

which is positively invariant and attracting for all $t > 0$, where

$$\begin{cases} S_1 = \dfrac{\Lambda_H}{\mu_H}, \\ S_2 = \dfrac{Q_E(\mathcal{R}_0 - 1)}{\mathcal{R}_0}, \\ S_3 = P_0(\mathcal{R}_0 - 1), \\ S_4 = \dfrac{Q_H(\mathcal{R}_0 - 1)}{\mathcal{R}_0}, \\ S_5 = \dfrac{\alpha_h Q_H(\mathcal{R}_0 - 1)}{(\alpha_s + \mu_s)\mathcal{R}_0}, \\ S_6 = \dfrac{\alpha_s \alpha_h Q_H(R_0 - 1)}{(\alpha_s + \mu_s)(\alpha_m + \mu_m)\mathcal{R}_0}, \\ S_7 = \dfrac{\alpha_m \alpha_s \alpha_h Q_H(\mathcal{R}_0 - 1)}{2\mu_a(\alpha_m + \mu_m)(\alpha_s + \mu_s)\mathcal{R}_0}, \\ S_8 = \dfrac{N_a \alpha_a \alpha_m \alpha_s \alpha_h Q_H(\mathcal{R}_0 - 1)}{2\mu_a(\alpha_e + \mu_e)(\alpha_m + \mu_m)(\alpha_s + \mu_s)\mathcal{R}_0} \end{cases} \tag{6.3.6}$$

with

$$\begin{cases} \mathcal{R}_0 = \left[\dfrac{\beta_H(\Lambda_H-\mu_H)\alpha_E}{\alpha_H\mu_H\Phi_H(\mu_E+\alpha_E)P_0}\right]\left[\dfrac{N_a\alpha_a\alpha_e\alpha_m\alpha_s\alpha_h}{2(\mu_h+\mu_h)(\mu_s+\alpha_s)(\mu_m+\mu_m)(\mu_e+\alpha_e)\mu_a}\right], \\ Q_E = \dfrac{N_a\alpha_a\alpha_m\alpha_s\alpha_h\alpha_e\beta_H(\Lambda_H-\mu_H)}{2\mu_a(\alpha_e+\mu_e)(\alpha_m+\mu_m)(\alpha_s+\mu_s)(\alpha_h+\mu_h)\Phi_H(\alpha_E+\mu_E)\mu_H}, \\ Q_H = \dfrac{\beta_H(\Lambda_H-\mu_H)}{\mu_H(\Lambda_H+\mu_H)(\alpha_h+\mu_h)\Phi_H}, \end{cases} \tag{6.3.7}$$

for $\Lambda_H > \mu_H$. Thus, whenever $\Lambda_H > \mu_H$, then the region Γ is positively invariant and attracting and it is sufficient to consider solutions of the model system (6.2.1) in Γ, since all solutions starting in Γ remain there for all $t \geq 0$. Hence, the model system is mathematically and epidemiologically well-posed and it is sufficient to consider the dynamics of the flow generated by model system (6.2.1) in Γ whenever $\Lambda_H > \mu_H$. We shall assume in all that follows (unless stated otherwise) that $\Lambda_H > \mu_H$ and $R_0 > 0$. In the next two subsection, we provide some results concerning the equilibrium states of the multiscale model system (6.2.1) and their stabilities. The multiscale model system (6.2.1) has two equilibrium states: the disease-free equilibrium state (DFE) and the endemic equilibrium state (EPP).

6.3.2 Disease-Free Equilibrium and Reproduction Number

We compute the disease-free equilibrium point of the model system (6.2.1) by setting the left-hand side of the equations of model system (6.2.1) equal to zero and also assume that $I_H = P_E = P_h = P_s = P_m = P_a = P_e = 0$. We further let

$$E_0 = \left(\frac{\Lambda_H}{\mu_H}, 0, 0, 0, 0, 0, 0, 0, 0\right), \tag{6.3.2.1}$$

denote the disease-free equilibrium of the model system (6.2.1). For the purpose of analyzing the stability of the DFE, we make the use of the basic reproduction number denoted as R_0. Generally, R_0 is a threshold value that is often used in public health to measure the spread of a disease in a given population.

6.3.2.1 Basic reproductive number of the embedded multiscale model system (6.2.1) for human ascariasis dynamics

The basic reproduction number of the multiscale model system (6.2.1) is calculated in this section using next generation operator approach described in [5]. Thus, the model system (6.2.1) can be

written in the form

$$\begin{cases} \dfrac{dX}{dt} &= f(X,Y,Z), \\ \dfrac{dY}{dt} &= g(X,Y,Z), \\ \dfrac{dZ}{dt} &= h(X,Y,Z), \end{cases} \tag{6.3.2.1.1}$$

where

(i) $X = S_H$ represents a compartment of susceptible individuals,

(ii) $Y = (I_H, P_E, P_h, P_s, P_m, P_a, P_e)$ represents all compartments of infected individuals that do not transmit the disease,

(iii) $Z = P_H$ represents a compartment of infected individuals who are capable of transmitting the disease.

Following [5] we define $\tilde{g}(X^*, Z)$ by

$$\tilde{g}(X^*, Z) = (\tilde{g}_1(X^*, Z), \tilde{g}_2(X^*, Z), \tilde{g}_3(X^*, Z), \tilde{g}_4(X^*, Z), \tilde{g}_5(X^*, Z), \tilde{g}_6(X^*, Z), \tilde{g}_7(X^*, Z)), \tag{6.3.2.1.2}$$

with

$$\begin{cases} 1.\ \widetilde{g}_1(X^*,Z) &= \dfrac{\beta_H\Lambda_H P_H}{\mu_H(\mu_H+\delta_H)(P_0+P_H)}, \\ 2.\ \widetilde{g}_2(X^*,Z) &= \dfrac{\alpha_e P_e[\widetilde{g}_1(X^*,Z)+1]}{(\mu_E+\delta_E+\alpha_E)}, \\ 3.\ \widetilde{g}_3(X^*,Z) &= \dfrac{\beta_H(\Lambda_H-\mu_H)P_H}{\mu_H(\mu_h+\alpha_h)\Phi_H(P_0+P_H)[\widetilde{g}_1(X^*,Z)+1]}, \\ 4.\ \tilde{g}_4(X^*,Z) &= \dfrac{\alpha_h P_h}{\alpha_s+\mu_s}, \\ 5.\ \tilde{g}_5(X^*,Z) &= \dfrac{\alpha_s P_s}{\alpha_m+\mu_m}, \\ 6.\ \widetilde{g}_6(X^*,Z) &= \dfrac{\alpha_m P_m}{2\mu_a}, \\ 7.\ \widetilde{g}_7(X^*,Z) &= \dfrac{N_a\alpha_a P_a}{2\mu_a(\alpha_e+\mu_e)}. \end{cases} \tag{6.3.2.1.3}$$

Therefore, in this case

$$h(X,Y,Z) = \frac{KP_H}{(P_0+P_H)} - \alpha_H P_H, \tag{6.3.2.1.4}$$

where

$$K = \frac{N_a\alpha_a\alpha_e\alpha_m\alpha_s\alpha_h\beta_H(\Lambda_H-\mu_H)\alpha_E}{2\mu_a\mu_H(\alpha_e+\mu_e)(\alpha_s+\mu_s)(\alpha_m+\mu_m)(\alpha_h+\mu_h)(\alpha_E+\mu_E)\Phi_H}. \tag{6.3.2.1.5}$$

Let $A = D_Z h(X^*, \tilde{g}(X^*,0),0)$ and further assume that A can be written in the form $A = M - D$, where

$$M = \frac{K}{P_0}, \quad D = \alpha_H. \tag{6.3.2.1.6}$$

The basic reproductive number is the spectral radius (dominant eigenvalue) of the matrix MD^{-1}, that is,

$$\begin{cases} \mathcal{R}_0 = \rho(MD^{-1}) = \left[\dfrac{\beta_H(\Lambda_H - \mu_H)\alpha_E}{\alpha_H\mu_H\Phi_H(\mu_E+\alpha_E)P_0}\right]\left[\dfrac{N_a\alpha_a\alpha_e\alpha_m\alpha_s\alpha_h}{2(\mu_h+\mu_h)(\mu_s+\alpha_s)(\mu_m+\mu_m)(\mu_e+\alpha_e)\mu_a}\right], \\ \\ = \mathcal{R}_{0_H}.\mathcal{R}_{0_h}. \end{cases} \tag{6.3.2.1.7}$$

Therefore, from the equation (6.3.2.1.7) we deduce that the basic reproductive number $\mathcal{R}_0$, has two main components which are as follows:

i. *The between-host scale partial reproductive number ($\mathcal{R}_{0_H}$)* which is the average number of infected humans arising from each infectious dose of ascaria parasite eggs ingested from the contaminated food or water by soil containing the eggs.

ii. *The within-host scale partial reproductive number ($\mathcal{R}_{0_h}$)* which is the amount of eggs produced by worms within a single infected human host and contributed to the contamination of the physical-soil environment.

In overall, from the expression of the reproductive number in equation (6.3.2.1.7) we can conclude that it is a function of both the within-host scale parameters and the between-host scale parameters. Therefore, the obtained results here show that the within-host scale and the between-host scale influence each other in a reciprocal way. In the next following two subsections, we further use basic reproductive number (6.3.2.1.7) to evaluate the local and global stability of the disease-free equilibrium (E_0) of the multiscale model system (6.2.1).

6.3.2.2 Local stability analysis of the embedded multiscale model disease-free equilibrium state

In this subsection, we determine the local stability of DFE of the model system (6.2.1). We linearize equations of the model system (6.2.1) in order to obtain a Jacobian matrix. Then we evaluate the Jacobian matrix of the system at the disease - free equilibrium (DFE),

$$E_0 = \left(\frac{\Lambda_H}{\mu_H}, 0, 0, 0, 0, 0, 0, 0, 0\right). \tag{6.3.2.2.1}$$

The Jacobian matrix of the model system (6.2.1) evaluated at the disease-free equilibrium state (DFE) is given by

$$J(E_0) = \begin{pmatrix} -\mu_H & 0 & 0 & -A_0 & 0 & 0 & 0 & 0 & 0 \\ 0 & -a_0 & 0 & A_0 & 0 & 0 & 0 & 0 & 0 \\ 0 & 0 & -a_1 & 0 & 0 & 0 & 0 & 0 & \alpha_e \\ 0 & 0 & \alpha_E & -\alpha_H & 0 & 0 & 0 & 0 & 0 \\ 0 & 0 & 0 & A_1 & -a_2 & 0 & 0 & 0 & 0 \\ 0 & 0 & 0 & 0 & \alpha_h & -a_3 & 0 & 0 & 0 \\ 0 & 0 & 0 & 0 & 0 & \alpha_s & -a_4 & 0 & 0 \\ 0 & 0 & 0 & 0 & 0 & 0 & \frac{\alpha_m}{2} & -\mu_a & 0 \\ 0 & 0 & 0 & 0 & 0 & 0 & 0 & N_a\alpha_a & -a_5 \end{pmatrix} \quad (6.3.2.2.2)$$

where

$$\begin{cases} a_0 = (\mu_H + \delta_H), \\ a_1 = (\mu_E + \alpha_E), \\ a_2 = (\mu_h + \alpha_h), \\ a_3 = (\mu_s + \alpha_s), \\ a_4 = (\mu_m + \alpha_m), \\ a_5 = (\mu_e + \alpha_e), \\ A_0 = \dfrac{\beta_H \Lambda_H}{\mu_H P_0}, \\ A_1 = \dfrac{\beta_H(\Lambda_H - \mu_H)}{\Phi_H \mu_H P_0}. \end{cases} \tag{6.3.2.2.3}$$

We consider stability of DFE by calculating the eigenvalues (λ_s) of the Jacobian matrix given by equation (6.3.2.2.2). The characteristic equation for the eigenvalues is given by

$$\Theta[\lambda^7 + \Phi_1\lambda^6 + \Phi_2\lambda^5 + \Phi_3\lambda^4 + \Phi_4\lambda^3 + \Phi_5\lambda^2 + \Phi_6\lambda + \Phi_7] = 0, \tag{6.3.2.2.4}$$

where

$$\Theta = (-\mu_H - \lambda)(-a_0 - \lambda). \tag{6.3.2.2.5}$$

It is clear from equation (6.3.2.2.4), that there are two negative eigenvalues (λ = -μ_H and λ = -a_0). Now in order to make conclusions about the stability of the DFE, we followed the Routh-Hurwitz criteria to determine the sign of the remaining eigenvalues of the polynomial

$$P(\lambda) = \lambda^7 + \Phi_1\lambda^6 + \Phi_2\lambda^5 + \Phi_3\lambda^4 + \Phi_4\lambda^3 + \Phi_5\lambda^2 + \Phi_6\lambda + \Phi_7 = 0 \tag{6.3.2.2.6}$$

where

$$\begin{cases} \Phi_1 &= a_5 + a_4 + a_3 + a_2 + a_1 + \alpha_H + \mu_a, \\ \Phi_2 &= a_5(\alpha_H + \mu_a) + k_0(a_5 + \alpha_H + \mu_a) + \alpha_H\mu_a + k_1, \\ \Phi_3 &= (a_5k_0 + k_1)(\alpha_H + \mu_a) + \alpha_H\mu_a(a_5 + k_0) + a_5k_1 + k_2, \\ \Phi_4 &= (a_5k_1 + k_2)(\alpha_H + \mu_a) + \alpha_H\mu_a(a_5k_0 + k_1) + a_5k_2 + k_3, \\ \Phi_5 &= (a_5k_2 + k_3)(\alpha_H + \mu_a) + \alpha_H\mu_a(a_5k_1 + k_2) + a_5k_3, \\ \Phi_6 &= \alpha_H\mu_a(a_5k_2 + k_3) + a_5k_2(\alpha_H + \mu_a), \\ \Phi_7 &= k_3a_5\mu_a\alpha_H[1 - \mathcal{R}_0], \end{cases} \tag{6.3.2.2.7}$$

with

$$\begin{cases} k_0 &= a_5 + a_4 + a_3 + a_2 + a_1, \\ k_1 &= a_1a_2 + a_3a_4 + (a_3 + a_4)(a_1 + a_2), \\ k_2 &= a_1a_2(a_3 + a_4) + a_3a_4(a_1 + a_2), \\ k_3 &= a_1a_2a_3a_4. \end{cases} \tag{6.3.2.2.8}$$

Using the Routh-Hurwitz stability criterion, the equilibrium state associated with the model system (6.2.1) is stable if and only if the determinants of all the Hurwitz matrices associated with the characteristic equation (6.3.2.2.6) are positive, that is

$$Det(H_j) > 0; \quad j = 1, 2, ..., 7 \tag{6.3.2.2.9}$$

where

$$\begin{cases} H_1 = \begin{pmatrix} \Phi_1 \end{pmatrix}; \quad H_2 = \begin{pmatrix} \Phi_1 & 1 \\ \Phi_3 & \Phi_2 \end{pmatrix}; \quad H_3 = \begin{pmatrix} \Phi_1 & 1 & 0 \\ \Phi_3 & \Phi_2 & \Phi_1 \\ \Phi_5 & \Phi_4 & \Phi_3 \end{pmatrix}; \\ H_4 = \begin{pmatrix} \Phi_1 & 1 & 0 & 0 \\ \Phi_3 & \Phi_2 & \Phi_1 & 1 \\ \Phi_5 & \Phi_4 & \Phi_3 & \Phi_2 \\ \Phi_7 & \Phi_6 & \Phi_5 & \Phi_4 \end{pmatrix}; \quad H_5 = \begin{pmatrix} \Phi_1 & 1 & 0 & 0 & 0 \\ \Phi_3 & \Phi_2 & \Phi_1 & 1 & 0 \\ \Phi_5 & \Phi_4 & \Phi_3 & \Phi_2 & \Phi_1 \\ \Phi_7 & \Phi_6 & \Phi_5 & \Phi_4 & \Phi_3 \\ 0 & 0 & \Phi_7 & \Phi_6 & \Phi_5 \end{pmatrix}; \end{cases} \tag{6.3.2.2.10}$$

and

$$\begin{cases} H_6 = \begin{pmatrix} \Phi_1 & 1 & 0 & 0 & 0 & 0 \\ \Phi_3 & \Phi_2 & \Phi_1 & 1 & 0 & 0 \\ \Phi_5 & \Phi_4 & \Phi_3 & \Phi_2 & \Phi_1 & 1 \\ \Phi_7 & \Phi_6 & \Phi_5 & \Phi_4 & \Phi_3 & \Phi_2 \\ 0 & 0 & \Phi_7 & \Phi_6 & \Phi_5 & \Phi_4 \\ 0 & 0 & 0 & 0 & \Phi_7 & \Phi_6 \end{pmatrix}; \\ H_7 = \begin{pmatrix} \Phi_1 & 1 & 0 & 0 & 0 & 0 & 0 \\ \Phi_3 & \Phi_2 & \Phi_1 & 1 & 0 & 0 & 0 \\ \Phi_5 & \Phi_4 & \Phi_3 & \Phi_2 & \Phi_1 & 1 & 0 \\ \Phi_7 & \Phi_6 & \Phi_5 & \Phi_4 & \Phi_3 & \Phi_2 & \Phi_1 \\ 0 & 0 & \Phi_7 & \Phi_6 & \Phi_5 & \Phi_4 & \Phi_3 \\ 0 & 0 & 0 & 0 & \Phi_7 & \Phi_6 & \Phi_5 \\ 0 & 0 & 0 & 0 & 0 & 0 & \Phi_7 \end{pmatrix}. \end{cases} \quad (6.3.2.2.11)$$

The Routh-Huiwitz criterion applied to Eq. (6.3.2.2.6) requires that the following conditions $C1$ - $C6$ be satisfied, in order to guarantee the local stability of the disease-free equilibrium point of

the model system (6.2.1).

$$\begin{cases} C1.\ \Phi_1,\Phi_2,\Phi_3,\Phi_4,\Phi_5,\Phi_6,\Phi_7>0,\ \ C2.\ \Phi_1\Phi_2-\Phi_3>0, \\ C3.\ \Phi_1(\Phi_2\Phi_3+\Phi_5)>\Phi_1\Phi_4+\Phi_3^2 \\ C4.\ \Phi_1[\Phi_2\Phi_3\Phi_4+\Phi_6(\Phi_1\Phi_2+\Phi_5)]+\Phi_3[\Phi_2\Phi_5+\Phi_7]+\Phi_4\Phi_5> \\ \quad \Phi_1[\Phi_2^2+\Phi_1^2\Phi_4+\Phi_2\Phi_7]+\Phi_3\Phi_6[\Phi_3\Phi_6^2+1]+\Phi_5^2, \\ C5.\ \Phi_1[\Phi_1\Phi_5\Phi_6(2\Phi_2+\Phi_3)+\Phi_2\Phi_3(\Phi_4\Phi_5+\Phi_7)+\Phi_3(2\Phi_6+\Phi_7)]+ \\ \quad \Phi_3^3(1+\Phi_5\Phi_4+\Phi_2\Phi_7)>\Phi_1[\Phi_1(\Phi_2\Phi_4\Phi_7+\Phi_4^2\Phi_5+\Phi_1\Phi_6^2+\Phi_6\Phi_7)+ \\ \quad \Phi_2(\Phi_3\Phi_5\Phi_6+\Phi_5^2)+\Phi_4(\Phi_3\Phi_7\Phi_5^2)]+\Phi_3(\Phi_3\Phi_6+\Phi_2\Phi_5^2+2\Phi_5\Phi_7), \\ C6.\ \Phi_1[\Phi_2\Phi_4\eta_0+\Phi_2\Phi_6\Phi_7(\Phi_3+\Phi_5)+2\Phi_4\Phi_6\eta_1]+\Phi_1^2\Phi_6[2\Phi_6(\Phi_2\Phi_3+\Phi_7)+\Phi_7\eta_2]+ \\ \quad \Phi_3\Phi_7(\eta_3+\Phi_7\eta_4)+\Phi_3\Phi_6\eta_5+\Phi_7\Phi_4\Phi_5^2+\Phi_7^3>\Phi_1[\Phi_2\eta_6+\Phi_6\nu_8+\Phi_7^2\Phi_6(2+\Phi_6) \\ \quad +\ 2\Phi_7\Phi_4\eta_7+\Phi_1^2(\Phi_7\Phi_6\eta_9+\Phi_4^2\Phi_5\Phi_6)+\Phi_6(\Phi_1^3\Phi_6+\Phi_5^3)+\Phi_7^2\eta_{10} \end{cases} \tag{6.3.2.2.12}$$

where

$$\begin{cases} \eta_0 &= \Phi_3\Phi_5\Phi_6 + \Phi_5\Phi_7 + \Phi_7^2, \\ \eta_1 &= \Phi_3\Phi_4\Phi_7 + \Phi_5^2, \\ \eta_2 &= \Phi_2\Phi_4 + \Phi_4^3 + 1, \\ \eta_3 &= \Phi_3\Phi_4^2 + 3\Phi_5\Phi_6 \\ , \eta_4 &= \Phi_2\Phi_4\Phi_7 + \Phi_2^2\Phi_7, \\ \eta_5 &= \Phi_3\Phi_6 + \Phi_2\Phi_5^2, \\ \eta_6 &= \Phi_3\Phi_4^2 + \Phi_3^2\Phi_6^2 + \Phi_5\Phi_6\Phi_7 + \Phi_4\Phi_7^2, \\ \eta_7 &= \Phi_3\Phi_6 + \Phi_4\Phi_5, \\ \eta_8 &= \Phi_2^2\Phi_5^2 + 2\Phi_3\Phi_5\Phi_6, \\ \eta_9 &= \phi_4\Phi_2 + \phi_4 + \Phi_2, \\ \eta_10 &= \Phi_3^3 + \Phi_1\Phi_6^2 + \Phi_2\Phi_5 \end{cases} \tag{6.3.2.2.13}$$

From equations (6.3.2.2.10) and (6.3.2.2.11) we note that all the coefficients Φ_1, Φ_2, Φ_3, Φ_4, Φ_5, and Φ_6 of the polynomial $P(\lambda)$ are greater than zero whenever $\mathcal{R}_0 < 1$. And we also noted that the conditions above are satisfied if and only if $\mathcal{R}_0 < 1$. Hence, all the roots of the polynomial $P(\lambda)$ are either negative or have negative real parts. The results are summarized in the following theorem.

Theorem 6.1. *The Disease-free equilibrium point of the model system (6.2.1) is locally asymptotically stable whenever* $\mathcal{R}_0 < 1$.

6.3.2.3 Global stability analysis of the embedded multiscale model disease-free equilibrium

We determine the global stability of DFE of the simplified multiscale model system (6.2.1) by using a next generation operator [5]. Thus the system (6.2.1) can be re-written in the form

$$\begin{cases} \dfrac{dX}{dt} &= F(X,Z), \\ \\ \dfrac{dY}{dt} &= G(X,Z), \end{cases} \tag{6.3.2.3.1}$$

where

- $X = S_H$ represents a compartment of uninfected humans, and
- $Z = (I_H, P_E, P_H, P_h, P_s, P_m, P_a, P_e)$ represents all compartments of infected and infectious components.

We let

$$E_0 = (X^*, 0) = \left(\frac{\Lambda_H}{\mu_H},\ 0,\ 0,\ 0,\ 0,\ 0,\ 0,\ 0,\ 0 \right), \tag{6.3.2.3.2}$$

denote the disease-free equilibrium (DFE) of the embedded multiscale model system (6.2.1). For X^* to be globally asymptotically stable, the following conditions (H1) and (H2) must be satisfied.

H1. $\dfrac{dX}{dt} = F(X,0)$ is globally asymptotically stable (g.a.s),

H2. $G(X,Z) = AZ - \hat{G}(X,Z)$, $\hat{G}((X,Z) \geq 0$ for $(X,Z) \in R^9_+$ where $A = D_Z G(X^*, 0)$ is an M-matrix and R^9_+ is the region where the model makes biological sense.

In this case,

$$F(X,0) = \left[\ \Lambda_H - \mu_H S_H \ \right], \tag{6.3.2.3.3}$$

and the matrix A is given by

$$A = \begin{bmatrix} -b_0 & 0 & \frac{\beta_H \Lambda_H}{\mu_H P_0} & 0 & 0 & 0 & 0 & 0 \\ 0 & -b_1 & 0 & 0 & 0 & 0 & 0 & \alpha_e \\ 0 & \alpha_E & -\alpha_H & 0 & 0 & 0 & 0 & 0 \\ 0 & 0 & \frac{\beta_H(\Lambda_H - \mu_H)}{\Phi_H \mu_H P_0} & -b_2 & 0 & 0 & 0 & 0 \\ 0 & 0 & 0 & \alpha_h & -b_3 & 0 & 0 & 0 \\ 0 & 0 & 0 & 0 & \alpha_s & -b_4 & 0 & 0 \\ 0 & 0 & 0 & 0 & 0 & \frac{\alpha_m}{2} & -\mu_a & 0 \\ 0 & 0 & 0 & 0 & 0 & 0 & N_a \alpha_a & -b_5 \end{bmatrix}. \quad (6.3.2.3.4)$$

where

$$\begin{cases} b_0 = (\mu_H + \delta_H), \\ b_1 = (\mu_E + \alpha_E), \\ b_2 = (\mu_h + \alpha_h), \\ b_3 = (\mu_s + \alpha_s), \\ b_4 = (\mu_m + \alpha_m), \\ b_5 = (\mu_e + \alpha_e). \end{cases} \quad (6.3.2.3.5)$$

and $\hat{G}(X,Z)$ given by

$$\hat{G}(X,Z) = \begin{bmatrix} \left(\frac{\Lambda_H}{P_0\mu_H} - \frac{S_H}{P_0+P_H}\right)\beta_H P_H \\ 0 \\ 0 \\ \left(\frac{\Lambda_H-\mu_H}{P_0\mu_H\Phi_H} - \frac{S_H-1}{(P_0+P_H)\Phi_H(I_H+1)}\right)\beta_H P_H \\ 0 \\ 0 \\ 0 \\ 0 \end{bmatrix} \tag{6.3.2.3.6}$$

It is clear that $\hat{G}(X,Z) \geq 0$ for all $(X,Z) \in R^9_+$, since $\Lambda_H/(\mu_H P_0) \geq S_H/(P_0+P_H)$ and $(\Lambda_H - \mu_H)/(P_0\mu_H\Phi_H) \geq [S_H - 1]/[(P_0+P_H)\Phi_H(I_H+1)]$. It is also clear that A is an M-matrix, since the off diagonal elements of A are non-negative. We state a theorem which summarizes the above result.

Theorem 6.2. *The disease-free equilibrium of model system (6.2.1) is globally asymptotically stable if* $R_0 \leq 1$ *and the assumptions* $(H1)$ *and* $(H2)$ *are satisfied.*

6.3.3 The Endemic Equilibrium and its Existence

In this section, we present some results concerning the existence of an endemic equilibrium solution for the model system (6.2.1). The endemic equilibrium state of the multiscale model system (6.2.1) is obtained by setting the left-hand side of the model to zero. Letting

$$E^* = (S^*_H, I^*_H, P^*_E, P^*_H, P^*_h, P^*_s, P^*_m, P^*_a, P^*_e) \tag{6.3.3.1}$$

be and endemic solution for the multiscale model system (6.2.1), the human ascariasis baseline

burden can be approximated using the endemic solutions of E^* given by equation (6.3.3.1). We now give expression for the endemic variables and their interpretation as follows: The endemic value of susceptible humans is given by

$$S_H^* = \frac{\Lambda_H(P_0 + P_H^*)}{(\beta_H + \mu_H)P_H^* + \mu_H P_0}. \tag{6.3.3.2}$$

From Eqn. (6.3.3.2) we note that the susceptible human population at endemic equilibrium is determined by the average time of stay in susceptible class and the rate at which new susceptible individuals enter into the susceptible class through birth. Individuals in the susceptible class leave the susceptible class either through infection or death. The endemic value of infected humans is given by

$$I_H^* = \frac{\beta_H P_H^* S_H^*}{(\mu_H + \delta_H)(P_0 + P_H^*)}. \tag{6.3.3.3}$$

We note from Eqn. (6.3.3.3) that the infected human individuals at the endemic equilibrium point is given by the average time of stay in the infected class, the rate at which susceptible individuals become infected and the density of susceptible individuals. The endemic value of ascaria worm eggs population in the physical soil environment is given by

$$P_E^* = \frac{\alpha_e P_e^*(I_H^* + 1)}{(\alpha_E + \mu_E)}. \tag{6.3.3.4}$$

We note from Eqn. (6.3.3.4) that the worm eggs population at equilibrium point is equal to the average life span of eggs, the rate at which each infected human host excretes ascaria worm eggs and the total number of humans infected. We note that this expression provides a link between the dynamics of the inside-host worm eggs and the outside-host environmental population dynamics of ascaria worm eggs. The endemic value of infective ascaria worm eggs population in the outside-host environment is given by

$$P_H^* = \frac{\alpha_E P_E^*}{\alpha_H}. \tag{6.3.3.5}$$

We note from Eqn. (6.3.3.5) that the ascaria worm eggs population at equilibrium point is equal to the rate at which ascaria worm eggs develop to become infective worm eggs and the average life span of infective worm eggs in the outside-host environment. The endemic value of within-host infective worm eggs in the human intestine is given by

$$P_h^* = \frac{\beta_H P_H^*(S_H^* - 1)}{(P_0 + P_H^*)(I_H^* + 1)(\alpha_h + \mu_h)\Phi_H}. \tag{6.3.3.6}$$

We note from Eqn. (6.3.3.6) we note that the average infective worm eggs population within a single infected human is equal to the average life-span of infective worm eggs within a single infected human host and the rate of infection of a single susceptible individual to become infected. We also note that this expression provides a link between the dynamics of the infective worm eggs within-host and human population dynamics. The endemic value of first stage worm larvae population inside an infected human host is given by

$$P_s^* = \frac{\alpha_h P_h^*}{(\alpha_s + \mu_s)}. \tag{6.3.3.7}$$

We note from Eqn. (6.3.3.7) that the first stage worm larvae population at equilibrium point is equal to the average life span of larvae, the rate at which each within-host ascaria worm eggs hatch . The endemic value of mature larvae population in the lungs of an infected human host is given by

$$P_m^* = \frac{\alpha_s P_s^*}{(\alpha_m + \mu_m)}, \tag{6.3.3.8}$$

We note from (6.3.3.9) that the mature larvae population in the lungs of an infected human host at equilibrium point is equal to the rate at which immature worm larvae migrate to the lungs and develop to become mature worm larvae and the average life span of mature worm larvae in the lungs. The endemic value of adult female worm larvae is given by

$$P_a^* = \frac{\alpha_m P_m^*}{2\mu_a}. \tag{6.3.3.9}$$

We note from Eqn. (6.3.3.9) that the adult female worm larvae population in the small intestine at equilibrium point is equal to the average life span of adult female worm larvae and the rate at which each mature worm larvae in the lungs migrate to the small intestine and develop to become adult female worm larvae. The endemic value of ascaria worm eggs population in the small intestine is given by

$$P_e^* = \frac{N_a \alpha_a P_a^*}{(\alpha_e + \mu_e)}. \tag{6.3.3.10}$$

We note from Eqn. (6.3.3.10) that the ascaria worm eggs population in the small intestine at equilibrium point is equal to the rate at which adult female worm release eggs, number of ascaria worm eggs produced by each adult female worm and the average life span of ascaria worm eggs in the small intestine.

6.3.3.1 Existence and uniqueness of the endemic equilibrium state

In this subsection, we present some results concerning the existence of an endemic equilibrium solution for model system (6.2.1). To determine the existence and uniqueness of the endemic equilibrium point (EEP) of the multiscale model system (6.2.1), we express the endemic values of the human ascariasis disease variables $S_H^*, I_H^*, P_E^*, P_h^*, P_s^*, P_m^*, P_a^*, P_e^*$ in terms of P_H^* as follows:

$$\begin{cases} S_H^*(P_H^*) = \dfrac{\Lambda_H(P_0+P_H^*)}{\mu_H P_0+(\beta_H+\mu_H)P_H^*}, \quad I_H^*(P_H^*) = \dfrac{\beta_H\Lambda_H P_H^*}{(\mu_H+\delta_H)[\mu_H P_0+(\beta_H+\mu_H)P_H^*]}, \\ P_h^*(P_H^*) = \dfrac{\beta_H}{(\mu_h+\alpha_h)\Phi_H}.\dfrac{Q_H^*(P_H^*)}{[I_H^*+1]}, \quad Q_H^*(P_H^*) = \dfrac{P_H^*[(\Lambda_H-\mu_H)(P_0+P_H^*)-\beta_H P_H^*]}{[\mu_H P_0+(\beta_H+\mu_H)P_H^*]}, \\ P_s^*(P_H^*) = \dfrac{\alpha_h\beta_H}{(\mu_s+\alpha_s)(\mu_h+\alpha_h)\Phi_H}.\dfrac{Q_H^*(P_H^*)}{[I_H^*+1]}, \\ P_m^*(P_H^*) = \dfrac{\alpha_s\alpha_h\beta_H}{(\mu_m+\alpha_m)(\mu_s+\alpha_s)(\mu_h+\alpha_h)\Phi_H}.\dfrac{Q_H^*(P_H^*)}{[I_H^*+1]}, \\ P_a^*(P_H^*) = \dfrac{\alpha_m\alpha_s\alpha_h\beta_H}{2\mu_a(\mu_m+\alpha_m)(\mu_s+\alpha_s)(\mu_h+\alpha_h)\Phi_H}.\dfrac{Q_H^*(P_H^*)}{[I_H^*+1]}, \\ P_e^*(P_H^*) = \dfrac{N_a\alpha_a\alpha_m\alpha_s\alpha_h\beta_H}{2\mu_a(\mu_e+\alpha_e)(\mu_m+\alpha_m)(\mu_s+\alpha_s)(\mu_h+\alpha_h)\Phi_H}.\dfrac{Q_H^*(P_H^*)}{[I_H^*+1]} \\ P_E^*(P_H^*) = \dfrac{\alpha_e N_a\alpha_a\alpha_m\alpha_s\alpha_h\beta_H Q_H^*(P_H^*)}{2\mu_a(\mu_e+\alpha_e)(\mu_m+\alpha_m)(\mu_s+\alpha_s)(\mu_h+\alpha_h)(\mu_E+\alpha_E)\Phi_H}. \end{cases} \tag{6.3.3.1}$$

Substituting the expression $P_E^*(P_H^*)$ of equation (6.3.3.1) into the equation for infective parasite eggs (P_H) in the outside-human-host scale environment which is given by:

$$\frac{dP_H(t)}{dt} = \alpha_E P_E(t) - \alpha_H P_H(t), \tag{6.3.3.2}$$

at endemic equilibrium, we get

$$P_H^{*2} + M_1 P_H^* + M_2 = 0, \tag{6.3.3.3}$$

where

$$\begin{cases} M_1 = \dfrac{\mu_H P_0}{\beta_H + \mu_H}\left[1 - \mathcal{R}_0\right] + \dfrac{N_E \beta_H}{\alpha_H(\beta_H + \mu_H)} + P_0, \\ M_2 = \dfrac{\mu_H P_0^2}{\beta_H + \mu_H}\left[1 - \mathcal{R}_0\right], \\ N_E = \dfrac{\beta_H \alpha_e N_a \alpha_a \alpha_m \alpha_s \alpha_h}{2\Phi_H(\mu_E + \alpha_E)(\mu_h + \alpha_h)(\mu_s + \alpha_s)(\mu_m + \alpha_m)(\mu_e + \alpha_e)\mu_a}. \end{cases} \tag{6.3.3.4}$$

Therefore,

$$P_H^* = \frac{1}{2}\left[-M_1 + \sqrt{M_1^2 - 4M_2}\right] > 0 \ for \ \ \mathcal{R}_0 > 1. \tag{6.3.3.5}$$

We note that $M_2 < 0$ for $R_0 > 1$, while M_2 is either positive or negative for $\mathcal{R}_0 > 1$. Therefore, we can conclude that the multiscale model system (6.2.1) has one positive endemic equilibrium for $\mathcal{R}_0 > 1$. Furthermore, based on the endemic equilibrium values of the model system (6.2.1) given by equation (6.3.3.1)), we can easily deduce that some of the between-host scale expressions depend on both the within-host and the between-host disease parameters, while the within-host scale expressions are determined by both the within-host and the between-host disease parameters. Therefore, the obtained results here show that the within-host scale and the between-host scale dynamics influence each other in a reciprocal way.

6.3.3.2 Local stability of the endemic equilibrium state

In this sub-section, we study the local asymptotic stability of the endemic steady state of the model system (6.2.1) by using the Center Manifold Theory described in [57]. In this case, we employ Center Manifold Theory by making the following change of variables: letting $S_H = x_1$, $I_H = x_2$, $P_E = x_3$, $P_H = x_4$, $P_h = x_5$, $P_s = x_6$, $P_m = x_7$, $P_a = x_8$, $P_e = x_9$. We also use the vector notation $\mathbf{x} = (x_1, x_2, x_3, x_4, x_5, x_6, x_7, x_8, x_9)^T$ so that the model system (6.2.1) can be written in the form

$$\frac{d\mathbf{x}}{dt} = \mathbf{f}(\mathbf{x}, \beta^*), \tag{6.3.3.1}$$

where

$$\mathbf{f} = (f_1, f_2, f_3, f_4, f_5, f_6, f_7, f_8, f_9). \tag{6.3.3.2}$$

Therefore, model system (6.2.1) can be re-written as:

$$\begin{cases} 1. \quad \dot{x}_1 = \Lambda_H - [\dfrac{\beta_H x_4(t)}{P_0 + x_4(t)} - \mu_H]x_1(t), \\ 2. \quad \dot{x}_2 = \dfrac{\beta_H x_4(t)}{P_0 + x_4(t)} - [\mu_H + \delta_H]x_2(t), \\ 3. \quad \dot{x}_3 = \alpha_e x_9(t)(x_2(t) + 1) - [\mu_E + \alpha_E]x_3(t), \\ 4. \quad \dot{x}_4 = \alpha_E x_3(t) - \alpha_H x_4(t), \\ 5. \quad \dot{x}_5 = \dfrac{\lambda_H(x_1(t) - 1)}{\Phi_H(x_2(t) + 1)} - [\alpha_h + \mu_h]x_5(t), \\ 6. \quad \dot{x}_6 = \alpha_h x_5(t) - [\alpha_s + \mu_s]x_6(t), \\ 7. \quad \dot{x}_7 = \alpha_h x_6(t) - [\alpha_m + \mu_m]x_7(t), \\ 8. \quad \dot{x}_8 = \dfrac{\alpha_m x_7(t)}{2} - \mu_a x_8(t), \\ 9. \quad \dot{x}_9 = N_a \alpha_a x_8(t) - [\alpha_e + \mu_e]x_9(t). \end{cases} \tag{6.3.3.3}$$

The Center Manifold Theory method involves evaluating the Jacobian matrix of the system (6.3.3.3) at the disease-free equilibrium E^0 denoted by $J(E^0)$. The Jacobian matrix associated with the system of equations (6.3.3.3) evaluated at the disease-free equilibrium (E_0) is given by

$$J_{\beta^*} = \begin{pmatrix} -\mu_H & 0 & 0 & -\dfrac{\beta^*\Lambda_H}{\mu_H P_0} & 0 & 0 & 0 & 0 & 0 \\ 0 & -z_0 & 0 & \dfrac{\beta^*\Lambda_H}{\mu_H P_0} & 0 & 0 & 0 & 0 & 0 \\ 0 & 0 & -z_1 & 0 & 0 & 0 & 0 & 0 & \alpha_e \\ 0 & 0 & \alpha_E & -\alpha_H & 0 & 0 & 0 & 0 & 0 \\ 0 & 0 & 0 & \dfrac{\beta^*(\Lambda_H - \mu_H)}{\Phi_H \mu_H P_0} & -z_2 & 0 & 0 & 0 & 0 \\ 0 & 0 & 0 & 0 & \alpha_h & -z_3 & 0 & 0 & 0 \\ 0 & 0 & 0 & 0 & 0 & \alpha_s & -z_4 & 0 & 0 \\ 0 & 0 & 0 & 0 & 0 & 0 & \dfrac{\alpha_m}{2} & -\mu_a & 0 \\ 0 & 0 & 0 & 0 & 0 & 0 & 0 & N_a\alpha_a & -z_5 \end{pmatrix} \tag{6.3.3.4}$$

where

$$\begin{cases} z_0 = (\mu_H + \delta_H), \\ z_1 = (\mu_E + \alpha_E), \\ z_2 = (\mu_h + \alpha_h), \\ z_3 = (\mu_s + \alpha_s), \\ z_4 = (\mu_m + \alpha_m), \\ z_5 = (\mu_e + \alpha_e). \end{cases} \tag{6.3.3.5}$$

Using the similar approach as in previous section, the basic reproductive number of model system (6.3.3.3) is as follows:

$$\mathcal{R}_0 = \frac{N_a\alpha_a\alpha_e\alpha_m\alpha_s\alpha_h\beta_H(\Lambda_H - \mu_H)\alpha_E}{2(\mu_h+\mu_h)(\mu_s+\alpha_s)(\mu_m+\mu_m)(\mu_e+\alpha_e)\mu_a\alpha_H\mu_H\Phi_H(\mu_E+\alpha_E)P_0}. \tag{6.3.3.6}$$

Let $\beta_H = \beta^*$ be a bifurcation parameter of the model system (6.3.3.3). Considering $\mathcal{R}_0 = 1$, and solve for β^* in equation (6.3.3.6), we obtain:

$$\beta^* = \frac{2(\mu_h+\mu_h)(\mu_s+\alpha_s)(\mu_m+\mu_m)(\mu_e+\alpha_e)\mu_a\alpha_H\mu_H\Phi_H(\mu_E+\alpha_E)P_0}{N_a\alpha_a\alpha_e\alpha_m\alpha_s\alpha_h\beta_H(\Lambda_H - \mu_H)\alpha_E}. \tag{6.3.3.7}$$

We can easily note that the linearized system of the transformed equations (6.3.3.3) with bifurcation point β^* has a simple zero eigenvalue. Hence, the center manifold theory [**?**] can be used to analyze the dynamics of (6.3.3.3) near $\beta_C = \beta^*$. We, therefore, apply Theorem 4.1 in Castillo-Chavez and Song [**?**] stated below as Theorem 6.3 for convenience, to show the local asymptotic stability of the endemic equilibrium point of (6.3.3.3) (which is the same as the endemic equilibrium point of the original system (6.2.1), for $\beta_C = \beta^*$).

Theorem 6.3. *Consider the following general system of ordinary differential equations with parameter ϕ:*

$$\frac{dx}{dt} = f(x,\phi), \quad f : R^n \times R \longrightarrow R, \quad f : C^2(R^2 \times R), \tag{6.3.3.8}$$

where 0 is an equilibrium of the system, that is $f(0,\phi) = 0$ for all ϕ, and assume that

A1. $A = D_x f(0,0) = ((\partial f_i/\partial x_j)(0,0))$ is a linearization matrix of the model system (6.3.3.8) around the equilibrium 0 with ϕ evaluated at 0. Zero is a simple eigenvalue of A, and other eigenvalues of A have negative real parts,

A2. matrix A has a right eigenvector u and a left eigenvector v corresponding to the zero eigenvalue.

Let f_k be the k^{th} component of f and

$$\begin{aligned} a &= \sum_{k,i,j=1}^{n} u_k v_i v_j \frac{\partial^2 f_k}{\partial x_i \partial x_j}(0,0), \\ b &= \sum_{k,i=1}^{n} u_k v_i \frac{\partial^2 f_k}{\partial x_i \partial \phi}(0,0). \end{aligned} \tag{6.3.3.9}$$

The local dynamics of (6.3.3.8) around 0 *are totally governed by* a *and* b *and are summarized as follows.*

1. $a > 0$, $b > 0$. *When* $\phi < 0$ *with* $|\phi| \ll 1$, 0 *is locally asymptotically stable, and there exists a positive unstable equilibrium; when* $0 < \phi \ll 1$, *0 is unstable and there exists a negative and locally asymptotically stable equilibrium.*

2. $a < 0$, $b < 0$. *When* $\phi < 0$ *with* $|\phi| \ll 1$, 0 *is unstable; when* $0 < \phi \ll 1$, *0 is locally asymptotically stable, and there exists a positive unstable equilibrium;*

3. $a > 0$, $b < 0$. *When* $\phi < 0$ *with* $|\phi| \ll 1$, 0 *is unstable, and there exists a locally asymptotically stable negative equilibrium; when* $0 < \phi \ll 1$, 0 *is stable and a positive unstable equilibrium appears;*

4. $a < 0$, $b > 0$. *When* ϕ *changes from negative to positive,* 0 *changes its stability from stable to unstable. Correspondingly a negative unstable equilibrium becomes positive and locally asymptotically stable*

For us to apply Theorem 6.3, the following computations are necessary (it should be noted that we are using β^* as the bifurcation parameter, in place of ϕ in Theorem 6.3).

Eigenvectors of J_{β^*}: For the case when $R_0 = 1$, it can be shown that the Jacobian matrix in (6.3.3.4) at $\beta_C = \beta^*$ (denoted by J_{β^*}) has a right eigenvector associated with the zero eigenvalue given by

$$\mathbf{u} = [u_1, u_2, u_3, u_4, u_5, u_6, u_7, u_8, u_9]^T, \tag{6.3.3.10}$$

where

$$\begin{cases} u_1 &= -\dfrac{\beta^*\Lambda_H}{\mu_C^2 P_0}, \\ u_2 &= \dfrac{\beta^*\Lambda_C}{P_0\mu_H}, \\ u_3 &= \dfrac{N_a\alpha_a\alpha_e\alpha_m\alpha_s\alpha_h\beta_H(\Lambda_H-\mu_H)}{2(\mu_h+\mu_h)(\mu_s+\alpha_s)(\mu_m+\mu_m)(\mu_e+\alpha_e)\mu_a\mu_H\Phi_H(\mu_E+\alpha_E)P_0}, \\ u_4 &= 1, \\ u_5 &= \dfrac{\beta^*(\Lambda_H-\mu_H)}{\mu_H\Phi_H(\mu_h+\alpha_h)P_0}, \\ u_6 &= \dfrac{\alpha_h\beta^*(\Lambda_H-\mu_H)}{\mu_H\Phi_H(\mu_h+\alpha_h)(\mu_s+\alpha_s)P_0}, \\ u_7 &= \dfrac{\alpha_s\alpha_h\beta^*(\Lambda_H-\mu_H)}{\mu_H\Phi_H(\mu_h+\alpha_h)(\mu_s+\alpha_s)(\mu_m+\alpha_m)P_0}, \\ u_8 &= \dfrac{\alpha_m\alpha_s\alpha_h\beta^*(\Lambda_H-\mu_H)}{\mu_H\Phi_H(\mu_h+\alpha_h)(\mu_s+\alpha_s)(\mu_m+\alpha_m)\mu_a P_0}, \\ u_9 &= \dfrac{N_a\alpha_a\alpha_m\alpha_s\alpha_h\beta^*(\Lambda_H-\mu_H)}{2\mu_H\Phi_H(\mu_h+\alpha_h)(\mu_s+\alpha_s)(\mu_m+\alpha_m)\mu_a P_0}. \end{cases} \tag{6.3.3.11}$$

In addition, the left eigenvector of the Jacobian matrix in (6.3.3.4) associated with the zero eigenvalue at $\beta_C = \beta^*$ is given by

$$\mathbf{v} = [v_1, v_2, v_3, v_4, v_5, v_6, v_7, v_8, v_9]^T, \tag{6.3.3.12}$$

where

$$\begin{cases} v_1 &= 0, \\ v_2 &= 0 \\ v_3 &= \dfrac{2(\mu_h+\alpha_h)(\mu_s+\alpha_s)(\mu_m+\alpha_m)\mu_a}{\alpha_E N_a \alpha_a \alpha_m \alpha_s \alpha_h}, \\ v_4 &= \dfrac{\beta^*(\Lambda_H-\mu_H)}{\alpha_H \mu_H \Phi_H P_0}, \\ v_5 &= 1, \\ v_6 &= \dfrac{(\alpha_h+\mu_h)}{(\alpha_h}, \\ v_7 &= \dfrac{(\mu_s+\alpha_s)(\alpha_h+\mu_h)}{(\alpha_s\alpha_h}, \\ v_8 &= \dfrac{(\mu_m+\alpha_m)(\mu_s+\alpha_s)(\alpha_h+\mu_h)}{(\alpha_m\alpha_s\alpha_h}, \\ v_9 &= \dfrac{2\mu_a(\mu_m+\alpha_m)(\mu_s+\alpha_s)(\alpha_h+\mu_h)}{N_a\alpha_a\alpha_m\alpha_s\alpha_h}. \end{cases} \tag{6.3.3.13}$$

Computation of bifurcation parameters a and b:

We evaluate the non-zero second order mixed derivatives of **f** with respect to the variables and β^* in order to determine the signs of a and b. The sign of a is associated with the following non-vanishing partial derivatives of **f**:

$$\begin{cases} \dfrac{\partial^2 f_1}{\partial x_3^2} &= \dfrac{2\beta^*\Lambda_H}{P_0^2\mu_H}, \\ \dfrac{\partial^2 f_2}{\partial x_3^2} &= -\dfrac{2\beta^*\Lambda_H}{P_0^2\mu_H}, \\ \dfrac{\partial^2 f_3}{\partial x_3^2} &= -\dfrac{2\beta^*(\Lambda_H-\mu_H)}{P_0^2\mu_H\Phi_H}. \end{cases} \tag{6.3.3.14}$$

The sign of b is associated with the following non-vanishing partial derivatives of $\mathbf{f}$:

$$\begin{cases} \dfrac{\partial^2 f_1}{\partial x_3 \partial \beta^*} &= -\dfrac{\Lambda_H}{\mu_H P_0}, \\ \dfrac{\partial^2 f_2}{\partial x_3 \partial \beta^*} &= \dfrac{\Lambda_H}{\mu_H P_0}, \\ \dfrac{\partial^2 f_4}{\partial x_3 \partial \beta^*} &= \dfrac{(\Lambda_H - \mu_H)}{\mu_H P_0 \Phi_H}. \end{cases} \tag{6.3.3.15}$$

Substituting expressions in Eqn. (6.3.3.11), Eqn. (6.3.3.13), and Eqn. (6.3.3.14) into Eqn. (6.3.3.9), we get

$$\begin{cases} a &= u_1 v_4^2 \dfrac{\partial^2 f_1}{\partial x_4^2} + u_2 v_4^2 \dfrac{\partial^2 f_2}{\partial x_4^2} + u_5 v_4^2 \dfrac{\partial^2 f_5}{\partial x_4^2}, \\ &= u_1 v_4^2 \left[\dfrac{2\beta^* \Lambda_H}{P_0^2 \mu_H}\right] + u_2 v_4^2 \left[\dfrac{-2\beta^* \Lambda_H}{P_0^2 \mu_H}\right] + u_5 v_4^2 \left[\dfrac{-2\beta^* (\Lambda_H - \mu_H)}{\Phi_H P_0^2 \mu_H}\right], \\ &= \dfrac{2\beta^* \Lambda_H}{P_0^2 \mu_H}.v_4^2 \left[u_1 - u_2\right] - u_5 v_4^2 \left[\dfrac{2\beta^* (\Lambda_H - \mu_H)}{\Phi_H P_0^2 \mu_H}\right] < 0, \end{cases} \tag{6.3.3.16}$$

since $u_1 - u_2 < 0$ and $u_5 > 0$.

Similarly, substituting expressions in Eqn. (6.3.3.11), Eqn. (6.3.3.13) and Eqn. (6.3.3.15) into equation (6.3.3.9), we get

$$\begin{cases} b &= u_1 v_4 \dfrac{\partial^2 f_1}{\partial x_3 \partial \beta^*} + u_2 v_4 \dfrac{\partial^2 f_2}{\partial x_3 \partial \beta^*} + u_5 v_4 \dfrac{\partial^2 f_5}{\partial x_{10} \partial \beta^*}, \\ &= v_4 \left[\dfrac{\Lambda_H}{P_0 \mu_H}.u_2 - \dfrac{\Lambda_H}{P_0 \mu_H}.u_1 + \dfrac{(\Lambda_H - \mu_H)}{\Phi_H P_0 \mu_H}.u_4\right], \\ &= \dfrac{\Lambda_H}{P_0 \mu_H}.v_4 \left[u_2 - u_1\right] + \dfrac{(\Lambda_H - \mu_H)}{\Phi_H P_0 \mu_H}.v_4 u_5 > 0, \end{cases} \tag{6.3.3.17}$$

since $(u_2 - u_1) > 0$, $u_5 > 0$, and $v_4 > 0$. Thus, $a < 0$ and $b > 0$. Using Theorem 6.3, item 4., we have established the following result which only holds for $\mathcal{R}_0 > 1$ but close to 1. The following Theorem summaries the results we obtained:

Theorem 6.4. *The endemic equilibrium guaranteed by the Center Manifold Theorem 6.3 is locally asymptotically stable for $R_0 > 1$ near 1.*

6.4 Numerical Analysis of the baseline multiscale model of ascariasis transmission dynamics

The behaviour of the human ascaria multiscale model system (6.2.1) was also numerically simulated using a Python program version V 2.6 on Windows 10 operation system. This was achieved to illustrate the analytical results we obtained in this chapter. We used the estimated parameter values presented in Table 6.2 and Table 6.3 for sensitivity and numerical analysis. Some of parameter values used from published literature and some were assumed as values of some parameters generally not reported in literature. However, for those parameters which are not reported in literature, their values were only indirectly approximated from inferences reported in the published literature. For instance, parameters marked [D^*] in Table 6.2 are demographic parameters which were chosen to be within ranges of values for developing countries. Also, parameters marked [H^*] in Table 6.3 are epidemiological parameters specific to human ascariasis infection that could not be found in literature, and thus were chosen to be within ranges of values for helminths infections. The initial conditions used for simulation are given by $S_H(0) = 2500$, $I_H(0) = 10$, $P_E(0) = 0$, $P_H(0) = 1.50$, $P_h(0) = 0$, $P_s(0) = 0$, $P_m(0) = 100000$, $P_a(0) = 0$, $P_e(0) = 50000$.

SL. No.	Parameter	Description	Value [Range explored]	Units	Source/ Rational
1.	Λ_H	Susceptible humans recruitment rate through birth	0.0001[0.0001-0.0003]	day^{-1}	[D^*]
2.	β_H	Human infection rate	0.1[0.3000-0.00300]	day^{-1}	[D^*]
3.	μ_H	Natural death rate of humans	0.00001[0.0001-0.00001]	day^{-1}	[D^*]
4.	δ_H	Disease induced death rate	0.004[0.004-0.0001]	day^{-1}	[D^*]
5.	P_0	Saturation constant of infective eggs	1000[100-10000]	day^{-1}	Assumed
6.	Φ_H	Proportion of new infections	0.03000[0.003-0.3000]	day^{-1}	Assumed
7.	α_E	Rate at which fertilized eggs become infective in the environment	0.1250[0.0181-0.1000]	day^{-1}	[69]
8.	μ_E	Natural decay rate of fertilized worm eggs in the environment	0.183561[0.079472-0.260274]	day^{-1}	[66]
9.	α_H	Natural decay of infective eggs in the environment	0.0357[0.0120-0.0357]	day^{-1}	[69]

Table 6.2: Parameter values for the multiscale model given by (6.2.1) associated with the outside-host disease dynamics.

SL. No.	Parameter	Description	Value [Range explored]	Units	Source/ Rational
1.	μ_h	Natural decay rate of infective eggs in the small intestine	1.427397[0.805479-2.276712]	day^{-1}	[H^*]
2.	α_h	Rate at which infective eggs hatched in the small intestine	0.1230[0.000-1.000]	day^{-1}	[72]
3.	μ_s	Natural death rate of immature worms in the small intestine	0.0400[0.000-0.000]	day^{-1}	[H^*]
4.	α_s	Migration rate of immature worm to lungs	0.2500[0.5000-1]	day^{-1}	[73]
5.	μ_m	Natural death rate of adult female worms within the human host	0.0667[0.0667-0.1000]	day^{-1}	[H^*]
6.	α_m	Migration rate of mature worm to small intestine	0.0714[0.0667-0.2000]	day^{-1}	[66, 69]
7.	N_a	Average number of eggs produced by adult female worm	10000.0[10000.0-20000.0]	day^{-1}	[69]
8.	α_a	Rate at which female worms produce eggs in the small intestine	0.0133[0.0133-0.0167]	day^{-1}	[66]
9.	μ_a	Natural decay rate of adult female worms within human host	0.0027[0.0014-0.0027]	day^{-1}	[69]
10.	α_e	Rate of excretion of the worm eggs into the environment	0.320548[0.019178-1.369863]	day^{-1}	[H^*]
11.	μ_e	Natural decay of worm eggs in the human host	0.0400[0.0400-0.0001]	day^{-1}	[H^*]

Table 6.3: Parameter values for the multiscale model given by (6.2.1) associated with the inside-host disease dynamics.

6.4.1 Sensitivity Analysis of the human ascariasis transmission metrics derived from the multiscale model

In this subsection, we carry out a sensitivity analysis to evaluate the relative change in the two main human ascariasis transmission metrics derived from the multiscale model system (6.2.1) when the within-host and between-host parameters in the multiscale model change. The two human ascariasis transmission metrics derived from the multiscale model system (6.2.1) are: the basic reproductive number (R_0) – which characterize the transmission of the disease at the

start of an infection, and the endemic value of infective worm eggs in the environment (P_H^*) – which characterize the transmission of the disease when it has reach an endemic level. Fig. 6.3 and Fig. 6.4 are tornado plots of the partial rank correlation coefficients (PRCCs) concurrently showing the effect of the within-host and between-host parameter variations on the two human ascariasis transmission metrics (R_0 and P_H^*) using parameter values in Table **??**.

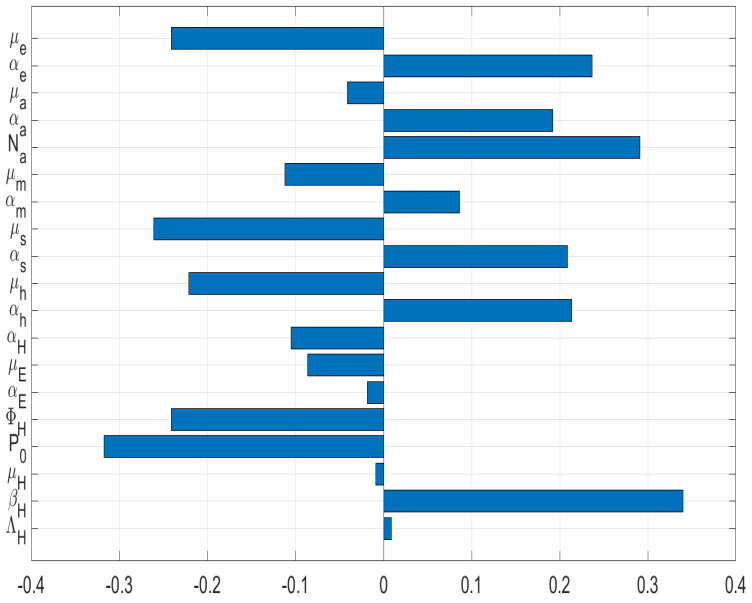

Figure 6.3: *Tornado plot of partial rank correlation coefficients (PRCCs) of all the model parameters that influence the human ascariasis transmission metric* R_0

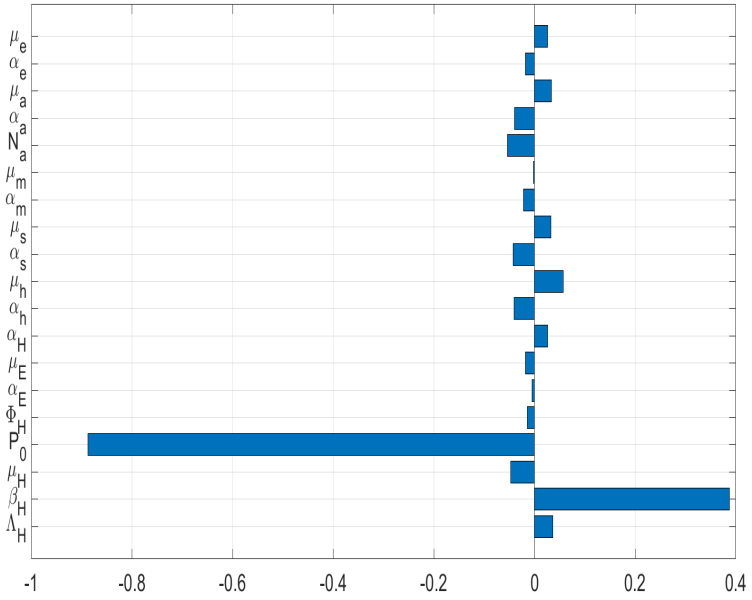

Figure 6.4: *Tornado plot of partial rank correlation coefficients (PRCCs) of all the model parameters that influence the human ascariasis transmission metric* P_H^*

From the sensitivity indices in Fig. 6.3) and Fig. 6.4, we deduce the following results:

(i) Some of the baseline parameters of the multiscale model (6.2.1) have positive PRCCs and some have negative PRCCs. This indicates that, parameters with positive PRCCs will increase the value of both R_0 and P_H^* when they are increased, while parameters with negative PRCCs will decrease the value of R_0 and P_H^* when they are increased.

(ii) For R_0, the most sensitive parameters at within-host scale are: μ_h, α_h, α_s, μ_s, α_m, μ_m, N_a, α_a, μ_a, α_e, and μ_e while the most sensitive parameters at between-host scale are β_H, P_0, Φ_H, and α_H. This implies that at the beginning of human ascaris infection care must be taken to the accuracy of those five between-host parameters and the five within-host parameters during the intervention.

(iii) For P_H^*, the sensitive of the transmission metric to the same parameters as for R_0 is variable, with P_H^* being highly sensitive only to the two between-host parameters (β_H and P_0) while remaining less sensitive to all the other parameters. This means that when human ascariasis is at the endemic level, interventions such as (a) vaccinations that reduces susceptibility of humans to infection, (b) good sanitary hygiene behavior that reduces the risk of an individual to contact with infective worm eggs in the environment need to be highly

considered as they are likely to have the highest benefits in reducing the transmission of human ascariasis in the community.

6.4.2 Evaluation of Reciprocal Influence Between Within-host scale and Between-host scale from Numerical Simulations of the Multiscale Model

In this subsection, we present evidence about the reciprocal influence between the between-host scale and the within-host dynamics of human sacariasis infection using results from the numerical simulations of the multiscale model system (6.2.1). The simulation of model (6.2.1) were carried out using a Python program version V 2.6 in the windows operation system (Windows 10).

6.4.2.1 Ascertaining the influence of between-host scale on the within-host ascaris disease dynamics

In this sub-section, we investigate through numerical simulation of the multiscale model system (6.2.1) the reciprocal effect of the between-host scale sub-model parameters on the within-host scale sub-model dynamics. Fig. 6.5 - Fig. 6.7 show the impact in the variation of the four between-host parameters (β_H, μ_E, α_H, P_0) on the dynamics of four selected key with-host variables (P_h, P_s, P_a, P_e). These parameters were only chosen as illustrative examples of the influence of outside-host (between-host) scale disease processes on within-host scale ascaria disease dynamics.

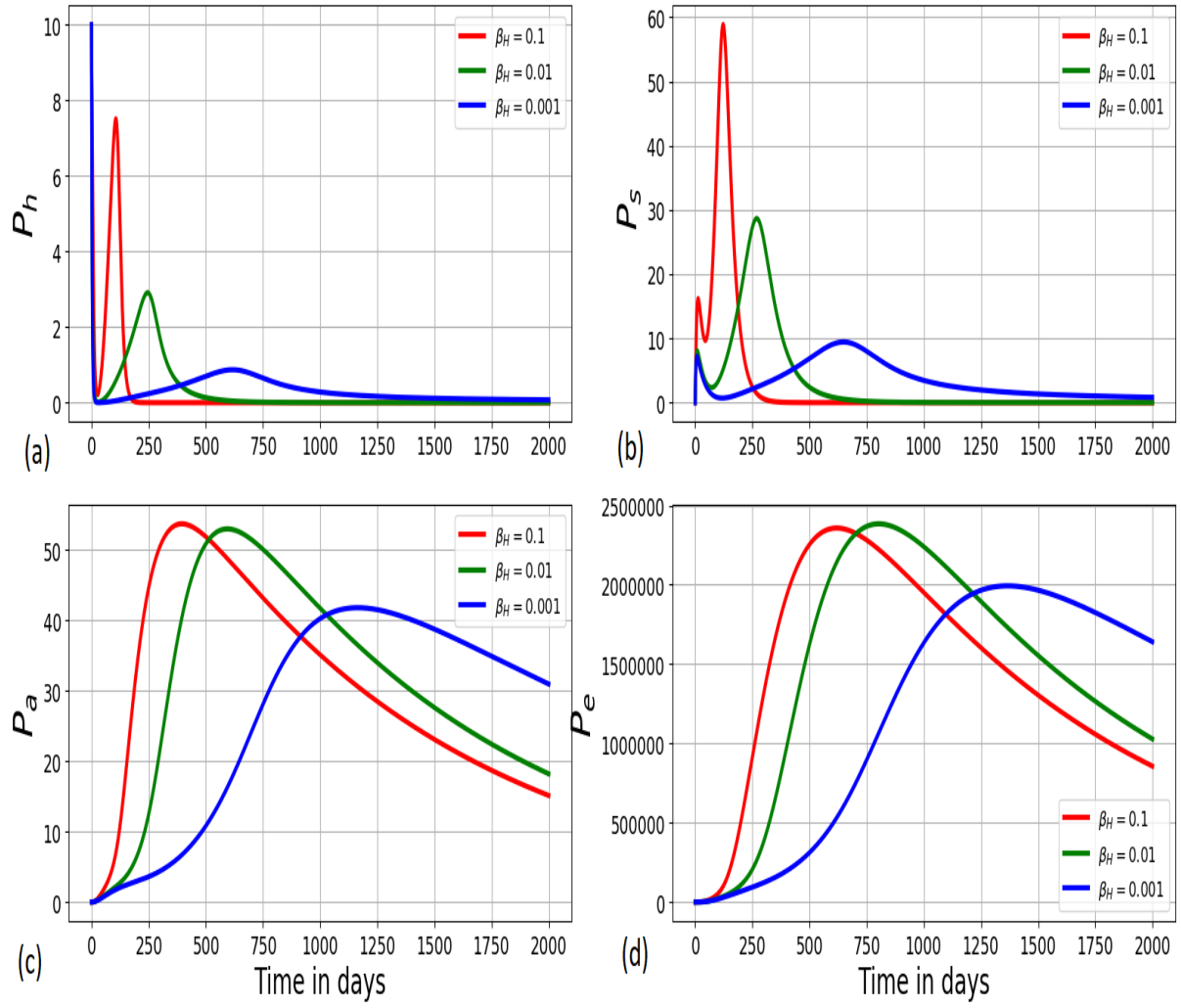

Figure 6.5: *Graphs of numerical solutions of model system (6.2.1) showing the influence of between-host transmission rate parameter (β_H) on the within-host scale population dynamics of (a) infective eggs (P_h), (b) first stage larvae (P_a), (c) adult roundworms (P_a), and (d) eggs (P_e) hatched by adult roundworms in the host small intestine for different values of β_H: β_H = 0.1, β_H = 0.01, and β_H = 0.001.*

Fig. 6.5 illustrates graphs of numerical solutions showing the variations in the population of (a) within-host infective eggs (P_h), (b) first stage larvae (P_a), (c) adult roundworms (P_a), and (d) hatched eggs (P_e) by adult roundworms in the human small intestine for different values of β_H: β_H = 0.1, β_H = 0.01, and β_H = 0.001. The results Fig. 6.5 show the influence of between-host disease process on within-host disease process of ascaria disease. In particular, the results show that as transmission rate of human ascariasis at the population level increases, the within-host infection intensity of the disease increases as well. Therefore, human behavioural changes (such as good hygiene and sanitation practices) which reduce individuals from contacting with

contaminated food or water with worm infective eggs from the soil reduces the infection intensity of the disease at an individual level.

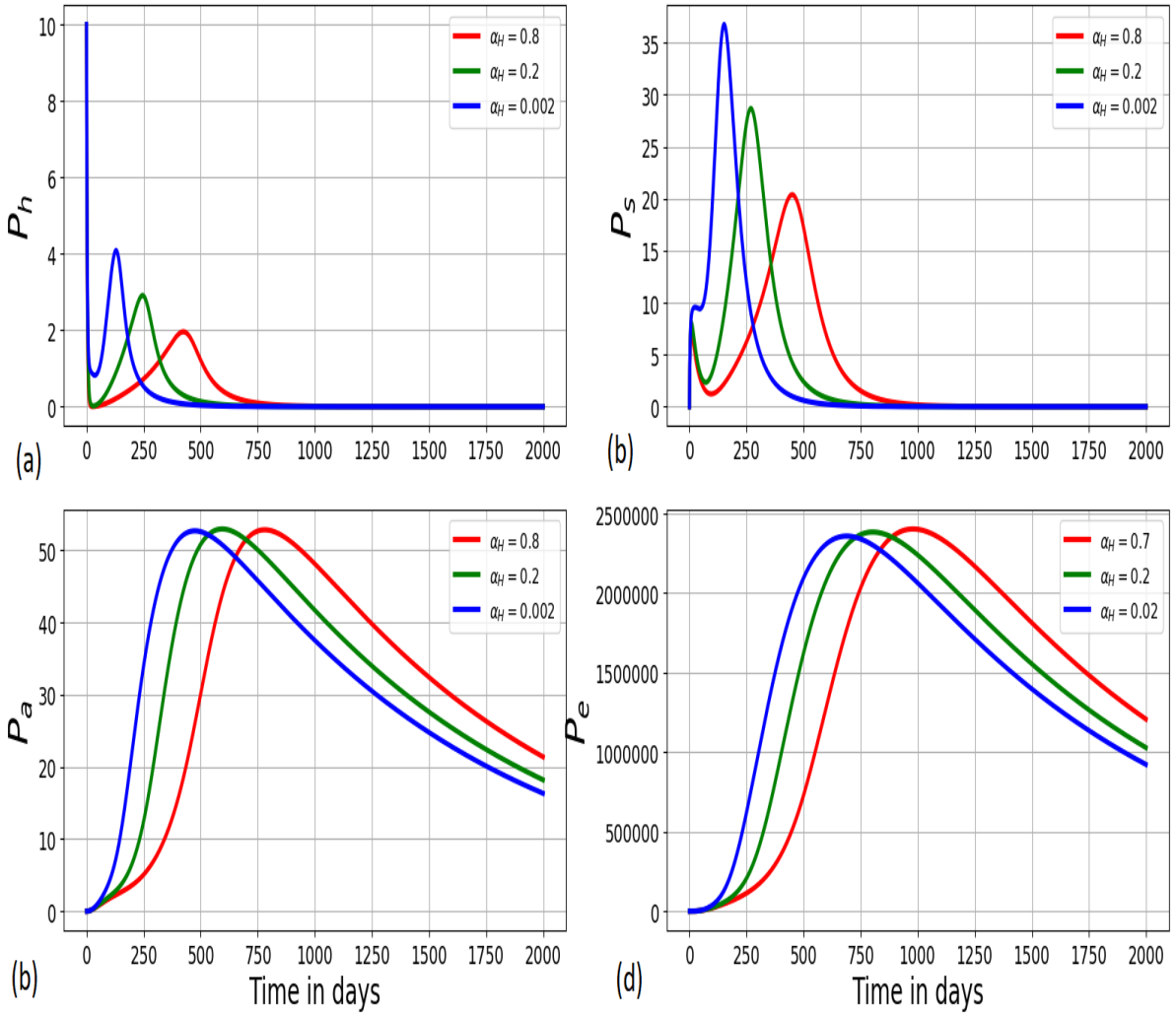

Figure 6.6: *Simulations of model system (6.2.1) showing impact of decay rate of infective eggs in the environment on the within-host scale population dynamics of (a) infective eggs (P_h), (b) first stage larvae (P_a), (c) adult roundworms (P_a), and (d) eggs (P_e) hatched by adult roundworms in the host small intestine for different values of α_H: α_H = 0.8, α_H = 0.2, and α_H = 0.002.*

Fig. 6.6 further illustrates graphs of numerical solutions showing the changes in (a) the within-host infective eggs in the human small intestine (P_h), (b) the within-host first stage larvae in the human small intestine (P_a), (c) adult roundworms in the human small intestine (P_a), and (d) hatched eggs (P_e) by adult roundworms in the human small intestine for different values of α_H: α_H = 0.8, α_H = 0.2, and α_H = 0.002. The results in Fig. 6.6 further shows that as the decay rate of infective worm eggs in contaminated food or water increase, there is a negligible or no change in the within-host infection intensity of the disease at an individual level. This

further demonstrates the influence of between-host disease transmission process on the within-host infection intensity of human ascariasis. Therefore, public health interventions intended to kill infective eggs from contaminated food or drinking water (through food or water treatment such as heating or chlorinate) would have beneficial effect at an individual through reduction of the infection intensity of the disease.

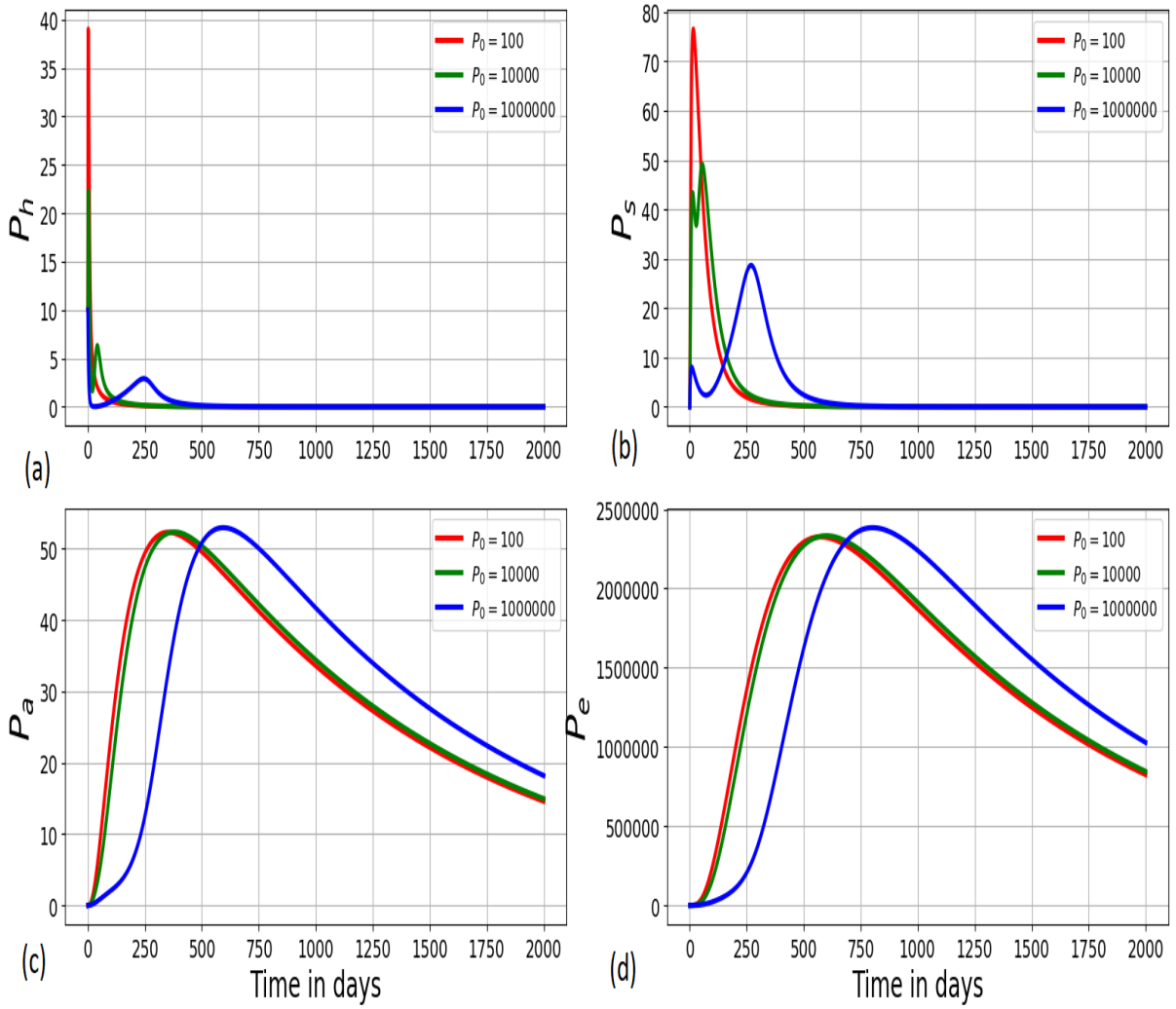

Figure 6.7: *Graph of numerical solutions of model system (6.2.1) showing effect of half saturation constant parameter (P_0) on the within-host scale population dynamics of (a) infective eggs (P_h), (b) first stage larvae (P_a), (c) adult roundworms (P_a), and (d) eggs (P_e) hatched by adult roundworms in the host small intestine for different values of P_0: $P_0 = 100$, $P_0 = 10000$, and $P_0 = 1000000$.*

Fig. 6.7 again illustrates graphs of numerical solutions showing the variations in (a) the within-host infective eggs in the human small intestine (P_h), (b) the within-host first stage larvae in the human small intestine (P_a), (c) adult roundworms in the human small intestine (P_a), and (d)

bottom right: hatched eggs (P_e) by adult roundworms in the host small intestine for different values of P_0: P_0 = 100, P_0 = 10000, and P_0 = 1000000. The results in Fig. 6.7 shows that the increase in the half saturation constant parameter (P_0) associated with infection of infective worm eggs results in a significant decline of the within-host ascariasis intensity. Therefore, sufficient distribution of vaccines in the population to reduce susceptibility of human to the disease will significantly reduce the infection intensity of the disease at an individual level.

Collectively, based on the numerical results in Fig. 6.5 - Fig. 6.7, we notice that the variation in the selected between-host scale parameters β_H, μ_E, α_H and P_0 corresponds to the the changes in the four key selected within-host scale variables P_h, P_s, P_a and P_e. This confirms that during disease dynamics between-host scale influences the within-host scale for human ascaria infection.

6.4.2.2 Ascertaining the influence of within-host scale on the between-host ascaris disease dynamics

This sub-subsection highlights some numerical results obtained from the investigation of the reciprocal influence of the within-host sub-model parameters on the between-host sub-model ascariasis transmission dynamics. Fig. **??** - Fig. 6.10 show the impact in the variation of three within-host parameters (α_s, μ_s, N_a) on the dynamics of three key between-host variables (S_H, I_H, P_E, P_H). Also, these parameters were only chosen as illustrative examples of the influence of inside-host (within-host) scale disease processes on between-host scale human ascariasis transmission dynamics.

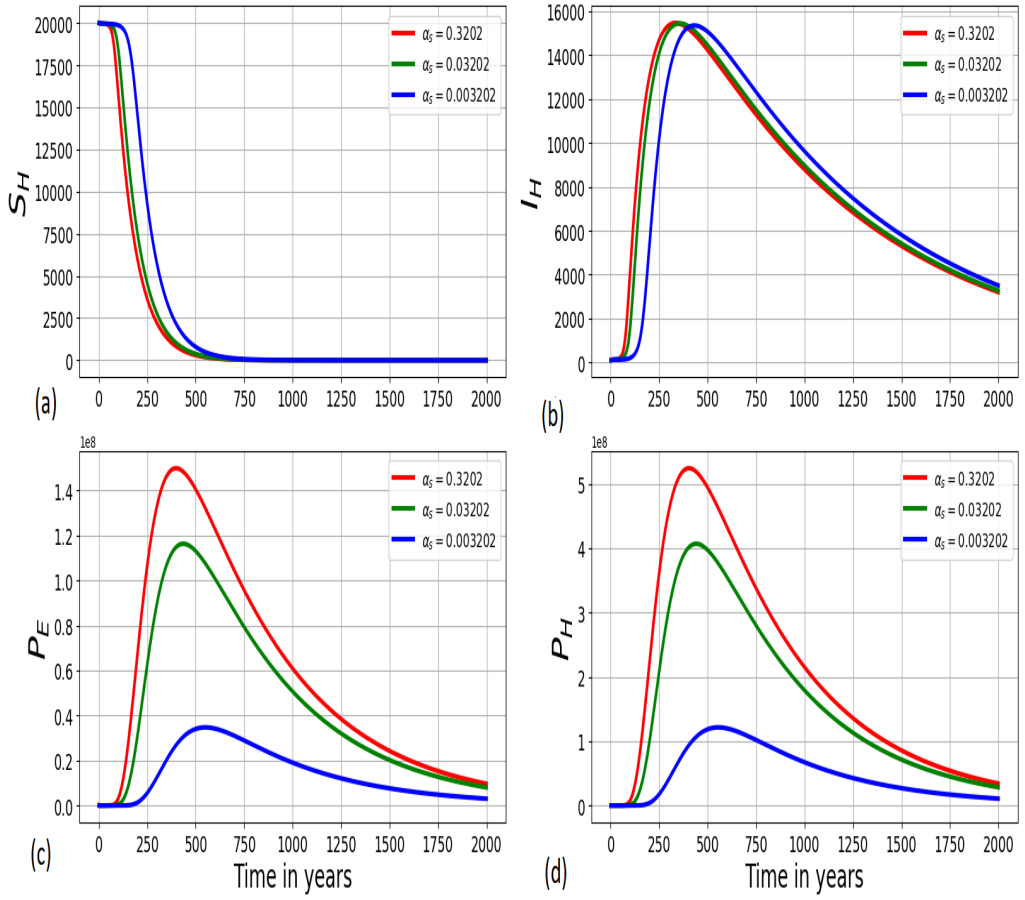

Figure 6.8: *Graph of numerical solutions of the model system (6.2.1) showing the influence of the rate of migration of mature worms α_s from the host's lungs to the host's small intestine on the between-host population dynamics of (a) susceptible humans (S_H), infected humans (I_H), fertilized worm eggs in the environment (P_E), and (d) infective fertilized worm eggs (P_H) in the environment for different values of α_s: $\alpha_s = 0.3202$, $\alpha_s = 0.03202$, and $\alpha_s = 0.003202$.*

Fig. 6.8 also shows graphs of numerical solutions of the multiscale model system (6.2.1) showing variations in (a) population of susceptible human (S_H), (b) population of infected human (I_H), (c) population of roundworm eggs (P_E) in physical environment, and (d) population of infective fertilized worm eggs in the physical environment for different values of α_s: $\alpha_s = 0.3202$, $\alpha_s = 0.03202$, and $\alpha_s = 0.003202$. The numerical results in Fig. 6.8 show that the between-host scale population of worm eggs (P_E and P_H) in the environment as well as infected human population (I_H) increase significantly in response to the increase in the rate of migration of first stage larvae from small intestine to the human host lungs whilst susceptible human population

(S_H) decreases. Therefore, any intervention mechanisms that is intended to block migration of worm larvae in the small intestine to human host lung may have a considerable effect on reducing transmission risk of human ascariasis at population/community level.

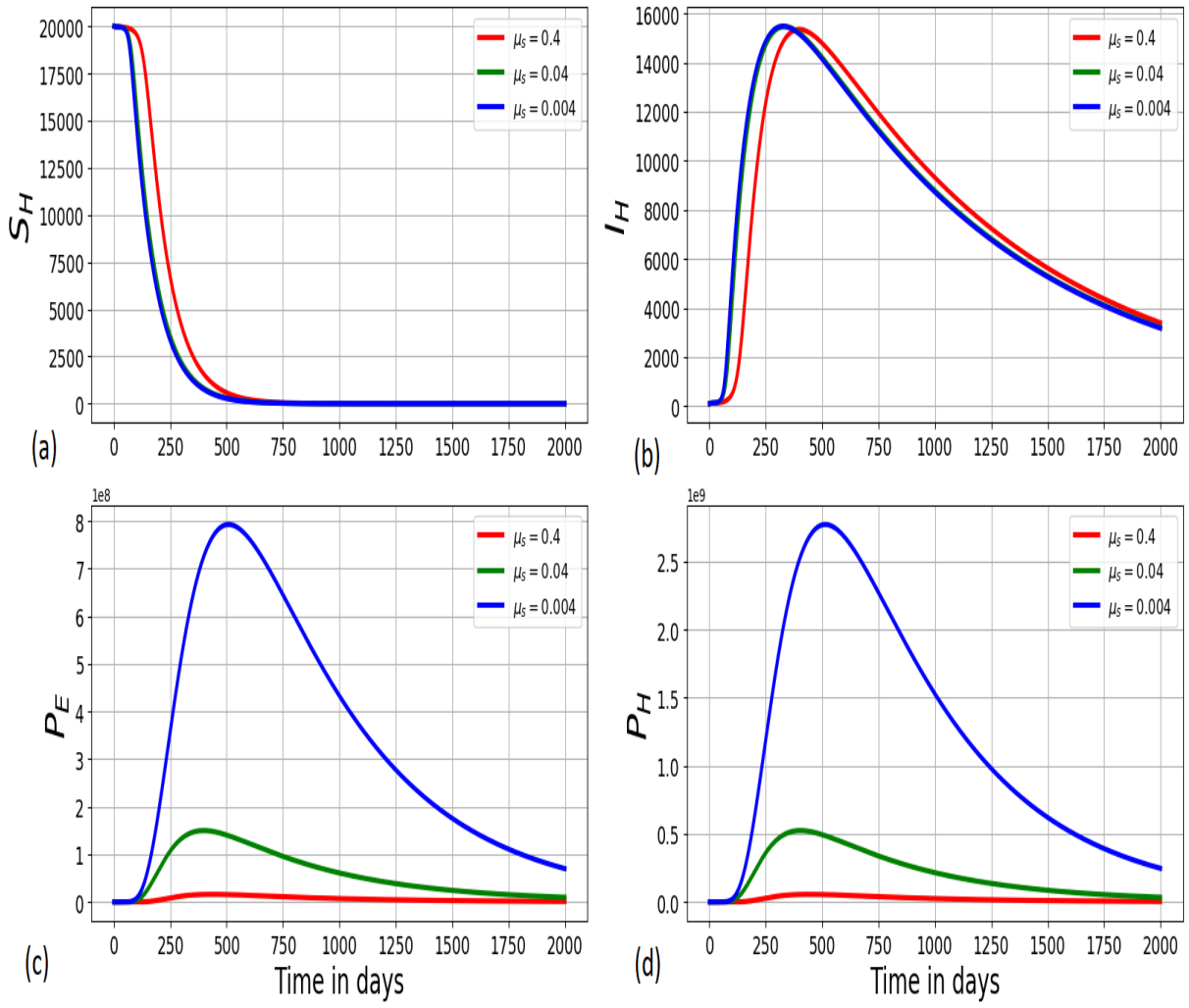

Figure 6.9: *Simulations of model system (6.2.1) showing the impact of decay rate of mature worm larvae in the host lungs on the between-host population dynamics of (a) susceptible humans (S_H), (b) infected humans (I_H), (c) fertilized worm eggs in the environment (P_E), and (d) infective fertilized worm eggs (P_H) in the environment for different values of μ_s: $\mu_s = 0.3$, $\mu_s = 0.025$, and $\mu_s = 0.003$.*

Fig. 6.9 further shows graphs of numerical solutions of the multiscale model system (6.2.1) showing variations in (a) population of susceptible human (S_H), (b) population of infected human (I_H), (c) population of roundworm eggs (P_E) in physical environment, and (d) population of infective fertilized worm eggs in the physical environment for different values of μ_s: $\mu_s = 0.4$, $\mu_s = 0.04$, and $\mu_s = 0.004$. The results in Fig. 6.9 demonstrate that as the death rate of the

mature worm larvae in the human host lungs increases, there is a significant decrease in the between-host scale population of worm eggs (P_E and P_H) which consequently further affects transmission of the disease in the human population level. Therefore, any interventions which enhance the killing of mature worm population in the lungs of an infected human host reduces transmission risk of the disease within communities.

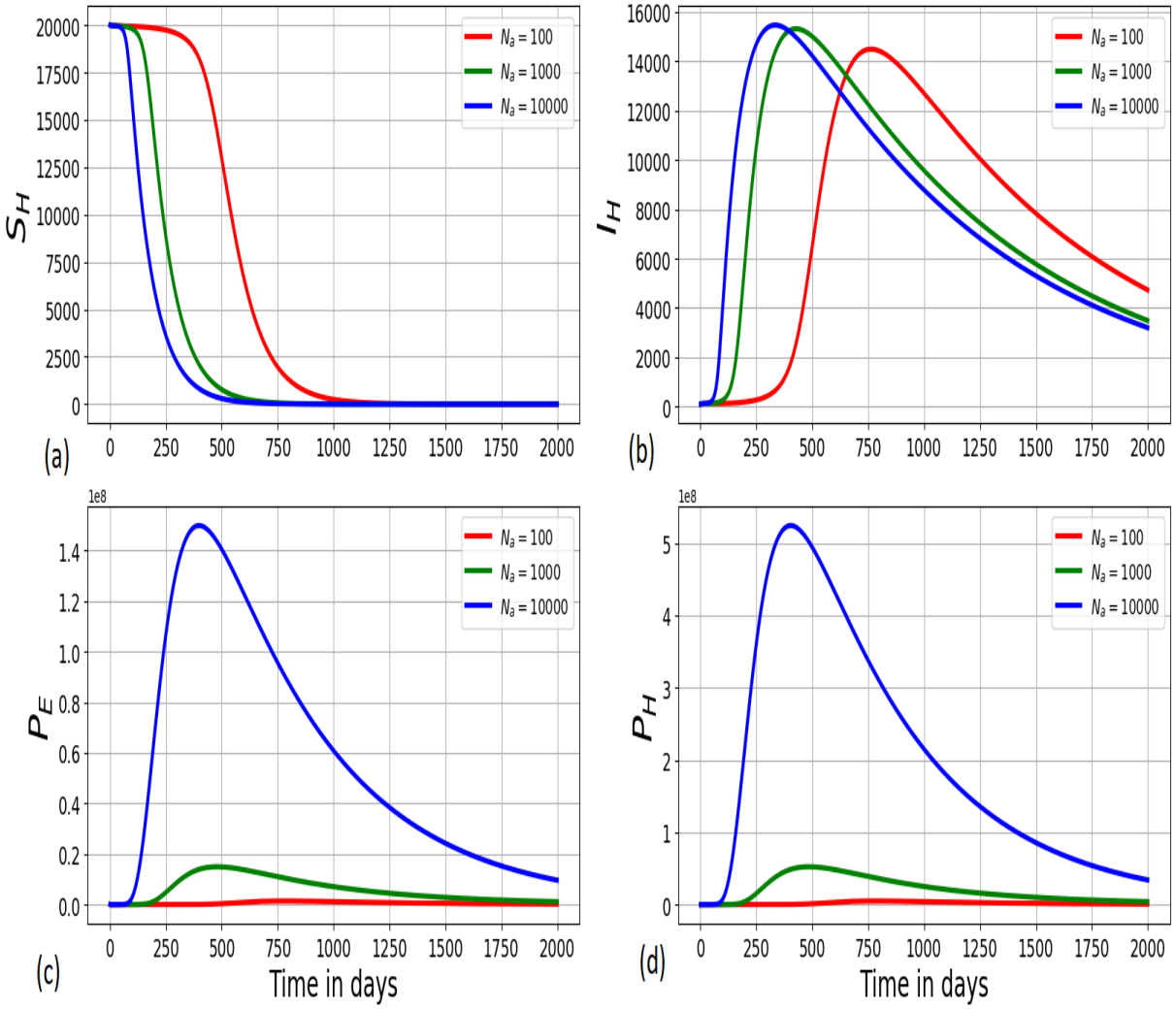

Figure 6.10: *Graphs showing the effect of average number of eggs (N_a) in the small intestine produced by adult roundworms on the between-host population dynamics of (a) top left: susceptible humans (S_H), (b) infected humans (I_H), (c) fertilized worm eggs in the environment (P_E), and (d) infective fertilized worm eggs (P_H) in the environment for different values of N_a: $N_a = 100$, $N_a = 1000$, $N_a = 10000$.*

Fig. 6.10 again shows graphs of numerical solutions of the multiscale model system (6.2.1) showing variations in (a) population of susceptible human (S_H), (b) population of infected human (I_H), (c) population of roundworm eggs (P_E) in physical environment, and (d) population of

infective fertilized worm eggs in the physical environment for different values of N_a: $N_a = 10$, $N_a = 100$, $N_a = 1000$. The results in Fig. 6.10 demonstrate that an increase in production of worm eggs per day by each pair of adult roundworm in the human host small intestine increases significantly the transmission risk of human ascariasis at population/community level. Therefore, any intervention mechanisms intended to reduce worm fecundity within an infected human host may significantly reduce the transmission risk of human ascariasis in the community.

Collectively, the numerical results in Fig. 6.8 - Fig. 6.10, we notice that as the selected within-host scale parameters μ_h, α_s, μ_s and N_a change, results to the changes in the between-host scale variables S_H, I_H, P_E and P_H. This confirms that during disease dynamics within-host scale influences the between-host scale for human ascaria infection.

6.5 Comparison of the Embedded Multiscale Model With the Nested Multiscale Multiscale Model

In this section, we compare the embedded multiscale model which has been extensively used in this chapter to study the multiscale dynamics of the population biology of ascaris with the corresponding nested multiscale model. The corresponding nested multiscale model can be derived from the embedded multiscale model (6.2.1) by removing the super-infection. Therefore, the nested multiscale model for ascaris becomes:

$$
\begin{cases}
i. \quad \dfrac{dS_H(t)}{dt} &= \Lambda_H - \dfrac{\beta_H P_H(t) S_H(t)}{P_0 + P_H(t) S_H(t)} - \mu_H S_H(t), \\
ii. \quad \dfrac{dI_H(t)}{dt} &= \dfrac{\beta_H P_H(t) S_H(t)}{P_0 + P_H(t)} - [\mu_H + \delta_H] I_H(t), \\
iii. \quad \dfrac{dP_E(t)}{dt} &= I_H(t)\alpha_e P_e(t) - [\mu_E + \alpha_E] P_E(t), \\
iv. \quad \dfrac{dP_H(t)}{dt} &= \alpha_E P_E(t) - \alpha_H P_H(t), \\
v. \quad \epsilon \dfrac{dP_h(t)}{dt} &= -[\mu_h + \alpha_h] P_h(t), \\
vi. \quad \epsilon \dfrac{dP_s(t)}{dt} &= \alpha_h P_h(t) - [\mu_s + \alpha_s] P_s(t), \\
vii. \quad \epsilon \dfrac{dP_m(t)}{dt} &= \alpha_s P_s(t) - [\mu_m + \alpha_m] P_m(t), \\
viii. \quad \epsilon \dfrac{dP_a(t)}{dt} &= \dfrac{\alpha_m}{2} P_m(t) - \mu_a P_a(t), \\
ix. \quad \epsilon \dfrac{dP_e(t)}{dt} &= N_a \alpha_a P_a(t) - [\mu_e + \alpha_e] P_e(t).
\end{cases}
\tag{6.5.1}
$$

where ϵ as previously defined is a constant highlighting the fast time-scale dynamics of the within-host model compared to the slow time-scale of the between-host scale dynamics, and it is assumed that $0 < \epsilon << 1$. Therefore, setting $\epsilon = 0$ we get:

$$(P_h^*, P_s^*, P_m^*, P_a^*, P_e^*) = 0. \tag{6.5.2}$$

Now, substituting $P_e^* = 0$ in the third equation of the nested multiscale model system (6.5.1) for P_E which is given by

$$\frac{dP_E(t)}{dt} = I_H(t)\alpha_e P_e(t) - [\mu_E + \alpha_E] P_E(t). \tag{6.5.3}$$

when the dynamics of the disease has reached an endemic level we get:

$$\frac{dP_E(t)}{dt} = -(\mu_E + \alpha_E) P_E(t). \tag{6.5.4}$$

Therefore, the solution of the expression (6.5.4) is

$$P_E(t) = P_E(0)e^{-(\mu_E+\alpha_E)t} \tag{6.5.5}$$

This implies that when t get larger, $P_E(t)$ converges to zero. That is,

$$P_E(t) \to 0 \quad \text{as} \quad t \to \infty \tag{6.5.6}$$

Using the same principles as in Eqs. (6.5.4), similar expressions can be derived for the remaining model variables so that

$$(S_H^*, I_H^*, P_E^*, P_H^*, P_h^*, P_s^*, P_m^*, P_a^*, P_e^*) = 0 \tag{6.5.7}$$

as the disease reaches an endemic level. But, this is not true because infectious disease system of this type do not clear themselves naturally as the within-host dynamics reaches endemic levels. Therefore, we can conclude that nested multiscale models are generally not appropriate in characterizing the dynamics of any type I environmentally-transmitted diseases.

6.6 Summary

The main objective of this study was to compare and identify between an embedded multiscale model and a nested multiscale model which is the most appropriate multiscale model in predicting the dynamics of an infectious disease that has no pathogen replication-cycle at the microscale with specific reference to human ascariasis. The embedded multiscale model for human ascariasis population biology was formulated based on the general multiscale model for type I environmentally-transmitted disease systems presented in the paper of the replication-transmission relativity theory for multiscale modelling of infectious disease systems by Garira [8]. While, the nested multiscale model for human ascariasis population biology was derived from the embedded multiscale used in this study by neglecting the effect of superinfection on the dynamics of the disease. The results of the embedded multiscale models (through mathematical and numerical analysis) show that superinfection continuously influence the dynamics of the disease throughout the infection. While, the nested multiscale model results show that during human ascariasis dynamics the model predict an endemic level of zero which correspond to a disease-free equilibrium state. However, this is not true because infectious diseases of this type continue to persist as they do not naturally clear themselves as they reach an endemic level. Based on these results obtained in the chapter, we established that during human ascariasis population dynamics, only the embedded multiscle model is appropriate for predicting disease dynamics.

In such a case, a nested multiscale model is inappropriate. Therefore, the results in this chapter are powerful evidence that for any infectious disease that has no pathogen replication cycle at the microscale, only the embedded multiscle model is appropriate for predicting disease dynamics. We anticipate that the results in this chapter will enable modelers to choose an appropriate multiscale model in the study of infectious diseases that has no pathogen replication cycle at the microscale beyond human ascariasis.

Chapter 7

Conclusion and Future Research Directions

7.1 Conclusion

In this study, we compared two different categories of multiscale models of infectious diseases, namely, nested multiscale models and embedded multiscale models, and identify between the two categories which one is most appropriate in characterizing the dynamics of infectious disease system with specific to two representative environmentally-transmitted disease systems which are ruminant paratuberculosis and human ascariasis. The two environmentally-transmitted diseases considered in this thesis represent infectious disease systems with replication-cycle at microscale (i.e. ruminant paratuberculosis) and infectious disease systems without replication cycle at the microscale (i.e. human ascariasis). Firstly, we developed a single-scale model that we progressively extended to develop nested multiscale models and embedded multiscale models that we then compare to determine they suitability in characterizing the multiscale dynamics of infectious diseases. To be more specific:

In **Chapter 2**, we presented a single-scale model for the transmission dynamics of environmentally-transmitted disease systems using ruminant paratuberculosis as a paradigm. The model was formulated based on the transmission mechanism theory [8], (i.e. single scale modelling of disease) which privileges the macroscale at every level of organization of an infectious disease system in

disease dynamics. The model was shown through mathematical analysis to be both mathematically and epidemiologically well-posed. We also performed sensitivity analysis study to assess the sensitivity of the two main disease transmission metrics derived from the model which are the basic reproduction number (R_0) and the endemic value of the environmental MAP bacteria (B_C^*) to all the parameters in the model using the Latin hypercube sampling scheme. Numerical simulations of the model variable were also done based on parameters identified to be more sensitive from sensitivity analysis. In this chapter, we demonstrated that although the model analyses were simple, the major weakness of the model was that it describes the replication dynamics of the pathogen within an infected host in a phenomenological manner which makes the model being unrealistic in predicting the dynamics of environmentally-transmitted disease systems. We therefore, anticipate that this kind of limitation of single-scale model can be overcome by extending the single-scale model to a multiscale model.

In **Chapter 3**, we presented nested multiscale model that integrates the within-host scale and between-host scale dynamics for PTB infection, with the main objective of investigating the influence of the variation in size of initial inoculum on the dynamics of the disease. We established (through numerical simulation of the PTB transmission multiscale model) that once the minimum infectious dose is consumed, then the infection at the within-host scale is sustained by pathogen replication. In particular, numerical results showed that as the initial inoculum increases, the time to reach the endemic state also increases at this scale domain. However, at the between-host scale, we observed that when the initial inoculum of MAP bacteria increased beyond the minimum infectious dose made no difference in the transmission dynamics of the disease. In this regard, we think that as the initial infective inoculum increases beyond the minimum infectious dose, the superinfection in the dynamics of PTB in ruminants has no effect on the dynamics of the disease. This is due to the replication of MAP bacteria at the within-host scale that sustains the disease dynamics at this scale. We further used nested multiscale model to enhance traditional single-scale model by estimating $\widehat{N}_c$ that is difficult to estimate using single scale. This was achieved by making the use of a fast-slow time scale based method which reduces dimension of the full nested multiscale model to become a simplified nested multiscale model. After estimating $\widehat{N}_c$, we showed that the simplified multiscale model for PTB infection is mathematically and epidemiologically well-posed. Furthermore, we investigated global stability for both the disease-free and endemic equilibrium states. We also perform a sensitivity analysis study to assess sensitivity (R_0) and (B_C^*) derived from the multiscale model to both the within-host scale and between-host scale parameters in the multiscale model using the Latin hypercube sampling scheme. The results from the sensitivity analysis for both R_0 and B_C^* indicated that care must be taken to the accuracy of the within-host model parameters such as the excretion rate of the

within-host MAP bacteria into the environment, the decay rate of the within-host MAP bacteria at the site of infection within an infected ruminants and the average number of the intracellular MAP bacteria excreted into extracellular environment by each bursting infected macrophages during the data collection if the efficient elimination of the burden of Paratuberculosis infection in a dairy farm level need to be achieved.

In **Chapter 4**, we developed an embedded multiscale model for the dynamics of ruminant paratuberculosis, with the main objective of investigating the role of superinfection on the multiscale dynamics of paratuberculosis in ruminants. We studied the mathematical properties of the multiscale model and established that the model is epidemiological and mathematically well-posed. We observed the same trends as in nested multiscale model results in Chapter 3, that superinfection of the ruminant by the bacteria before it recovers from prior infection by PTB infection does not significantly alter the total pathogen load within an infected ruminant. In particular, Fig. 4.6 - Fig. 4.8 showed the impact in the variation of three selected within-host parameters (α_c, μ_c, N_m) on the population dynamics of three key between-host variables (S_C, I_C, B_C), while Fig. 4.3 - Fig. 4.5 showed the impact in the variation of three important between-host scale parameters (β_C, α_C, B_0) on the population dynamics of four selected key with-host scale variables (I_m, B_c, T_1, T_2). Collectively, the numerical results in Fig. 4.6 - Fig. 4.5 confirmed that once the infection has successfully established at the within-host scale the replication of MAP bacteria sustain the dynamics of PTB disease at this scale domain. The results of sensitivity analysis of R_0 further indicated that the variation of the within-host scale parameters in particular the decay rate of the within-host MAP bacteria population have significant effect on the transmission risk of the disease at the ruminant population level. Therefore, taking into account that there is no drugs for PTB infection (intervention which is administrated at within-host scale), the output of results of sensitivity analysis as indicated in the Tornado plot in Fig. 4.2 reveals that the development of a drug that kills and restricts replication of MAP bacteria at the within-host scale would have beneficial effect on the reduction of the transmission risk of the disease among the ruminants at the herd level.

In **Chapter 5**, we compared the full nested multiscale model, simplified nested multiscale model and the embedded multiscale model for ruminant paratuberculosis described in **Chapter 3** and **Chapter 4**, respectively, to ascertain their suitability in characterizing the intrinsic dynamics of PTB in ruminants as well as the disease is under the influence of health interventions. We established the fact that both the full nested and the embedded multiscale models predict the same pattern of the intrinsic dynamics of an PTB infection and the predicted pattern did not change under the influence of PTB health interventions. This indicates that both the full nested and

the embedded multiscale models can equally be used to characterize an infectious disease that involves a pathogen replication-cycle at the microscale such as PTB. However, the simplified multiscale model seem to predict a high pathogen load as well as a lower impact of effectiveness of intervenion on reducing the burden of the disease. This is because in the simplified multiscale model infection at the microscale has been allowed to progress for sometime before interventions are implemented.

In **Chapter 6**, we compared an embedded multiscale models with a nested multiscale modelling in predicting the dynamics of environmentally-transmitted diseases that have has no pathogen replication cycle at the microscale with specific reference to human ascariasis. Human ascariasis is among neglected tropical diseases that has been and continue to be a cause of public health concern in many low and middle income countries. It is caused by the parasite ascaris lumbricoides that has a complex life-cycle associated with seven main life stages of which two occur outside-host/geographical environment and two take place inside-host/biological environment. The development of an embedded multiscale model for human ascariasis population biology was based on the general multiscale model for type I environmentally-transmitted disease systems presented in [8]. On the other hand, the derivation of a nested multiscale model for human ascariasis population biology was based on the embedded multiscale by neglecting the effect of superinfection on the dynamics of the disease. For an embedded multiscale model, we studied its mathematical properties and established that the multiscale model is epidemiologically and mathematically well-posed. Through investigating the potential influence of superinfection on the dynamics of the disease, we established that during human ascariasis dynamics, superinfection has a significant influence on the increase of infectiveness of an individual. However, in the case of a nested multiscale model, we established (through mathematical analysis of the multiscale model) that during human ascariasis dynamics the model predict an endemic level of zero which correspond to disease-free equilibrium states. But, this is not the case because infectious diseases of this type continue to persist as they do not naturally clear themselves as they reach an endemic level. Therefore, the results in this chapter are powerful evidence that for any infectious disease that has no pathogen replication cycle at the microscale, only the embedded multiscle model is appropriate for predicting disease dynamics. Whereas a nested multiscale model is inappropriate.

The major innovations of this study are as follows: (i) the establishment of scientific evidence that show that for type II environmentally-transmitted diseases, both the NMSM and the EMSM can equally be used to characterize their intrinsic disease dynamics and when they are under the

influence of health intervention mechanisms; (ii) the use of simplified nested multiscale modelling to enhance single-scale modelling in estimating a composite parameter that is difficult to estimate using single-scale models; and (iii) establishment of scientific evidence that show that only an embedded multiscale model is suitable for modelling type I environmentally-transmitted diseases and that a nested multiscale model is inappropriate in modelling type I environmentally-transmitted diseases. We anticipate that this study will enable modelers to choose an appropriate multiscale model in the study of infectious diseases. However, the most challenge we face in this study is the scarcity of multiscale empirical data for models validations. All of our multiscale models developed in this study we not validate due to the scarcity of multiscale empirical data. We do acknowledge that the availability of a relevant multiscale empirical dataset would have aided in estimating key disease parameter and testing possible control scenarios for any infectious disease systems beyond Paratuberculosis and Ascariasis considered in this study.

7.2 Future Research Directions

Since focus of this study was only on comparing the appropriateness of nested and embedded multiscale models in predicting the dynamics of two representative of environmentally-transmitted diseases, for future research directions the following aspects can be take into consideration:

1. Intensive study to compare the suitability in predicting the dynamics of infectious disease systems among all the five different generic categories of multiscale model beyond nested multiscale model and embedded multiscale model would be helpful in the selection of an appropriate category.

2. The comparison between NMSM and EMSM categories was done based on infectious disease systems that are environmentally-transmitted diseases. Therefore, it would be important to consider also infectious diseases that are directly-transmitted diseases to compare the appropriateness of these two multiscale models in prediction of the dynamics of infectious disease systems.

3. It is also imperative to investigate if these two categories of multiscale models accurately predict the dynamics of an infectious disease to the existing empirical data.

4. Furthermore, in relationship to paratuberculosis multiscale models developed in Chapter 3 and Chapter 4, these multiscale models do not take into account the formation of granuloma within an infected ruminant. A possible extension of the work in this study is to

investigate if the two multiscale models predict the same pattern when taking into account granuloma formation on the transmission dynamics of the disease among ruminants.

5. In addition, the multiscale models presented in Chapter 6 did not take into account other factors that determine disease dynamics such as climate, immune response, and demographic structure of the population. We think that these factors are important in determining human ascariasis disease dynamics.

Bibliography

[1] W. Garira. "the research and develoment process for multiscale models of infectious disease systems". 10.1371/journal.pcbi.1007734, 2020.

[2] CDC. Parasites - ascariasis. Available from https://www.cdc.gov/parasites/ascariasis/biology.html, Accessed on October 17, 2019.

[3] Daniel Bernoulli and Sally Blower. An attempt at a new analysis of the mortality caused by smallpox and of the advantages of inoculation to prevent it. *Rev. Med. Virol*, 14:275–288, 2004.

[4] H.W. Hethcote. The mathematics of infectious diseases. *SIAM Rev.*, 42(4):599–653, 2000.

[5] C. Castillo-Chavez, Z. Feng, and W. Huang. *"On the computation Ro and its stability,"In: Mathematical Approaches for Emerging and Reemerging Infectious Diseases: An Introduction, IMA*, volume Vol. 125 of *229-250.* Springer - Velgar, 2002.

[6] W. Garira. The dynamical behaviours of diseases in africa. In Joachim P. Sturmberg and Carmel M. Martin, editors, *Handbook of Systems and Complexity in Health*, pages 595–623. Springer New York, 2013.

[7] D.M. Hartley, J.G. Morris, and D.L. Smith. Hyperinfectivity: A critical element in the ability of v. cholerae to cause epidemics? *PLoS Med*, 3:pp. 0063–0069pp. 0063–0069, 2006.

[8] W. Garira. The replication-transmission relativity theory for multiscale modelling of infectious disease systems. *Scientific Reports*, 9(16353), 2019. https://doi.org/10.1038/s41598-019-52820-3.

[9] W. Garira, D. Mathebula, and R. Netshikweta. A mathematical modelling framework for linked within-host and between-host dynamics for infections with free-living pathogens in the environment. *Mathematical Biosciences*, 256:58–78, October 2014. ISSN 0025-5564. doi: 10.1016/j.mbs.2014.08.004.

[10] R. Netshikweta and W. Garira. A multiscale model for the world's first parasitic disease targeted for eradication: Guinea worm disease. *Computational and Mathematical Methods in Medicine*, 29, 2017. (Article ID 1473287).

[11] Z. Feng, J. Velasco-Hernandez, and B. Tapia-Santo. A mathematical model for coupling with-host and between-host dynamics in an environmental-driven infectious disease. mathematical biosciences. *Mathematical Biosciences*, 242(1):49–55, 2013.

[12] Z. Feng, X. Cen, Y. Zhao, and J.X. Velasco-Hernandez. Coupled within-host and between-host dynamics and evolution of virulence. *Mathematical Biosciences*, 270, 2015. 204e212.

[13] X. Cen, Z. Feng, and Zhao. Emerging disease dynamics in a model coupling within-host and betwen-host system. *J. Theor. Biol*, 361:pp. 141–151, 2014.

[14] X. Wang and J. Wang. Disease dynamics in a coupled cholera model linking within-host and between-host interactions. *J. Biol. Dyn.*, 11:pp. 238 – 262, 2017.

[15] M. Konboon, M. Bani-Yaghoub, P.O Pithua, N. Rhee, and S.S Aly. A nested compartmental model to assess the efficacy of paratuberculosis control measures on u.s. dairy farms. *Plos ONE*, 13(10), 2018. e0203190.

[16] W. Garira and M.C. Mafunda. From individual health to community health: towards multiscale modelling of directly transmitted infectious disease systems. *J. Biol. Syst.*, 27(1): 131–166, 2019.

[17] W. Garira and D. Mathebula. A coupled multiscale model to guide malaria control and elimanation. *Journal of Theoretical Biology*, 475:34–59, 2019.

[18] W. Garira and F. Chirove. A general method for multiscale modelling of vector-borne disease systems. *Interface Focus*, 10(20190047), 2019. http://dx.doi.org/10.1098/rsfs.2019.0047.

[19] W. Garira. A primer on multiscale modelling of infectious disease systems. *Infectious Disease Modelling.*, 3:176–191, 2018.

[20] W. Garira. A complete categorization of multiscale models of infectious disease systems. *Journal of biological dynamics*, 11(1):378–435, 2017.

[21] M.J. Keeling and K.T.D. Eames. Networks and epidemic models,. *J. R. Soc. Interf.*, 2(4): pp. 295– 307, 2005.

[22] T. Kostova. Persistence of viral infections on the population level explained by an immunoepidemiological model. *Math. Biosci.*, 206(2):pp. 309–319, 2007.

[23] Vickers M.D. and Osgood N.D. A unifed framework of immunological and epidemiological dynamics for the spread of viral infections in a simple network-based population. *Theor. Biol. Med. Modell.*, 4(1):p. 49., 2007.

[24] H.C. Tuckwell, L. Toubiana, and J.F. Vibert. Spatial epidemic network models with viral dynamics. *Phys. Rev. E*, 57(2):pp. 2163 – 2169, 1998.

[25] Bennett S. and E.M. Riley. The statistical analysis of data from immuno-epidemiological studies. *J. Immunol. Methods*, 146(Suppl. 2):pp. 229–239, 1992.

[26] A.V.D. Roux and A.E. Aiello. Multilevel analysis of infectious diseases. *J. Infect. Dis.*, 191 (Suppl. 1):pp. S25–S33, 2005.

[27] T.E.M. Elfaki, K. Arndts, A. Wiszniewsky, Ritter, I.A. M. Goreish, M.E.Y.A. Atti El Mekki, S. Arriens, K. Pfarr, and R. Fimmers et al. Multivariable regression analysis in schistosoma mansoni infected individuals in the sudan reveals unique immuno-epidemiological profles in uninfected, egg+ and non-egg+ infected individuals. *PLoS Negl. Trop. Dis.*, 10(5):p. e0004629, 2016.

[28] A.L. Bauer, C.A. Beauchemin, and Perelson A.S. Agent-based modeling of host-pathogen systems: The successes and challenges. *Inf. Sci.*, 179(Supp. 10):pp. 1379 – 1389, 2009.

[29] J.E. Mellor, J.A. Smith, G.P. Learmonth, V.O. Netshandama, and R.A. Dillingham. Modeling the complexities of water, hygiene, and health in limpopo province, south africa. *Environmental Science & Technology*, 46(24):13512–13520, 2012. doi: doi:10.1021/es3038966.

[30] H.M. Yang. Malaria transmission model for different levels of acquired immunity and temperature-dependent parameters (vector). *Rev. Saude Publica*, 34(03):pp. 223 – 231, 2000.

[31] C. Chiyaka, W. Garira, and Dube S. Transmission model of endemic human malaria in a partially immune population. *Math. Compt. Modell.*, 46(05):pp. 806 – 822, 2007.

[32] J. Labadin, C.M.L. Kon, and S.F.S. Juan. Deterministic malaria transmission model with acquired immunity. In *in Proceedings of the World Congress on Engineering and Computer Science*, volume 2, pages pp. 20–22, 2009.

[33] M.A. Gilchrist and D. Coombs. Evolution of virulence: Interdependence, constraints, and selection using nested models. *Theor. popul. Biol.*, 62(02):pp. 145 – 153, 2006.

[34] Z. Feng, J. Velasco-Hernandez, B. Tapia-Santo, and M.C.A. Leite. A model for coupling within-host and between-host dynamics in an infectious disease. *Nonlinear Dyn.*, 63(3): pp.401–411, 2012.

[35] M.A. Gilchrist and Sasaki A. Modeling host-parasite co-evolution: a nested approach based on mechanistic models. *J Theor Biol*, 218:289–308., 2002.

[36] M. Martcheva and S.S. Pilyugin. An epidemic model structured by host immunity. *J. Biol. Syst.*, 2006.

[37] Angulo, F. O. Milner, and L. Sega. A sir epidemic model structured by immunological variables. *J. Biol. Syst*, 21(Supp. 4):pp. 1340013, 2013.

[38] A. Gandolf, A. Pugliese, and C. Sinisgalli. Epidemic dynamics and host immune response: A nested approach. *J. Math. Biol.*, 70(3):pp. 399–435, 2015.

[39] S.H. Steinmeyer, C.O. Wilke, and K.M. Pepin. Methods of modelling viral disease dynamics across the within- and between-host scales: The impact of virus dose on host population immunity. *Philos. Trans. R. Soc. B: Biol. Sci.*, 365(1548):1931–1941, 2010.

[40] M. Legros and S. Bonhoeffer. A combined within-host and between-hosts modelling framework for the evolution of resistance to antimalarial drugs. *J. R. Soc. Interf.*, 2016.

[41] N. Martcheva, M. Tuncer and Kim Y. On the principle of host evolution in host-pathogen interactions. *J. Biol. Dyn.*, 11(Supp. 1):pp. 107–119, 2017.

[42] J.W. Rudge, J.P. Webster, D.B. Lu, T.P. Wang, G.R. Fang, and M.G. Basanez. Identifying host species driving transmission of schistosomiasis japonica, a multihost parasite system, in china. *Proc. Natl. Acad. Sci.*, 110(28):pp. 11457–11462, 2013.

[43] D. Heinzmann, A.D. Barbour, and P.R. Torgerson. A mechanistic individual-based two-host interaction model for the transmission of a parasitic disease. *Int. J. Biomath*, 4(04):pp. 443 – 460, 2011.

[44] WHO. Food-borne diseases. https://www.who.int/news-room/fact-sheets/detail/food-safety., . Accessed on Act 2019.

[45] C.L.F. Walker, J. Perin, J. Katz, J.M. Tielsch, and R.E. Black. Diarrhea as a risk factor for acute lower respiratory tract infections among young children in low income settings. *Journal of Global Health*, 3(1):010402., 2013. doi:10.7189/jogh.03.010402.

[46] WHO. Soil-transmitted diseases. https://www.who.int/news-room/fact-sheets/detail/soil-transmitted-helminth-infections., . Accessed on October 2019.

[47] W. Garira and D Mathebula. Development and application of multiscale models of acute viral infections in intervention research. *Math Meth Appl Sci.*, pages 1 – 27, 2020. DOI: 10.1002/mma.6119.

[48] S. Ott, S. Wells and B. Wagner. Herd-level economic losses associated with johne's disease on us dairy operations. *Preventive veterinary medicine*, 40:179–192, 1999.

[49] M. Boots. A general host–pathogen model with free–living infective stages and differing rates of uptake of the infective stages by infected and susceptible hosts. *Researches on Population Ecology*, 41(2):189–194, 1999.

[50] C.P. Bhunu, W. Garira, and Z. Mukandavire. Modeling hiv/aids and tuberculosis coinfection. *Bulletin of Mathematical Biology*, 71(7):1745–1780, 2009.

[51] H. J. B. Njagavah and F. Nyambaza. Modelling the impact of rehabitation amelioration and relapse on the prevalence of drug epidemics. *Journal of Biology Systems*, 21(1), 2012.

[52] G. Magombedze, C.N. Ngonghal, and C. Lanzas. Evalution of the "iceberg phenomenon" in johne's disease through mathematical modelling. *PLoS ONE*, 8(10), 2013. e76636.

[53] G. Magombedze, S. Eda, and V.V. Ganusov. Competition for antigen between th1 and th2 responses determines the timing of the immune response switch during mycobaterium avium subspecies paratuberulosis infection in ruminants. *PLoS Comput Biol,*, 10(1), 2014. e1003414.

[54] M. Martcheva, S. Lenhart, S. Eda, E. Klinkenberg, D. Momotani, , and J. Stabel. An immuno-epidemiological model for johne's disease in cattle. *Veterinary Research*, 46(1): 69, 2015.

[55] R.J. Chiodini, W.M. Chamberlin, J. Sarosiek, and R.W. McCallum. Crohn's disease and the mycobacterioses: a quarter century later. causation or simple association? *Critical reviews in microbiology*, 32:59–93, 2012.

[56] M. Martcheva, M.D. Todorov, and C.I Christov. An immuno-epidemiological model of paratuberculosis,. In *in AIP Conference Proceedings*, volume 1404, page p. 176, 2011.

[57] K. R. Schneider. Applications of centre manifold theory. applied mathematical sciences 35. berlin-heidelberg-new york, springer-verlag 1981. xii, 142 s., dm 32,-. us $ 14.60. isbn 3-540-90577-4. *ZAMM - Journal of Applied Mathematics and Mechanics / Zeitschrift für Angewandte Mathematik und Mechanik*, 62(10):571–571, 1982.

[58] F. Bastida and R.A. Juste. Paratuberculosis control: A review with a focus on vaccination. *Journal of Immune Based Therapies and Vaccines*, 9(8), 2011.

[59] R. Mitchell, R. Whitlock, Stehman, A. S. Benedictus, and et al. Chapagain. Simulation modeling to evaluate the persistence of mycobacterium avium subsp. paratuberculosis (map) on commercial dairy farms in the united states. *Preventive veterinary medicine*, 93 (10):360–380, 2008.

[60] P. Marce, C. Ezanno, M.F. Weber, H. Seegers, D.U. Pfeiffer, and C. Fourichon. Invited review: Modeling within-herd transmission of mycobacterium avium subspecies paratuberculosis in dairy cattle: A review. *Journal of Dairy Science*, 93(19):4455–4490, 2010.

[61] M. Martcheva. An immuno-epidemiological model of paratuberculosis. https://pdfs.semanticscholar.org/0090/c48945aedb167a146f32ab80bf6dd2c1e260.pdf.

[62] J. Robins, S. Bogen, A. Francis, A. Westhoek, and Kanarek et al. Agent-based model for johne's disease dynamics in a dairy herd. *Vet. Res.*, 46(58), 2015.

[63] P.O Pithua N. Rhee S.S Aly M. Konboon, M. Bani-Yaghoub M. A nested compartmental model to assess the efficacy of paratuberculosis control measures on u.s. dairy farms. *PLoS ONE*, 13(10):e0203190., 2018.

[64] R.M. Anderson and R.M. May. Helminth infections of humans: mathematical models, population dynamics, and control. *Adv. Parasitol*, 24:1e101, 1985.

[65] WHO. Water sanitation health: Disease risk ascariasis, . Available from https://www.who.int/water_sanitation_health/diseases-risks/diseases/ascariasis/en/, Accessed on October 17, 2019.

[66] Z.S. Pawlowski. *Ascariasis: Host-Pathogen Biology*, volume 4. Oxford University Press., July 1982.

[67] R. M. Anderson. Depression of host population abundance by direct life cycle macroparasites. *J. Theor. Biol.*, 82:283–311, 1980.

[68] M.E. Scott. Ascaris lumbricoides: A review of its epidemiology and relationship to other infections. *Ascaris lumbricoides: A review of its epidemiology and relationship to other infections*, 66(722), 2008.

[69] R. M. Anderson. Population dynamics of human helminth infections: control by chemotherapy. *Nature*, 297:557–563, 1982.

[70] A. C. Fowler and T. Déirdre Hollingsworth. The dynamics of ascaris lumbricoides infections. *Bulletin of Mathematical Biology*, 78(4):815–833, April 2016. ISSN 1522-9602.

[71] E.L. Davis, L. Danon, Prada J.M., S.A. Gunawardena, J.E. Truscott, and J. et al. Vlaminck. Seasonally timed treatment programs for ascaris lumbricoides to increase impact—an investigation using mathematical models. *PLoS Negl Trop Dis*, 12(1):p. e0006195, 2018.

[72] W.D. Ransom, B.H. Foster. Observations on the life history of ascaris lumbricoides. *US Dept. Agric. Bull.*, 817, 1920.

[73] F.W. Douvres and F.G. Tromba. Comparative development of ascaris suum in rabbits, guinea pigs, mice and swine in 11 days. *Proc Helm Soc Wash*, 38:246e52, 1971.